Università degli Studi di Palermo

Department of Engineering

Doctorate in Mechanical, Manufacturing, Managment and Aerospace Innovation (M3AI)

XXXVII Cycle of Doctorate

Advanced Biomechanical Modeling of Spine. *In-vitro* Testing and Finite Element Modelling

PHD THESIS

ENG. VINCENZA SCIORTINO

DOCTORATE COORDINATOR

PROF.SSA GIOVANNA LO NIGRO

TUTOR

PROF.SSA DONATELLA CERNIGLIA

CO-TUTOR

PROF. TOMMASO INGRASSIA

PROF. SALVATORE PASTA

ACADEMIC YEAR 2023-2024

Contents

List of Figures

List of Tables

Acronyms

FSU *Functional Spinal Unit*

IVD *Intervertebral Disc*

AF *Annulus Fibrous*

NP *Nucleus Pulpous*

ECM *Extracellular Matrix*

CEP *Cartilaginous Endplate*

IAR *Instantaneous Axis of Rotation*

ICR *Instantaneous Center of Rotation*

ROM *Range of Motion*

EZ *Elastic Zone*

NZ *Neutral Zone*

PMMA *Poly(methyl methacrylate)*

NR *Nucleus Replacement*

DHR *Disc Height Reduction*

IDP *Intradiscal Pressure*

MRI *Magnetic Resonance Imaging*

CT *Computer Tomography*

LIF *Lumbar Interbody Fusion*

PLIF *Posterior Lumbar Interbody Fusion*

ALIF *Anterior Lumbar Interbody Fusion*

LLIF *Lateral Lumbar Interbody Fusion*

OLIF *Oblique Lumbar Interbody Fusion*

TLIF *Transverse Lumbar Interbody Fusion*

FEM *Finite Element Modelling*

PCA *Principal Component Analysis*

SSM *Statistical Shape Modelling*

MRE *Medical Reverse Engineering*

Abstract

The focus of this thesis is spinal column, one of the most complex and fundamental anatomical structures in the entire human body with the main functions to support upright posture, provide movements and protect the central nervous system.

The aim of the thesis was to investigate spinal anatomy and biomechanics through *in-vitro* experimental campaigns conducted on human cadavers and animal specimens and through a computational approach. The acquired anatomical, biomechanical and experimental knowledge were then exploited for seeking and employing a mathematical model that could simulate the biomechanical response of the intervertebral disc under prolonged loads. In addition, an infinite population of spinal geometries was created,i.e. a 3D atlas of the pathological lumbar spine, by using the advanced technology available today of finite element modeling. The goal was to create useful tool for the bioengineering field that could be exploited to have access to accurate geometries of spinal columns. These geometries can be used to perform computational simulations that can be used in clinical practice for the fabrication of medical devices and for the simulation of surgical procedures. Finally, the last research step was to create a finite element model of the spine to be validated through experimental data.

This thesis has been divided into five main chapters, each one addressing one crucial aspect. The first two chapters provide a detailed background on the anatomy and biomechanics of the spine; while the last 3 chapters encapsulate the innovative research work conducted over the three years of doctoral studies, in which published works and those still in the process of publication have been included, those have enriched the literature with new concepts and instruments never before presented.

Chapter 1 presents a detailed description of the anatomical structures of the spine in its major regions: cervical, thoracic, lumbar, sacral and coccygeal. Indeed, each region has been described as unique in its anatomy, morphology and function. Specifically, more attention has been placed on the intervertebral disc as it is a key element in spinal biomechanics, separating the vertebrae and acting as a shock

absorber to distribute forces along the spine and providing spinal flexibility. It is crucial to analyze it from a biomechanical point of view as it is one of the first spinal components to develop degenerative diseases.

Chapter 2 covers the study of the spinal biomechanics. Hence, several key biomechanical concepts were introduced such as: the Functional Spinal Unit (FSU), which is the smallest functional unit of the spine, consisting of two adjacent vertebrae and the intervertebral disc separating them; the global reference system for an FSU; and the major movements, i.e., flexion, extension, axial rotationl, and lateral bending. The remaining part of the chapter focused on experimental tests employed to study in spine biomechanics to measure key parameters such as flexibility, creep, and stress relaxation. Employing experimental tests enables the quantification of deformation phenomena which occur over time, offering new perspectives to better understand the long-term behaviour of the spine under repeated and chronic stress conditions.

Chapter 3 focused on the main degenerative diseases of the spine, with special emphasis on the pathologies affecting the intervertebral disc. Degenerative disc diseases are generally related to aging and mechanical deterioration of the intervertebral discs, but they are also influenced by genetic and biomechanical factors. Indeed, disc herniation is characterized by the leakage of the nucleus pulposus across weakened annulus fibrosus fibers, leading to acute pain. It is one of the most common disorders afflicting a large portion of the world's population. In addition, the final part of the chapter provide an overview of surgical treatments for spinal diseases, such as spinal fixation and spinal fusion, as well as innovations in the field of disc Nucleus Replacement (NR). Indeed, a schematic review on the nucleus replacement has been published, representing a major focus of the research work in this thesis. This schematic review was an historical one, and it was the very first in its kind presented in the literature. The reviews covered the nucleus replacement history from 1955 until today, presenting the nucleus replacement as a promising alternative to fusion, as it preserves vertebral mobility and reduces the risks associated with postoperative stiffness.

Chapter 4 is the experimental section of this thesis work, in which two innovative research papers were included. In this chapter, the concepts learned in Chapter 2 were implemented to conduct *in-vitro* experimental campaigns on bovine tails and human cadavers, aiming to simulate the actual biomechanical conditions of the human spine. Specifically, the aim was to obtain experimental data which could be

used to perform viscoelastic analysis of tissues, using prolonged tests to measure creep deformation, through which mathematical modelling of disc biomechanical behavior followed. A novel aspect of modelling intervertebral disc biomechanics was introduced with the fractional calculus matheamtical tool. Indeed, it was shown how fractional calculus, compared with classical models, can offer a more accurate description of nonlinear mechanical behavior of tissues.

Finally, **Chapter 5** is the computational section, where how Finite Element Modeling (FEM) can be used to simulate the biomechanical behavior of the spine is presented. The chapter contains four research papers. First, the main key aspects to consider in realizing a FEM of the spine were presented, aiming to replicate accurately and precisely the interactions between the different components of the spine under different loading conditions. The next step involved the creation of a three-dimensional atlas based on data from patients with spinal diseases. The greatness of these research papers are about of the creation of this 3-D atlas which offers the possibility to virtually simulate the effects of pathologies and to have available an infinite population of different anatomical geometries. Finally, the chapter ends with the presentation of a new finite element model that was built on a patient-specific basis, which was then validated through experimental data.

Chapter 1

Spinal anatomical structures and functions

1.1 The Spinal Column

The spine is composed by a total 24 vertebrae, in addition to the sacrum and the coccyx (Figure 1.1). The main functions of the spine are to maintain the body in upright position, to support the weight of the head, neck and trunk, to transfer this weight to the lower limbs, to protect the spinal cord and to provide a pathway for the spinal nerves from the cord along all adjacent zones [1–8].

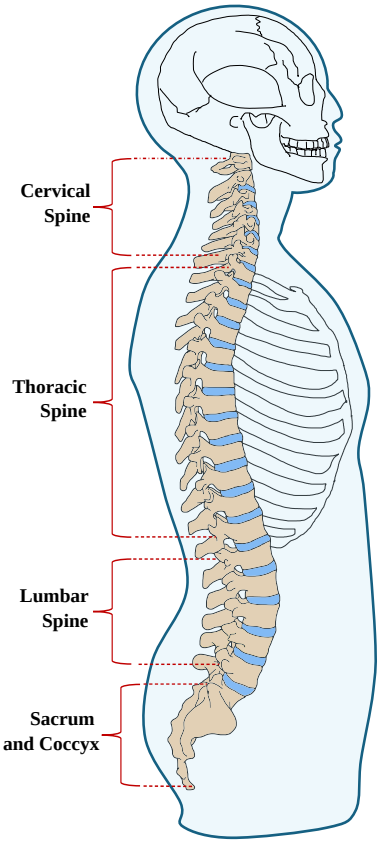

Figure 1.1. *© Spine and its regions: Cervical, Thoracic, Lumbar, Sacrum and Coccyx.*

There are five distinct zones in the vertebral column: cervical (7 vertebrae), thoracic (12 vertebrae), lumbar (5 vertebrae), sacral, and coccygeal regions, as reported in Figure 1.2. Each spinal region has different characteristics and functions, and at the junction between two distinct areas, the two vertebrae present intermediate anatomical features between the upper and lower zones [1–8].

Looking at the sagittal plane, the spine is not purely rigid and straight. Indeed, an adult spinal column has four different curvatures (see Figure 1.2), which can be divided into primary (before birth) and secondary curvatures (after birth):

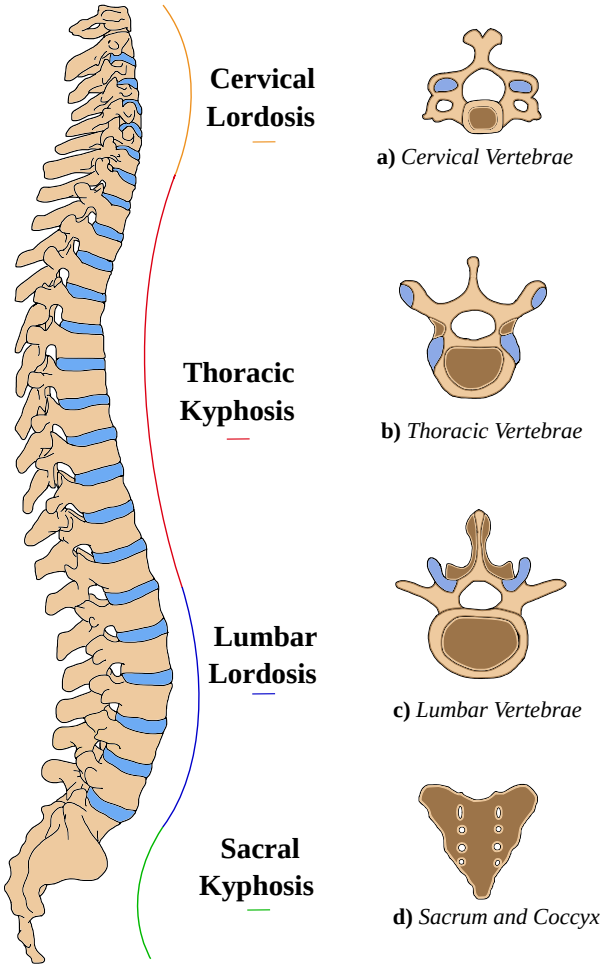

Figure 1.2. *© Cervical and Lumbar lordosis, and Thoracic and Sacral kyphosis. Schematic representation of the vertebrae in the different regions:* ***a)*** *Cervical;* ***b)*** *Thoracic;****c)*** *Lumbar ;****d)*** *Sacrum and Coccyx.*

1. **Cervical curvature or cervical lordosis.** This is a secondary curvature that is developed once the infant learns to balance the head's weight on the neck's vertebrae.

2. **Thoracic curvature or thoracic kyphosis.** This is a primary curvature that

anatomically has the function of containing the organs in the thorax (heart and lungs).

3. **Lordosis curvature or lumbar lordosis.** This is a secondary curvature that is created to balance the weight of the trunk on the lower limbs, thus developing the ability to maintain the upright posture.
4. **Kyphosis curvature or sacral kyphosis.** This is a primary curvature anatomically designed to carry the abdominopelvic organs.

Despite their different function related to the specific area, all vertebrae have the same anatomical structure that can be described as follows [1–8] (see Figure 1.3):

- ➢ **Anteriorly** there is the vertebral body. This is the region that enables the transmission of weight along the axis of the spine. The vertebral body presents a spherical or oval shape, from which the vertebral arch extends posteriorly. Each vertebra binds with the adjacent one through ligaments, and they are separated from each other by intervertebral discs.
- ➢ **Posteriorly** each vertebra has a **vertebral arch** or also referred to as a neural arch. It delimits the lateral and posterior margins of the vertebral hole that surrounds and along which there is the spinal cord. Besides possessing a floor (posterior surface), the vertebral arch has **pedicles** and **laminae**. The peduncles delimit the posterior- and lateral margins of the body, while the laminae extend dorsally and medially to complete the roof. The fusion of the laminae results in the **spinal process**, i.e. the posterior part of the vertebrae, which can also be seen and palpated through the skin. In addition, there are the transverse processes that join the pedicles and act as attachment sites for the muscles.
- ➢ The **articular processes** are the junction between the pedicles and laminae. There are the superior (cranially) and inferior (projected) articular processes.
- ➢ All 24 vertebral arches create the **vertebral foramen**, which contains the spinal cord and allow the passage of nerves coming from or directed to the spinal cord.

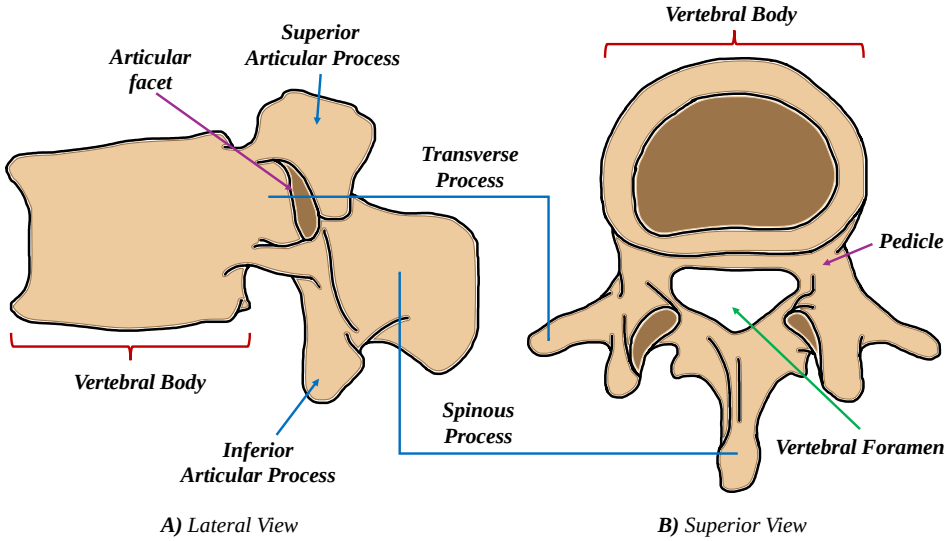

Figure 1.3. *© Lateral and Superior view of a vertebra, with the main anatomical features.*

Lastly, numerous vertebral joints allow the relative movements between pairs of vertebrae. Each articular process has a smooth surface called the facet joint.

Table 1.1. *The main characteristics for each spinal region about vertebral body and hole, spinal and transversal process and functions.*

	Vertebral Body	**Vertebral Hole**	**Spinal Process**	**Transversal Process**	**Functions**
Cervical	Small, oval, curved faces	Large	Long, bifid, directed downwards	Transverse hole	Skull, spinal, cord support. Stabilize brain, position and control head's movement
Thoracic	Medium size, heart-shaped, flatten faces, rib facets	Medium	Long, thin, not bifid, directed downwards	Facet joints in all vertebrae except T11-12	Support weight of Head, neck, upper limbs and protect organs. Rib joints allow chest volume to change for lungs expansion
Lumbar	Large, oval, flatten faces	Small	Smoothed, large, posteriorly directed	Short, absense transverse hole	Support weight of neck, upper,limbs, organs, thoracic abdominal cavity

1.1.1 Cervical Spine

The cervical area has a total of 7 vertebrae, which extend from the cranial occipital bone to the thoracic vertebrae, with a cervical lordotic curvature between 13 and 25 degrees. The cervical vertebrae own peculiar characteristics, especially the first, second and seventh vertebrae, as they are defined as **atypical** ones, while the remaining ones share common characteristics. The cervical vertebral body is small with a triangular large vertebral hole which contain the spinal cord. Here, the spinal cord is quite big, since it is the area that connects most of the nerves from the encephalon to the rest of the body. The spinal process of the C3-C6 vertebrae is relatively pointed, palpable at the skin of the posterior neck and very prominent, which is why it is called **bifid** [1–10]. The cervical spine is divided into three parts:

1. **Suboccipital zone.** It involves only the C1 vertebra (see Figure 1.4). C1 is called "Atlas" because it supports the head while articulating with the condyles of the cranial occipital bone. The name comes from Greek mythology: Atlas supports the world as the C1 sustain the head.

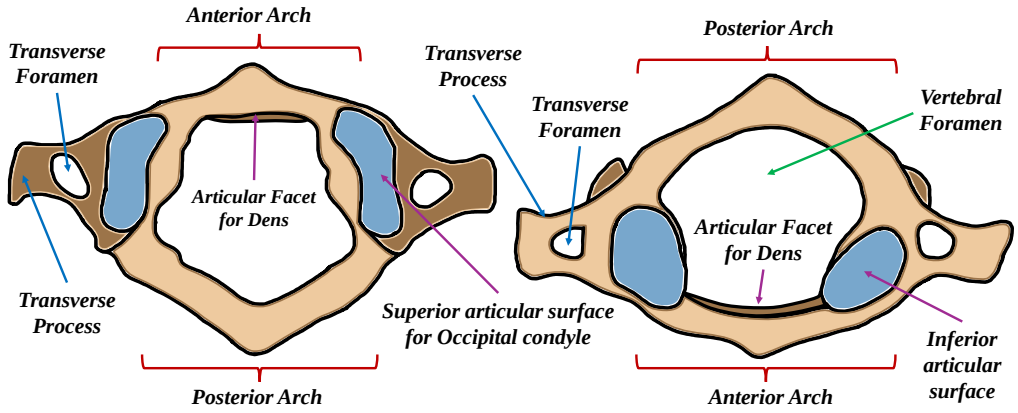

Figure 1.4. *© Superior and Inferior view for C1 vertebrae with its main anatomical features.*

The vertebral joint does not allow axial rotation, but a small amount of forward flexion and backward extension. The C1 vertebra differs from the other vertebrae due to the two vertebral arches, the lack of a vertebral body, the presence of oval upper and round lower facet joints, and the larger vertebral hole, compared to other vertebrae, which accommodate the large size of the spinal cord, preventing its injury during movement. The Atlas flexes and

extends, but the cardinal movement is axial rotation. C1 is the pivot of the axial movements on the medial axial joint. The Atlas lowers or pivots during axial rotation and rises when the movement is reversed. The wing joints are the brake of the rotation of the atlas, which is very wide, as they block the anterior dislocation of the head. Indeed, if these are damaged, they cause rotational instability.

2. **Superior Transition zone.** It is composed by C2 (see Figure 1.5), known as the **Epistrophe**. The Atlas fuses with the epistrophe and this fusion is called the tooth or odontoid process of the epistrophe. The fusion is the reason why there is no intervertebral disc between the C1 and C2 vertebrae. The lateral articular process creates the lateral atlas-axial joint. The lateral process has a caudal and lateral slope (slope) that stabilizes the atlas. The posterior movements of C1 are blocked by the odontoid process, i.e., **dens**. The anterior process is blocked by the transverse ligament.

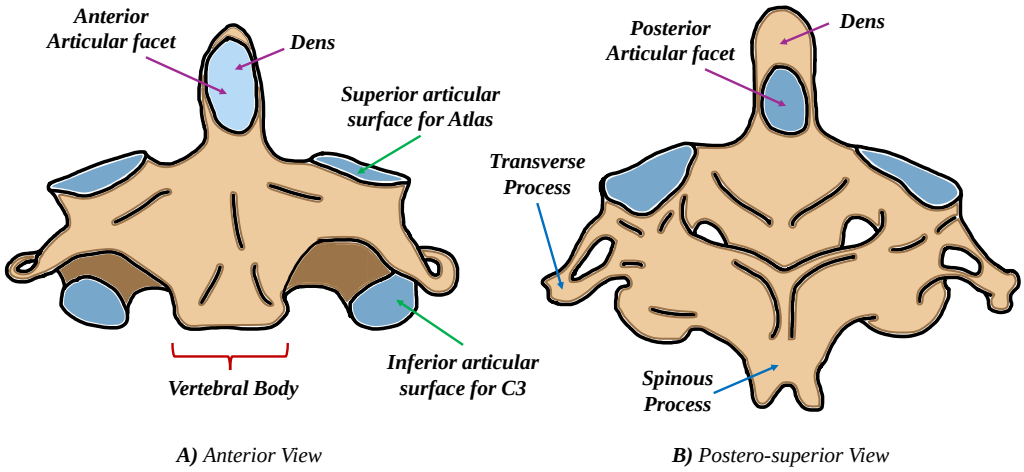

Figure 1.5. *© Superior and Inferior view for C2 vertebrae with its main anatomical features.*

3. **Inferior Transition or Typical zone.** This zone consists of the remaining cervical vertebrae which have common features. Centrally there is the vertebral body and laterally the two articular processes, where the muscles act and on which they are attached. The transverse processes protrude laterally from the articular pilasters and are joined posteriorly to the laminae that support the spinous processes. The uncinate processes, which arise from the superior and posterolateral margin of each side, are also located at the base of the articulations between the vertebral bodies. The weight-bearing axis

of these vertebrae transmits the head's weight along the anterior canal along the vertebral body to the next one and through the posterior canals and the zygapophyseal joints. The load then passes from the occipital bone to the atlas, and then to C2, where it is discharged to the other vertebrae by the lateral processes and centrally with the vertebral bodies. Finally, the C7 vertebra is referred as **the prominent vertebra** (see Figure 1.6).

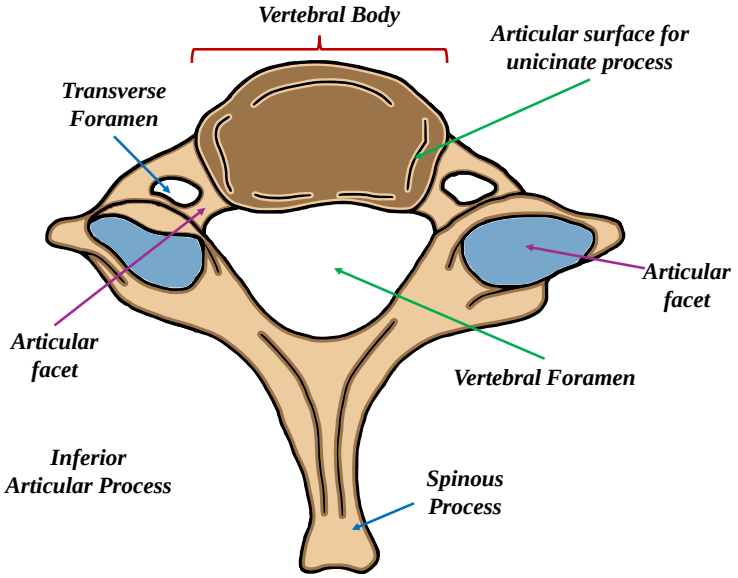

Figure 1.6. *© Superior view for C7 vertebrae with its main anatomical features.*

This vertebra differs from the others. It is the interface between the cervical and thoracic areas, acting as a contact bridge between cervical lordosis and thoracic kyphosis. The C7 vertebra has a long, thin spinous process ending in a large, prominent tubercle that can be noted under the skin at the base of the posterior neck. The transverse processes are extended for muscle insertion, while the transverse holes are reduced or absent.

1.1.2 Thoracic spine

The thoracic area consists of 12 vertebrae. The main characteristic is the **heart shape** of the vertebral body, which is slightly more massive than the cervical vertebrae (see Figure 1.7). The **vertebral hole** is circular in shape and a bit smaller than the cervical one. The spinous processes of the T10-T12 vertebrae are thicker and show characteristics of the lumbar region. The kyphotic curvature angle is about 45 degrees, and it may range between 20 and 70 degrees with age and disease development.

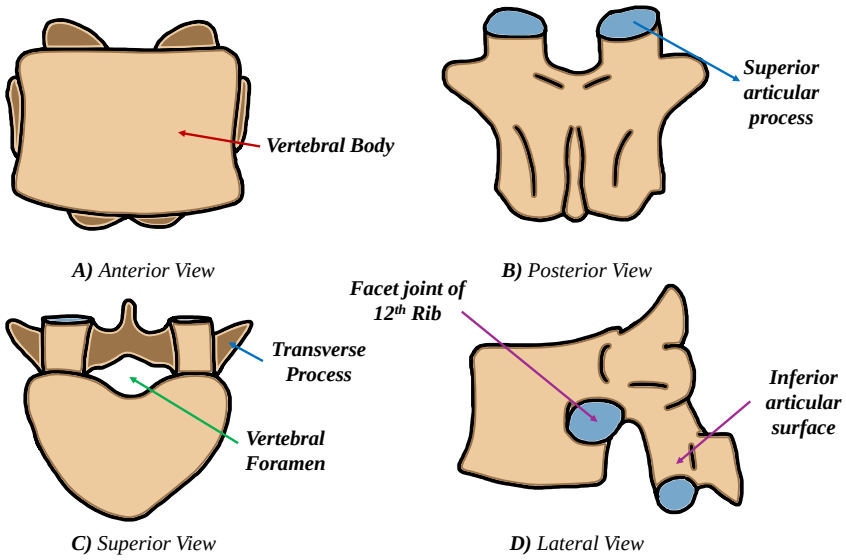

Figure 1.7. *© Thoracic vertebrae (T12) in the anterior, posterior, superior and lateral views, with its main anatomical features.*

The **thoracic-lumbar transition zone** is critical because possess the function of stabilizing the curvature change from kyphosis to lordosis. This area is often subjected to fracture from compression or dislocation following a bad fall or impact. All thoracic vertebrae, except T11 and T12, articulate with the ribs at the dorso-lateral surface of their vertebral body. From T1 to T8 there are the upper and lower rib facets, while from T9 to T12 there is only a single facet on each side. The ribs contact the vertebrae at two points at the level of the costal facet and at the level of the transverse costal facet. The purpose of this double joint is to limit precisely the thoracic vertebrae mobility [1–8].

1.1.3 Lumbar spine

The lumbar spine is composed by the **largest vertebrae** of the human body (1.8). The lumbar vertebrae are divided into vertebral body, posterior elements and pedicles. The posterior elements have two laminae with two transverse, four articular and one spinous processes [1–8]. The **vertebral body** has an ovoid structure shaped like a drum, with the main function to support high load which are progressively greater toward to the sacrum. Its slightly concave surfaces, known as vertebral endplates, facilitate the intervertebral discs attachment and increase resistance to load bearing because of their large size. The vertebral plates are almost parallel, while the others follow the lordotic curvature. L1 and L2 show a greater height posteriorly than anteriorly, while the L4 and L5 plates have a greater height anteriorly [1–8].

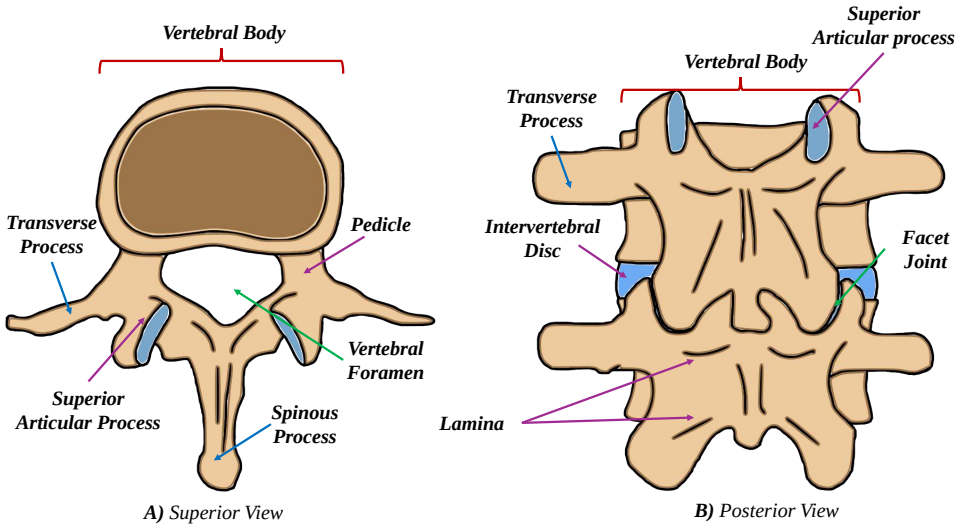

Figure 1.8. *© Lumbar vertebrae in superior and posterior view with its main anatomical features.*

There are **no facet joints** on the sides of the body or on the transverse processes, and the vertebral hole is triangular. The more massive shape is dictated as the lumbar vertebrae must support the greater weight. The vertebral architecture is designed to support high compressive forces, owing to the shell of cortical bone with a thickness of less than 0.4 mm . This is reinforced by the internal spongy portion of the bone, trabecular bone, which reinforces the bone structure through thin vertical and horizontal structures, i.e. interconnected by vertical and horizontal trabeculae. The cavities created by the trabeculae allow the arteries to supply nutrients to the structure and the intervertebral disc [1–8].

The **pedicles** have an oval shape and are very large compared to the other spinal areas. The average height of the peduncles differs from lumbar vertebrae considered, reaching up to about 19 mm in the L5. The pedicles' function is to provide the attachment for the posterior spinal structures, which are formed by the laminae of the corresponding spinal processes. The **transverse and spinous spinal processes** have several functions such as providing attachment for the muscles. Meanwhile, the articular processes have the function of contributing to the kinematics of the lumbar region and to transmit and distribute load between the anterior and posterior regions. The **vertebral foramen** is very large, compared to the other regions. Excessive compression damage is often present in this area, especially at the intervertebral disc level. Low back pain is often linked to the lumbar area by herniated discs, which we will be discussed in detail later. The spinal processes are very massive and represent the insertion zone of the muscles, which strengthen and regulate the lordosis [1–8].

1.1.4 Sacrum and cocyx

The **sacrum** is the fusion of five sacral vertebrae which begin to fuse after puberty and its complement occurs between the ages of 25 and 30. Its structure (see Figure 1.9) provides protection for the reproductive, digestive and urinary organs [1–8, 11].

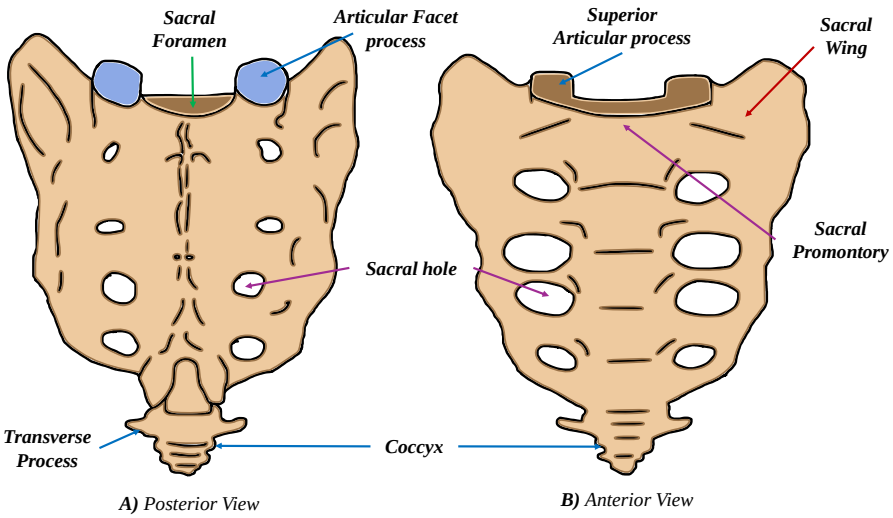

Figure 1.9. *© Sacrum and Coccyx in the anterior and posterior view with its main anatomical features.*

Furthermore, it enables the connection between the axillary skeleton and the pelvic girdle of the appendicular skeleton through a pair of articulations. This vertebral area provides a large surface for the muscle insertion, especially for the hamstring muscles. The sacral promontory is present, which is especially essential in women for labor and delivery. There is also the sacral canal, where the nerves and spinal cord branch off. The spinous processes, once fused, create the median sacral crest, leading to the creation of sacral holes which represent the fusion. The **sacral kyphosis** is prominent, and in the male sex the width of the curvature is greater. Several joints and ligaments are fundamental to the stabilization of the area. The wedge-like shape has the main function of providing the support for transferring the weight of the body along then lower limbs. Lastly, about the **coccyx,** it is formed by 3-5 (often 4) coccygeal vertebrae, which fuse once the human reaches the adult age. The coccyx provides many insertion sites for ligaments and sphincter muscle of the anus. The first two coccygeal vertebrae have transverse processes and unfused vertebral arches; in addition, the laminae of the first vertebra are called coccygeal horns and join the sacral horns

1.2 Intervertebral Disc

The ***Intervertebral Disc*** **(IVD)s** act as separators and **shock absorbers** between the vertebrae, and anchors them together, for each vertebra from the epistrophe (C2) to the sacrum (S1) [1, 2, 6, 7, 12–17]. Figure 1.10 shows a schematic representation of two vertebrae separated by the intervertebral disc, with the ***Cartilaginous Endplate*** **(CEP)** and the inside structure of a vertebral body.

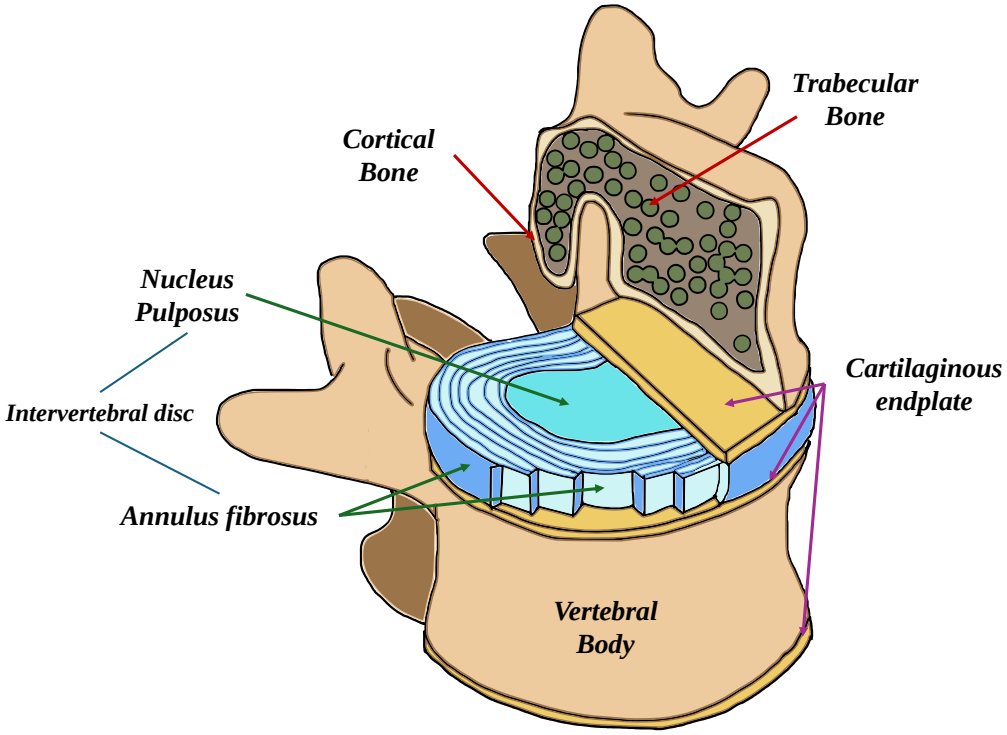

Figure 1.10. *© Schematic representation of two vertebrae separated by the intervertebral disc, with the cartilaginous endplates and the inside structure of a vertebral body*

The main functions of the intervertebral disc are separating the individual vertebrae and transmit load between adjacent vertebrae. The disc has a cartilaginous type of structure with remarkable dimensions compared to other cartilaginous structures. It is a fibrocartilaginous cushion that provides precisely this dampening function and composed of the ***Annulus Fibrous*** **(AF) and** ***Nucleus Pulpous*** **(NP)** [1, 2, 6, 7, 12] . The disc has a physiological diameter and height of approximately 7-10 mm, and 30-40 mm [16, 17]. The fibrous annulus circumferentially surrounds and encapsulates the nucleus pulposus, and it involves an highly organized, fiber-reinforced fibrous and fibrocartilaginous structure. The **AF collagen fibers** are enclosed in concentric lamellae called **layers** and are alternately arranged at approximately 30 degrees [13–17] (see Figure 1.11).

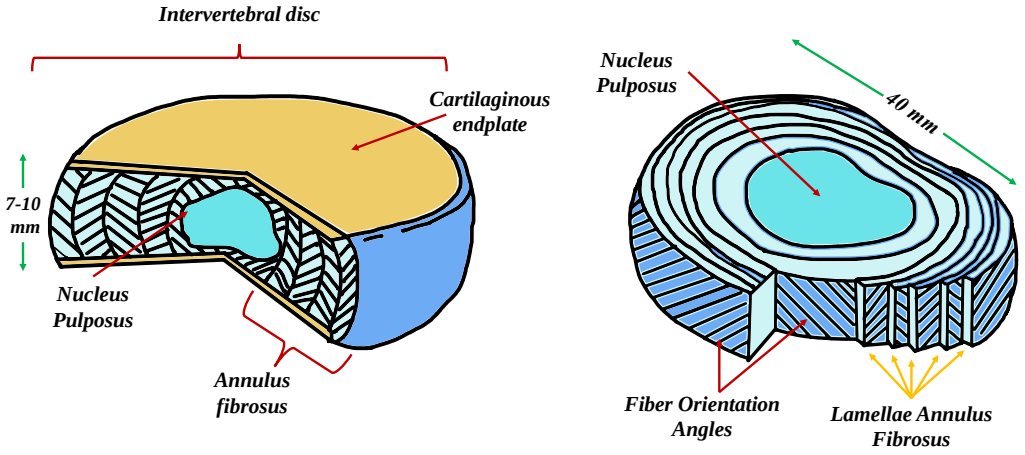

Figure 1.11. *© Intervertebral disc structure composed of NP and AF with its fiber orientation angles and Lamellae.*

The fibrous annulus develops around the first and second year of life and it has between 15 and 25 dense layers of parallel fibrous laminae. **Outer and inner rings** can be distinct. AF is thicker in the posterior region as it has fewer collagen fibers there, but they are more tightly packed together [18–21].

Indeed, the outer ring is the one that contains the densest fibrous lamellae. The fibers originate and insert into the cortical bone at the contact between the two vertebrae where the disc is included. The **lamellae** are almost exclusively **type I collagen** and exclusively consisting of **fibroblasts**. The lamellae thickness and fiber angles follow a strong radial gradient; indeed, the thickness grows from 0.05 mm to 0.5 mm from the outside to the inside, while the angle grows radically from about 30 degrees to about 45 degrees within the AF[18–21].

1.2.1 IVD composition

The **NP** has a soft, elastic and gelatinous body, which is composed of 75% water. It is predominantly composed of hyaline-like cartilage, although the water content in the extracellular matrix is much higher. The nucleus pulposus is responsible for the disc's elasticity and cushioning function [1, 2, 6, 7, 12–17].

Above and below, the IVD is covered by thin plates composed of hyaline and fibrous cartilage, i.e. the **CEP**. These structures are loosely attached to the vertebrae and closely connected to the fibrous ring, aiming to stabilize the IVD position, working together with the intervertebral ligaments[21–23]. Besides water, the disc also consists of solutes and macromolecules, namely **collagen** and **proteoglycans** [24] which account for 95% of the tissue's protein composition (see Table 1.2)

Table 1.2. *Distribution in % of the main components in the IVD*

Percentage distribution of the main components in the intervertebral disc			
	Outer annulus	**Inner annulus**	**Nucleus pulposus**
Water	65	70	75
Collagen I	55	45	5
Collagen II	10	10	15
Collagen V	Small quantity	Small quantity	-
Proteoglycans	15	30	55

There are also other molecules besides collagen, such as elastin and lipids, that compose the disc's ***Extracellular Matrix*** **(ECM)**, but their contribution at the mechanobiological level has not been explored in depth in the literature. Although, there are some studies that suggest their function is to support the integrity maintenance of the inter-lamellar structure made in collagen fibers and the recovery of the disc's lamellar organization after loading and unloading [1, 2, 6, 7, 12–17, 24–28].

The most ubiquitous protein in the human body is **collagen**. The basic molecular unit is the tropocollagen, a protein that has three polypeptide sinistrorsal chains, wrapped together in such a way to create a right-handed helix. The single left-handed chains can be different from each other, in fact, there are 19 different types of collagens based on their possible combinations. Collagen has an important function in the biomechanical response of a tissue: it confers extreme resistance to tensile stress states, to plastic deformation and rupture, providing high strength [29–31]. The collage's mechanical contribution is determined by the intermolecular bonds formed between the helix chains, which stabilize the structure and make it very strong. **Type I** collagen fibers aim to resist tensile forces. **Type II** collagen fibers aim to resist compressive forces. Type I and type II collagen are the main types of collagens found in the intervertebral disc, and the nucleus contains mainly type II collagen in small fibrils, as collagen is better suited to support compressive loads.

Besides, the t**hree-dimensional network of the small fibrils** is distributed in an isotropic space, without any privileged orientation. In the **IVD's annulus fibrosus**, the packing of the type II collagen fibrils is less dense than in other types of cartilage, as more deformability in tissue space is required. The outer annulus, on the other hand, has a greater amount of type I cartilage, as in tendons and ligaments, as it must be able to withstand high uniaxial tensile stresses. The lamellae of the annulus have fibrils organized into fibers with an orientation of approximately 30°, except for the outermost lamina which has a vertical orientation. These fibers are

organized in concentric cylindrical layers (15 or 25 layers), and for each layer of lamellae, the collagen fibers are arranged parallel to each other, with alternating oblique sides [18–21].

The **elastin protein**, due to the presence of hydrophobic domains, has excellent characteristics: it responds elastically to stress. After being stressed, once it is unloaded, it would be return to its initial configuration without any modification of its native structure. The energy stored during the stress is entirely returned at the unloading (perfectly elastic return). At the structural level, elastin does not present regularity, so it is not a crystalline protein. The individual amino acids of the protein chain give elastin specific properties: the protein has a high mobility that allows it to assume different configurations. Its main function is to confer elasticity to the structures, which it is going to compose. In addition, elastin also provides high resilience, i.e., high impact resistance [29–31].

Proteoglycans are special proteins whose main task is to support **glycosaminoglycans** (GAGs, i.e., carbohydrates present at the membrane surface and inner) in their functions and activities. Indeed, they are large molecules composed by glycosaminoglycans chains, having a strong negative charge, fundamental in the biomechanical response of the IVD. Among their functions there are the hydration maintenance and conferring compressibility and tensile strength to the tissue [29–31].

1.2.2 IVD in the spinal region

The **cervical disc** has unique characteristics. Besides possessing the nucleus and the annulus fibrosus, it also has the **Luschka joints**, i.e., the uncovertebral joints. Luschka's articles are joints formed after only 9 years old, whose function is to allow coupled movements in combination of lateral flexion and axial rotation, thus improving the overall movements of the vertebral region. The nucleus is not located centrally but posteriorly, while the annulus does not surround the nucleus completely, indeed it is more prominent anteriorly. The **nucleus** is fibrocartilaginous upon reaching maturity, whereas it was previously gelatinous. The **annular fibers** have an orientation that varies longitudinally to the deepest layers, providing a half-moon shape to the AF. In the posterior end, there is only a small layer of longitudinal fibers covering the nucleus [9, 10].

The **thoracic disc** is anatomically influenced by the biomechanical characteristics it must possess to support loads and ensure spinal movement. The anterior section

of the disc is compressed by the body's weight. In uncompressed conditions, the disc generally has a wedge shape, leading to a significant difference in height between the anterior and posterior portions. The anterior zone is approximately 20% higher than the posterior. The T1-4 and T-7 discs have a relatively flat shape, while the T4-5 region has a **higher posterior height**. Owing to the higher compression loads,the central disc anterior zone is often exposed to pathological conditions. The thoracic disc appears to be lower if compared to the cervical or lumbar regions, although the AF is the thickest and strongest between the regions. Meanwhile, the **nucleus** appears to be relatively small, since the loads are generally absorbed by the facet or thoracic cage. Indeed, thoracic hernias are rare and often asymptomatic.

The **lumbar discs** present an high anterior height, leading to a lumbar lordosis degree of approximately 60 degrees. Consequently, they are the largest and the thickest in height. This important difference in both sizes depends precisely on the biomechanical function that lumbar discs have, i.e. they must support greater weight and higher mechanical pressure. The lumbar disc contains a higher nucleus pulposus content than the annulus fibrosus part. This is intended to ensure a greater capacity to absorb shocks and to better distribute forces. Lumbar discs allow greater flexion and extension, although rotation is limited as it requires action from the lower back. Controversially, cervical discs are those that provide a greater range of motion, ensuring exactly greater mobility of the neck. Whereas the thoracic discs allow an inferior range of movement due to the presence of the rib cage, which restricts movement [32].

1.2.3 IVD nutrition

The intervertebral disc lacks innervation and vascularization, indeed it is an **avascular tissue**. Intervertebral disc cells require nutrients if to fulfil their physiological tasks, while their metabolic wastes must be removed from the ECM. These transports of substances result complex, given the avascular characteristics. The only regions of the intervertebral disc where there is a scattered and poor network of capillaries is the outermost annulus region. These blood vessels at the edges of the disc structure are responsible for nutrient supply and waste removal. The nucleus and inner annulus are also supplied through the cartilaginous endplates, which have a **capillary network** that is indeed crucial in the nutrient supply [25–28] (see Figure 1.12).

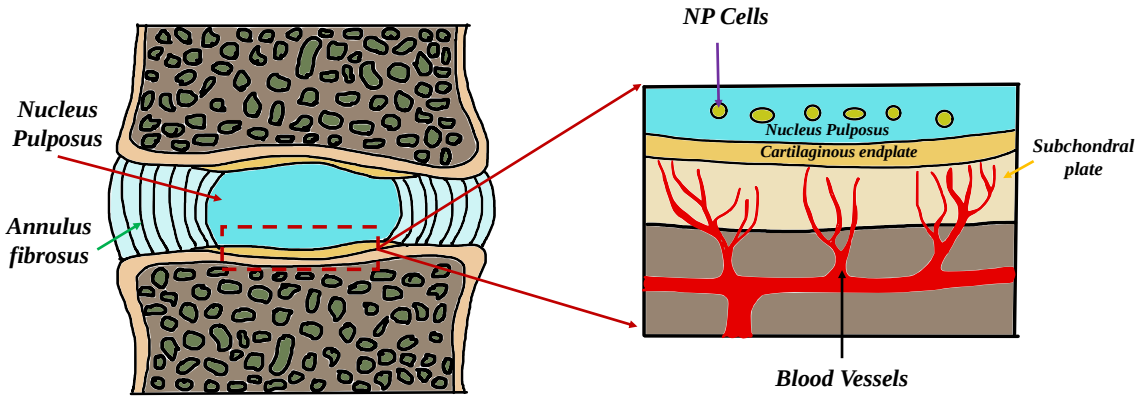

Figure 1.12. *© IVD nutrition supply and enlargement of the poor network of capillaries building the IVD supply thought the cartilaginous endplate.*

The nutrition of the disc is provided through a **diffusion process**, and this is fundamental for the prevention of degenerative disc pathologies. The tissue's nutrients are oxygen, glucose, substrates to produce the extracellular matrix, amino acids and sulphate. The flow of these nutrients occurs through the exchange mechanism between the capillaries surrounding the tissue and the dense extracellular matrix of the disc. The same mechanism is followed for metabolic waste products to be removed from the tissue. The nutrient transport is well complex. Small solutes such as glucose, lactic acid and oxygen are transported by diffusion. . Figure 1.13 shows a diagram of the nutrient concentrations along the IVD location between CEPs and IVD.

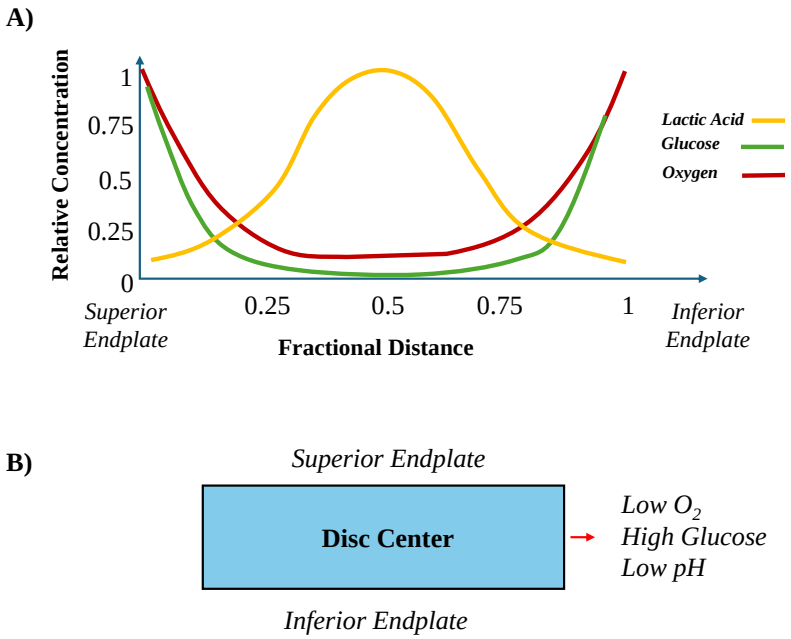

Figure 1.13. *© **A)** Relative concentrations vs. Fractional Distance diagram of IVD nutrients. **B)** Schematic representation of the diagram about the IVD nutrient distribution at the disc center.*

Concentration gradients are responsible for nutrients transports. The movements of fluids in and out of the disc are responsible for the changes in disc height during the day and night. The fluids accumulated during the night, in the recovery phase, increase the disc's height, are slowly tossed out during the day, i.e. the loading phase, due to the compressive loads that the disc is subjected to during the day, thus decreasing its height.

Disc cells take energy from **glycolysis**. They use small amounts of oxygen, thus producing limited CO2. The cells' activity depends on extracellular oxygen concentrations and pH, although the influence of these factors in numbers has not yet been clarified in the scientific community. It appears that acidic pH levels can be negative for the disc cell, leading to matrix breakdown and cell death [25–28].

There is strong evidence that **disc degeneration** may be related to a decrease in nutrient supply. The capillary bed architecture and porosity of the cartilaginous endplate influence and ensure nutrient delivery. Hence, a decrease in nutrients provided to the disc may occur because of several pathological phenomena that affect blood supply, such as atherosclerosis, thrombolytic disorders, sickle cell anemia, or even exposure to vibration or smoking, or even subchondral bone sclerosis or cartilage calcification. High lactic acid levels or alterations in the acidic pH level can affect nutrient influx. Therefore, the nutrient gradients necessary for the diffusion phenomena are highly variable depending on the location of the intervertebral disc considered. Hence, the **disc center** has the lowest concentrations of glucose and oxygen, with high metabolic concentration of lactic acid, which produces a very acidic pH. When the nutrient supply is limited due to a pathological condition, such as atherosclerotic disease or calcification of the cartilaginous endplate, the reduced nutrient flow can cause the death of cells in the center of the nucleus pulposus, leading to the early stages of disc degeneration [25–28].

All these pathological changes are unfortunately not yet 100% proven to be a direct cause of loss nutrient supply which can be correlated to disc degeneration. However, these conclusions have been substantiated by some *in-vivo* observations conducted to study nutrient transport in the disc organism in animals. In addition, the natural advancement of age is also a major contributor to changes in the capillary network density, which limits nutrient supply. Together with the inevitable and eventual calcification of the CEP caused by aging, they are the major factors in disc degeneration [25–28] .

1.3 Accessories structures

There are several accessory structures that contribute towards and provide the wide range of functions and movements to the spine. These structures are the **intervertebral joints**, **spinal ligaments** and **spinal muscles**. Intrinsic paraspinal ligaments and muscles hold the vertebrae together and both control and limit the spinal motion. The movements of each vertebral segment are established by the facet joints, except for the atlas and axis. However, the spinal stability and movement control itself depend, indeed, on the muscles and ligaments [1, 2, 6, 7, 12–17].

1.3.1 Spinal joints

All vertebrae from the second cervical vertebra to the first sacral vertebra articulate with each other through intervertebral joints, and synovial joints between the facet joints, as reported in each figures representing a specific spinal region. The joints between the facet joints are called **zygapophyseal joints** which connect the upper and lower articular processes of adjacent vertebrae. The surfaces of these joints are covered with hyaline cartilage, and their dimensions and structures vary depending on the vertebral zone considered. These joints are responsible for small relative movements between adjacent vertebrae that when added together provide the movements of flexion, extension, lateral bending and axial rotation. The facet joints change their structure and functions depending on the region considered [1, 2, 6, 7, 12–17].

The **cervical joints** provide high flexibility compared to the other regions. They have two cartilaginous surfaces, the meniscoid, or synovial fold, and the capsular ligament. They are attached to the vertebral arch, transferring most of the compressive load to the lower segments and they promote the cervical flexibility, together with the disc, thus protecting the spinal cord [1, 2, 6, 7, 12–17].

The **thoracic facet joint**s limit the range of motion in flexion/extension and axial rotation. Indeed, the inclination angle of the facet joints is gradually increasing as they move downwards, converging towards the frontal plane. The right facet joints are more vertical and appear almost parallel to the sagittal plane than the left side. Overall, the thoracic facets are oriented parallel to the frontal plane, so that may provide resistance to anteroposterior translation and to resist axial loads. In the transition zone between lumbar and thoracic, the facet joints abruptly change their orientation from frontal to sagittal orientation; meanwhile, in the transition from

cervical to lumbar the change of orientation is gradual [1, 2, 6, 7, 12–17].

The **lumbar facet joints** present a sagittal orientation, with an angle of 120-150 degrees. This different orientation from other spinal areas ensures a more efficient distribution between the intervertebral discs and the facets, providing greater resistance against translation and rotation movement [1, 2, 6, 7, 12–17].

1.3.2 Spinal Ligaments

The **ligaments** have the main function to promote spinal movements and to provide the spinal stability. There are several intervertebral ligaments (see Figure 1.14) which are inserted in the vertebral bodies and processes [1, 2, 6, 7, 12–17]:

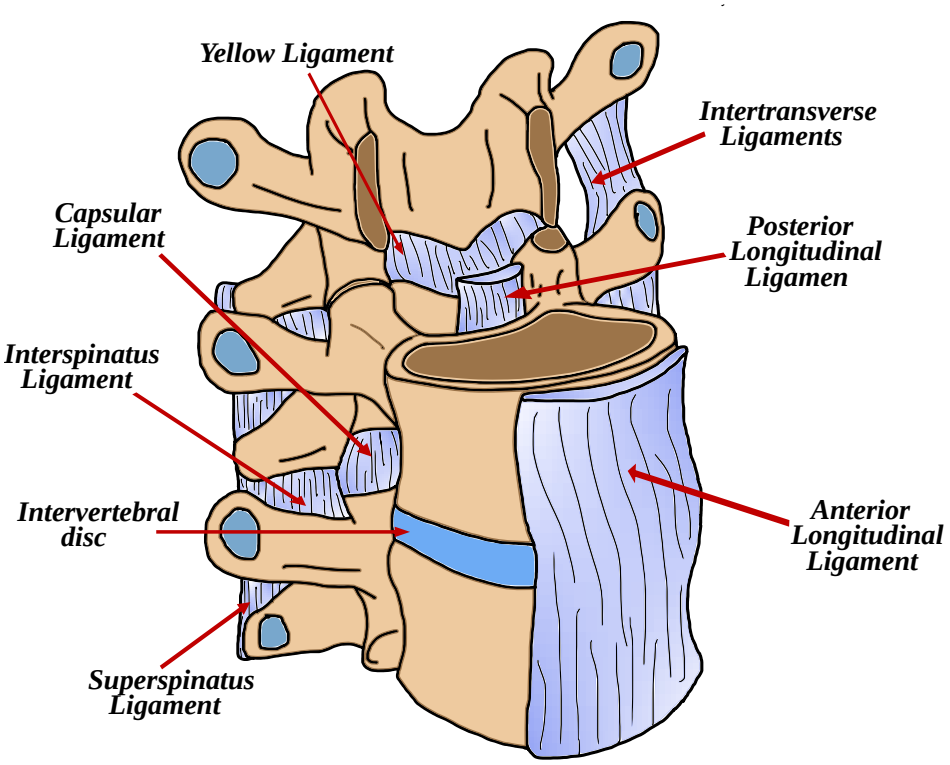

Figure 1.14. *© The main Ligaments in the spinal region.*

- The **anterior longitudinal ligament** adheres to the intervertebral discs and the anterior surface of each vertebral body.
- The **posterior longitudinal ligament** is parallel to the previous one, but it adheres to the posterior surfaces of the vertebral bodies. The cervical spine lacks of posterior ligaments.
- The **ligamenta flava** (i.e., yellow ligament) connect the laminae of adjacent vertebrae and it covers the dorsal surface of the spinal canal. It is characterized

by strong elastic bonds that cover the space between the different laminae. The ligament stretches laterally and elongates under tension, promoting flexion of the spine.

- ➢ The **interspinous ligaments** connect the spinous processes of adjacent vertebrae.
- ➢ The **supraspinous ligament** interconnects the apexes of the spinous processes from C7 to L3 or L4. The nuchal ligament, on the other hand, is the supraspinous ligament that extends from C7 to the base of the skull.

The **posterior longitudinal ligament** extends from the axis to the sacrum and forms the anterior wall of the spinal canal. It is very wide across the cervical and thoracic parts of the spine. The ligament shrinks from the L1 lumbar spine to half its original width. It appears firmly attached to each intervertebral disc through the cartilaginous endplate. The open space between the posterior longitudinal ligament and the vertebral body is known as the anterior epidural space, which is crucial for herniated discs, resulting with its narrowing, an inherent weakness of the structure. The posterior longitudinal ligament has the function of resisting the flexion movement of the lumbar area[1, 2, 6, 7, 12–17].

Meanwhile, the **anterior longitudinal ligament** of the lumbar spine, located ventrally, has the main function of resisting the extension movement of the lumbar region. The nuchal ligament begins at C7 and extends cranially to the external occipital crest. This ligament acts as the string of an arch when the head is upright, maintaining cervical lordosis without any muscular effort. If the neck is tilted forward, the elasticity of the ligament brings the neck back into an upright position. In a car accident, the injury to this ligament, which is generally the one that ensures the stability and balance of the head, is mentioned[1, 2, 6, 7, 12–17].

1.3.3 Spinal Muscles

The spinal muscles have a key function in **stabilizing** the skeleton and in ensuring the motion of the skeletal joint system. Hence, the muscles act as shock absorbers, by dissipating externally applied loads and so protecting internal structures and organs[1, 2, 6, 7, 12–17]. The spinal muscles are stratified, and they can be differentiated in **deep and superficial muscles** (see Figure 1.15).

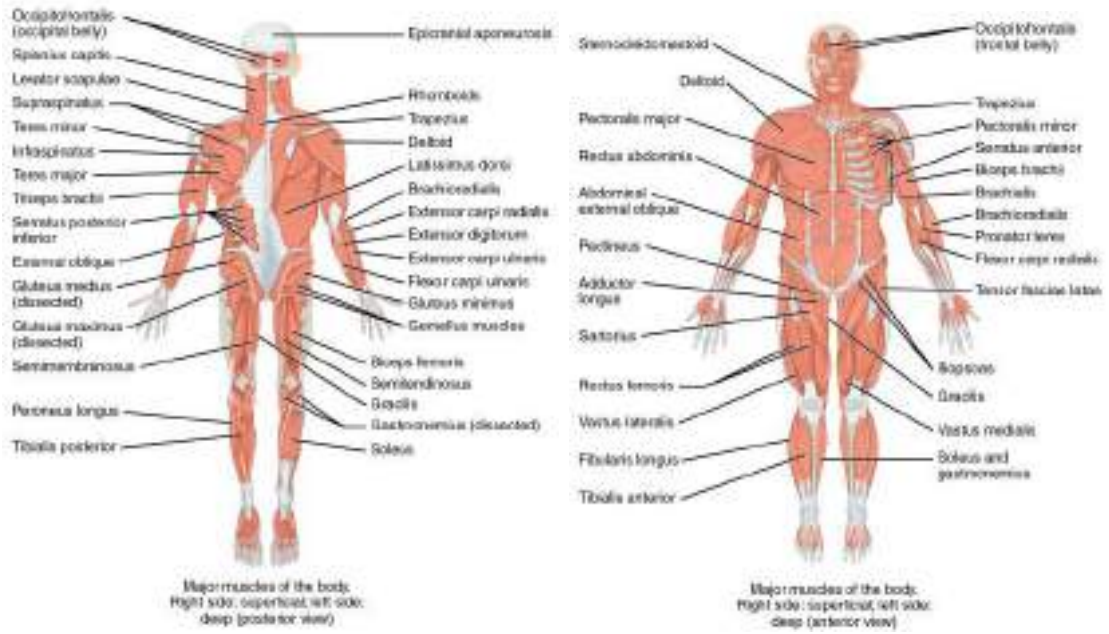

Figure 1.15. *Major spinal muscles in the anterior and posterior view. Right side: superficial muscles. Left side: deep muscles.* ***Source:*** *Wikimedia Commons.*

The **deepest muscles** are the intrinsic muscles, i.e. the actual back muscles that also have innervations from the posterior branches of the spinal nerves. In contrast, the superficial muscles are the extrinsic muscles, which are inserted on the bones of the upper limbs and are innervated by the anterior branches of the spinal nerves.

Intrinsic muscles are divided into superficial and deep muscles. The superficial intrinsic muscles are the erectors of the paraspinal column, which extend along the entire column from the occipital bone to the sacrum. In addition, there are the splenius muscles of the upper back and neck. These muscles are responsible for keeping the upright standing [1, 2, 6, 7]. The **deep intrinsic muscles** are the transverse-spinal muscles, which insert obliquely and longitudinally, establishing a cable system that supports the lateral stability of the column, as well as for maintaining the upright posture and for the rotation of the column itself. The deepest muscles are the interspinal and intertransverse muscles, which are composed of many small muscles, and they contribute to maintaining posture [1, 2, 6, 7].

The superficial spinal muscles are the following[1, 2, 6, 7, 12–17]:

- **Trapezius muscle.** This muscle inserts from the occipital bone to the lower thoracic vertebrae and laterally to the scapula. Its motor function is to allow the movements of the scapula and spine by acting as an extensor of the head and neck.

➢ **Latissimus Dorsi.** This muscle is very large with a fan shape, which inserts to the spinous processes and supraspinous ligaments of the T7 and L5 vertebrae, as well as to the sacral segments, iliac head and the last ribs. Its basic function is to support the lumbar spinal biomechanics, although it plays a more important role in shoulder movements.

➢ **Levator Scapulae.** It is located on the side of the neck and originates from the cervical transverse processes of the C1 and C4 vertebrae, inserting on the scapula. Its function is to elevate the scapula. When the scapula is stable, the muscle provides lateral flexion and extension of the cervical spine.

➢ **Rhomboid Major and Minor.** The rhomboid major inserts from the thoracic spinous processes from T2 to T5, while the rhomboid minor inserts at the spinous processes of the C7 and T11 vertebrae. They are superficial muscles, but deeper than the trapezius. They act as stabilizers of the scapula, acting as antagonists of the trapezius to pull the scapula toward the spine.

➢ **Serratus Posterior Superior and Posterior Inferior.** They have function in breathing for the rib movements.

About deep spinal muscles, i.e., **the erector spinal muscles**[1, 2, 6, 7, 12–17]:

➢ **Splenius Capitis and cervicis.** These are the muscles that connect the skull to the spine. There is the splenius muscle of the neck and head, which together provide lateral flexion, extension and rotation of the cervical spine.

➢ **Iliocostalis.** There are Iliocostalis of the cervical, thoracic and lumbar region. The cervical one is the smallest and its main function is to act synergistically with the splenius cervicis during the flexion and extension of the neck. The thoracis one support the thoracic region movements. Lastly, the Iliocostalis Lumborum acts as axial extensors and rotators for the lower lumbar levels, also providing axial flexion, extension and rotation movement. Furthermore, when these muscles contract, they create the indirect "arch" effect that accentuates the lumbar lordosis.

➢ **Longissimus.** They are the Longissimus capitis, cervicis and thoracis. The capitis and cervicis work together to allow the flexion, extension and axial rotation of the head and neck. The longissimus thoracis is the largest one and its function is to act at the thoracic level and on the ribs, as well as it can

increase lumbar lordosis in contraction, while also acting as a flexor of the lumbar and thoracic region.

- ➢ **Spinalis.** They are in the cervical, thoracic and lumbar region. Its main function is to support and contribute to the flexion, extension and axial rotation movements.
- ➢ **Multifidus.** Located deeper than the other muscles, it inserts on the transverse and spinous processes in all spinal levels. It is most developed at the lumbar level, creating the arching cord effect between the lumbar vertebrae, thus emphasizing the lordosis. It has a main extensor function, and it also acts as a stabilizer to minimize shear and compressive loads on the facet joints.
- ➢ **Iliac muscles.** They are the psoas major, psoas minor, and quadratus lumborum. The psoas major has the main function of hip flexor and thigh rotation. It has a key role in stabilizing the vertebral column by connecting the lumbar area with the pelvis, thus supporting posture maintenance and vertebral movements. The Psoas minor contributes not only to influencing hip flexion, but also provides support in posture and lumbar curvature. Lastly, the Quadratus lumborum has the main function of ensuring lateral extension and flexion movements of the lumbar spine and maintaining upright posture. It also allows lateral flexion of the thorax, as well as stabilizes the pelvis, while maintaining the alignment and stability of the lumbar region.

Lastly, **the thoracic fascia support**, stabilize and distribute loads on the spine, working in synergy with the Spinal muscles. Whereas, the Abdominal Muscles stabilize the trunk, by creating intra-abdominal pressure that has the function of protecting the spine, while working with the Thoracic Fascia to maintain posture and reduce the risk of injury.

Chapter 2

Spinal Biomechanics and Testing

2.1 Spinal glossary

Spinal biomechanics refers to the study of the movements and dynamics of the spine and its main structures, including the analysis of internal and external forces, as well as the study of the mechanical response of bones, intervertebral disc and all accessory structures. The goal is to provide support to clinical and rehabilitation practice aiming to assist physicians in the patient care, by designing and realizing medical devices, thus optimizing surgical interventions [2, 33–46].

Hence, ***in-vitro* and *in-vivo* experimentation** on human beings and animals has a significant influence on the comprehension of spinal biomechanics. Parameters and fundamental notions will be defined in the following glossary [2, 33–46], which will be use in the following sections of the chapters:

- ***Functional Spinal Unit* (FSU) or motion segment**. It consists in two adjacent vertebrae including the intact intervertebral disc and ligaments. This is the smallest unit of the spine which can describe the general mechanical behavior of a specific region of the spine (see Figure 2.1).
- **Intact specimen**. It is a fresh or frozen spine that must be tested, with a specific length and intact ligaments and intervertebral disc that includes at least one (FSU).
- **Injured or defect specimen**. It is a spinal segment with an existing or created pathology to the ligamentous components, bony tissue, or IVD which can include one or more FSUs.
- **Relative motion**. It is the movement between pairs of vertebrae and represents the transformation from one local coordinate system to the other.

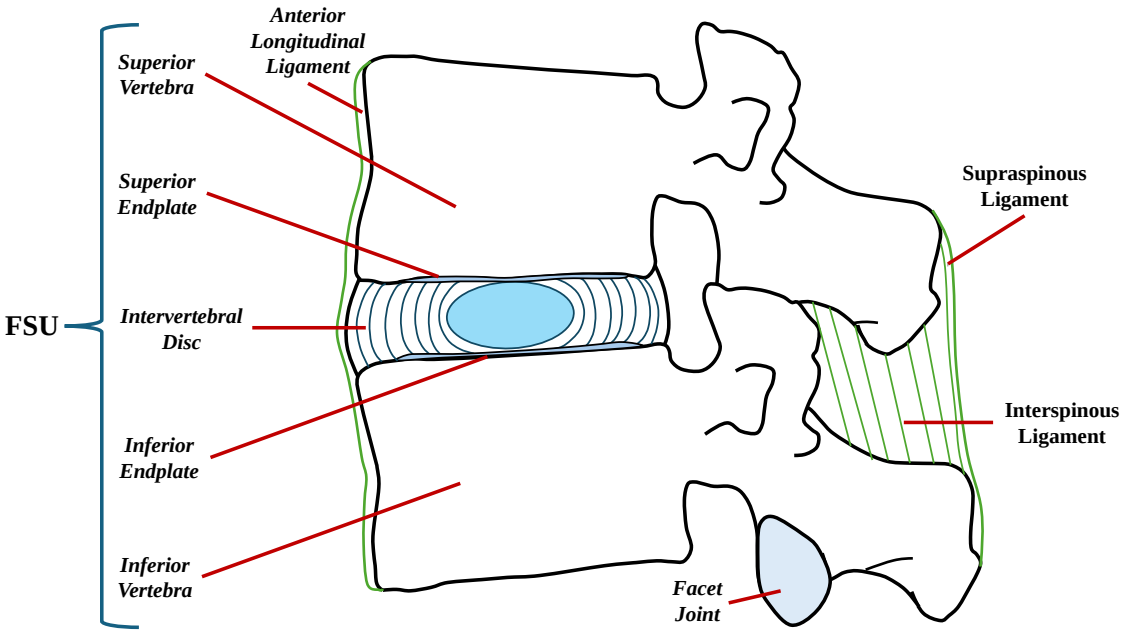

Figure 2.1. *© Schematic representation of the FSU, with the IVD, vertebrae, cartilaginous endplate, facet joint and with some of the main ligaments.*

➢ **Axis of Rotation**. An ***Instantaneous Axis of Rotation*** **(IAR)** is defined as a straight line that is attached to a moving body through which all points of the body rotate at a specific time instant.

➢ **Centre of Rotation**. The ***Instantaneous Center of Rotation*** **(ICR)** is defined as the fixed point of a body through which the circular trajectory along which all points of the body move is centered (see Figure 2.2).

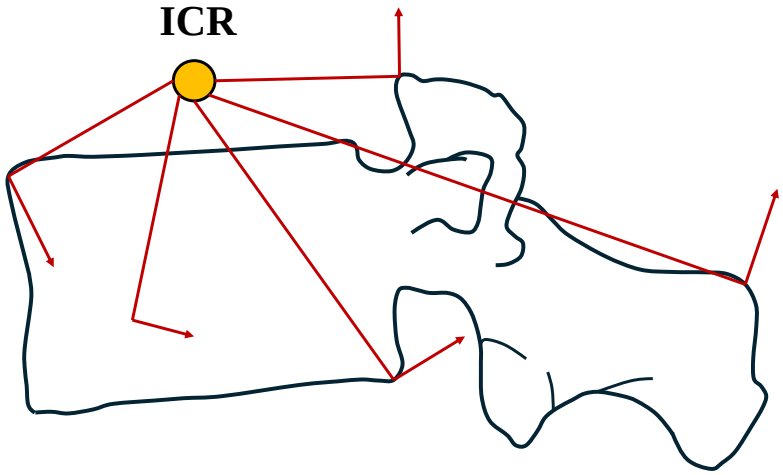

Figure 2.2. *© ICR for a vertebral body, representing the circular trajectory along which the body move is centered.*

➢ **Spinal coordinate system**. It is a specific three-dimensional, orthogonal,

right-handed coordinate system designed for the spine with the following axis: X forward or ventral, Y to the left, and Z above or cranial (see Figure 2.3). Hence, the sagittal plan is the x–z plane, the frontal plane is the y–z plane, and the transverse plane is the x-y plane of the coordinate system.

➢ **Primary loading directions**:

- **Lateral bending** is a pure moment applied in the +/– Mx direction.
- **Flexion/extension** is a pure moment in the +/– My direction.
- **Axial rotation** is a pure moment applied in the +/– Mz direction.
- **Anterior/posterior shear** is a force applied in the +/– Fx direction.
- **Left/right lateral shear** is a force applied in the +/– Fy direction.
- **Distraction/compression** is a force applied in the +/– Fz direction.

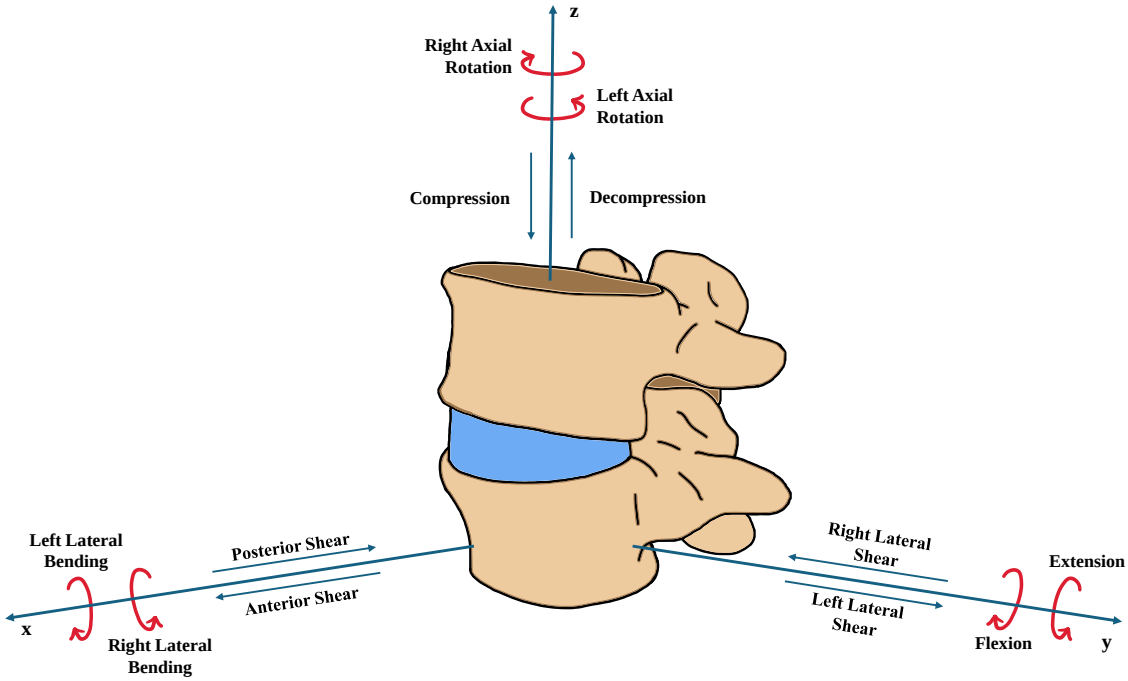

Figure 2.3. *© Primary loading directions in the spinal global coordinate system, including Right/Left Lateral Bending, Right/Left Axial Rotation, Right/Left Lateral Shear, Flexion/Extension and Compression/Decompression.*

➢ **Global coordinate system**. In *in-vitro* experiments the origin of the coordinate system is situated in the middle of the lower side in the most cranial vertebra. The specimen alignment should be adequate to simulate the upright position.

➢ **Local coordinate system**. The origin of a local coordinate system should be in a biomechanically relevant point (see Figure 2.4). It should be the mid-point in the frontal plane of the terminal endplates' margins of the adjacent vertebral bodies.

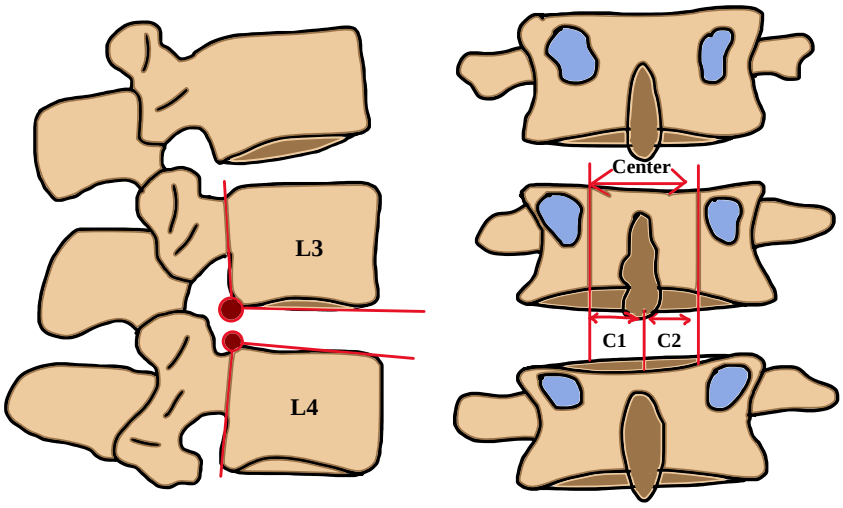

Figure 2.4. *© Example of the suggested local coordinate systems in the sagittal and posterior view.*

➢ **Primary motion**. It is a consequence of the body movement along the direction in which the load was applied.

➢ **Preconditioning**. It is critical in testing specimens to minimize viscoelastic behavior and obtain reproducibility measurements.

➢ ***Neutral Zone*** **(NZ)**. It provides a measure for the laxity of the spinal specimen. Indeed, it describes the range in which the specimen is moving without an applied load. The NZ can be calculated as the difference in angle at zero load between the two phases of movement (see Figure 2.5).

➢ ***Elastic Zone*** **(EZ)**. It is the strain measured from the end of the neutral zone to the peak load point (see Figure 2.5).

➢ ***Range of Motion*** **(ROM)**. It is the sum of the NZ and the EZ in one direction of motion (e.g., flexion, or axial rotation to the right, see Figure 2.5).

➢ **Viscoelasticity**. Viscoelastic materials exhibit an intermediate behaviour between the classical behaviour of fluid and solid. Indeed, they present an elastic and viscous mechanical response, resulting in an extraordinary non-conservative behaviour with a time-dependent mechanical response.

➢ **Energy dissipation**. The distinctive feature of viscoelasticity is the energy dissipated during the loading and unloading phases that is observed in the stress-strain curves (see Figure 2.5). The area enclosed by the stress–deformation curve is defined as the energy dissipated during the loading and unloading phase, and it represents the viscoelastic characteristic of a biological structure.

➢ **Neutral position**. It is the computed midpoint between two zero-load points derived from the hysteresis curve, one for each phase of movement (see Figure 2.5).

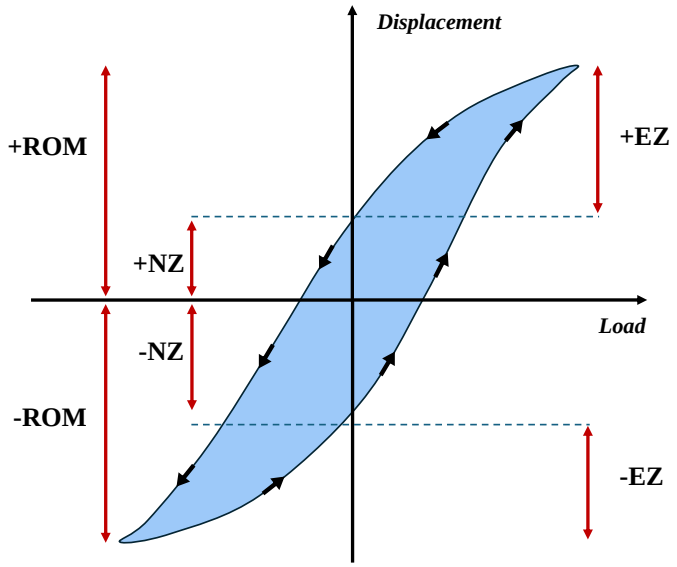

Figure 2.5. *© Hysteresis curve displacement vs. load with the indicated ROM, NZ and EZ.*

➢ **Flexibility**. It describes the ability of the spine to deform in response to an applied load in a specific load direction under the application of an applied pure moment and in static conditions.

➢ **Stiffness**. It refers to the deformation of the specimen as a measure of its mechanical strength. In the EZ, it is defined as the ratio between load and strain according to Hooke's Generalized Constitutive Law. Since the load-deformation characteristics of specimens are nonlinear, it is important to provide the points at which stiffness is calculated.

➢ **Clinical Instability**. Clinical instability denotes the loss of the spinal column's ability to maintain physiological conditions, due to the development of degenerative conditions. Clinical instability can often be related to pain and neurological dysfunction. Indeed, increased zona neutral (NZ) may also be

associated as an indicator of clinical instability.

- ***Intradiscal Pressure* (IDP)**. It is the hydrostatic pressure at the nucleus pulposus, and it is usually measured with pressure transducers during *in-vitro* tests. IDP is influenced by increasing or decreasing external loads, although IDP is never zero under unloading conditions due to disc swelling.
- **Swelling**. It refers to fluid accumulation in biological tissues, specifically it refers to the hydration of the intervertebral disc owing to its proteoglycan content and the resulting osmotic gradient, which ensures the fluid uptake from the external environment. Swelling is a direct consequence of IDP under resting conditions.

Laslty, in the **recommendations** from Wilke et al. (1998) [34], the requirements that a machine should have to test spinal specimens are introduced as follow:

1. The spine tester should allow the fixation and testing of specimens from all regions of the spine: single or polysegmental specimens.
2. Specimens should move unconstrained in all six degrees of freedom.
3. All six loading components (flexion/extension, lateral bending, axial rotation, left/right and anterior/posterior shear, and axial compression/decompression) should be applicable without any manipulation of the specimen.
4. Any combination of loading should be possible.
5. Loads should be applicable continuously or gradually.
6. Muscle forces should be able to be simulated.

These are the **basics** for dealing with the subsequent sections of this thesis.

2.2 Spinal Biomechanics

The spine biomechanics is complicated by the **upright posture** which impose a gravitational compressive load and anterior bending moment to the spine, that make more intricate the mechanics. Here, the muscular component is essential in preserving the upright posture, as previously discussed. The **muscles** act similarly to **tensioned cables**, ensuring the spine remains correctly aligned while standing [2, 33–45]. The spine can be divided biomechanically into two portions [46]:

1. **The anterior column**. It involves the vertebrae, intervertebral discs, and anterior ligaments, and it is responsible for compression load resistance and supports about 60%-90% of the load in normal standing.
2. **Posterior column**. It consists of the posterior bony structures and the posterior ligaments, and it supports about 10%-40% of the load in normal standing.

The spine is exposed to **gravitational forces** resulting from the body segments' mass, **external forces** and moments generated by physical activity and to muscle tension. **Compressive forces** estimated from in vivo experiments, using kinematic and electromyographic data, have recorded values of 200-300N in supine posture and 1400N in standing posture. Such actions as simple bending can double the intradiscal pressure, and if bending is associated with lifting a 20kg weight in flexed posture these values can also be increased four or five times. Shear forces are also present, and they are generated between the intervertebral disc and vertebral endplate during flexion/extension movements as well as from compressive loading. However, these forces are minimized by the action of the muscle component, which indeed plays a key role in stabilizing the spine [2, 33–46].

The relevance of the **muscle component i**n resisting high loads on the spine was highlighted by Patwardhan et al. (1999) [47]. In early investigations on human cadaveric vertebrae, it has been observed that when they were loaded with a vertical compressive load, the vertebrae experienced deformations, bending and buckling to the breaking point even for small loads within a few hundred Newtons. However, it was well known that the spine could support much higher loads, even exceeding 3000N. This is enabled by the action of the muscles. The muscles ensure that any eccentric compressive load becomes a **follower load**, which is a **non-conservative** load that follows the spinal curvatures. The path of the follower force is tangent to the spinal curvature through the vertebral center of rotation [47–50] (see Figure 2.6).

The **follower load function** is to minimize the shear forces induced by compressive loading, allowing the spine to support loads that it would not be able to support without this mechanism. The follower force is the key point against spinal instability. Having a strong muscular component is equivalent to having a highly stable spine, which even with small imbalances in equilibrium, for example owing to herniated disc, is still able to maintain its stable configuration[47–50]. Hence,

the **spine's stability** is unique, and an alteration of this stability can arise from pathologies such as herniated discs, scoliosis, resulting in altering the physiological stress state in one or more FSUs and it can be assessed by the loss of stiffness or increased mobility. When these conditions lead to significant pain and discomfort, surgical intervention may be necessary.

Hence, the instability can be classified into **micro-instability or macro-instability. Micro-instability** refers to instability caused by the normal degenerative process associated with advancing age; whereas **macro-instability** refers to instability caused by a spinal fracture or dislocation[47–50].

The next sections deal more closely with the biomechanical behavior of the intervertebral disc and bone component, focusing also on the differences at the biomechanical level between the cervical and lumbar region.

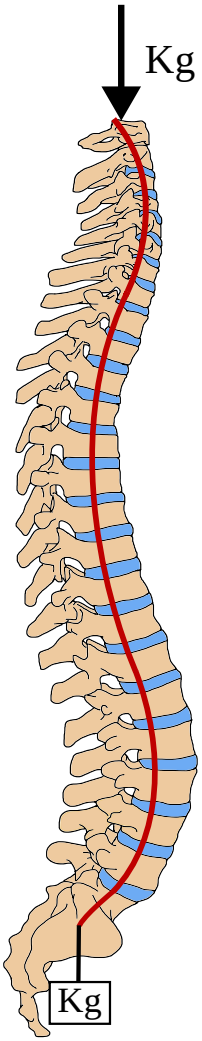

Figure 2.6. *© Action of the muscle components which convert a compressive axial load in a follower load applied along the center of rotation for each vertebra.*

2.2.1 Intervertebral disc

The intervertebral disc acts as a shock absorber to spinal loads, thus ensuring compressive strength and providing **flexibility and mobility** to the spine. Its native structure creates a unique distribution of stresses from external loads in the nucleus and fibrous annulus. The stresses within the NP are predominantly hydrostatic, with specific **intradiscal pressure (IDP) values**, which can be measured in-vivo by needle pressure transducers. Indeed, many measurements have been made on subjects engaging in different activities, from simple standing to heavy lifting [51–53](see the Figure 2.7 for IDP values).

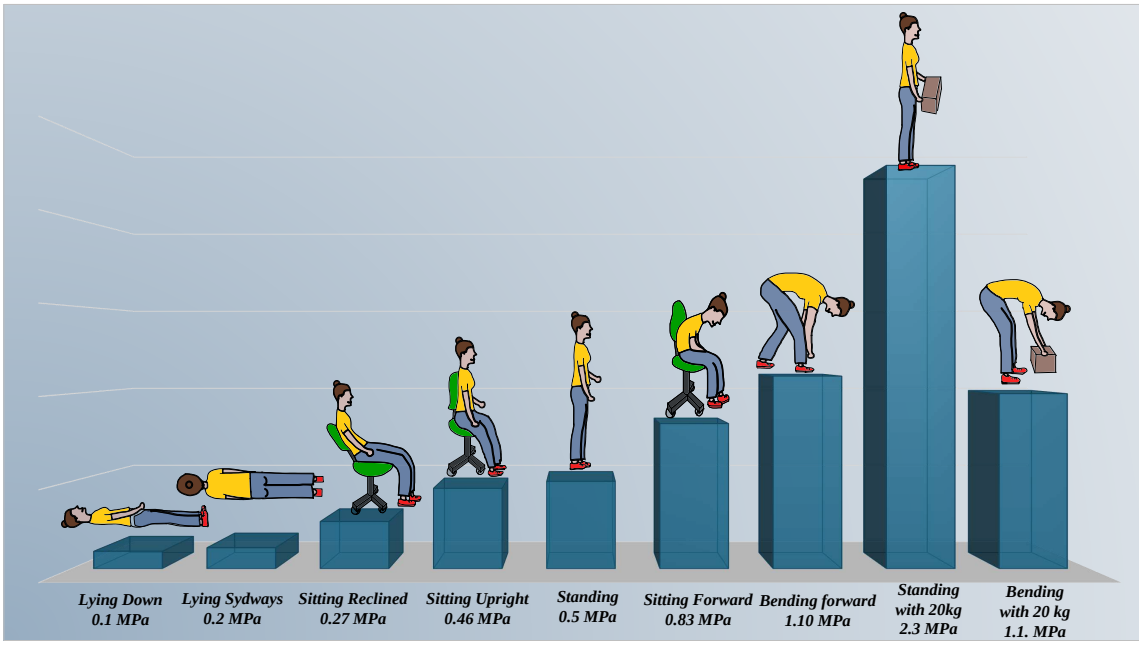

Figure 2.7. *© Intradiscal Pressure in-vivo measurements in different movements, i.e., Lying down and sideways, sitting reclined, upright and forward, bending forward without and with 20kg, standing without and with 20 kg.*

IDP values range from a supine resting value of 0.1-0.2 MPa to a peak of 2.3 MPa in flexion with weight lifts. Indeed, the stresses are also **posture-dependent:** the anterior or posterior part of the disc is more stressed if one has a posture in flexion or extension, respectively [51–53]. Furthermore, **stress profilometry** is also based on in-vivo measurements using a pressure transducer, aiming to record the stress distribution along the disc structure.

Figure 2.8 shows how the load is distributed along the **different positions** of the AF (outer and inner) and in the nucleus pulposus for a lumbar IVD in the healthy and pathological conditions. It was observed how the stresses increased as

the applied load increased. In addition, the **hydrostatic stresses** remain uniform in the core and in the inner portions of the annulus. However, the stresses appear to be direction-dependent and are always lower at the outer ring [2, 33–46, 51–53].

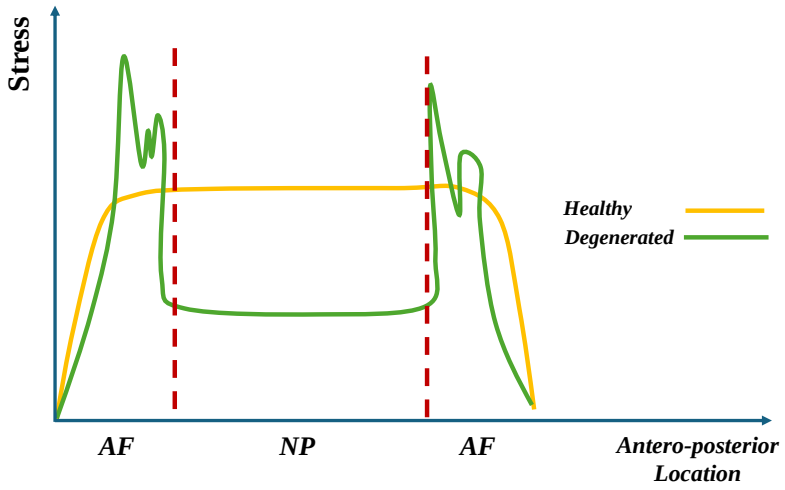

Figure 2.8. *© Stress profile [54] in the sagittal plane for a lumbar healthy and degenerated IVD.*

The intervertebral disc tension state has manifold complexities. Given an FSU, if an axial compressive force is applied to the segment, the **swelling phenomenon** is visible in Figure 2.9. The AF generates tension by swelling radially along all directions. As a result of the compressive force action, the disc flattens and swells at the sides, assuming a **swelled shape** [2, 24, 33–46, 54–58].

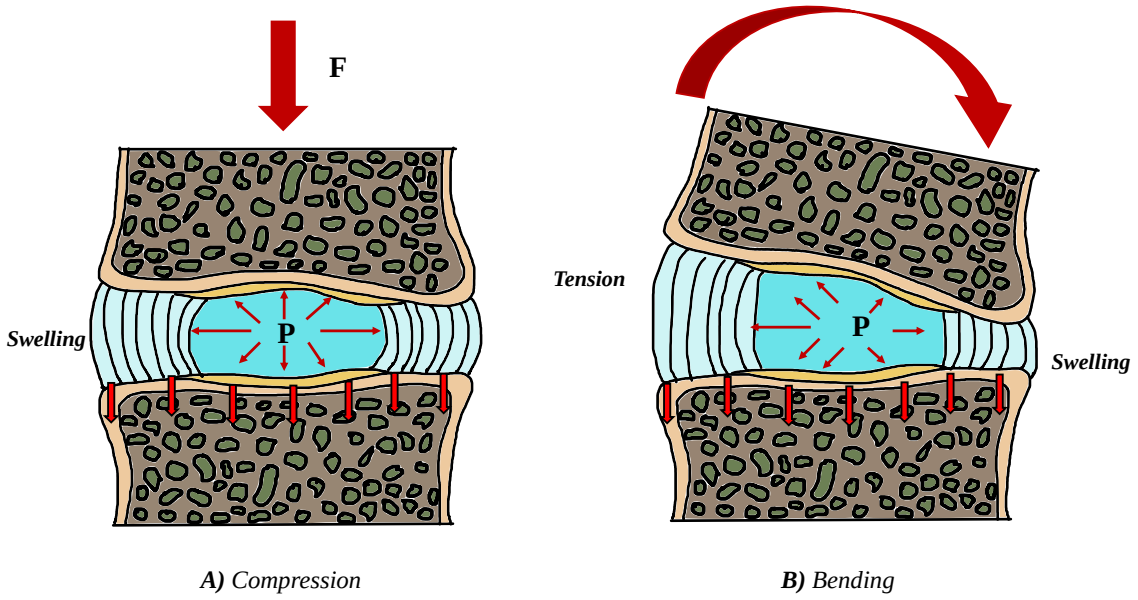

Figure 2.9. *© **A)** Swelling of the AF caused by increased IDP in the nucleus during Compression. **B)** Swelling and stretching of the AF caused by increased IDP in the nucleus during Bending.*

The **swelling effect** is caused by the tangential forces established at the contact between disc and vertebrae because of friction. The tangential forces resist movement by leading the central material to stand immobile and so bringing the disc to assume this shape. Anatomically, the swelling phenomenon is also caused by the anchoring action created between the fibrous annulus and the cartilaginous endplate. Uniform tension is created along the AF directs the NP fluid centrally, allowing load distribution from one vertebra to another across the fibrous annulus [2, 24, 33–46, 54–58].

The h**ydrostatic pressure** of the NP is generated by its high-water content, exhibiting incompressible behavior. In addition, the proteoglycans in the NP are mainly responsible for the IVD bulging as they capture water while balancing the tensile forces of the AF fibers, thus achieving equilibrium. Swelling increases as applied load increases, although this load distribution between NP, AF and intradiscal pressure is always present even in the resting condition. Indeed, the pressure will never be zero in the annulus. Once there is an increase in load, the swelling phenomenon is very pronounced. After these loads are removed, the NP pressure stabilizes ensuring the restoration of normal disc height by returning to the equilibrium state [2, 24, 33–46, 54–58].

The **intradiscal pressure** induces all structures to move away from the nucleus, so pulling the upper vertebra away from the lower one while the annulus will move radially outward. The IDP distribution is greatest at the nucleus center, and decays progressively moving from the nucleus outward from the annulus. The pressure generated in the annulus is not only a consequence of the applied external load (weight and muscle forces), but it is also dependent on the compressive action of the annulus fibers. The fibers are inclined toward each other and are inclined to join the two contiguous vertebral bodies. Therefore, the fibers bring the two vertebral bodies closer together by increasing the load on the nucleus pulposus because of the pressure exerted by the nucleus [2, 24, 33–46, 54–58].

The fibers' angle depends exactly on the stress conditions so that they can support the loads induced by flexion and torsion. Furthermore, the fibrous annulus has a role in restricting spinal motion. The concentric lamellae orientation with the different orientation degrees allows one-half of the AF layers to resist deformation from torsion in one direction, while the other half moves in response to torsion in the opposite direction, while also succeeding in resisting deformations dictated by

vertical compressive forces.

Hence, if a compressive load is applied in flexion, it can be observed from Figure 2.9 how the swelling phenomenon always occurs, but it appears that the posterior AF elongates leading the nucleus to flow posteriorly, in the opposite way to the direction of flexion. this mechanism allows a balancing of pressures and stresses, while still managing to maintain uniform pressure across the cartilaginous endplate [2, 24, 33–46, 54–58].

At the mechanical level, NP has nearly **isotropic properties,** while AF has **anisotropic mechanical properties** due to the collagen fiber orientation and organization. In addition, interactions are established between water and collagen fibers within the IVD, which therefore also allows poroelastic behavior caused by the exit or entry of water into this structure.

Lastly, **osmotic effects** in the disc structure are also essential in the biomechanical response of the disc, which reflect the high negative charge of proteoglycans. Osmotic pressure involves a force generated by the difference in solute concentrations, i.e., proteoglycans, between the NP and the fibrous annulus, which therefore has the tendency to drive water in or out of the disc to ensure osmotic balance. Since the NP has high concentrations of proteoglycans, it attracts water by osmosis, thus keeping the disc hydrated. Maintaining disc hydration is critical for maintaining the disc height and thus the ability to shock-absorb. In addition, osmotic pressure also allows loads to be properly distributed, as discussed above [2, 24, 33–46, 54–58].

2.2.2 Vertebral bones

The vertebral bone provides the structural and mechanical support for the spine, withstanding most of the compressive load according to Rockoff (1969) [59]. The cortical component of the vertebral body supports from **25% to 55% of the total compressive load,** with a Young's modulus of about 12.000 MPa for the cortical bone, meanwhile the Young's modulus of the trabecular component is around 90 MPa. Overall, the **compressive strength** of the whole vertebral body is estimated to be between 4.000 and 7.000N. Although the presence of cortical and trabecular bone, a vertebra is very light. The structure is designed to reduce stress to the joints and provide cushioning and thus energy absorption and dissipation, allowing it to withstand high mechanical loads [2, 33–46, 59–61].

Therefore, vertebral bone can be viewed as a **hierarchical structure material**,

as reported in Figure 2.10. It involves:

- ➢ **Nano-structural components** involve the type I collagen fibers and hydroxyapatite.
- ➢ **Micro-structural components** consist of osteon and trabeculae, along with the mineralized collagen fibril lamellae.
- ➢ **Macro-structural components** is composed of the vertebra within the cortical and trabecular bone.

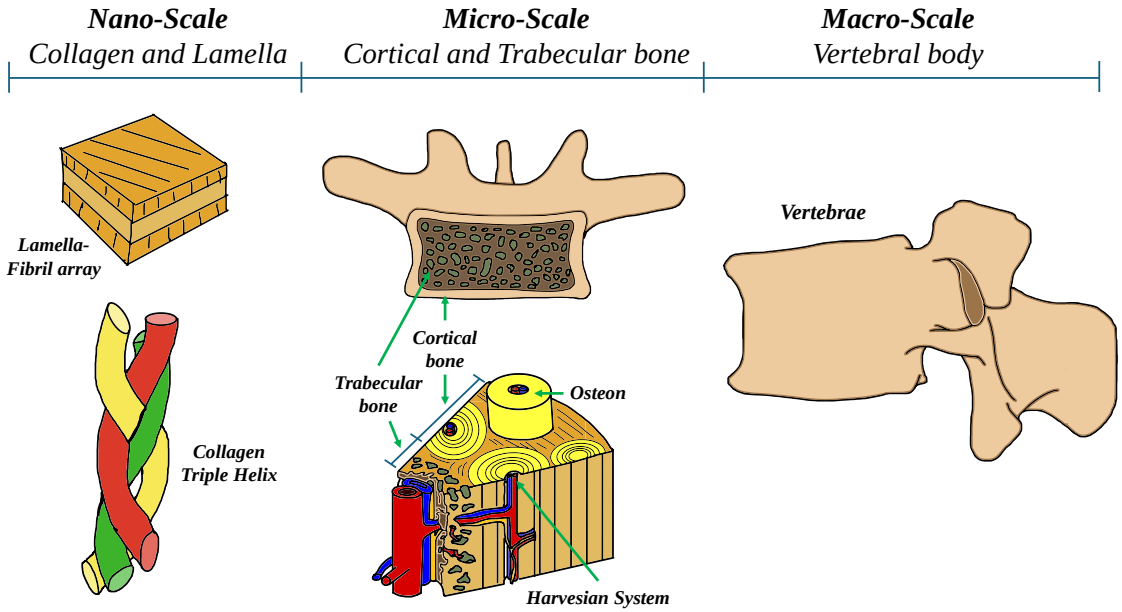

Figure 2.10. *© Hierarchical structure of the vertebrae.*

At the **macroscopic level**, the internal structure of the vertebral bone is unique due to the composite structure created by the assembly between the trabecular component, i.e. the spongy bone, and the cortical bone shell.

The **spongy bone** is formed by the trabeculae each about 200 μm thick, resulting in very light weight and providing dynamic load support; meanwhile, the **compact bone** is a very dense bone which is responsible precisely for mechanical stiffness. In conjunction, the two bone structures work together to combine their characteristics and weaknesses, thus creating a unique structure. A weakness of cortical bone is its inability to resist transversal compression; however, the horizontal trabeculae act as internal reinforcement thus preventing the cortical bone from collaring, providing resilient characteristics while the vertical ones support the compact bone [2, 33–46, 59–61].

At the **microscopic level**, the cortical bone porosity is about 6% with thickness in millimeters. The blood vessels are surrounded by a structure called an **osteon or Havers system** that involves from 3 to 8 concentric bone lamellae with vertical arrangement, where Osteons consist of mineralized collagen fibers.

Trabecular bone is composed of an interconnected, foam-like network of many lamellae. The single lamella is composed of mineralized collagen fibrils with an optimized orientation which depend on the load distribution, thus providing anisotropic characteristics. Indeed, bone is classifiable as a **composite, anisotropic and porous cellular solid,** although preferential directions can be identified based on the load acting on the trabecular bone. Hence, the whole vertebra can be classified as an orthotropic and transversely isotropic material. Lastly, at the nano-structural level, the bone material is composed of carbonated hydroxyapatite nanoparticles and collagen fibrils[2, 33–46, 59–61].

The mechanical response of the bone is crucial especially when evaluating the risk of bone fractures. Biomechanically, **bone mineral density** is intended as an indicator of bone strength. Hence, alterations in this parameter can result in either weakening or stiffening of the bone structure, potentially causing clinical problems for patients. Looking at the horizontal load direction for a FSU, as the force applied increases, the IDP increases in the distribution between vertebra, IVD and CEP can be observed in Figure 2.9. The increase in pressure induces the arising of tension in the outer fibers of the fibrous annulus, as well as a central compressive load at the vertebral canter in the lower and upper portions.

A **deflection curve** of the upper and lower vertebral endplate will result, leading to an imprinted deformation that may result as a possible fracture point. Therefore, there is equal load distribution transmitted from the vertebral body to the cartilaginous endplate, which is then passed to the IVD. The IVD increases the intradiscal pressure, and it consequently raises the tensile stress on the annulus fibers, which deform radially, generating the swelling phenomenon, thus allowing a proper load transmission along the entire FSU [2, 33–46, 59–61].

2.2.3 Spinal regions

The **cervical spine** exhibits intricate and sophisticated kinematics due its **saddle shape** and its facet joints orientation. Indeed, the movements in this region involve combined flexion/extension, lateral bending, and axial rotation. The ROM is a key

parameter in describing the biomechanical and kinematic behavior of any spinal segment. In pathological conditions, the physiological ROM is often altered, making it a valuable measure for assessing the severity of the clinical situation and quantifying the patient's pain[2, 33, 46, 59–61].

Over the years, scientists have provided manifold contributions about the spinal ROM. Table 2.1 shows an overview about the ROM in average of the cervical region during the flexion, extension, axial rotation and lateral bending movements [2, 60, 62]. About **cervical IDP**, there are few data in the literature since the cervical discs, unlike the lumbar ones, are very small; consequently, it is very complex to insert measuring devices into the nucleus pulposus. About the physiological load distribution, this is distributed anteriorly and posteriorly due to the head weight and the muscle component. It is estimated that the anterior part of the vertebrae, together with the discs, transmits 36% of the load to the thoracic spine. In contrast, the remaining load is distributed equally through the facet joints of the posterior portions [2, 60, 62] (32% load transmitted for each side, see Figure 2.11).

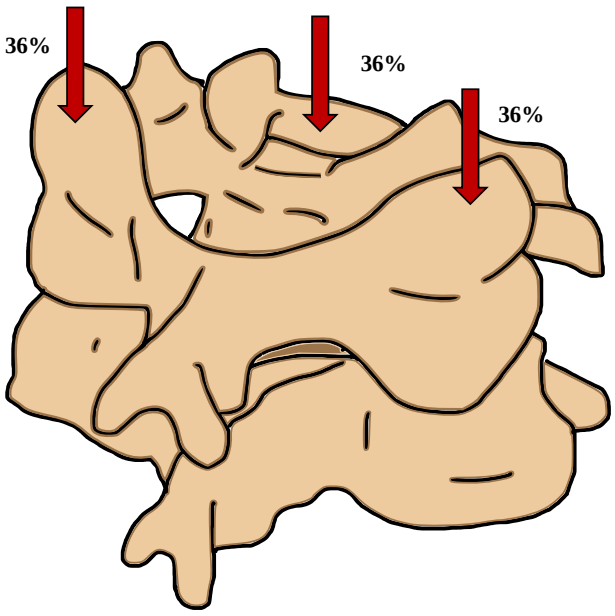

Figure 2.11. *© Load distribution in the cervical zone.*

The **thoracic spine** is frequently associated with **spinal fractures** leading to the risk of neurological dbecause of the small diameter of the spinal canal. However, the muscle component and the rib cage provide a great biomechanical support, which made it difficult to be damaged. Indeed, the injuries occurring in this region are often associated with impact or shock trauma, like sharp falls or highway accidents,

where the impact power allows the energy storage necessary to reach the fracture point of the thoracic vertebral component. Fractures often occur at the T9-T12 region which is the thoracolumbar junction area. Table 2.1 shows an overview about the ROM in average of the thoracic region in flexion, extension, axial rotation and lateral bending [2, 36, 37, 46].

The **lumbar spine** is the anatomical region with the highest strength, since it must support the weight of the entire upper body, while also offering greater protection to the spinal cord due to a larger spinal foramen. It allows all **6 degrees of freedom**, including rotations and translations along the main axes. For the lumbar spine, the ROM appears to be an indicator of the physiological status. Table 2.1 shows an overview about the ROM in average of the cervical region in flexion, extension, axial rotation and lateral bending [2, 36, 37, 46, 60, 63, 64].

Table 2.1. *ROM data [2] for humans in Flexion/Extension, lateral bending, Axial rotation*

		Flexion Extension	**Lateral Bending**	**Axial Rotation**
Species	**FSU**	**ROM (°)**	**ROM (°)**	**ROM (°)**
	C1-2	20	8	-
	C2-3	10	20	6
	C3-4	15	22	14
	C4-5	20	22	14
	C5-6	20	15	14
	C6-7	17	14	12
	C7-T1	9	8	4
	T1-2	4	10	18
	T2-3	4	12	16
	T3-4	4	10	16
	T4-5	4	12	16
	T5-6	4	12	16
	T6-7	5	12	14
	T7-8	7	12	14
	T8-9	7	12	12
	T9-10	7	12	8
	T10-11	9	14	4
	T11-12	12	18	4
	T12-L1	12	16	4
	L1-2	12	12	4
	L2-3	14	12	4
	L3-4	15	16	4
	L4-5	16	12	4
	L5-S1	17	6	2

Among ***in-vitro* and *in-vivo* studies** there is a clear difference in ROM among the distinct spinal sections, for instance in lumbar levels L4-5 and L5-S1 there is an increase in ROM *in-vitro* for flexion/extension tests, which in in vivo measurements does not appear. Similar was the case for lateral bending experiments, where the ROM appeared identical in the in vitro experiments between the distinct lumbar segments, while *in-vivo* there was a decrease for the last two lumbar segments from L4 to S1. This may be explained by the missing muscle component which is always absent in *in-vitro* experiments due to obvious limitations in laboratory experiments [2, 33–46, 59, 61].

About the **facet joints,** they do not directly support axial loads except in lordosis extension, even though they play a key role in just allowing movements and resisting flexion/extension, lateral bending and rotation in different ways depending on the anatomical region considered. Indeed, the relative motion associated with each FSU is related precisely to the facet joint orientation. Coronal orientation of the facet joints in the cervical spine allows rotation and flexion/extension, whereas sagittal orientation allows flexion/extension but limits rotation [2, 33–46, 59, 61].

2.3 Experimental tests on the spine

Spine biomechanics is extremely helpful to study spinal diseases and injuries. Several kinds of biomechanical testing protocols may be employed, including **flexibility** or **creep and stress relaxation tests.**

Aside from the test employed, the preconditioning is always necessary, for example unloading and loading ten cycles, and it is recommended for several reasons [2, 33–46]:

- ➢ To minimize viscoelastic effects in the flexibility test.
- ➢ To activate the specimen to trigger its biomechanical response.
- ➢ To simulate the effects caused by the muscle component action and body weight.

Lastly, regardless of the protocol and machine used for testing, the calibration of the machine and any tracking system is always mandatory. Afterwards, all procedures for implementing the testing protocol can be followed. The following section outlines the main steps to follow in performing biomechanical testing on the spine.

2.3.1 Specimen for testing

A **biomechanical test** can be considered more reliable if it is performed *in-vivo* on living subjects or *in-vitro* on fresh or frozen human cadaver specimens. Obviously, human specimens when available are not from young people, but from older adults who often have disc degeneration or other pathologies. Indeed, this is a major limitation, since the conclusions drawn from experiments performed on already degenerated or osteoporotic specimens are limited, and therefore must be well discussed and adapted for each case, as well as looking if the conclusions may be equivalent equally on healthy specimens. Specimens with lesions or tumors should be excluded from the studies because the pathological effects alter the results of the experiments far too much[2, 33–46].

The **specimen storage process** must be well performed and organized sufficiently to ensure that all specimens are labeled according to age, gender, weight, size, and death cause, while also annotating bone quality (measuring bone mineral density) or disc height by measurements obtained from MRI or CT examinations.

The **human specimen preservation** steps are the following [2, 33–46, 64]:

- ➢ The specimen must be collected fresh from the defunct body, with most muscle mass dissected. The specimen is then sealed in double or triple plastic bags.
- ➢ The specimen should remain frozen at -20/-30 °C and should be thawed several hours before the test gradually by placing it in a cold room at low temperatures first, and then bringing it back to room temperature before the test. Studies have shown that freezing and thawing, if done properly, have reduced effects on bone and disc biomechanical behavior.
- ➢ Specimens cannot be fixed with formalin, as this preservation method has been shown to drastically alter the biomechanical properties of the specimen.

Once the **specimen is thawed,** the preparation starts. Operators must have taken essential **safety precautions** in laboratory practices as working with human specimens can bring serious risks of infection, i.e., AIDS or hepatitis. Figure 2.12 shows the step followed for the preparation of a human specimen.

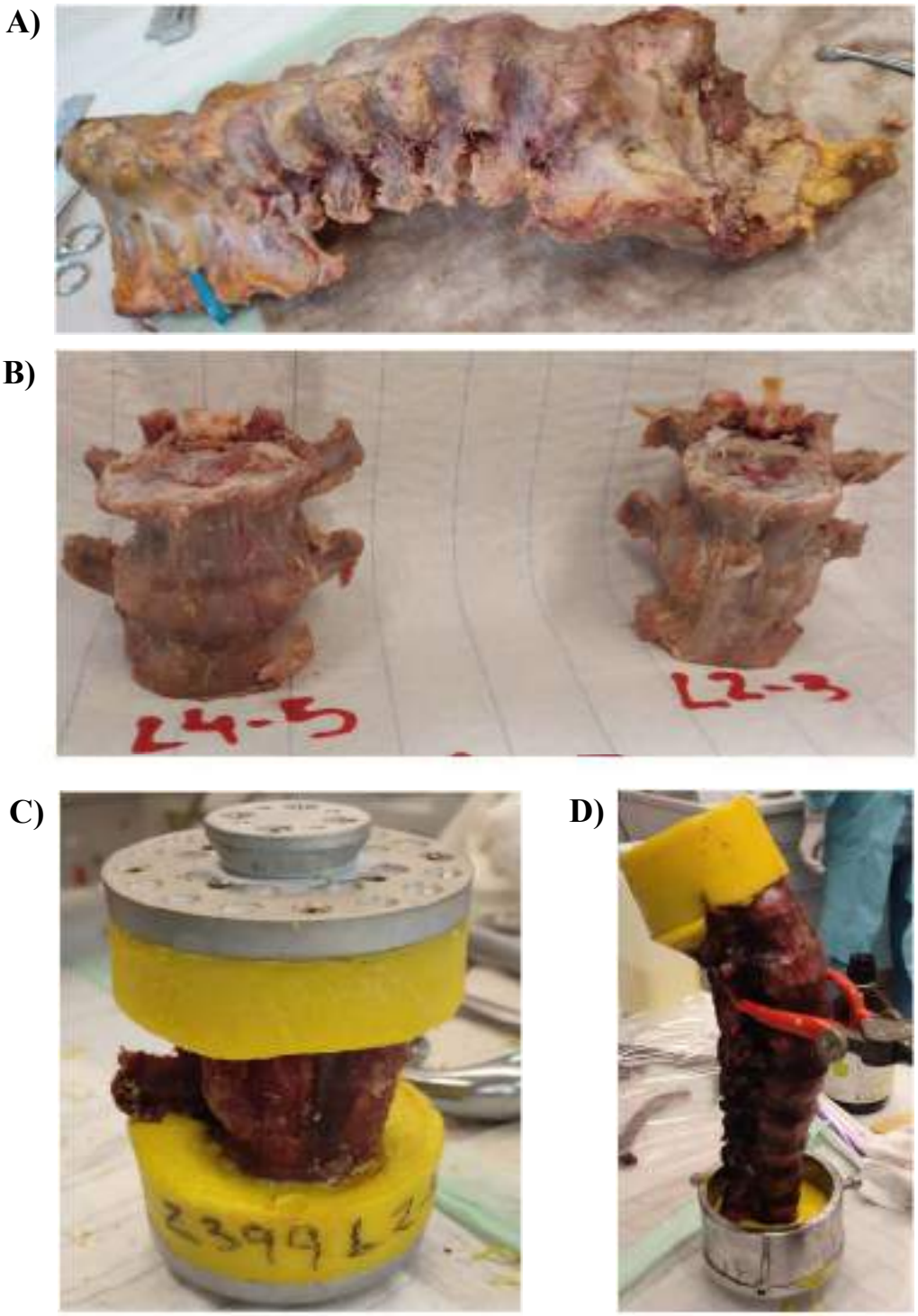

Figure 2.12. *© A) Humna lumbar spine thawed. B) L2-3 and L4-5 FSUs isolated and prepared. C) Embedding and preparation of the specimen to be attached to the testing machine.*

The **specimen preparation procedure** requires that the specimen should be muscle-free, but with all ligamentous and bony structures intact (see Figure 2.12A). Then, the spinal segments are isolated if required. For example, Figure 2.12B) shows the isolation of two lumbar FSUs. To ensure the attachment of specimen

to the testing machine, the cranial and caudal ends are embedded in a polymeric or low melting point alloy (i.e., ***Poly(methyl methacrylate)*** **(PMMA)**). For the specimen anchoring to the PMMA, screws are inserted into the specimen with threads [2, 33–46] (see Figure 2.12C).

The **availability of human specimens** is, for several reasons, very **limited**. Hence, the use of **animal specimens** is necessary. There are several studies that have used calf, sheep or pig for early testing in the research or experimental stages, for example, in performing stability tests on new implants [2, 34, 65–69].

Specimen preparation for animal is almost the same to human, as shown in Figure 2.13 an example for bovine tails. Animal specimens can also be frozen, stored in two plastic bags and labeled by animal race and age, also associating radiographic data if needed.

Figure 2.13. *© **A)** Fresh bovine tail; **B)** C3Y-4 Bovine tail embedded and prepared for testing.*

Specifically, Chapter 4 will focus on experiments performed on bovine tails since bovine tails are widely cheap. At the anatomical level, animal specimens do not perfectly replicate human anatomy, but it has been observed that there are instead **several similarities** at the biomechanical level. One benefit of using animal specimens is the availability of having fresh specimens in high numbers. Several studies have been reported in the literature where they have evaluated whether **bovine tails** can be used as a model for the human lumbar spine. Indeed, DNA, proteoglycan and collagen contents in bovine intervertebral discs have been analysed to estimate changes in matrix contents compared with humans. Overall, the bovine disc is very similar to human lumbar disc, although there are differences.

Table 2.2 shows an anatomical comparison between human and bovine [2].

Table 2.2. *Data extracted from [2] for a anatomical comparison between humans and cows.*

Intervertebral disc Human vs. Bovine (Thoracic)						
Species	**Height [mm]**	**Medio lateral width [mm]**	**Antero posterior width [mm]**	**Disc area [mm2]**	**NP area [mm2]**	**Ratio NP/Disc area**
1						
1	11.3 ± 0.3	55.9 ± 9.4	37.2 ± 4.7	1727 ± 550	479 ± 110	0.28
1						
1						
1	6.9 ± 0.35	28.9 ± 2	27.8 ± 1.3	622 ± 71	176 ± 22	0.28
1						

Tables 2.3 shows the biomechanical performance in flexibility tests of cows [2].

Table 2.3. *Data extracted from [2] about the ROM of cows in Flexion/Extension, lateral bending, Axial rotation*

		Flexion Extension	**Lateral Bending**	**Axial Rotation**
Species	**FSU**	**ROM (°)**	**ROM (°)**	**ROM (°)**
	T6-7	4	10	9
	T7-8	4	9	10
	T8-9	5	10	10
	T9-10	5	10	10
	T10-11	4	10	8
	T11-12	5	9	6
	T12-T13	4	9	2
	T13-L1	5	10	2
	L1-2	6	13	2
	L2-3	6	14	3
	L3-4	7	12	2
	L4-5	7	12	2
	L5-L6	10	10	4

Biomechanical tests should be done between 20°C and 30°C and should not be performed for more than 20 hours exposure at room temperature, to avoid the specimen properties alteration. If a testing temperature close to body temperature is desired, it should be considered that the cellular autolytic process is accelerated; therefore, the test length duration is not more than 20 hours, but it is significantly lowered. Specimens must be kept hydrated while performing the test. There are several methods, one example is just spraying the specimen with saline solution

periodically [2, 33–46].

The **planning process** of the **test protocol** is crucial. Before the experiment is performed, the protocol must be clearly decided, according to the experimental design. Furthermore, the test must be performed repeatedly under identical conditions for obtaining at least three result values for each test, where any deviation from the protocol must be noted. The data generated from the experiments are recorded and then analyzed in different ways according to the test purposes [2, 33–46].

To avoid confusion during data acquisition, it is essential to ensure that all sample information is accurately recorded and properly associated. The **raw data** collected will primarily consist of a simple load versus displacement curves. From these curves, it is possible to derive important metrics, such as ROM, NZ, stiffness, hysteresis, stress-strain curves, and other relevant information depending on the test's objectives. Once the collection and analysis of test data is completed, it is important to present the key findings clearly and concisely, whether in a scientific article, conference paper, technical report, or book chapter [2, 33–46]. Practical examples will be provided in the following chapters.

2.3.2 Flexibility test

Flexibility tests are common tests adopted to investigate the spinal column's biomechanical behavior. These tests involve the application of **pure moments** in flexion, extension, lateral bending and axial rotation, which are applied directly to the spinal segment one direction at a time. The resulting three-dimensional motion is recorded through a **camera system** that tracks the movement.

The spatial position of the spinal segment can be recorded by placing markers on the specimen in a visible manner for the cameras. The markers can be attached by screws and inserted into either bone or PMMA block, as an example see Figure 2.14, to ensure rigid positioning. The markers by moving as a rigid body they will allow the tracking of the spinal specimen's movement [2, 33–46].

The data obtained from the motion recording are analyzed, and the measured common parameters are ROM, NZ, stiffness hysteresis, coupled motion, axis of rotation, etc. A preconditioning phase often precedes the flexibility test, which aims to simulate body weight and muscle effects. An amplitude of ± 7.5 Nm is suggested when using pure moment loading in the lumbar spine; for the thoracic spine ± 5 Nm; for the cervical spine ± 1 Nm at C1-2 and in the other segments ± 2.5 Nm [2, 34,

46]. Once the data have been processed, **statistical comparisons** are conducted between test groups, calculating correlation coefficients to identify important factors. Several types of analysis can also be done, depending on the overall aim of the test.

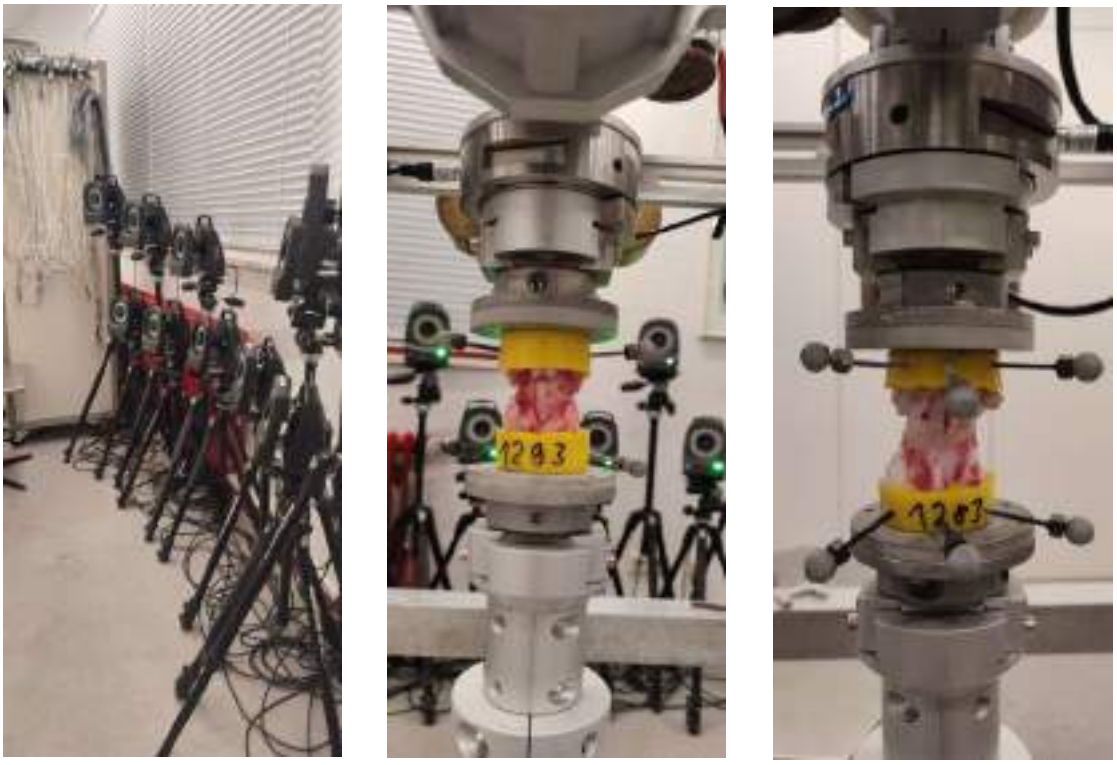

Figure 2.14. *© Track motion system and placement of the specimen in the universal spine tester.*

2.3.3 Creep and stress relaxation tests

The intervertebral disc is often modelled as a viscoelastic material. The disc has a high-water component, coupled with other substances that give it its solid compactness. Therefore, the disc can be seen as a hybrid material that exhibits intermediate characteristics between solid and fluid, hence its viscoelastic nature. The tissue's viscoelasticity at the mechanical level has also been found experimentally, as discussed in previous sections. Indeed, specimens are often subjected to long-term creep or stress relaxation tests to evaluate the biomechanical behaviour of IVD [43, 70–73].

Creep is a viscoelastic phenomenon which occurs when a material subjected to constant stress exhibits time-dependent deformation. Creep testing consists in the application of a stress history to the sample (see Figure 2.15A). It can be observed that the mechanical strain response predicts a continuous growth until a constant value is reached. The strain-time plot, for an imposed unit stress history, will be representative of the material **Creep function** $J(t)$. The Creep Function is an

increasing monotonous function, as can be seen in the figure. Indeed, spinal specimens are often subjected to compressive creep tests, with multiple loading and unloading steps, to study the mechanical response and fluid exchange of the IVD over time [43, 71–73].

Meanwhile, Relaxation is a viscoelastic phenomenon that occurs when a material subjected to constant deformation exhibits time-dependent stress. Stress Relaxation testing consists in the application of a strain history to the sample (see Figure 2.15B). It can be observed that the mechanical strain response predicts a continuous growth until a constant (zero) value is reached. The stress-time plot, for an imposed unit strain history, will be representative of the material **Stress Relaxation function** $G(t)$, which is a monotonically decreasing function, as can be seen in the figure. Like creep, relaxation tests with compressive loading and unloading phases are used to study the response IVD and its fluid exchange [43, 71–73].

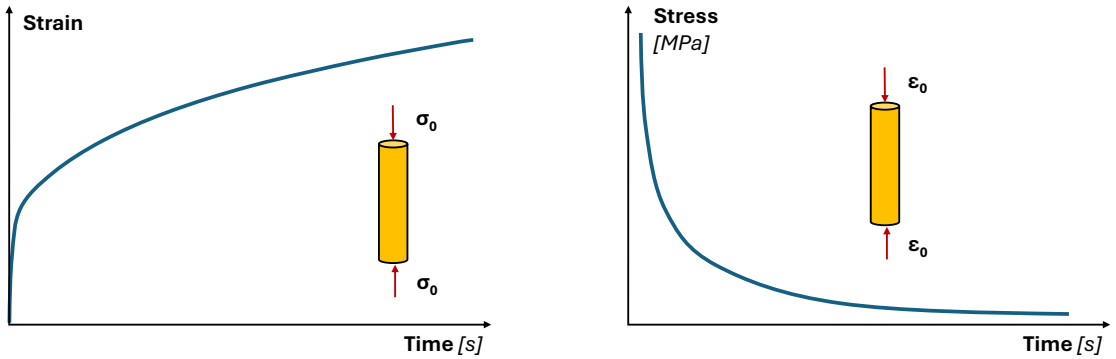

Figure 2.15. *© **A)** Creep curve from long-term test. **B)** Stress relaxation curve from long-term test.*

Where σ_0 is the stress expressed in engineering terms which is described as a force (F_0) per unit area (A_0) and where ϵ_0 is the strain expressed in engineering terms which is described as the change in length of the sample relative to its initial length. in the following sections, creep tests will be reconsidered in depth, as they have been an important focus of this thesis.

Chapter 3

Spinal Diseases and Clinical Treatments

3.1 Back pain

Back pain is a historically well-known disease. Since ancient societies, there have been efforts to understand the nature of this condition. The ancient societies thought that pain was related to supernatural demonic forces, leading to the more naturalistic and critical view of the ancient Greeks (Hippocrates) and Egyptians. However, it was only near '900s, that earlier concepts of spinal pathologies were widely studied and discovered. The pioneer was **Georgle Schmorl** (1861-1932), a German, who first systematically described all the normal anatomical structure of vertebrae and discs, including morphology of age-related disc degeneration, disc protrusions and annulus tears. Back pain is one of the most common causes of absence from work, resulting in health and economic burden for countries. A variety of pathologies can afflict the spine, influencing disc height, spinal mobility, and affecting changes in the accessory structures [1, 2, 32, 74–79].

Spinal pathologies can be subdivided according to location and progression sequence whether at the intervertebral disc, involving NP, AF, and endplate, or whether involving facet joints, ligaments, or spinal canal. Pathology characterization is based on the imaging approach should follow these steps [1, 2, 80]:

1. Characterize the affected segments involved in the pathological process.
2. Identify the sequence of degeneration and predict potential abnormalities.
3. Detect any hidden or subtle abnormalities.
4. Assist clinicians in identifying the source of pain and neurological symptom.
5. Determine the most effective treatment plan for the patient.

The North American Spine Society's (NASS) Evidence-Based Guideline Development Committee has recommended, as the gold standard for confirmation of spinal disease, the ***Magnetic Resonance Imaging*** **(MRI)** and multidetector ***Computer Tomography*** **(CT)** [1, 2, 32, 74–79].

3.2 Disc Degeneration Diseases

Disc degeneration occurs with advancing age, although it can also be present in non-elderly adults. The biomechanics of the healthy disc have already been analyzed in the previous chapter. From the second life decade, aging affects NP composition and nutrient transport, causing a decrease in proteoglycan synthesis by reducing the ability to generate hydrostatic pressure in response to stimuli [12–14, 56, 74–89]. The loss of proteoglycans, and thus glycosaminoglycans, is directly responsible for the reduction in osmotic pressure and hydration. The disc becomes more fibrotic and less gelatinous. Therefore, due to the **failure** of the NP to hydrate properly, the disc is no longer able to distribute load evenly across the endplates and loses the ability to swell. This alteration in load distribution can lead to significant complications, from **endplate fracture** to **osteophyte formation**.

As a result, the AF thickens, and the collagen fibers are no longer highly organized. There is also a small **alteration in collagen** content, but the disc degeneration is not related with this, but with the disorganization that occurs between the collagen fibers. These alterations change the IVD elastic zone stiffness by expanding the discal NZ and limiting disc mobility. In addition, disc degeneration is also commonly followed by **facet joint degeneration**. The alterations in disc mobility and the decrease in disc height led to an acceleration of the erosion process of articular cartilage because of increased contact pressures between the upper and lower facets, resulting in subluxation events, for example.

Lastly, all these phenomena alter the stability of the spine leading the patient to have problems at the clinical level, which may often require surgery to relieve pain. As a result of **degenerative processes,** the spine experiences vertical instability as the IVD, facet joints, and ligamentous structures are no longer able to maintain the anatomical alignment and anatomical position of the spinal segment. Instability usually occurs in the cervical and lumbar areas and it is presented clinically as intermittent low back pain [12–14, 56, 74–77, 79–89].

3.2.1 Disc Herniation

Considering the hypothesis that disc degeneration starts at the NP, the following is the explanation of the **pathology progression**. The NP may experience degeneration, due to combined effects, such as abnormal mechanical stress, advancing age etc. The NP dehydrated reduces the IDP leading to an increase in the mechanical load on the fibrous annulus, which experiences changes at the anatomical and morphological level. The increased loads acting on the AF result in **injury or rupture** of the fibrotic structure, from which disc herniation may result. In addition, structural weakness of the annulus will be reflected in possible difficulty in maintaining alignment and anatomical position between adjacent vertebrae, thus leading to instability and eventual spondylolisthesis [12–14, 56, 74–77, 79–89].

Disc displacement is defined as the displacement of disc material outside the limits of the disc space. It is classified as diffuse dislocation, or **protrusion**, or focal dislocation, which would be **herniation**, and then **extrusion** with sequestration [80–89] (see Table 3.1 for the classification).

Table 3.1. *Description of disc displacement different scenario.*

	Diffuse		**Focal (Herniations)**		
	Disc Bulging	**Annular Bulging**	**Protrusion**	**Extrusion**	**Extrusion with sequestration**
Description	Disc height Preserved	Disc height reduced	Absence or minimal	AF completely damaged	Damage AF with injury to posterior ligament

Disc herniation is defined as the local displacement of nucleus pulposus outside the intradiscal space through the AF, where a fragment of NP migrates from its original position outward. Differentiating the different types of disc herniation is crucial (see Figure 3.1). Herniation can result in [80–89]:

- ➢ **Protrusion**. It is a displacement of disc material from its original position, resulting without or with minimal destruction of the AF.
- ➢ **Extrusion**. It occurs as a displacement of disc material with continuity outside the disc space with complete disruption of the AF. The extrusion in the sagittal plane can cause inflection of the posterior longitudinal ligament and neurological symptoms associated with pain.

➢ **Extrusion with sequestration**. It is as an extruded focal displacement of disc material without any continuity. Sequestration can be subsegmental, i.e., the extruded NP material extends along the posterior longitudinal ligament. If the extruded NP material provokes a complete disruption of the AF and the posterior longitudinal ligament, the sequestration is defined as transligamentous. This herniation is associated with neurological symptoms and pain.

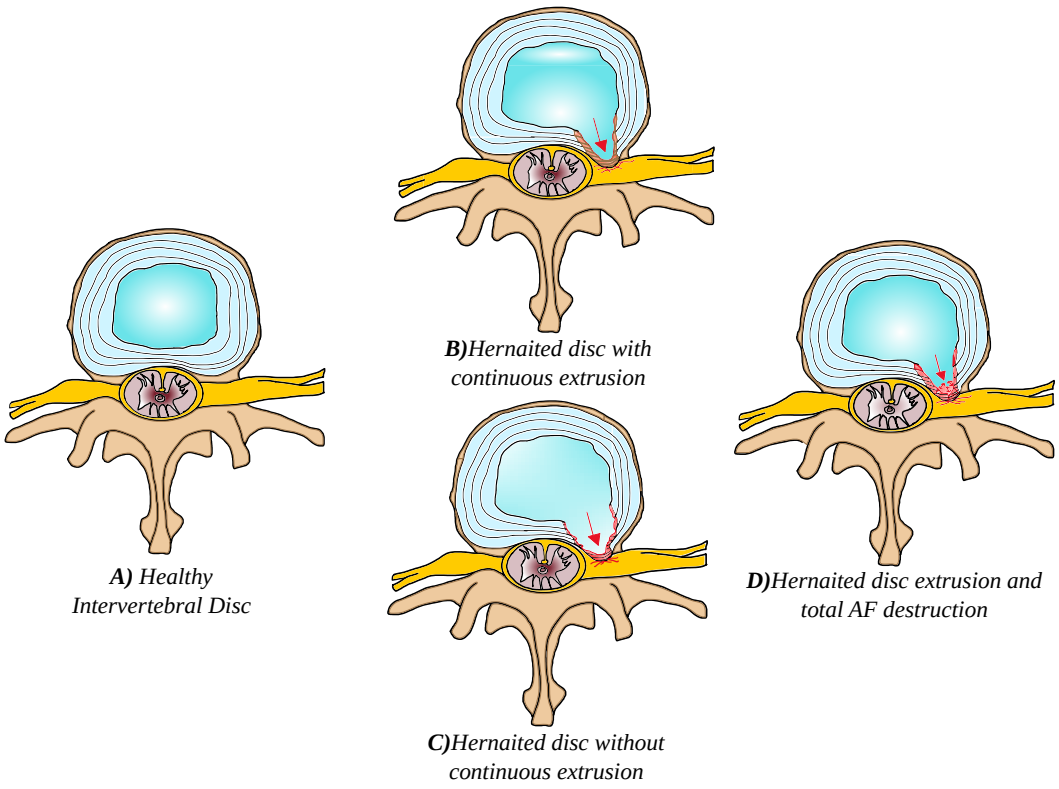

Figure 3.1. *© Schematization of* ***A)*** *healthy IVD;* ***B)*** *IVD with continuous extrusion;* ***C)*** *IVD with extrusion which is not continuous;* ***D)*** *IVD with extrusion and total AF destruction.*

The disc displacement can occur in the anterior or posterior plane, hence the classification of herniation as c**entral, or paracentral, foraminal, or extraforaminal** [80–89] and the herniation may migrate **superiorly or inferiorly** (see Figure 3.2). **Herniated discs,** special sequestrations, can **recede spontaneously.** These phenomena are still not fully understood today. However, when the disc material sequesters into the epidural space, it activates the immune system response, thus provoking the autoimmune and inflammatory responses, which will lead the disc material to neovascularization, enzymatic degradation, and phagocytosis by macrophages [80–89].

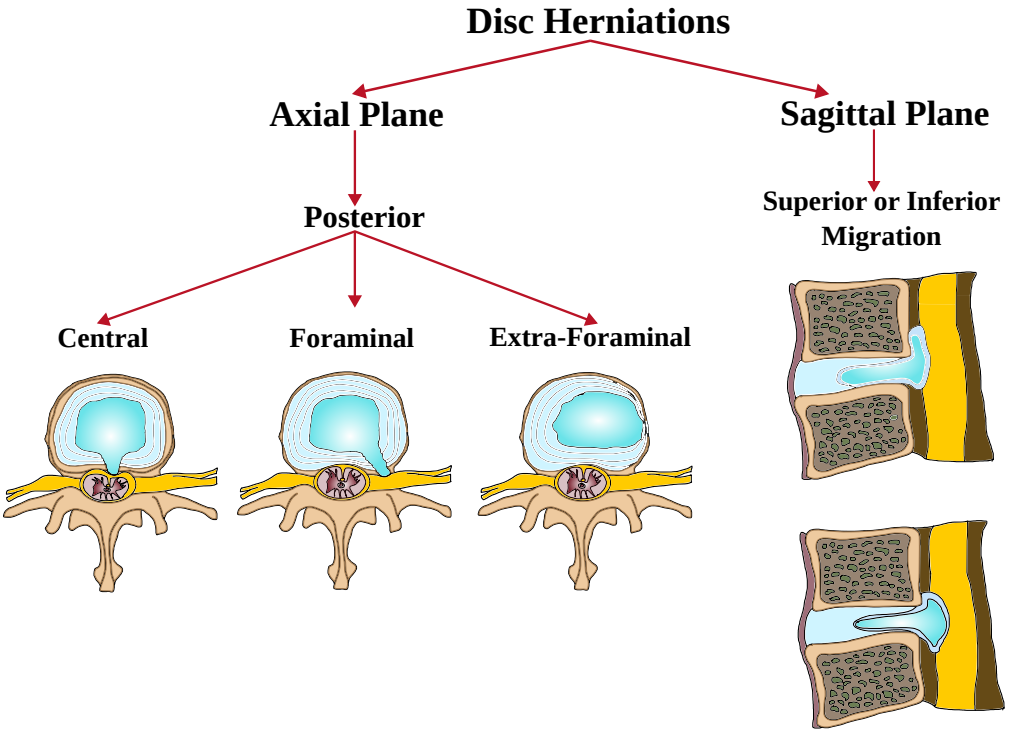

Figure 3.2. *© Disc herniation scenario in the axial and sagittal plane.*

There are several factors that lead to disc herniation. Decreased NP hydration, **imbalance** in nutrient exchange between NP and AF, thickening of AF, and collagen increase may lead to all these complex pathological phenomena [80–89]. Figure 3.3 shows what happen at thew **biological level** when the disc is herniated.

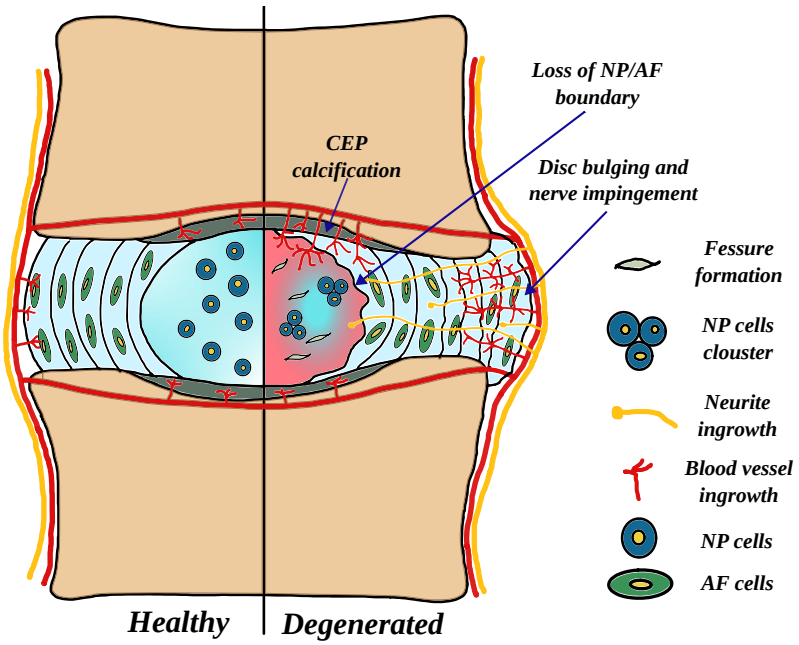

Figure 3.3. *© Comparison between healthy and herniated disc at the biological level.*

Dehydration is seen as the triggering agent in the pathogenesis of degenerative disc disease. Although, the origin of early intervertebral disc degeneration is still unknown, even though there are several studies that have considered the idea that the genetic component may play a key role in the disease's progression. However, it is the physical and external environment that strongly influence the mechanobiology of the intervertebral disc [80–89].

Hence, disc herniations are not only associated with degenerative diseases or the course of aging, but **spinal overloads** may also be one causes of the pathology occurrence. Indeed, disc herniation often occurs in adults who still have high IDP. For example, disc protrusion can appear where the IDP is still high with the fibrous annulus also intact and disc height preserved. Annulus tears can then lead to disc herniation. Therefore, degeneration will then bring to a decrease in IDP, eventually resulting in a collapse of the disc space, with subsequent reduction in height and closeness between the vertebral bodies. As a result, an increased vertical load will act on the annulus, leading to annulus protrusion, caused by its radial outward bulging or bending.

Disc disease is often associated with pain. **Low back pain**, intended as the nerve pain production, is caused by an inflammatory signaling mechanism that is established in the pathological IVD. The NP represents an immune-privileged area in the human body, since it is confined within the IVD. As the NP is extruded into the epidural space outside its physiological boundary, it becomes immunoreactive. Therefore, the extruded NP provokes a response from the immune system thus generating the inflammatory signaling mechanism [80–89].

Several complications are associated with herniation. Besides back pain, which may vary in intensity and duration from patient to patient, neurological complications are common, resulting from the compression of nerve roots and spinal cord. The compression can lead to pain, muscle weakness, numbness, and loss of function. There are also vascular complications to be considered. In addition, these symptoms are also associated with **biomechanical limitations**, such as limitation of trunk flexion, as well as increased leg pain during straining or in the sitting position. Hence, herniated disc causes instability of the injured FSU, and an increase in ROM and NZ. These conditions lead to higher stresses acting on the facet joints and excessive swelling of the annulus fibrosus: the intervertebral disc will act as a deflated tire, thus greatly accelerating the disc degeneration process [4, 75, 79, 82, 90, 91].

The **clinical treatment** of patients with symptomatic herniated discs often involves nonoperative management. **Conservative treatments** appear to be the primary choice, involving a multi-modal approach with anti-inflammatory drugs (local corticosteroid injections), education and physiotherapy [4, 75, 79, 82, 90, 91]. On the other hand, **surgical treatments** may involve different procedures which will be discussed in the next sections.

3.2.2 Endplate in Disc Degeneration Disease

The cartilaginous endplate is the **interface** between the vertebral body and the disc. Its purpose is to maintain the structural integrity of the IVD, ensuring the normal nutrient transport mechanism, thus enabling the normal physiological functioning of the structure. Furthermore, it acts as not only a **physical/structural interface** but also as a mechanical interface between disc and vertebra, since it facilitates load distribution between the two components. The association between endplate morphology and disc degeneration remains **unclear**. However, it is possible to state that most likely the endplate plays a crucial role in the initiating mechanism of disc degeneration. Indeed, several studies have been done on the possible injuries that may involve the endplate[2, 25, 27, 92, 93].

There are four different types of lesions extrapolated from [2] (see Figure 3.4):

1. **Schmorl's nodes**. The endplate injury or fracture is directly caused by the NP pushing through the endplate until it is destroyed. This injury involves only the center of the endplate and usually happens in the lumbar area, without invasion of the spinal canal. Schmorl's hernia is named after George Schmorl, who introduced the concept that the endplate irregularity may be important in the evaluation of disc degeneration.
2. **Rupture of the endplate junction**. The endplate junction is destroyed by herniation, where the NP forces its way through the AF, thus causing the sequestration and leading to a complete rupture of the annulus-endplate bond.
3. **Mid-span rupture**. The nucleus pulposus extrudes out by rupturing through the annulus breaking it in half, maintaining the junctions with the endplate.
4. **Calcification**. Endplate calcification occurs and affects the entire plate

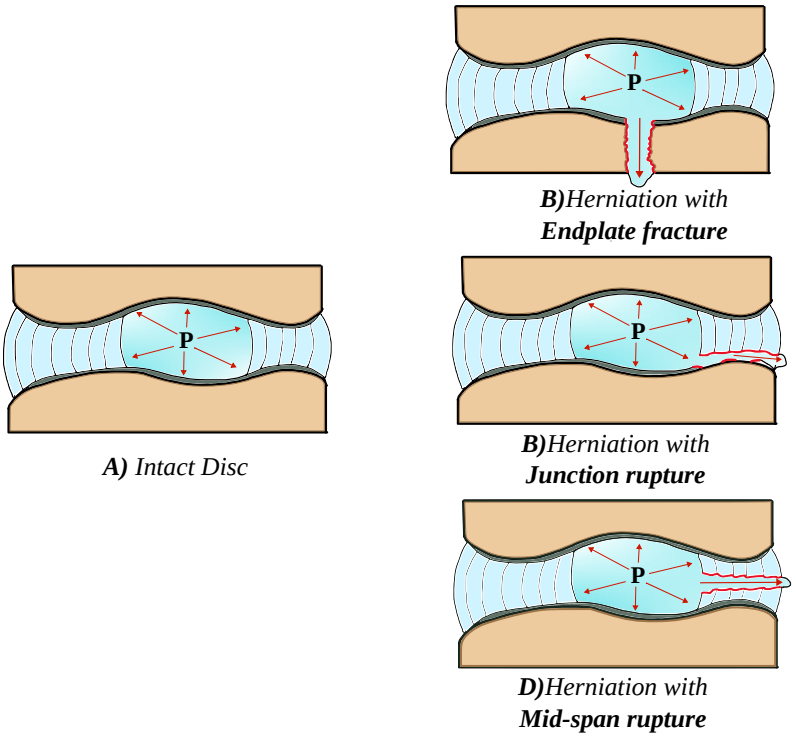

Figure 3.4. *© Endplate role in disc herniation [2]:* ***A)*** *Intact disc;* ***B)*** *Endplate fracture;* ***C)*** *Endplate junction rupture;* ***D)*** *Mid-span rupture.*

3.2.3 Other spinal diseases

Spondylosis is a spinal pathological situation that afflicts the endplates and facet joints. Hypertrophic changes in these two structures unfortunately occur, which are called **Osteophytes**. Osteophytes are outgrowths of bone, growing along the vertebral body or along the capsular insertion of the facet joints. They are usually asymptomatic, but when associated with other conditions such as osteoarthritis, wear and inflammation, they can cause stiffening with decreased spinal mobility, and possibly even pain [2, 4, 80, 94].

Another pathology that can afflict the spine is **Spondylolisthesis**, which consists of forward slippage of one vertebra relative to the other, leading to misalignment and several clinical consequences. Surgical techniques are often adopted to treat this pathology. Spondylolisthesis can be classified into **degrees** according to the severity of the pathology. The classification is based on the **sliding percentage** of the vertebra as follows [2, 4, 80, 94] (see Figure 3.5):

- ➢ **Grade I**. From 0% to 25%.
- ➢ **Grade II**. From 25% to 50%.

➢ **Grade III**. From 50% to 75%.

➢ **Grade IV**. From 75% to 100%.

➢ **Spondyloptosis**. It is defined as L5 vertebra sliding in with the entire vertebral body of L5 lying below the top of S1. It is the most severe degree of possible slippage.

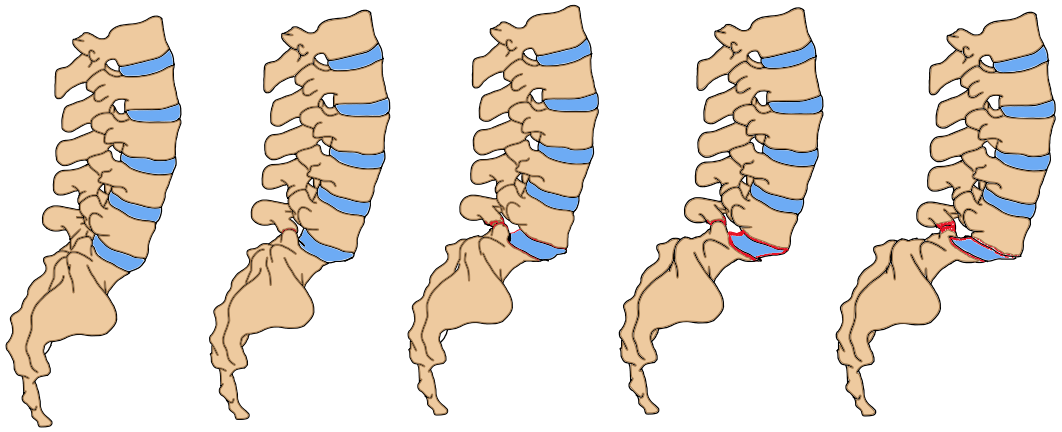

Figure 3.5. *© Classification of Spondylolisthesis according to the severity of the pathology.*

Spinal fractures are very common especially at the thoracolumbar junction. In 2013 a classification system was developed by the AOSpine Spinal Cord Injury and Trauma Knowledge Forum, an international group of academic spine surgeons, called **AOSpine thoracolumbar spine injury classification system** (Vaccaro et al., 2013). This system provided the following classification of fracture injuries into three types [2, 4, 80, 94, 95] (see Figure 3.6):

➢ **Type A**. Compression injuries of the anterior elements of the spine, i.e., vertebral body and/or disc. Injuries are caused by failure under axial compression. There are five other sub-categories of subtype A0, A1, A2, A3, and A4 differentiated into minor fractures, or fractures involving or not the endplates, or whether they involve the posterior wall, or combination of all these.

➢ **Type B**. Posterior tension band injuries if they involve the PLC and posterior arch, and anterior tension band injuries if they involve the ALL and anterior disc, but do not include translations. Posterior band injuries come from a flexion distraction injury mechanism, while anterior band injuries come from a hyperextension distraction mechanism. The subtypes of type B1, B2, and B3

injuries differ according to the destruction zone whether that is anterior, or posterior.

➢ **Type C**. Translational injuries involve dislocation or translational displacement beyond the physiological range of the spinal cranial and caudal parts in any plane, including to destruction of the anterior and posterior tension bands.

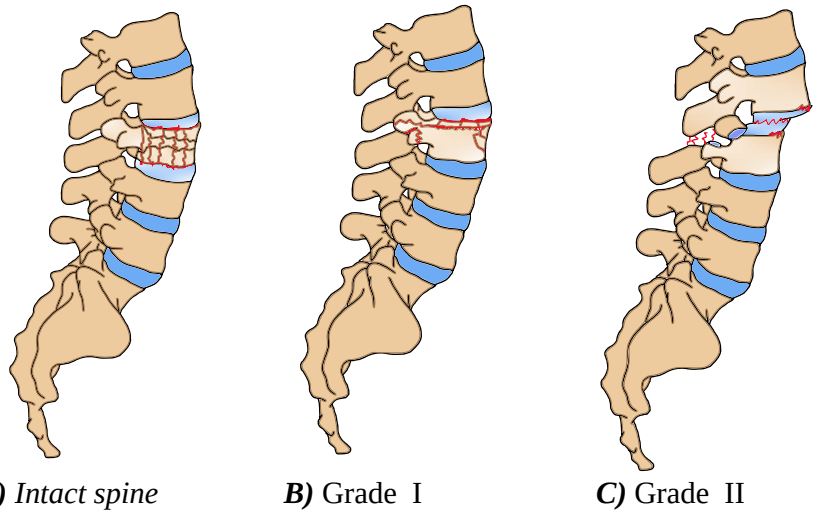

A) *Intact spine* ***B)*** Grade I ***C)*** Grade II

Figure 3.6. *© Fracture injury classification according to the AOSpine thoracolumbar spine injury classification system.*

In addition, lesions are also classified under **neurological status** [2, 4, 80, 94, 95]:

➢ **N0**: Neurologically intact

➢ **N1**: Transient neurological deficit, which is no longer present

➢ **N2**: Symptoms or signs of radiculopathy

➢ **N3**: Incomplete injury of the spinal cord or cauda equina

➢ **N4**: Complete spinal cord injury

➢ **Nx**: Undeterminable neurological status.

The **treatment** of fracture injuries can differ depending on the type of injury, and generally involves spinal fixation or spinal fusion by using bone graft. However, the goal of any treatment is to ensure **stabilization** of the spinal segment, reduce the fracture, decompress neural elements with patients with neurological deficits, and restore sagittal alignment.

Lastly, **scoliosis** is a condition that often afflicts even younger patients, which involve the appearance of a spinal curvature in the coronal plane which is normally straight. The severity of scoliosis, as well as the choice of possible clinical treatment, whether conservative or surgical, depends on the degree of scoliosis as measured by Cobb's method. Figure 3.7 shows how the Cobb's angle is measured.

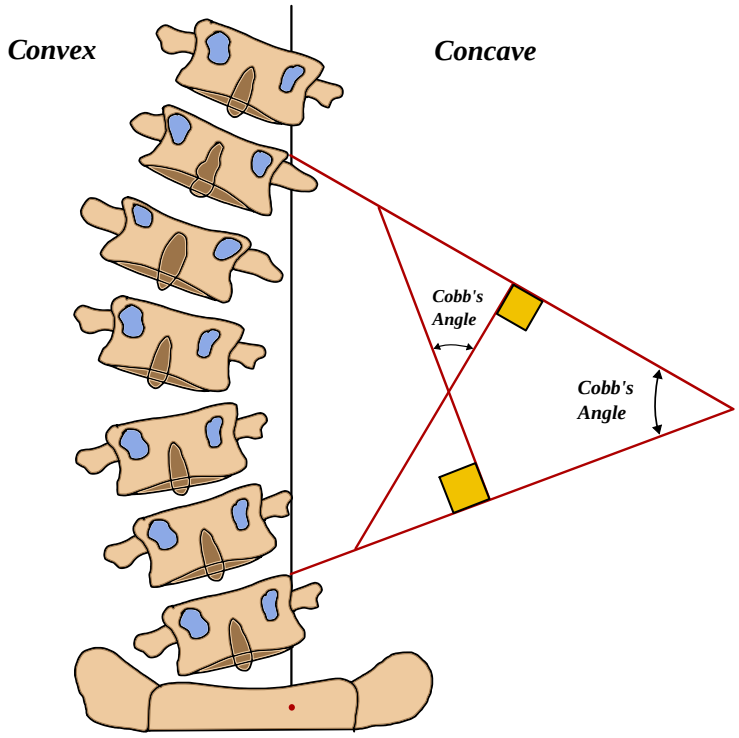

Figure 3.7. *© Measurements method of the Cobb's angle.*

Two lines are drawn in the coronal plane. One line is tangent to the plane of the more inclined upper vertebra; meanwhile, the other tangent to the more inclined lower vertebra, the angle formed by these two lines will be Cobb's angle [2, 4, 96]. Table 3.2 shows the classification of scoliosis severity according to the degree measured.

Table 3.2. *Clinical treatment based on Cobb's angle.*

Cobb's Angle	Clinical Treatment
<5°	Absence of scoliosis
5°-20°	Scoliosis with a low risk of evolution
20°-40°	Evolved but contained scoliosis, treatable by non-crucial medical treatment
>40°	Severe scoliosis, necessarily treated with surgery

3.3 Surgical Treatments

Spinal fixation and **fusion surgeries** are the gold standard for surgical treatment of spinal pathology. The main goal of these procedures is to **restore spinal stability**, now disrupted by pathology, and to interrupt the degenerative process and provide pain relief [2, 4, 97–101]. Figure 3.8 shows a schematic representation of these two surgical treatments for one FSU.

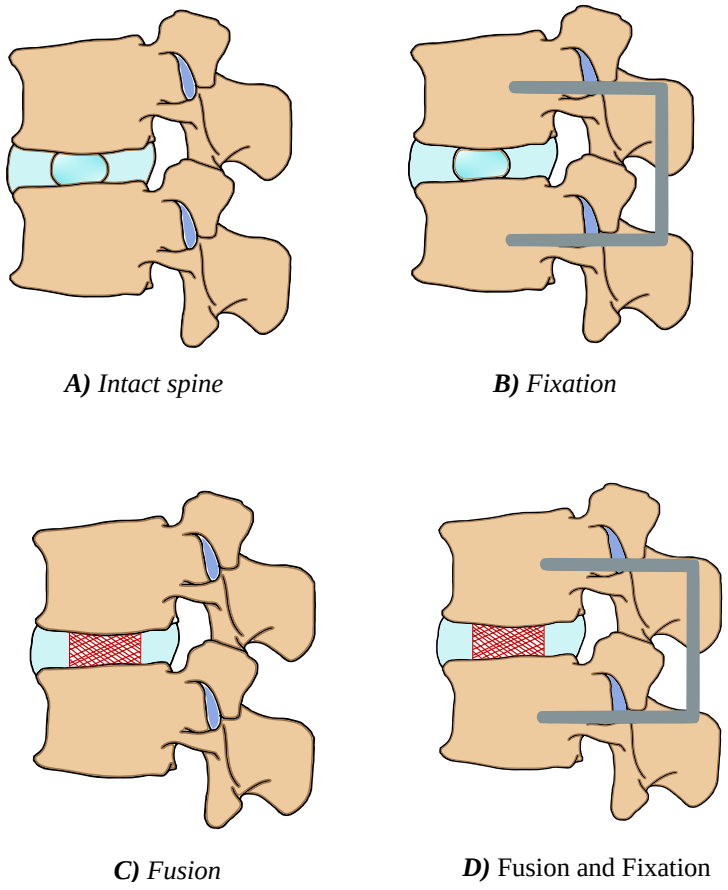

Figure 3.8. *© The main surgical techniques [2]:* ***A)*** *FSU intact,* ***B)*** *FSU treated with fixation;* ***C)*** *FSU treated with fusion;* ***D)*** *FSU treated with fixation and fusion.*

3.3.1 Spinal Fixation

Spinal fixation can be done through different anchoring components such as **pedicle screws** that are connected to longitudinal and transverse elements, such as plates or rods or connectors [2, 4, 97–101], as reported in Figure 3.9.

Pedicle screw fixation was developed in 1963 by Roy-Camille. Screws can be placed via pilot hole and threading, in the posterior vertebral section through minimally invasive techniques involving facet joint cleaning, soft tissue removal and

then pedicle wall inspection. **Screw placement** is crucial, as incorrect placement can cause transient or permanent injury, such as root pain, weakness or loss of sensation, paralysis, and severe vascular damage. Indeed, screw placement is always accompanied by an intraoperative radiographic control [2, 4, 97–101].

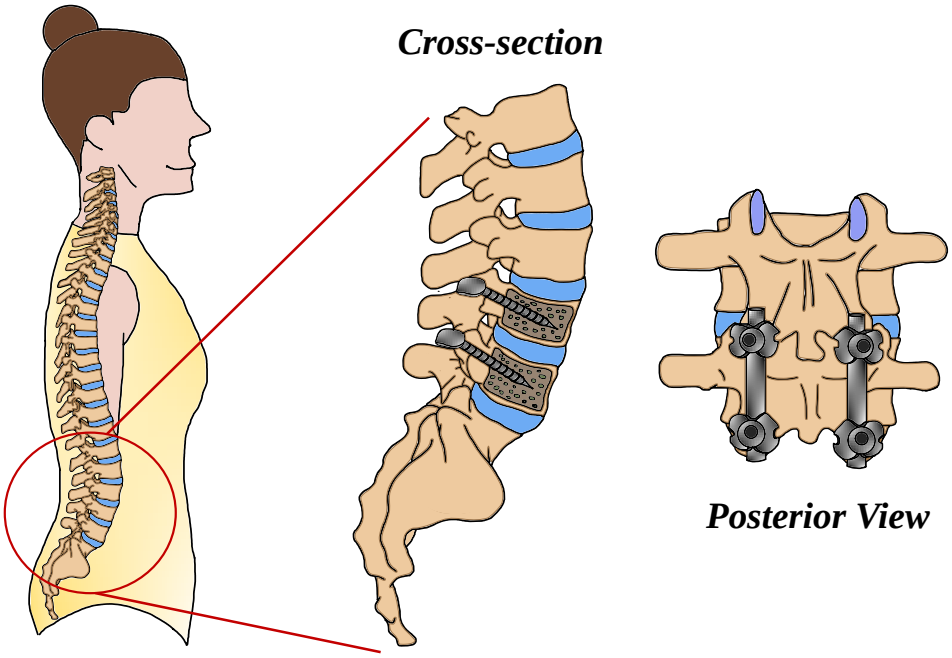

Figure 3.9. *© Spinal fixation surgery with road and screws in the lumbar area.*

At the **biomechanical level**, spinal fixation offers immediate stability to the spine by rigidly immobilizing the degenerated vertebrae. However, the procedure increases the spinal stiffness, restricting the natural kinematic movement of adjacent vertebral segments, also altering their load distribution and overall biomechanics. In vitro flexibility tests on human specimens have shown how the insertion of rigid instrumentation can provide multidirectional stability to the involved spinal tracts. Further, the **stabilization effect** is conferred and improved over time by the processes of bone remodeling, as new bone tissue is formed around the implants over time, helping to provide greater spinal strength and fusion [2, 4, 97–101].

3.3.2 Spinal Fusion

Among the most common surgical treatments to treat degenerative disease or trauma there is ***Lumbar Interbody Fusion*** **(LIF)**. The procedure involves the insertion of an implant, cage, space or graft, into the intervertebral space created following discectomy and preparation of the endplate surfaces [2, 4, 102–107].

There are several ways by which the procedure is performed (Figure 3.10):

- ➢ **Posteriorly**, i.e., *Posterior Lumbar Interbody Fusion* (PLIF).
- ➢ **Anteriorly**, i.e., *Anterior Lumbar Interbody Fusion* (ALIF).
- ➢ **Laterally**, i.e., *Lateral Lumbar Interbody Fusion* (LLIF).
- ➢ **Obliquely**, i.e., *Oblique Lumbar Interbody Fusion* (OLIF).
- ➢ **Transversely**, i.e., *Transverse Lumbar Interbody Fusion* (TLIF).

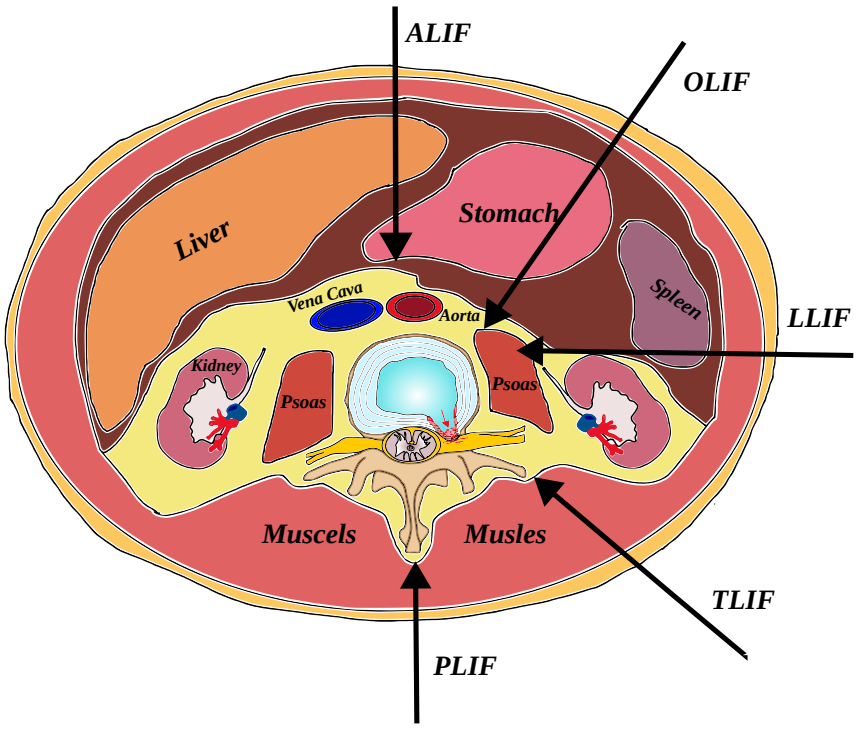

Figure 3.10. *© Lumbar interbody fusion with the different access.*

Spinal fusion is still under investigation to better understand its potential and improve approaches and the production of new cages or implants or spinal grafts. Some of these surgeries can also be performed **minimally invasively**. Anterior approaches involve surgery with anterior access to the transverse process followed by creation of retroperitoneal corridor to the lumbar spine (ALIF,OLIF,LLIF). In contrast, posterior approaches involve surgery with passage through the spinal canal and then to the interbody space (PLIF,TLIF). The posterior approach is generally the one most suitable combined with spinal fusion procedure, thus involving the insertion of screws and metal rods to make a spinal fixator, and immobilize the spinal tracts affected by the pathology [2, 4, 102–107].

The **PLIF approach** provides a good view for the surgeon of the nerve roots, restoring disc height, allowing neural decompression while keeping all posterior structures intact. The procedure is done through a single incision, which is a great advantage for the surgeon. The approach brings post-operative disadvantages. The patient may delay recovery and mobilization because of the muscle trauma associated with the approach [2, 4, 102–107].

The **TLIF approach** is used to stabilize the spine following failure of conservative treatment. This approach provides direct, unilateral access to the foraminal space, greatly reducing surgical trauma to the muscles, and preserving all ligamentous spinal structures, which allows the stabilization of the segmental biomechanics without altering its native structure. Patient recovery time with this technique is faster [2, 4, 102–107].

ALIF involves an anterior approach. Surgical planning is critical so that during surgery the surgeon avoids vital structures such as large blood vessels and the lumbar plexus. The abdominal vessels and organs should be moved to expose the disc and endplate. Once the disc has been exposed, the bony surfaces of the endplate are prepared and a partial discectomy can be performed, followed by the insertion of a spinal graft or implant (spinal cage) to restore the intervertebral disc height, which ensures the stabilization of the spinal segment biomechanics. The vascular anatomy makes ALIF appropriate for L4/L5 and L5/S1 and is limited for L2/L3 and L3/L4. Advantages concern the facility of having direct access to the disc and the effective stabilization of the spine, restoring vertebral height, lordosis, and alignment, and a single surgical incision. However, there are many contraindications, such as abdominal infections and vascular damage [2, 4, 102–107].

OLIF procedures are relatively recent procedures that have been accepted by the medical community only recently. The OLIF procedure with its lateral and oblique incision through the psoas provides direct and easier access to the spinal space without the need to dissect muscles or manipulate blood vessels and abdominal organs. Lastly, the LLIF procedure provides minimally invasive lateral access. A lateral incision is made to access the disc space and insert a disc cage. The approach is very useful being that it is minimally invasive, and it preserves the surrounding muscles and tissues [2, 4, 102–107].

3.3.3 Final remarks

Spinal fixation has been presented as the gold standard, reporting good or even excellent clinical outcomes. However, it should be emphasized that although the clinical outcomes and success of the procedure are more than satisfactory, spinal fixation unfortunately limits spinal mobility in a non-negligible way, as well as also it involves some **postoperative complications** related to overload and stiffening by the fused spinal segments. Indeed, a widely debated issue is that following spinal fixation, the patient may experience a risk of early degeneration of the adjacent segments to fused ones. It is assumed that this risk is a direct consequence to the **hypermobility** and overload required to compensate the flexibility loss of the treated segments [2, 4, 102–107]. However, research is still ongoing and there is no certainty about this, but nonetheless, this surgical procedure is and remains the therapeutic gold standard for spinal pathologies; even though, spinal fixation remains the **gold standard**.

3.4 Disc Nucleus Replacement

The previous sections have described the different strategies for treating spinal disc disease. Spinal fusion is the surgical gold standard, although as has already been pointed out, it is unable to preserve the spinal mobility and flexibility. This section focuses on the clinical treatment for disc herniation through disc nucleus replacement, a technology designed specifically to maintain physiological mobility, in contrast to spinal fusion. The following concepts are based on the comprehensive research review published by Wilke, H. J. and **Sciortino V.** (2024) [108].

3.4.1 Rationale

Several attempts have been made to embrace surgical procedures that can preserve spinal motion and keep anatomical structures intact. The first surgical technologies involved **sequestrectomy** and partial time **discectomy** [109, 110]. **Sequestrectomy** involves removal of only herniated disc fragments, which if they compress the spinal nerves can cause low back pain [111].

Such technology can be combined with the partial discectomy technique, which involves removal of the portion extruded on the outside and the portion extruded along the annulus [112, 113]. These procedures could also involve the complete

removal of the nucleus, thus defining the complete **nucleotomy** technique. Initially, all these surgical treatments create benefits for patients by removing pressure on the nerves.

However, **partial NP removal** causes not only reduction in disc height, but the disc can no longer properly distribute loads along the spinal structures, also leading to recurrence risks with **re-herniation** [114]. Instead, **complete removal** of the NP results in total collapse of the intervertebral disc height. Nevertheless, the aim of any surgical strategy is to restore the physiological and biomechanical condition of the biological tissue, while keeping the structure intact in some way.

Indeed, another alternative that has been approached is ***Nucleus Replacement (NR)***. This technique preserves the IVD structure while maintaining the fibrous annulus and the NR in place (Bao et al. 1996) aiming to make sure that **physiological movements are preserved** [97, 115–117]. The idea behind nucleus replacement, although simple and elegant, is not easily accomplished.

Figure 3.11 shows an ideal NR used to restore disk height.

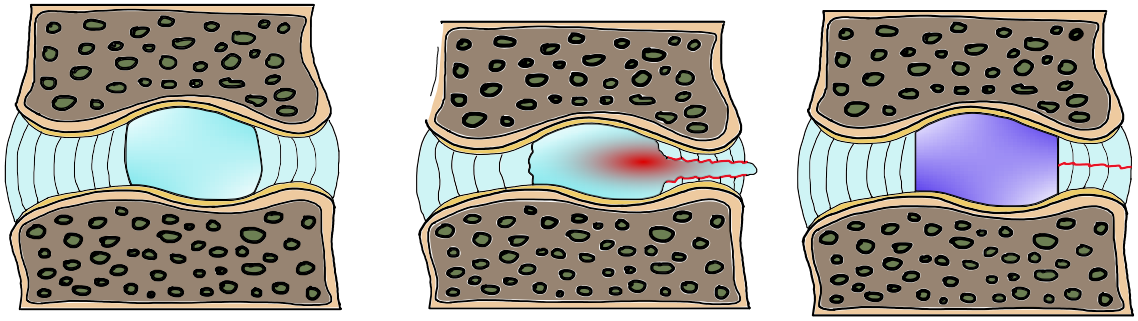

Figure 3.11. *© **A)** Healthy functional spinal segment. **B)** Herniated functional spinal segment. **C)** Functional spinal segment with an ideal NR*

Nucleus Replacement (NR) should not cause re-herniation or prolapse [101, 118, 119]. The longevity of the employed device, as well as its possible deterioration over the years, is a significant issue. However, the main problems with this treatment are potential **extrusion** and **migration**, likely caused by the implantation methodology [117, 120, 121]. Nucleus pulposus replacement represents a strategy with **huge potential**, one that could ensure the slowdown and eventual halting of the degenerative process the functional spinal segment is undergoing. NR employs nucleus prostheses which are designed to substitute the degenerated nucleus entirely. The **NR surgery** involves several steps.

Figure 3.16 shows schematically the workflow of replacing the nucleus pulposus with an example of NR, i.e. Prostethic Disc Nucleus (PDN) which will be described extensevely in the next sections.

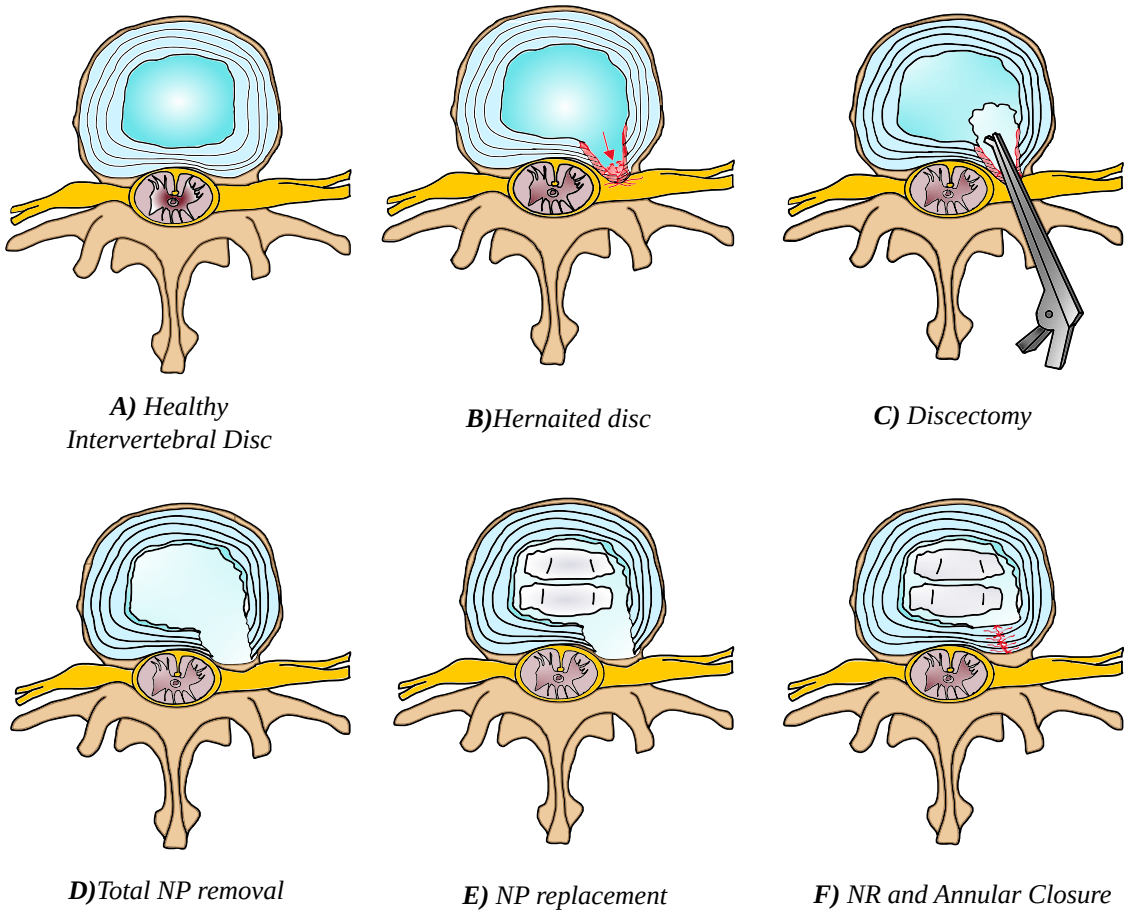

Figure 3.12. *© NR replacement and annular closure surgery: A) Healthy disc. B) Herniated disc. C) Discectomy. D) Dissected disc. E) PDN implanted. F) Annular closure.*

First, a **partial discectomy** is performed, which involves creating a hole, along the AF to reach the NP. The next step involves the removal of the damaged nucleus and consequently its replacement with the NR, which can be of different kinds as we have seen. Finally, the last step, still under investigation, is the hole closure that has been created along the AF, that it is not always performed [113, 116, 121].

Therefore, for the nucleus replacement insertion is required making a hole in the fibrous annulus. Initially, such a hole was not thought to be a problem, even if the herniation and extrusion phenomena are directly related to the lesions and tears in the fibrous annulus. Only afterwards, it was realized that the migration and extrusion phenomena of implanted NRs and re-herniation were related to this hole which was damaging the still-intact annulus. The hole represents an **escape**

channel for the NR implant, which then migrates and extrudes out via the same channel by which it was implanted. Hence, investigations are looking for techniques to **close** or **repair the annulus**, even though these treatments have never been used in clinical treatment yet.

There are several strategies and methods reported in the literature [113, 116, 121–128]:

- ➢ **Repair methods through suture**. This method involves the use of suture devices, which have received either CE mark or FDA approval to repair the annulus fibrosus.
- ➢ **Gap-filling repair methods**. This method involves the use of a patch or void filler created in a cellular component. These void fillers are mainly hydrogels, or sponges, like are collagen, hyaluronic acid, PLA.
- ➢ **Repair methods through a tissue engineering approach**. The goal behind this technique is to mimic the collagen fiber architecture of the AF, using scaffolds cultured with cells that must mimic AF cells and fiber alignment. The research is still ongoing.

Several biomechanical studies have been performed to evaluate **repair techniques** for the annulus fibrosus. Huer et al (2008) [122] and Zengerle [123] used a suturing closure technique with a combination between glue and suture to repair the annulus. They provided a mechanical testing protocol to evaluate the annulus closure methods using animal specimens, which can also be used by other researchers to pursue research on this issue. Vergroesen et al (2015) [124] proposed a biodegradable glue for annulus closure, with the aim to evaluate its feasibility and biomechanical properties. Sloan et al (2020) [125] conducted in vitro studies in sheep for a combined nucleus replacement and annulus fibrous repair approach. They demonstrated the value of the **integrated strategy.** Their histological analysis showed that the annulus fibrous preserved its morphologically and functionally.

Even today, a gold standard for the treatment of disc degeneration has not been identified owing to the **overwhelming complexity** of the disease. The aim of this paper was to create a systematic review on nucleus replacement, with the intention of collecting the existing literature so that conclusions could be drawn about the future of this clinical practice.

3.4.2 Materials and Methods

This systematic literature review was conducted pragmatically according to the following **Prisma Diagram** in Figure 3.13, by using scientific and engineering databases, i.e., Web of Science, PubMed, and Scopus taken from [108].

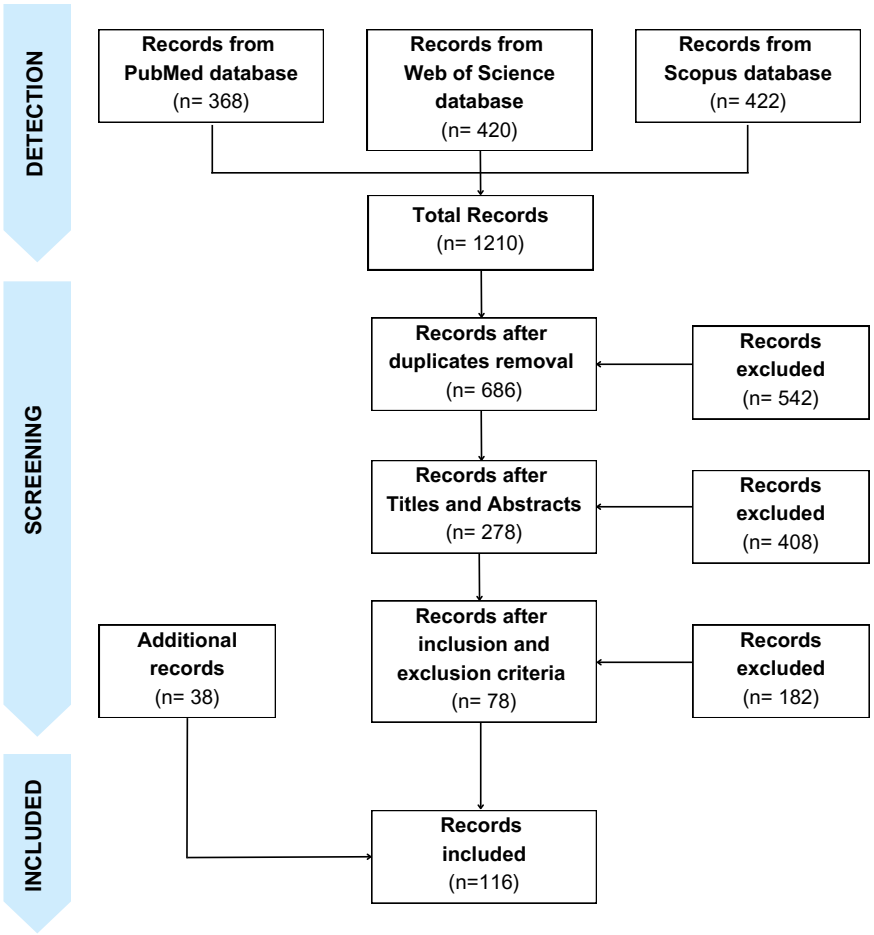

Figure 3.13. *Prisma diagram with the schematic illustration of the search strategy in literature about the disc nucleus replacements.* ***Source:*** *Wilke et al. (2024) [108].*

The search was done by **keywords**, i.e., "disc", "nucleus" and "replacement". From 1210 records selected up to November 2023, the duplicates were removed reaching 686 records. Hence, the screening was done by reading the title, and abstract and establishing inclusion/exclusion criteria.

Lastly, additional records were added from external sources, including a total of 116 records in the revision. After the records selection, the information about the NR design and development year (if detected), **biomechanical tests** conducted for its characterization, failure and/or successful implantation (if available), **clinical trial** (if conducted), or **FDA approval** (if received) or **CE mark** (if received) [108].

Table 3.3 shows the inclusion and extrusion criteria with the workflow selection followed by Wilke et al. (2024) [108].

Table 3.3. *Keywords, inclusion and exclusion criteria*

Keywords, exclusions and inclusion criteria	**N°**
(TITLE-ABS-KEY (disc) AND TITLE-ABS-KEY (nucleus) AND TITLE-ABS-KEY (replacement))	1210
After duplicates removal	686
After reading abstracts and titles	278
Inclusion criteria: English language; devices, prostheses, and biomaterials; clinical trials; biomechanical and characterization; surgical procedures.	
Exclusion criteria: No English language; histologicy; finite element models; studies with CT and MRI analysis; total disc replacement device; prevention study; articles that cannot be found.	78
Additional papers	38
Total records included in the review	116

Figure 3.14 shows a network between the items that were found in the 1210 selected records, i.e., 45 items were identified and placed in 3 cluster groups, pictured in 3 different colors, according to open-source software [108] (VOSviewer, version 1.6.19).

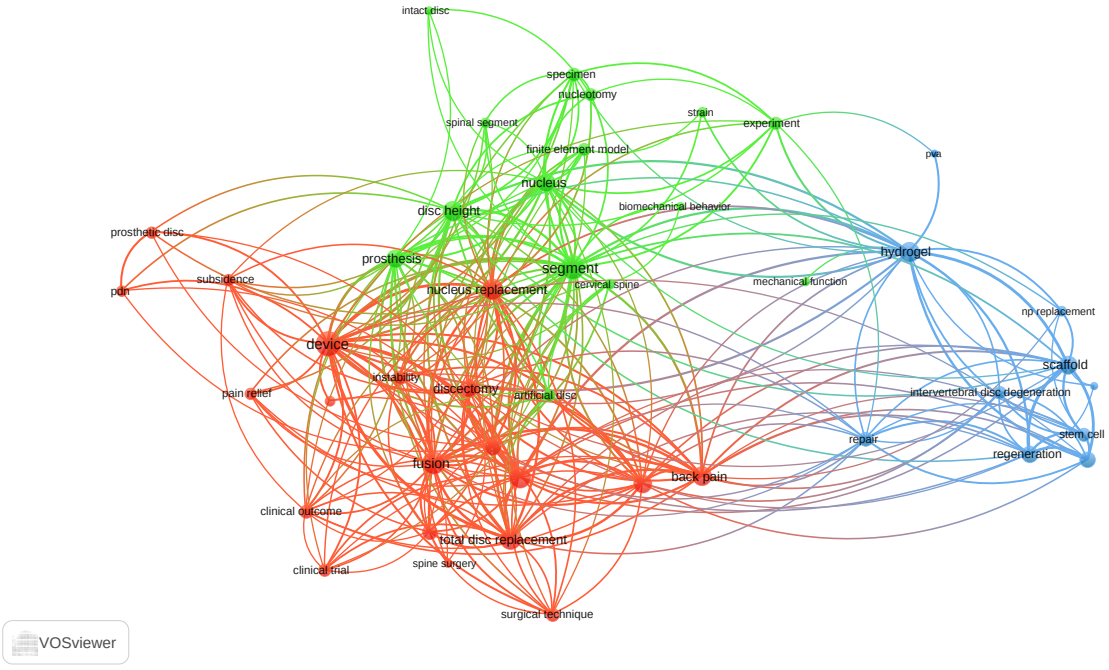

Figure 3.14. *Network visualization by Title, Abstract, Keywords showing the adequacy and adherence to the purpose.* ***Source:*** *Wilke et al. (2024) [108].*

The network was created by a **co-occurrence analysis,** which consists of a bibliographic analysis where the closeness for each pair of articles is determined by the amount of references they share, by which clustering clusters are then identified. Figure 3.14 shows how the dataset was correctly identified being focused on recurring words like PDN, hydrogel, Nucleus replacement, clinical trial, intervertebral disc degeneration, nucleotomy, and repair [108].

3.4.3 Results

The collection of all these information aimed to create a **historical overview** of the nucleus replacement, including most of the nucleus replacement that have been presented over the years in the literature.

After screening, this review included a total of 116 records identified according to the inclusion and exclusion criteria. The **first NR** in history was in 1955 by the David Cleveland, which injected PMMA into the disc space. Figure 3.15 shows the historical record of publications over the years from the initial dataset and the added papers [108, 117, 121, 129–142].

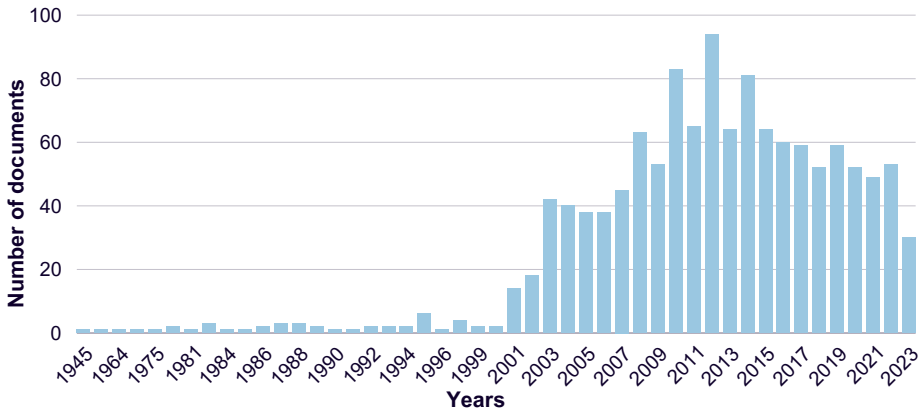

Figure 3.15. *Documents published over the years on nucleus replacements.* ***Source:*** *Wilke et al. (2024) [108]*

General fundings

Figure 3.16 shows a **Historical Timeline** from 1955 to today of nucleus pulposus replacements identified by the systematic literature search conducted.

The following is a **list** and **description** of a few of the main NRs [108, 117, 121, 129–142] (see Figure 3.17) found in literature:

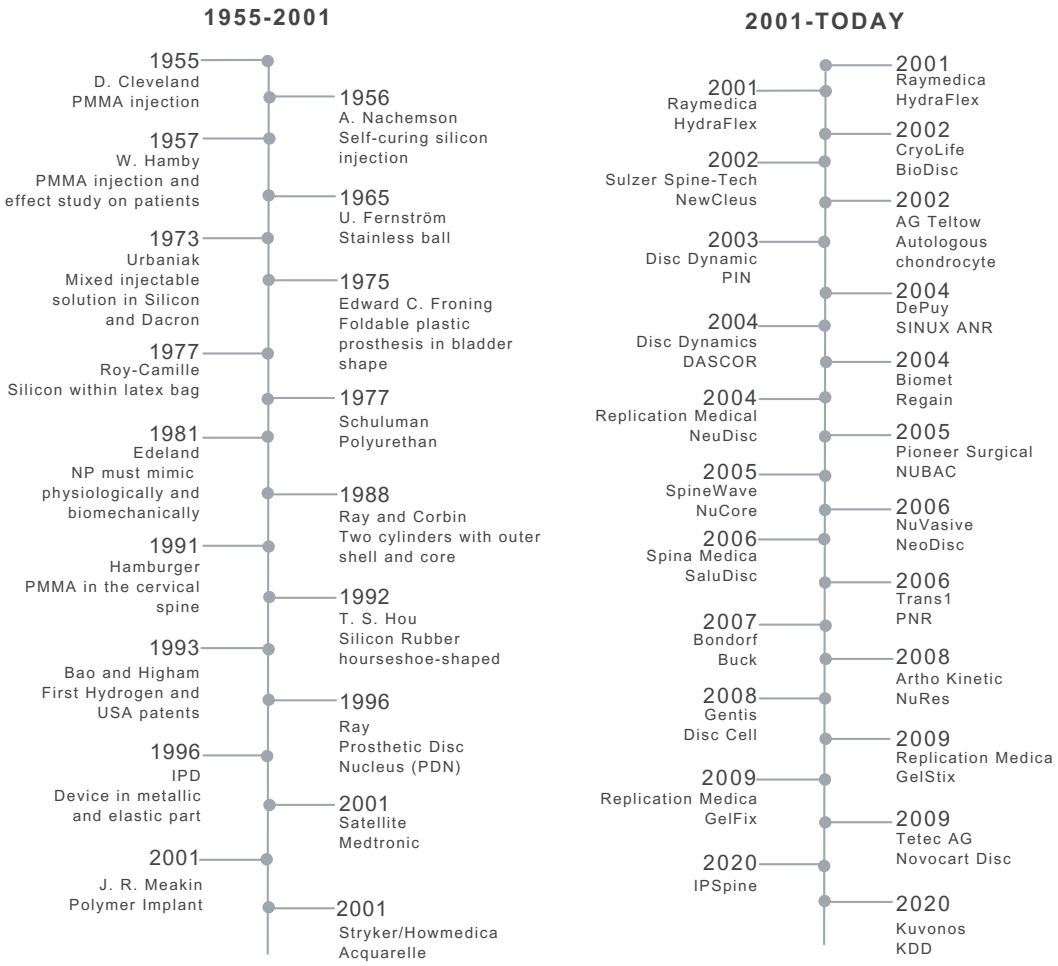

Figure 3.16. *Historical Timeline from 1955 to today of nucleus pulposus replacements identified by the systematic literature search conducted.* ***Source:*** *Wilke et al. (2024) [108]*

- **1955**: D. Cleveland was the first to clinically treat nucleus pulposus replacement. He injected Poly(methyl methacrylate) (PMMA) into 14 patients after discectomy to restore disc height and spinal stability.
- **1956**: A. Nachemson was the pioneer of the soft NR concept, by designing the first surgical procedures with self-curing silicone injected into the disc space. Even if the silicone material appears as a good substitute, there were several clinical complications that limited the clinical study success.
- **1965**: U. Fernström created the Fernstrom ball, which can be intended as the first NR. It is a metal spheres, that when implanted, it allowed the restoration in disc height ensuring the relative motion. His studies involved the implantation of the metal spheres in 125 patients. The clinical outcomes

involved extrusion, migration, and penetration of the device into both vertebrae, due to the sphere's high stiffness.

- **1981**: Edeland was the first to realize that disc NR should mimic the native tissue at the biomechanical and biological level. Indeed, he designed an NR device with viscoelastic properties capable of increasing or decreasing its water content as the load is applied, just as the disc does. Unfortunately, he never succeeded in realizing this device.
- **1988**: Ray and Corbin have created the precursor NR which has recorded the highest number of implantations in humans, with many clinical trials as well. The device involved two cylinders with a flexible and strong double spiral of polymer fibers as the outer material, and hyaluronic acid was injected inside. The design has been modified over the years to the Prostethic Nucleus Device (PDN) which will be discussed in detail in the following sections.
- **1993**: Bao and Higham represent the first ones who applied the principles conceived by Edeland. They designed a NR made of hydrogel. They decided to use a hydrogel with 70% water, aiming to mimic the physiological characteristics of the native tissue. They received U.S. patents. No information about patient implantation or clinical trials was found. The practice of using hydrogel as NR was well accepted by later scholars.
- **1996**: This year matches the year RayMedica produced PDN, a NR that involves a polyacrylonitrile-polyacrylamide (HYPAN) hydrogel core and a polyethylene (PE) envelope. Indeed, PDN is the NR more investigated. The procedure involved the implantation of the dehydrated PDN, and once water hydrated the device, the envelope controlled its swelling. Clinical outcomes resulted often in migration and extrusion. Several clinical trials have been conducted which will be discussed in the following sections. Indeed, PDN obtained the CE mark and the IDE approval from the FDA.
- **1996**: Dynamic Spine produced a mechatronic device, i.e., Intervertebral prosthetic disc (IPD), involving a metal and elastic part with springs. Biomechanical testing have shown how the device implantation led to a total destruction of the two vertebrae and of the entire intervertebral disc structure.
- **2001**: Satellite is a revisited Fernström's sphere in cobalt chrome produced by Medtronic. The device received the FDA approval in 2005, but the clinical

outcomes resulted in high risk of failure. Hence, the FDA approval was withdrawn in 2007.

- **2001**: Aquarelle is a NR produced by Stryker/Howmedica, that involved a preformed polyvinyl alcohol (PVA)-based, bullet-shaped hydrogel. The implant had viscoelastic characteristics as well as containing 80% water. The implantation involved the injection of the device in a semi-hydrated state, followed by its expansion. Several clinical trials have been conducted in Europe.
- **2002**: Newcleus is a NR composed by a preformed polymeric coiled implant of urethane polycarbonate elastomer (PCU) produced by Sulzer/Spine-Tech. Clinical trials have been done and the outcomes will be discussed in the following section.
- **2002**: NR as autologous disc chondrocyte transplantation was proposed by AG Teltow, Germany. Chondrocytes were collected and expanded in culture. The implantation involved the insertion of chondrocytes back into the disc, which remained viable and reproduced an extracellular matrix (ECM). A first clinical trial was done. With a 5-year follow-up, this clinical trial was the first involving a biological treatment for disc degeneration.
- **2004**: DASCOR is an injectable polyurethane NR produced by Disc Dynamics. The implantation involved the injection via a balloon and the in situ curing of the device. The device received the CE mark in 2007 and the IDE approval in 2006. Several clinical trials have been conducted and the outcomes will be discussed in the following sections.
- **2004**: SINUX ANR is an injectable liquid polymer of polymethylsiloxane (PMSO) NR produced by DePuy Spine within situ curing. The device received the CE mark in 2004.
- **2004**: NeuDisc is a modified polyacrylonitrile preformed NR reinforced with a Dacron mesh produced by Replication Medical. The dehydrated device is implanted, and it hydrates and expands once water is in contact with it. No information about the clinical trials conducted.
- **2004**: Regain is a one-piece metal NR composed of pyrocarbon produced by Biomet EBI Medical Systems. Biomechanical tests have been conducted,

followed by obtaining the CE mark in 2004 and performing clinical trials.

- **2005**: NuCore is an injectable protein NR involving a synthetic silk-elastic copolymer, which it was created by DNA bacterial synthesis, produced by Spine Wave. It obtained the IDE approval in 2006, followed by clinical trials which the outcomes will be discussed in the following sections.
- **2005**: NUBAC is a two-piece mechanical NR in PEEK produced by Pioneer Surgical Technology. It obtained the CE mark in 2005 and the IDE approval in 2006, followed by clinical trials which outcomes will be discussed in the following sections.
- **2007**: PNR (Percutaneus nucleus replacement) is a special NR which consist of a mechanical system with titanium screws connected to a curable material representing the nucleus, produced by TranS1. It is possible to implant the device percutaneously only in the nucleus between L5 and S1, maintaining the AF and ligaments intact. Clinical trials have been done and it obtained the CE mark in 2007.
- **2007**: BuckTSP is a NR involving a knitted titanium device produced by Bondorf and Buck Fmmb. It has a shape like a bovine nucleus pulposus and a rough surface.
- **2009**: GelStix and GelFix are NRs with shape memory hydrogel produced by Replication Medica. The devices received the CE mark in 2010, followed by clinical trials which outcomes will be discussed in the following section.
- **2009**: Novocart Disc is an injectable NR based on human albumin functionalized with maleimide and autologous disc chondrocytes. There are preclinical studies, and a combined Phase I/II study testing initial safety and efficacy of the device with a follow-up of 5 years.
- **2020**: iPSpine represent a new biological therapy, developed by a large EU-consortium (European Unions Horizon 2020 Research 52 and Innovation Program iPSpine, Grant/Award Number: 825925). This technology involves induced pluripotent stem cells (iPSCs) reprogrammed into mature spinal disc cells, aiming to treat disc degeneration.
- **Others NRs information can be found in Wilke et. al. (2024) [108]**.

Table 3.4 shows the list of the main NR features, including manufacturer, geometry

material, if clinical trials have been conducted, and whether it has received CE mark or FDA approval. Figure 3.17 represents the main NR of the design.

Table 3.4. *The main NR information about manufacture, shape, material, clinical trial, CE or IDE or FDA received.* ***Source:*** *Wilke et al. (2024) [108]*

NR	Company	Preformed	Injectable	Material	Clinical Trial	CE	FDA	IDE
PMMA	D. leveland	✗	✓	Polymer	✓	✗	✗	✗
Fernström ball	Fernström	✓	✗	Stainless steel	✓	✗	✗	✗
Poly urethane	Schulman	✗	✓	Polymer	✓	✗	✗	✗
PDN	RayMedica	✓	✗	HYPA-PE	✓	✗	✗	✓
Satellite	Medtronic	✓	✗	Chrome-Cobalt	✓	✗	✓	✗
Aquarelle	Stryker-Howmedica	✓	✗	PVA-hydrogel	✓	✗	✗	✗
Hydraflex Nucleus	RayMedica	✓	✗	Hydrogel	✓	✓	✗	✓
BioDisc	Cryolife	✗	✓	Hydrogel	✓	✓	✗	✗
Newcleus	Sulze-Spine -Tech	✗	✗	Elastomer	✓	✗	✗	✗
Chondro-transplant Disc	AG Teltow	✗	✓	Autologous disc chondrocyte	✓	✗	✗	✗
DASCOR	Disc Dynamics	✓	✓	Polymer	✓	✓	✗	✓
Sinux ANR	Sinite-DePuy Spine	✗	✓	Polymer	-	✓	✗	✗
NeuDisc	-	✗	✓	Hydrogel	✓	✗	✗	✓
Regain	EBI medical System	✓	✗	Pyrocarbon	✓	✓	✗	✗
NuCore	Spine Wave	✗	✓	Protein Polymer	✓	✗	✗	✓
NuBac	Pioneer Surgical Technology	✓	✗	PEEK	✓	✓	✗	✓
SaluDisc	Spine Medica	✗	✓	Hydrogel	-	✗	✓	✓
PNR	TranS1	✓	✗	Titanium and curable material	✓	✓	✗	✗
NeoDisc	NuVasive	✓	✗	Silicone and polyester	✓	✗	✗	✓
GelStix	Replication Medica	✗	✓	Hydrogel	✓	✓	✗	✗
GelFix	Replication Medica	✗	✓	Hydrogel	-	✓	✗	✗
Novocart Disc	Tetec AG	✗	✓	Hydrogel	✓	✗	✗	✗
BIOSTAT BIOLOGX	Spinal Restoration	✗	✓	Fibrin	✓	✗	✓	✗

Figure 3.17. *The main Nucleus replacement devices: A) Ray and Cobin. B) Bao's hydrogel. C) PDN. D) Satellite. E) Aquarelle. F) Newcleus. G) DASCOR. H) Neudisc. I) Regain. L) NUBAC. M) PNR. N) Knitted Titanium.* ***Source:*** *Wilke et al. (2024) [108].*

Classification, Requirements and Biomechanical test

Nucleus replacement can be classified as follows [4, 8, 98, 108, 117, 121, 129–143] (see Figure 3.18).

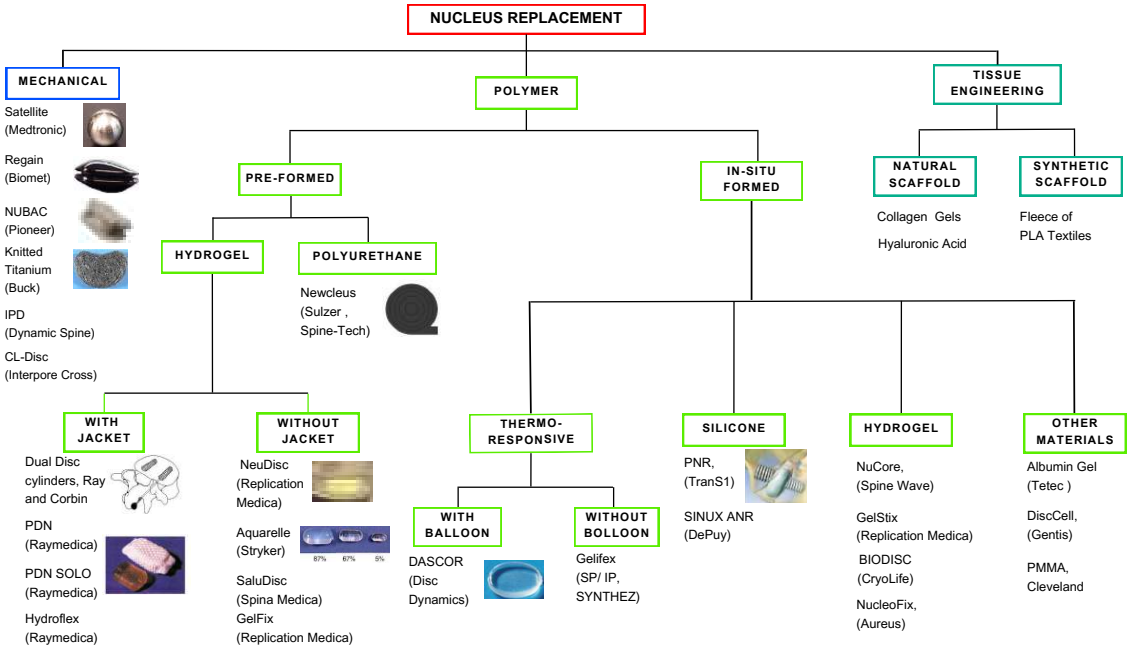

Figure 3.18. *Classification of the NR.* ***Source:*** *Wilke et al. (2024) [108].*

1. **Mechanical devices**. NR made in metallic materials can ensure biocompatibility, high mechanical strength, and durability, without any shock-absorbing capacity. At the biomechanical level, they are unable to maintain a uniform stress distribution at the endplates' surfaces. These are pre-formed devices with a predefined design and geometry. Therefore, there are the one-piece or two-piece devices, based on the components. Some examples are Satellite, Regain, and NUBAC. The implantation procedure involves the insertion directly to the disc space.

2. **Polymeric devices**. Nucleus replacement made in polymeric material are classified according to their design and implantation technique. Indeed, there are two categories of polymeric device:

   ➢ **Pre-formed polymeric devices**. These NRs are made in polyurethane or hydrogel, and they can be implanted dehydrated or partially hydrated. The implantation procedure involves a permeable balloon, or fibrous jacket. Newcleus is an example of polyurethane polymeric device. Pre-formed NRs made in hydrogel can be classified according to the presence or not of a jacket. PDN is pre-formed device with a jacket. Aquarelle, GelFix and NeuDisc are examples of pre-formed device without a jacket.

   ➢ **In-situ formed polymeric devices**. These NRs assume their shape once implanted in situ. The implantation procedure involves a minimally invasive technique to create a hole in the AF with a needle from which the biomaterials is injected, and it will polymerize assuming its shape or it will fill the disc cavity. The in-situ formed polymeric devices can be classified in four categories: thermo-responsive, with or without baloon; silicone and hydrogel. A thermo-responsive device with balloon is Dascor and without balloon is GelFix. GelStix, and NuCore are examples of hydrogel in-situ polymeric device; meanwhile PNR is a silicone one.

3. **Tissue engineering approach**. It is a powerful tool in the regeneration or healing of biological tissues, thus ensuring the recovery of their native biomechanical and physiological functions. A tissue engineering approach involve three fundamental actors: signal (for cell differentiation and growth), cell (response to signaling processes) and scaffold (acting as a structure in

which the cells can grow, differentiate, and communicate). The aim is to induce differentiation and cell growth of the proteoglycans of the NP and the collagen of the AF. These strategies can be used for repair and regeneration [97, 144–148].

To classify a device, implant, or biomaterial that can be used as nucleus replacement, it is required to satisfy **clinical and biomechanical criteria and requirements** [108, 117, 121, 129–142, 149–151]:

- ➢ The discal space available should not be less than 5mm.
- ➢ The implant should relief the patient from low back pain.
- ➢ It should be present spondylolisthesis and Schmorl's nodes.
- ➢ The implant should minimize the re-herniation and prolapse phenomena.
- ➢ The annulus fibrosus and vertebral endplates should be intact.
- ➢ The implantation of the device should preserve the adjacent FSU.
- ➢ The implantation should be reversible.
- ➢ Durability and biocompatibility of the implant.
- ➢ The implant should mimic the behaviour of the native structure.
- ➢ The implant should minimize extrusion and migration phenomena.
- ➢ The implant should ensure the alignment and stability of the FSU involved.
- ➢ The implant should be able to reestablish the normal stress state distribution.
- ➢ The stiffness should such that it avoids damage or remodeling of the endplates.

Lastly, the patient should, also, be eligible for the NR implantation: state of the endplates, body mass index (BMI), disc height, AF integrity and disc degeneration degree must be evaluated [149–151].

Besides fulfilling criteria and requirements, a NR also must have been **tested biomechanically** to evaluate its performance at the mechanical and biological level. Materials, geometry, manufacturing, and implantation technique are crucial in the **design planning**. The **performance** of the device is assessed by mechanical test. Static tests enable to establish the stiffness and yield point of the NR device; meanwhile, dynamic tests are necessary to evaluate the fatigue resistance for at

least 10,000,000 cycles without failure or, collapse, or permanent deformation of the implant. Also, other tests are required for the evaluation of **biocompatibility and degradability**, essential for the resistance in the human body environment.Once the mechanical and biological features are assessed, the **biomechanical test** must be performed as *in-vitro* test on animals, and then, human cadavers, to ensure the device's performance in physiological conditions [123, 152–154], aiming to prevent the falling.

From this systematic review, it has been possible to identify the lack of data in the existing literature related to biomechanical studies conducted on NRs. Figure 3.19 shows an example of biomechanical *in-vitro* test on human cadaver spines, obtained with three different NRs (Textile, Sinux and Collagen Type 1-Gel).

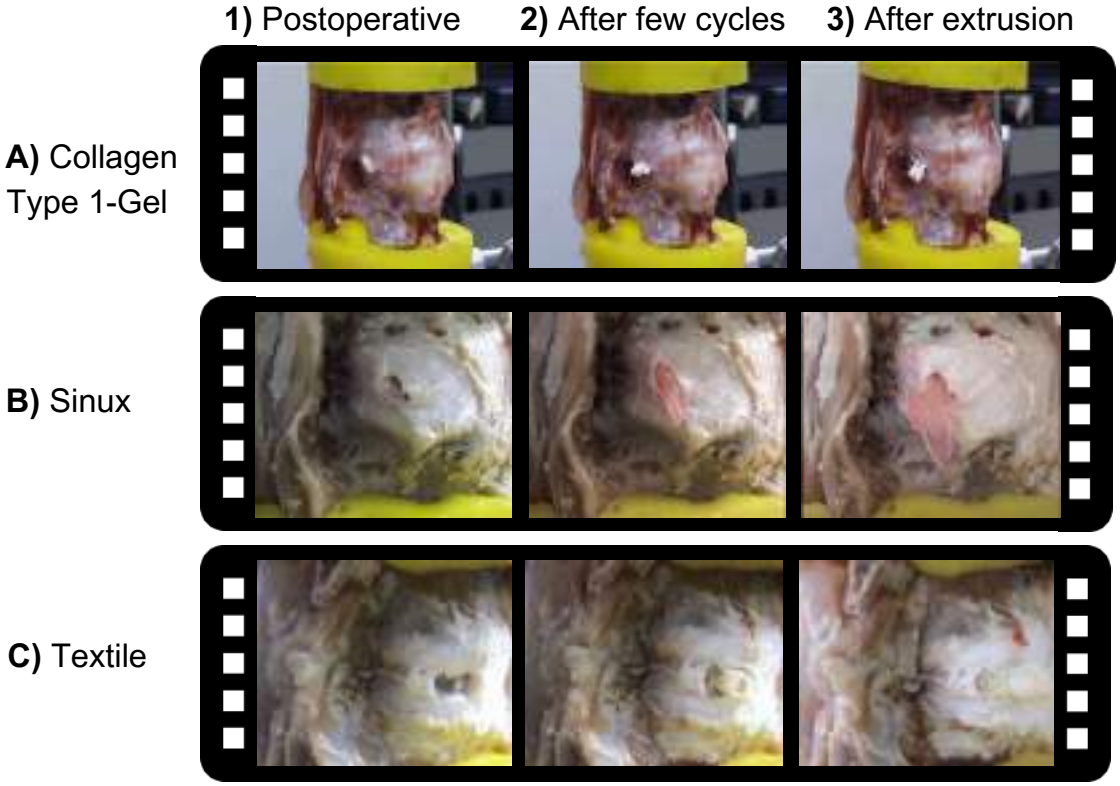

Figure 3.19. *Clips taken from videos recorded during experiments in different timestep:* ***A)*** *Lateral bending on a FSU with Collagen-Type 1-Gel (Col1-Gel) (Arthro-Kinetics) NR;* ***B)*** *Complex loads with Sinux NR;* ***C)*** *Complex loads with Textile NR.* ***Source:*** *Wilke et al. (2024) [108]*

The images were extracted from video recordings at three different time steps of a simple flexibility test (Fig 3.19C) and a complex loading test done with simultaneous combined flexion/extension, lateral bending, axial rotation and compression loads applied (Fig 3.19A-B). All experimental tests resulted in a complete extrusion of the NR implanted. Therefore, biomechanical testing is **imperative** to avoid disastrous

situations, such as extrusion and implant migration, from being experienced during clinical trials on patients who are serving as "guinea pigs" for new surgical procedures.

Clinical trials

Over the years several NRs have been authorized for clinical trials in human patients [121, 129–142, 149–151]. The clinical trials considered in this review work [108] can be classified in:

- **Short-term clinical trial** with a follow-up from 0 to 1 year.
- **Mid-term clinical trial** with a follow-up from 1 to 3 years.
- **Long-term clinical trial** with a follow-up greater than three years.

Prosthetic Nucleus Device (PDN) (RayMedica) involves a two pellet-shaped hydrogel cores that result attached within a constraining woven jacket in polyethylene with shape memory (Figure 3.17C). This implant is flexible and inelastic thank to the jacket, allowing the hydration. The coating will maintain the implant's shape under loading; meanwhile the hydrogel core is the spacer to restore the disc height and preserve flexibility. The device is implanted through a minimally invasive surgical procedure. Several biomechanical studies have been conducted on the PDN under different loading conditions. The PDN could restore ROM, NZ and disc height. The clinical trials were a short-term and long-term one and they involved 423 patients. The adverse events to the implantation procedure were manifold: endplate changes, high subsidence, and high migration and reoperation rate [108, 117, 121, 129–142, 149–151, 155, 156].

DASCOR, (Disc Dynamics) consists in an injectable polyurethane NR that cures in-situ in 12-15 minutes (Figure 3.17G). The implantation procedure includes a balloon, which is used to create the disc space for the material injection to fill the cavity created by the discectomy, involving static and dynamic test to assess the stiffness, shear properties, fatigue resistance and strength, and durability. Biomechanical *in-vitro* testing involved flexibility tests on human cadaveric spines. From these experimental tests, DASCOR maintains the ROM and restores the disc height, without extrusion, endplate damage, or vertebral fractures. The clinical trials were long-term and mid-term one. The adverse events to the implantation procedure were manifold: endplate changes, migration, subsidence and device explant [108, 117, 121, 129–142, 149–151].

NUBAC, (Pioneer Surgical Technology) is a mechanical nucleus replacement in polyetheretherketone (PEEK) (Figure 3.17L). The device presents three components: an internal ball/socket and two endplates. Mechanical testing has been conducted to evaluate resistance, biodurability and biocompatibility. Biomechanical dynamic tests have been performed to evaluate fatigue characteristics and to assess the extrusion risk. NUBAC was able to restore the disc height, ROM, and to maintain flexibility, without extrusion or damage to the endplate or bone. The clinical trials were short-mid and long-term one. The adverse events to the implantation procedure were manifold: endplate changes, migration, subsidence and device extrusion [108, 117, 121, 129–142, 149–151].

Newcleus (Sulzer Medica) is an in-situ nucleus replacement in polycarbonate urethane (PCU) with a spiral shape that is created in situ (Figure 3.17I). Static and fatigue mechanical tests have been performed to evaluate fatigue, strength and the wear resistance, followed by flexibility tests. The device was not always able to maintain flexibility and its implantation led to endplate deformation without migration. It was conducted only one short-term clinical trial with five patients. Owing the absence of data, it was not possible to evaluate the performance of the device.

NuCore (Spine Wave) is an injectable disc nucleus replacement manufactured by Spine Wave. It is a non-hydrogel nucleus rDNA-based synthetic protein copolymer that is composed of silk and elastin. It is an NR that cures in situ forming a very resistant, adhesive, and durable hydrogel. Once the NR is cured, this injected material is very resistant to extrusion phenomena thanks to the adhesive properties. This was tested in pre-clinical bench and animal testing. The first feasibility pilot study involved 14 patients for a mid-term clinical trial, with a follow-up at 6 and 12 weeks and 6, 12, and 24 months after surgery. The clinical data showed endplate changes of 64.3%. No migration or extrusions were observed. The clinical trial showed how NuCore seems to provide a restoration of the disc height and to protect the disc from collapse and degenerative cascade events. There was also no clinical evidence of any immunologic reaction to the NuCore material.

Others nucleus replacements clinical trials:

- **Satellite** involved only one short-term clinical trial with four patients between 2007 and 2009, with catastrophic results, i.e., loss of disc height and sphere subsidence (Figure 3.17D).

- **PNR** involved a long-term clinical trial with 26 patients, with catastrophic results, i.e., reoperation rate of 57.7% and silicon migration (Figure 3.17M).
- **GelStix** involved a small clinical trial with 29 patients between 2013 and 2017. After a follow-up of 12 months, 86.2% of the patients were satisfied from the the procedure. GelStix leads to clear improvements with pian relief, contributing to disc height restoration.
- **NOVOCART Disc plus** involved a clinical trial in a multicenter, randomized, controlled phase I/II study with 120 adult patients to evaluate the applicability, safety and efficacy in repairing herniated discs and adjacent degenerated discs.

3.4.4 Future Horizons and final remarks

Previous sections have covered a comprehensive review on all past nucleus replacements and their associated failures with clinical trials. The future of nucleus replacement procedure is the **Regenerative medicine and tissue engineering techniques.** These advanced technologies represent the new frontiers of bioengineering. the idea behind nucleus replacement is to mimic the native functions of the tissue and to avoid damage to structures that are still intact [97, 108, 144–148].

In tissue engineering, **Scaffolds** allow the manufacture of devices that mimic the structure and properties of the intervertebral disc, providing structural support. The scaffolds may be made from engineered biomimetic materials or biodegradable materials. Scaffolds in biomimetic materials promote integration within surrounding tissues, and allow the growth and proliferation of differentiated cells, whose purpose is to promote regeneration of damaged tissue [97, 108, 144–148].

Biodegradable biomaterial scaffolds promote tissue regeneration by releasing growth factors, like IGF-1 and bone morphogenetic protein (BMP), which influence IVD metabolism positively, stimulating proteoglycan synthesis and improving disc height and collagen production. The combined action of biodegradable materials with growth factors, as they biodegrade over time, emerges as a promising strategy for replacing damaged discs, providing a more durable and biologically consistent solution [97, 108, 144–148].

In addition, **regenerative medicine technologies,** such as cell therapy, may also be fundamental in promoting intervertebral disc healing. Such examples include the implantation of autologous chondrocytes and stem cells to treat disc degeneration.

However, many challenges remain, including fully understanding the pathogenesis of disc degeneration and optimizing biochemical signals to induce cells to differentiate properly [97, 108, 144–148].

This systematic review created an extensive **historical overview**, which had never been done before, as it included several aspects about the topic, exploring in depth the biomechanical aspects and clinical trials conducted over the years.

Disc nucleus replacement has been proposed as a treatment for degenerative disc disease for more than 70 years, demonstrating continuous evolution, although it has encountered significant challenges in clinical practice. Nucleus replacement is intended to restore the intervertebral disc's function while maintaining its mobility and height. However, in all the clinical trials that have been analyzed over different nucleus replacement, numerous problems have been experienced that have consistently obstructed the technology from becoming a clinical gold standard. The leading nucleus replacement devices, such as the PDN (Raymedica), DASCOR (Disc Dynamic), have shown high rates of **surgical complications,** including migration and implant extrusion. Although many of these devices have received approvals from regulatory entities like FDA or CE mark, several NR have been subsequently withdrawn from the market due to unsuccessful clinical outcomes [108].

Hence, it is still unknown the biological and mechanical processes that regulate disc degeneration, despite technological advances. This makes it difficult to develop solutions which are either effective, safe and durable. Tissue regeneration, as already discussed, is an exciting prospect, but its clinical application is complex and requires further research.

In conclusion, the coming future of disc nucleus replacement appears **promising**, driven by technological developments and improvements in clinical outcomes and yet still far from being a permanent clinical solution. However, further research efforts to overcome the current biomechanical and biological challenges is critical, aiming to ensure the long-term safety and efficacy of these techniques for the benefit of patients.

Chapter 4

Experimental tests on human cadavers and bovine tails, and modeling

4.1 Biomechanical behaviour modeling

Mathematical models may be used to describe the biomechanics phenomena which the IVD exhibit, thereby succeeding in simplifying the inherent complexity of this biological tissue [73, 157–165]. There are two kinds of modeling:

- **Numerical models**, usually the finite element ones, which will be extensively discussed in chapter 5.
- **Analytical model**s, which include mathematical modeling representing the disc geometry in a simplified manner as if it is a compact structure, involving few boundary conditions and assumptions.

The IVD has a **biphasic structure**, where the NP represents the fluid part by absorbing shocks and distributing loads among the spinal components, while the AF represents the solid part by providing stability and strength. At the microstructural level, the woven network of AF collagen fibers and the high-water content, along with the gel-like consistency of NP, are responsible for the intermediate viscoelastic behavior between solid and fluid of IVD. The mechanical interactions between NP and AF complicate the experimental studies in measuring and analyzing the load distribution, strength and deformation of the disc. Hence, there is a need to model the mechanical response of the IVD through **mathematical models**, which can provide a suitable method to simulate and understand the disc's biomechanical response in a **reproducible manner**. Indeed, analytical models simplify the geometry and composition of the disc, portrayed as a compact structure [73, 157–165].

Biomechanical behavior modeling of the IVD through mathematical models can be crucial in clinical practice and in the design of medical devices, suitable to replace the degenerated IVD. Any mathematical model made has limitations, as assumptions and simplifications are always done to simulate the real behaviors of the analyzed structures. However, although several limitations exist, the models can still be capable to simulate the real behaviors of biological structures in physiological and pathological situations. The main point is that any model must obviously be validated through experimental data. Multi-phase models such as poroelastic models have been exploited to describe the viscoelastic character of IVD, additionally including osmotic effects [73, 157–165]. However, this thesis project focused on mathematical modeling of the IVD's viscoelastic behavior by using rheological models, power laws and fractional calculus, as will be presented in the next sections of this chapter.

The focus of this chapter will be analytical modeling of disc biomechanics, where some notions on **viscoelasticity** (creep, stress relaxation, and rheological models) will be provided first, followed an introduction about the **fractional calculus tool**. Lastly, a detailed description of three original research articles, about the intervertebral disc modeling based on experiment data from in vitro tests performed on bovine and human specimens, will be included in the following chapter.

4.1.1 Viscoelasticity: Creep and Stress Relaxation

Viscoelasticity is a physical and mechanical phenomenon directly dependent on the molecular and microstructural nature of the structure. Biological materials exhibit **creep** and **relaxation phenomena**. If subjected to a constant load, these materials possess a time-dependent strain non-linear response, i.e., creep, whereas if subjected to a constant strain, they have a time-dependent stress non-linear response, i.e., relaxation. The non-linear mechanical response is associated with important dissipative phenomena. **Advanced mathematical models** are needed to adequately and efficiently describe the time-dependent properties in viscoelastic materials [43, 71–73, 157–165].

First, a viscoelastic material presents an **intermediate** mechanical response between solid and liquid . Hence, it is useful to remember that the mechanical response of an elastic spring is described by **Hooke's law** as follows [43, 71–73]:

$$\sigma = E\varepsilon \tag{4.1}$$

Where E is the **Young Modulus** (which is a force per unit area). It is evident that there is a linear and constant relationship over time relationship between stress and strain. Meanwhile, the mechanical response of a viscous liquid represented by a viscous dashpot is described by **Netwon-Petroff's law** as follows [43, 71–73]:

$$\sigma = \eta\dot{\varepsilon} \tag{4.2}$$

Where η is **a** (which is a pressure for second). Here there is a linear dependence between stress and strain and proportional to the strain time derivative.

Biological tissues are never subjected to the same constant strain and deformation value instant by instant, but this will depend by the physiological activities. The Boltzmann superposition principle of effects can be used to describe the application of an arbitrary tension or deformation values during a creep or stress relaxation tests. This principle allows to investigate an overall phenomenon as the sum of the individual effects contributing to its realization [43, 71–73].

If a deformation history is considered, the following considerations can be done:

- For $t \leq 0$ no deformation has been applied.
- For $t > 0$ the deformation is non-zero.

The strain will be a function of time. Indeed, for each time instant the applied strain will be different. Figure 4.1 shows the strain increment corresponding to the time interval between τ and $\tau + \Delta\tau$:

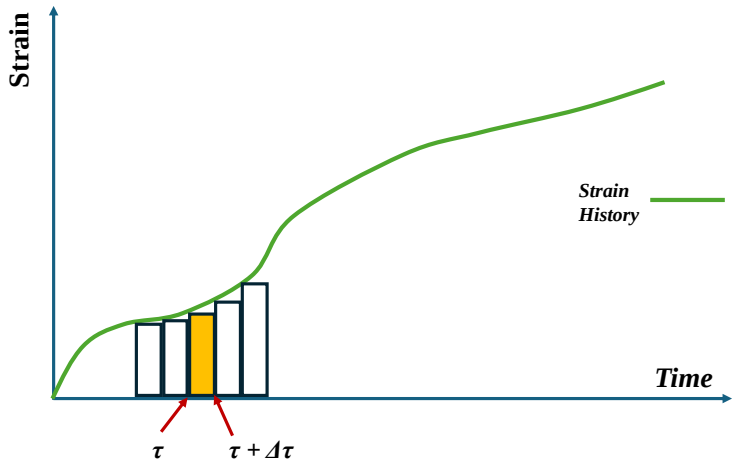

Figure 4.1. *Arbitrary strain history applied.*

By considering this deformation history, the function can be split into many

deformation intervals corresponding to successive time steps. The deformation history is seen as the sum of all these increments:

$$\varepsilon(t) = \varepsilon_0 + \varepsilon_1 + \dots \tag{4.3}$$

Where ε_0 is at the initial instant t_0, ε_1 is at the next instant time t_1 and thus on until the last moment of generic τ. Hence, through the linear formulation and the **Boltzmann principle** [43, 71–73], it is possible to identify the corresponding tension history as:

$$\sigma(t) = \varepsilon_0 G(t - t_o) + \varepsilon_1 G(t - t_1) + \dots \tag{4.4}$$

Where $G(t - t_o)$ is defined as the **Relaxation function** at a specific time instant. The (4.4) can be generalized:

$$\sigma(t) = \sum_{j=0}^{n} \varepsilon_j G(t - t_j) \tag{4.5}$$

Assuming that the strain history is a continuous and derivable function, it is possible to extend the strain increment summary as the **called Boltzmann Integral** [43, 71–73]:

$$\sigma(t) = \int_0^t G(t - \tau)\, \dot{\varepsilon}(t)\, d\tau \tag{4.6}$$

Where $\dot{\varepsilon}(\tau)$ is the **strain history.** The same assumptions can be done for an applied tension history. Hence the deformation history will then result:

$$\varepsilon(t) = \int_0^t J(t - \tau)\, \dot{\sigma}(t)\, d\tau \tag{4.7}$$

Where $\dot{\sigma}(\tau)$ is the [43, 71–73]and $J(t)$ is defined as the **Creep function**.

Lastly, by calculating the **Laplace transform** (see in the Appendix) of the B**oltzmann-Volterra integral** of stress and strain (with $\sigma_0 = 0$ and $\varepsilon_0 = 0$) the fundamental relation of **Linear Hereditary** [43, 71–73] may be obtained as follows:

$$\hat{J}(s)\, \hat{G}(s) = \frac{1}{s^2} \tag{4.8}$$

4.1.2 Rheological models

Rheological models are mathematical mechanical models that describe the relationship between stress and strain in viscoelastic materials by using springs and dampers. Classic rheological models consist of the combination between dashpots and springs in series or in parallel [43, 71–73, 166–168]. The most important and employed in literature are the following (see Figure 4.2):

- ➢ **Maxwell 's model**: a spring in series with a dashpot.
- ➢ **Kelvin-Voigt's model**: a spring in parallel with a dashpot.
- ➢ **First Solid Linear Standard Model (SLS1)**: the Kelvin-Voigt's model in series with a spring.
- ➢ **Second Standard Linear Solid Model (SLS2)**: Maxwell's model in parallel with a spring.

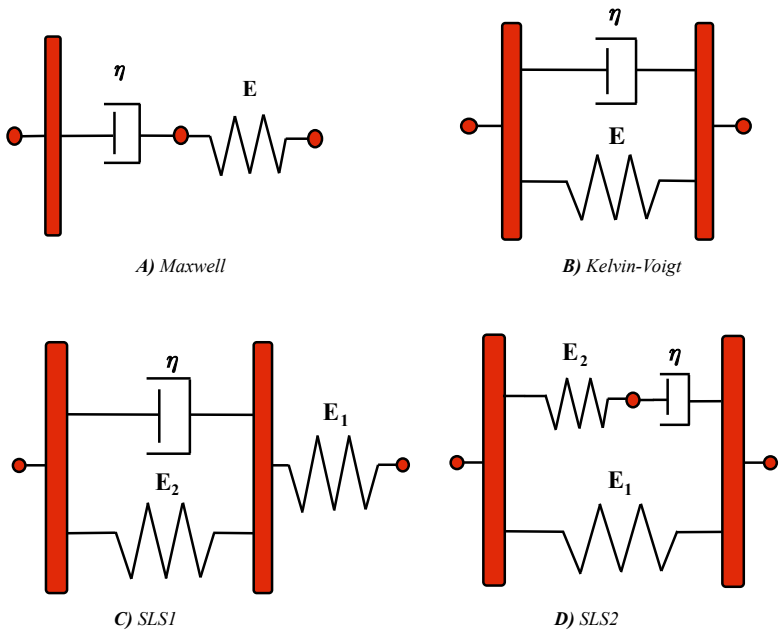

Figure 4.2. *Classical Rheological models:* ***A)*** *Maxwell;* ***B)*** *Kelvin;* ***C)*** *SLS1;* ***D)*** *SLS2.*

From here, the formulations of the governing equations for the Maxwell and Kelvin-Voigt's models are presented [43, 71–73, 166–168]. By considering the **Maxwell's model**, the series arrangement allows that the stress measured at the spring and dashpot is the same, and therefore identical to the output tension:

$$\sigma(t) = \sigma_E(t) = \sigma_\eta(t) \tag{4.9}$$

Where $\sigma_E(t)$ and $\sigma_\eta(t)$ are, respectively, the spring and the dashpot stress. The deformation will be the sum between the strain of the individual components:

$$\varepsilon(t) = \varepsilon_E(t) + \varepsilon_\eta(t) \tag{4.10}$$

Using (4.1) and (4.2) and manipulating the equation appropriately, the governing equation of the Maxwell's model is obtained as follows:

$$E\dot{\varepsilon}(t) = \frac{\sigma(t)}{\tau} + \dot{\sigma}(t) \tag{4.11}$$

Where $\tau = \frac{\eta}{E}$ is the time constant. By performing a **stress relaxation test**, the relaxation function to a constant input strain is:

$$\sigma(t) = \sigma_0 e^{-\frac{t}{\tau}} \tag{4.12}$$

Where σ_0 is the first stress value.

Maxwell's governing equation can be used only for stress relaxation, not for creep, because by performing a creep test the Maxwell's model gives a linear creep function. Hence, this model is **not a representative** model of viscoelasticity [43, 71–73, 166–168].

By considering a **Kelvin-Voigt's model**, the parallel arrangement allows that the strain measured at the spring and dashpot is the same, and therefore identical to the output strain:

$$\varepsilon(t) = \varepsilon_E(t) = \varepsilon_\eta(t) \tag{4.13}$$

Where $\varepsilon_E(t)$ and $\varepsilon_\eta(t)$ are, respectively, the spring and dashpot strain. The stress will be the sum of the stress individual components:

$$\sigma(t) = \sigma_E(t) = \sigma_\eta(t) \tag{4.14}$$

Where $\sigma_E(t)$ and $\sigma_\eta(t)$ are, respectively, the spring and dashpot stress. Using 4.1) and (4.2) and manipulating the equation appropriately, the governing equation of the Kelvin-Voigt's model is obtained as follows:

$$\dot{\varepsilon}(t) + \frac{\varepsilon(t)}{\tau} = \frac{\dot{\sigma}(t)}{\eta} \tag{4.15}$$

Where $\tau = \frac{\eta}{E}$ is the time constant. By performing a stress relaxation test, the creep function to a constant input strain is:

$$\varepsilon(t) = \varepsilon_0 \left(1 - e^{-\frac{t}{\tau}}\right) \tag{4.16}$$

Where ε_0 is the first strain value.

Kelvin-Voigt's governing equation can be used only for creep, not for stress relaxation, because by performing a relaxation test the Kelvin-Voigt's model gives a linear relaxation function. Hence, this model is, also, **not a representative** model of viscoelasticity.The classical Kelvin and Maxwell models are **unable** to describe the mechanical behaviour of a viscoelastic material.

Instead, the **SLS1 and SLS2 models** present more **complex** governing equations, resulting in Creep and Stress Relaxation Functions able to describe the creep and relaxation tests of a viscoelastic materials [43, 71–73, 166–168].

The governing equations, respectively, for SLS1 and SLS2 are the following:

$$\sigma(t) + \frac{\eta}{E_1 + E_2}\dot{\sigma}(t) = \frac{E_1 E_2}{E_1 + E_2}\,\varepsilon(t) + \frac{E_1 \eta}{E_1 + E_2}\dot{\varepsilon}(t) \tag{4.17}$$

$$\sigma(t) + \frac{\eta}{E_2}\dot{\sigma}(t) = E_1\,\varepsilon(t) + \frac{(E_1 + E_2)\eta}{E_2}\dot{\varepsilon}(t) \tag{4.18}$$

These models are better than the previous ones, but still **do not represent** the exact mathematical formulation for viscoelastic materials. Consequently, the search for n**ew mathematical modeling** has been pursued.

4.1.3 Fractional Calculus

In recent decades, **fractional calculus** has emerged as an **excellent** mathematical tool to adopt in the engineering modeling of viscoelastic behavior or diffusive phenomena. Indeed, this mathematical tool has already been used in the bioengineering field, for example, in the investigation of lung mechanics to better understand both pulmonary physiology and pathology. The theoretical basis on fractional calculus dates back over a century, although even today the **full potential** of this mathematical tool has not yet been exploited considering the difficulty involved in using it. The description of the viscoelastic mechanical response in polymers was made by the researcher **Nutting**, who found that the link between strain-time and force-time

could be determined through a **Power law** [43, 71–73, 166–173]:

$$u = at^n F^m \tag{4.19}$$

This formulation was the beginning of the research for alternative forms to express the Creep and Relaxation functions that would best describe the viscoelastic mechanical response under imposed loading or deformation history. Hence, the C**reep and Stress Relaxation functions** were expressed as **power laws** of time[43, 71–73, 166–173]:

$$J(t) = \frac{C_\beta \, t^\beta}{\Gamma(1+\beta)} \tag{4.20}$$

$$G(t) = \frac{C_\beta \, t^{-\beta}}{\Gamma(1-\beta)} \tag{4.21}$$

Where $\Gamma(\beta)$ is the **Euler Gamma** (see Appendix) and C_β is a characteristic material constant equal to $C_\beta = E_0 {\tau_0}^\beta$ (which is a pressure for time up to beta), with E_0 representing the Young's modulus of the material, meanwhile τ_0 is a time constant.

Using (4.20) and (4.21) relations e by replacing them in the Boltzmann integral in (4.6) e (4.7), the **fractional constitutive relation** between stress and strain history are the following[43, 71–73, 166–173]:

$$\sigma(t) = \frac{E_0 {\tau_0}^\beta}{\Gamma(1-\beta)} \int_0^t (t-\tau)^{-\beta} \, \dot{\varepsilon}(t) \, d\tau = E_0 {\tau_0}^\beta \left(D_{0^+}^\beta \varepsilon\right)(t) = C_\beta \left(D_{0^+}^\beta \varepsilon\right)(t) \tag{4.22}$$

$$\varepsilon(t) = \frac{1}{G_0 \Gamma(1+\beta)} \int_0^t (t-\tau)^{\beta-1} \, \sigma(t) \, d\tau = \frac{1}{G_0 {\tau_0}^\beta} \left(I_{0^+}^\beta \sigma\right)(t) \; = \frac{1}{C_\beta} \left(I_{0^+}^\beta \sigma\right)(t) \tag{4.23}$$

Where $\left(D_{0^+}^\beta \varepsilon\right)(t)$ is the β order Fractional Caputo Derivative (see Appendix) of the strain, while $\left(I_{0^+}^\beta \sigma\right)(t)$ is the Fractional Integral of Reimann-Liouville (see Appendix).

The Boltzmann convolution integral now encloses a **power law as kernel**. Through these generalized linear laws, it is possible to characterize the viscoelastic behaviour of a biological tissue.

Hence, Scott-Blair introduced the Springpot (see Figure 4.3) as a mathematical tool to describe the intermediate behaviour between solid and fluid of a viscoelastic material by using the fractional constitutive stress-strain law [43, 71–73, 166–173].

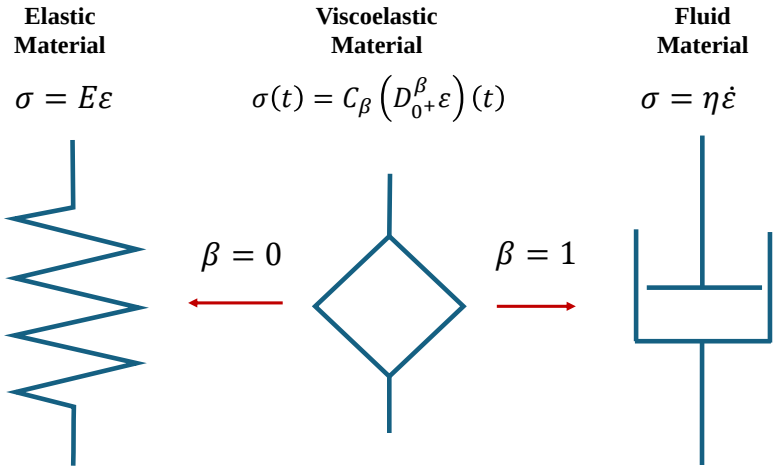

Figure 4.3. *Springpot for the viscoelastic characterization between solid and liquid.*

Indeed, the **Springpot** is built as the conjunction between a spring and a dashpot [43, 71–73, 166–173]:

- If $\beta = 0$, the mechanical response is given by Hooke's law of a spring, in which the stress depends on the zero-order derivative of the strain.
- If $\beta = 1$, the mechanical response is given by the Newton-Petroff law of a dashpot, in which stress depends on the one-order derivative of strain.
- If $0 < \beta < 1$, the mechanical response is given by the **fractional law**, in which stress is related to the fractional order β derivative of strain.

Indeed, about C_β, if $\beta = 0$, C_β will give the Young's modulus of the spring; meanwhile, if $\beta = 1$, C_β will give the viscosity of the dashpot.

Hence, the **intermediate behaviour** is described through the fractional formulation and parameters that are entirely dependent on material characteristics. The relationship between stress and deformation will be capable to incorporate the two extreme behaviors. **Fractional calculus represents** a means by which the barriers presented by complex geometries and interactions can be overcome [43, 71–73, 166–173].

4.1.4 Fractional Rheological Model

Fractional calculus can be used to generalize the classical rheological models aiming to improve their performance in modeling the viscoelastic behaviour. There are several formulations of different **fractional rheological models.** Fractional rheological models with their governing equations are the following [43, 71–73, 166–173]:

➢ **Generalized Maxwell's model**: a spring and a springpot connected in series (see Figure 4.4A). The formulation of the governing equation is made in the same of the classical Maxwell's model. Hence, the governing equation of the Generalized Maxwell's model is the following:

$$E\varepsilon\left(t\right)=\sigma\left(t\right)+\frac{E}{C_{\beta}}\left(I_{0^{+}}^{\beta}\sigma\right)\left(t\right) \tag{4.24}$$

Where $C_{\beta}=E_{0}{\tau_{0}}^{\beta}$ is the Springpot parameter, while $\left(I_{0^{+}}^{\beta}\sigma\right)\left(t\right)$ is the Right Fractional Riemann-Liouville integral of the stress.

➢ **Generalized Kelvin-Voigt's model**: a spring and a springpot connected in parallel (see Figure 4.4B). The formulation of the governing equation is made in the same of the classical Kelvin-Voigt's model. Hence, the governing equation of the Generalized Kelvin-Voigt's model is the following:

$$\sigma\left(t\right)=E\varepsilon\left(t\right)+C_{\beta}\left(D_{0^{+}}^{\beta}\varepsilon\right)\left(t\right) \tag{4.25}$$

Where $C_{\beta}=E_{0}{\tau_{0}}^{\beta}$ is the Springpot parameter, while $\left(D_{0^{+}}^{\beta}\varepsilon\right)\left(t\right)$ is the Caputo Fractional derivative of the strain.

➢ **Generalized First and the Second Standard Linear model (SLS1 and SLS2)** (see Figure 4.4C-D).The governing equations of these two models are easily derived as has already been done for the other rheological models, they are respectively for the SLS1 and SL2 as follows:

$$\sigma(t)+\frac{C_{\beta}}{E_{1}+E_{2}}\left(D_{0^{+}}^{\beta}\sigma\right)\left(t\right)=\frac{E_{1}E_{2}}{E_{1}+E_{2}}\ \varepsilon\left(t\right)+\frac{E_{1}\eta}{E_{1}+E_{2}}\dot{\varepsilon}\left(t\right)\left(D_{0^{+}}^{\beta}\varepsilon\right)\left(t\right) \tag{4.26}$$

$$\sigma(t)+\frac{C_{\beta}}{E_{2}}\left(D_{0^{+}}^{\beta}\sigma\right)\left(t\right)=E_{1}\ \varepsilon\left(t\right)+\frac{(E_{1}+E_{2})C_{\beta}}{E_{2}}\left(D_{0^{+}}^{\beta}\varepsilon\right)\left(t\right) \tag{4.27}$$

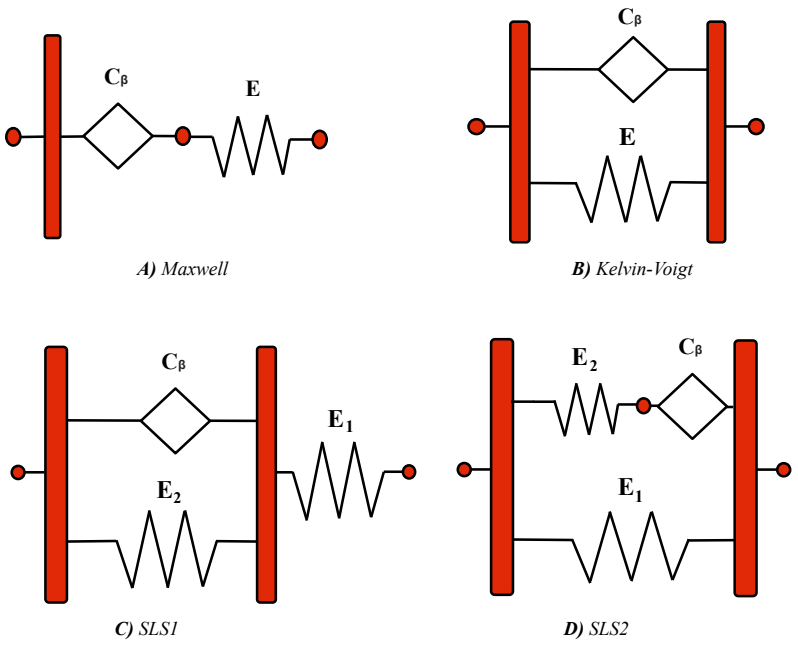

Figure 4.4. *Springpot for the viscoelastic characterization between solid and liquid.*

These fractional rheological models are **certainly better** than the classical ones, since they manage to describe the Creep and Stress Relaxation curves well, as it will be demonstrated in the next section of this chapter.

4.2 Classical Rheological models for IVD

The previous sections have described the different mathematical strategies available for the mechanical modeling. Hence, this section contains an overview of the literature on IVD modeling by using classical rheological models. All the concepts that will follow have been extracted from the research paper published by **Sciortino, V.**, et al. (2022) [174]. This paper aimed to present a small overview of IVD modeling to **emphasize** the potential and negative aspects of the current mathematical models adopted. This overview present the idea how the **fractional calculus** could be the **breakthrough** in the the IVD's mechanical modeling.

4.2.1 Review of the literature

In the literature, several **long-term experimental tests** are present that have been performed to characterize the biomechanical response of the IVD. Looking at an **analytical approach,** it is evident from the literature that classical rheological models have often been used to describe the creep or Relaxation stress curves

of the IVD. A detailed search on the state of the art in the literature involving intervertebral disc biomechanics was conducted through Scopus by a **keyword search,** i.e., rheological models, intervertebral disc, modeling. Table 4.1 summarizes the main results of the literature search, including a total of 10 articles selected according to the significance of the papers and the results obtained.

Table 4.1. *Rheological models in IVD modelling.* ***Source:*** *Sciortino et. al (2023) [174].*

Main records involved in the paper overview		
First Author	**Aim**	**Models used**
Burns M. L. [175]	Experimental test involved 8 h of Creep Test, to study the long-term response of IVD	Kelvin-Voigt, SLS1 and Burger
Keller, T. S. [176]	Experimental test involved 30 min of Creep Test to study the mechanics of lumbar spine	Kelvin-Voigt
Li, S. [177]	Experimental test involved Creep and Dynamic tests to study the IVD viscoelasticity	SLS1 and Burger
Ekstrom, L. [178]	Experimental test involved Dynamic test at different frequency/load to study the IVD viscoelasticity	SLS1 and Burger
Lu, Y. M. [179]	Experimental test to study the IVD viscoelasticity and the effect of fluid loss in the intradiscal pressure	SLS1
Campana, S. [180]	Studying the damage of intervertebral disc. The experimental protocol involved Creep Test	SLS1
Hwang, D. [181]	Experimental test involved Creep Test with pre-stress and excise phase to study the IVD viscoelasticity	SLS2
Araujo, A. R. [182]	Experimental test involved static and dynamic test to study disc's biomechanical properties.	5-parameter
Yang, X. [183]	Experimental test involved Creep Test of vibration at different frequencies to study the disc degeneration	SLS1
HeiNZ, A.[184]	Modeling the biomechanical response of the IVD	SLS1

By examining these papers, it was possible to observe that the disc's viscoelastic behaviour has not yet been accurately described. More specifically, the following are

the main advantages and disadvantages of the models used by the authors [175–184]:

1. **Kelvin-Voigt model and Maxwell model**.Some authors [175, 176] have highlighted how the Kelvin-Voigt model is not suitable for describing relaxation behavior, given the linear nature of its function, while it can instead describe the Creep curve. The same is equally true for the Maxwell model, which cannot describe creep behavior, since the linear nature of the mathematical law, while it can describe the stress relaxation one. However, although the models can potentially describe the creep and stress relaxation curves overall, there are some problems in the fitted data concerning the start and end of the creep test curve that cannot be neglected, which thus excludes them from the possible analytical models to be adopted to study the IVD biomechanical behavior.
2. **SLS1 and SLS2 models**. Many authors [175, 177–181, 183, 184] have used these equivalent models, as they are better at fitting the creep curve data. However, both models are unable to describe the upward ramp of the creep curve, thus losing a key source of information about the IVD creep response.
3. **Burger's model and multiparametric models**. These models have been used by [176, 182, 183]. The accuracy and precision of a multi-parameter model is greater than the SLS1 and SLS2 models. However, although at the analytical level multi-parameter models may do well, they lose out on interpretation of the results, as the excessive parameters make most of them meaningless, and they become a purely mathematical artifice. Therefore, they are not the solution for describing disc biomechanics.

Therefore, rheological models have **several critical issues** in capturing data. These issues may depend on their governing equations themselves, which struggle to interpret the data because of the variability in applied load and creep rate over time, as well as their simplicity in how they were formulated. Hence, the need arises to have new analytical methods through which IVD can be modelled. It was suggested that fractional calculus is the possible breakthrough in modeling disc biomechanics, specifically reffering to fractional rheological models, which have not yet been used in intervertebral disc biomechanics [43, 71–73, 166–173].

Fractional calculus for **modeling biological materials** has already been exploited in the literature, showing satisfactory results. The same might also be done with the intervertebral disc. Indeed, in the following sections of this chapter, the

application of fractional calculus in describing the biomechanical behaviour of the bovine tails intervertebral disc will be observed, representing the first step to more accurate modeling of disc mechanics.

4.3 *In-vitro* test on human cadavers

The contents of this section are extracted from the research paper published by **Sciortino, V.**, et al. (2024) [185]. This paper's purpose was first to show how the classical rheological models and Nutting's Power law can be valuable tools to adopt in modeling the creep behaviour, and secondly to emphasize that such models have some critical issues, which should be addressed if the most accurate modeling of IVD is desired.

4.3.1 Daily and Nightly activities of the IVD

The anatomical structure and function of the IVD have already been extensively described in previous sections. Here, it is important to emphasize why the **long-term behavior** of the intervertebral disc is being investigated. The 24 hours that compose a single day of a human being are divided into 16 hours of normal activities during day and 8 hours of rest during night. Therefore, the intervertebral disc exhibits a distinct balance between **daily** (16 hours loading) and **nightly** (8 hours unloading) activities. At the physiological level, this balance is reflected in behaviour of the nucleus pulposus [58, 158, 160, 161, 186–192].

NP exhibits **extraordinary** biomechanical properties, i.e., stiffness, compressive strength, and swelling characteristics. The NP shape and IDP vary over time as water content and physiological stresses on the spine change. These changes depend precisely on the loading or unloading conditions that alternately operate throughout the day in the disc. During the 16 hours of daily activity, there is a **reduction in disc height,** while during the 8 hours of rest at night there is a **recovery in disc height.** Hence, during the day a person present a small reduction in his height, while during the night the millimeters lost during the day are recovered. Therefore, this is also happening because of nutrient transport arising through the cartilaginous endplates, which allow water to enter or leave the NP [58, 158, 160, 161, 186–192].

Considering all these aspects, it is crucial to describe and model the viscoelastic characteristics of the IVD to fully understand its **loading and unloading mecha-**

nism. The modeling of the time-dependent mechanical response of the disc is indeed central in comprehend the complicated relationship between external loads and the **mechanobiology** of the IVD and its homeostasis. Succeeding in mathematically modeling these phenomena would prove to be a valuable approach to simplify truly complex mechanobiological phenomena, related to the mechanism behind daily and nightly activities affecting NP pressure, disc height, water transport, hydration, cell viability, matrix synthesis, and mechano-sensitive activity [58, 158, 160, 161, 186–192].

Therefore, aiming to model the disc biomechanics under long loads, **an *in-vitro* experiment** was conducted using cadaveric human lumbar spine columns for creep test [185]. The adopted models were evaluated on the creep data to determine whether they could provide a good modeling and fit of IVD creep behaviour, followed by correlation and linear regression analysis [58, 158, 160, 161, 186–192].

4.3.2 Materials and Methods

A total of **seven lumbar segments** (L4-5, Figure 4.5) from frozen human spines with mean age of 48 years were used for the experimental procedure [185] (Table 4.2). All samples were examined for signs of severe deformity, degeneration or bony defects, and those samples with a degree of disc degeneration greater than 1 were excluded. The specimens were frozen at -20 °C in triple plastic bags and were thawed at 4 °C for 16 h before the experiment. The preparation of the specimens involved the removal of muscle and fat, while maintaining the IVDs intact (Figure 4.5A).

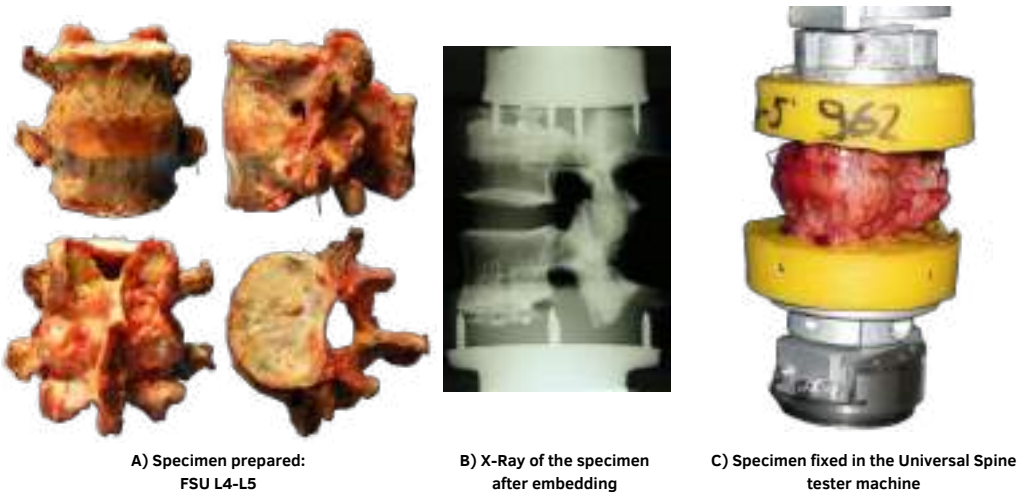

Figure 4.5. ***A)*** *Specimen prepared;* ***B)*** *X-Ray of the specimen;* ***C)*** *Specimen fixed in the machine ready to be tested.* ***Source:*** *Sciortino et al. (2024) [185]*

The next step involved embedding the cranial and caudal extremities in PMMA (Technovit 3040, Heraeus-Kulzer, Wertheim/Ts, Germany), resulting in securing fixation to the testing machine by using screws placed prior to encapsulation, followed by radiography (Figure 4.5B). The specimens were then fixed between flanges and secured to the **spine tester machine** (Figure 4.5C). Prior to performing the test protocol, the specimens were brought to a neutral position by clamping the freedom degrees in the gimbal system, thereby ensuring only axial translation, which was measured through an inductive linear displacement sensor (BTL2-P1-0225, Balluff, Neuhausen, Germany) connected to the spine tester. The **test protocol** included a non-destructive creep test performed with 500N of compression applied vertically to the upper endplate (to simulate upper body loading according to the experimental procedure already evaluated [192]) for 15 minutes.

Displacement creep curves as a function of time were extrapolated for each specimen, using *Disc Height Reduction* (DHR) as the reference parameter to analyze. The DHR was measured experimentally through the displacement sensor, considering it as the lowering of the specimen after the load was applied, if the lowering affects only the IVD. Maximum DHR values were identified for each specimen (Table 4.2).

Table 4.2. *Information extracted from Sciortino et al (2024) [185] about age, sex, grade of degeneration and Max value of Disc height reduction of the specimens.*

Specimen	Age	Sex	Max value DHR [mm]
1	48	Male	1.17
2	58	Female	1.44
3	57	Female	1.38
4	54	Male	1.24
5	59	Female	1.26
6	48	Female	0.91
7	58	Female	1.00

Creep curves were modelled through **classical rheological** models and **Nutting's power law** (Wolfram Mathematica v13.0, Wolfram Research, Champaign, Illinois, USA). A correlation analysis between the identified model parameters and the maximum value reached by the DHR was done through the software RStudio v2023.12.0 (Posit, PBC, Vienna, Austria), indicating as significant correlations those with Pearson correlations (r) greater than 0.5 and setting a significance value (p-value less than 0.05) [185].

4.3.3 Mathematical models

Several attempts have been made in the literature to model the time-dependent behavior of IVD through using different mathematical models as already metioned in the previous section. In this paper [185], the following are the mathematical steps to obtain the governing equations in terms of displacement $u(t)$ and force $F(t)$ for the following models adopted [58, 158, 160, 161, 186–192]:

➢ **Maxwell's model**. From the Figure 4.2A, the total displacement is the sum of its individual displacement components: $u(t) = u_E(t) + u_D(t)$. Where the total force, as they are placed in series, is the same between spring and dashpot: $F(t) = F_E(t) = F_D(t) = \frac{\eta A}{l_0}\dot{u}_D(t)$. Where specifically the displacement derivative of the dashpot is expressed as follows: $\dot{u}_D(t) = \dot{u}(t) - \dot{u}_E(t)$, with $\dot{u}_E(t) = \frac{l_0}{EA}\dot{F}(t)$. The time constant is the ratio of viscosity to Young's modulus $\tau_0 = \frac{\eta}{E}$. Substituting all this into the force relation and for a creep test with a constant force, the governing equation is obtained:

$$\dot{F}(t) + \frac{F(t)}{\tau_0} = k\dot{u}(t) \tag{4.28}$$

With $k = \frac{EA}{l_0}$ which is the spring rigidity. For creep test $F(t)$ is a constant force $\dot{u}(t) = \frac{F}{k\tau_0} \rightarrow u(t) = \frac{F}{k\tau_0}t + C_1$ and by imposing the boundary condition $u(0) = 0 \rightarrow C_1 = -\frac{F}{k\tau_0}$. The creep function for Maxwell's model is obtained:

$$u(t) = \frac{F}{k\tau_0}(t - 1) \tag{4.29}$$

➢ **Kelvin-Voigt's model**. From the Figure 4.2B, the total force is the sum of its individual force components as follows: $F(t) = F_E(t) + F_D(t)$. Where the total displacement, as they are placed in parallel, is the same between spring and dashpot $u(t) = u_E(t) = u_D(t)$. The dashpot and spring forces can be expressed as follows: $F_D(t) = \frac{\eta A}{l_0}\dot{u}(t)$ and $F_E(t) = ku(t) = \frac{EA}{l_0}u(t)$. The time constant is the ratio of viscosity to Young's modulus $\tau_0 = \frac{\eta}{E}$. Substituting all this into the force relation and for a creep test with a constant force, the governing equation is obtained:

$$\dot{u}(t) + \frac{E}{\eta}u(t) = \frac{F(t)l_0}{\eta A} \tag{4.30}$$

$\dot{u}(t) + \frac{E}{\eta}u(t) = \frac{Fl_0}{\eta A}$. By solving first-order differential equations with $u_{hom} = C_1 e^{-\frac{t}{\tau_0}}$ and $u_{part} = C_2$, where $\frac{E}{\eta}C_2 = \frac{Fl_0}{\eta A} \rightarrow C_2 = \frac{Fl_0}{EA} = \frac{F}{k}$, it is obtained $u(t) = C_1 e^{-\frac{t}{\tau_0}} + \frac{F}{k}$. By imposing the boundary conditions $u(0) = 0 \rightarrow C_1 = -\frac{F}{k}$, the creep function for Kelvin-Voigt's model is obtained:

$$u(t) = \frac{F}{k}\left(1 - e^{-\frac{t}{\tau_0}}\right) \tag{4.31}$$

➢ **SLS1's model** (Figure 4.2C). The mathematical steps are like the previous one. The governing equation in terms of displacement and forces is as follows:

$$\frac{\dot{F}(t)}{k_1} + \frac{F(t)\,l_0}{\eta A}\left(\frac{k_2 + k_1}{k_1}\right) = \dot{u}(t) + \frac{E_2}{\eta}u(t) \tag{4.32}$$

For creep test $F(t)$ is a constant force and by solving first-order differential equations with $u_{hom} = C_1 e^{-\frac{t}{\tau_2}}$ and $u_{part} = C_2$, where $\frac{E_1}{\eta}C_2 = \frac{Fl_0}{\eta A}\left(1 + \frac{E_1}{E_2}\right) \rightarrow C_2 = \frac{F}{K_1} + \frac{F}{K_2}$, it is obtained $\mathrm{u}(t) = C_1 e^{-\frac{t}{\tau_0}} + \frac{F}{k_1} + \frac{F}{k_2}$. By imposing the boundary conditions $u(0) = \frac{F}{k_1} \rightarrow C_1 = -\frac{F}{k}$, the creep function for SLS1's model as a function of displacement and applied force is obtained:

$$u(t) = \frac{F}{k_1} + \frac{F}{k_2}\left(1 - e^{-\frac{t}{\tau_2}}\right) \tag{4.33}$$

➢ **SLS2's model** (Figure 4.2C). The mathematical steps are like the previous one. The governing equation in terms of displacement and forces is as follows:

$$\dot{u}(t)\,[k_1 + k_2] + \frac{k_2 k_1 l_0}{\eta A}u(t) = \dot{F}(t) + \frac{1}{\tau_2}F(t) \tag{4.34}$$

For creep test, F(t) is a constant force and by solving first-order differential equations with $u_{hom} = C_1 e^{-\frac{k_1}{\tau_2(k_1+k_2)}t}$ and $u_{part} = C_2$, where $\frac{k_2 k_1 l_0}{\eta A(k_1+k_2)}C_2 = \frac{E_2 F}{A(k_1+k_2)} \rightarrow C_2 = \frac{F}{k_1}$, it is obtained $u(t) = C_1 e^{-\frac{k_1}{\tau_2(k_1+k_2)}t} + \frac{F}{k_1}$. By imposing the boundary conditions $u(0) = \frac{F}{k_1+k_2} \rightarrow C_1 = -\frac{k_2 F}{(k_1+k_2)k_1}$, the creep function for SLS2's model as a function of displacement and applied force is obtained:

$$u(t) = \frac{F}{k_1} - \frac{k_2 F}{(k_1 + k_2)\,k_1}\left(e^{-\frac{k_1}{\tau_2(k_1+k_2)}t}\right) \tag{4.35}$$

➢ **Nutting's Power Law**. This power law represents the creep function between

displacement, force and time as follows:

$$u(t) = CF^{\alpha}t^{\beta} \tag{4.36}$$

Where C, α and β are characteristic of the material. This is a general law obtained experimentally as already described in the previous section, describing the viscoelastic behaviour of materials.

Table 4.3 shows schematically and immediately the governing equations of the mathematical models adopted to describe the creep curves extrapolated from the in vitro experiments. The model parameters are as follows Spring **Stiffnesses** (k, k_1, k_2); **Viscosity** of the shock absorbers (η) and the **time constants,** which are the time required to reach the regime (τ_0, τ_1, τ_2).

Table 4.3. *Five mathematical models adopted with their governing equation and the corresponding creep function.* ***Source:*** *Sciortino et al. (2024) [185].*

Model	Creep Function
Maxwell	$u(t) = \frac{F}{k\ \tau_0}(t-1)$
Kelvin-Voigt	$u(t) = \frac{F}{k}\left(1 - e^{-\frac{t}{\tau_0}}\right)$
SLS1	$u(t) = \frac{F}{k_1} + \frac{F}{k_2}\left(1 - e^{-\frac{t}{\tau_2}}\right)$
SLS2	$u(t) = \frac{F}{k_1} - \frac{k_2 F}{(k_1+k_2)k_1}\left(1 - e^{-\frac{k_1}{\tau_2(k_1+k_2)}t}\right)$
Power Law	$u(t) = CF^{\alpha}t^{\beta}$

4.3.4 Results

The specimens have shown an **immediate reduction** in disc height from its initial value with an average of 0.94 mm ± 0.19 mm. After 15 minutes, the disc height was decreased with mean values of 1.14 mm ± 0.24 mm (Table 4.2). This meant that the IVDs lost 0.20 mm in only 15 minutes of compression [185]. Therefore, each creep curve was modelled with the different mathematical models to find the best fit for the original data. Figure 4.6 shows a creep curve of one specimen fitted with the rheological models and the power law, plotting an enlargement of the steady-state part of the curve [185].

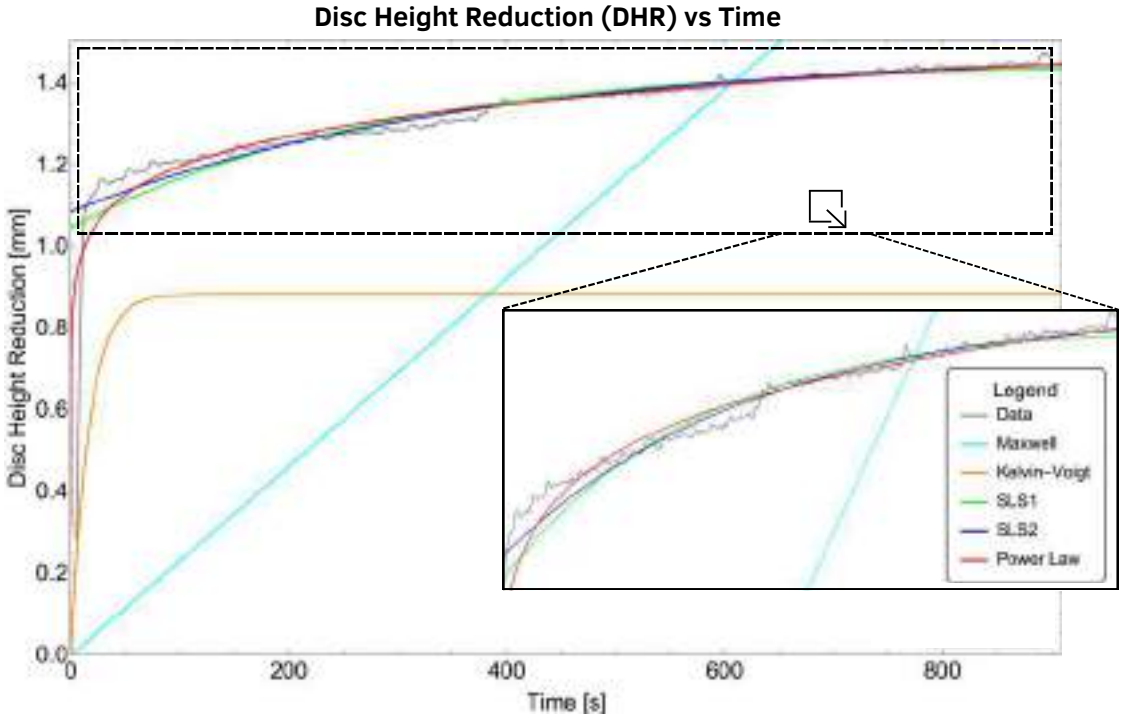

Figure 4.6. *Creep curve modelled for one specimen with the Maxwell, Kelvin-Voigt, SLS1, SLS2 models and Power law, with an enlargement of the regime part.* ***Source:*** *Sciortino et. al (2024) [185]*

Table 4.4 shows the average parameters of the Maxwell, Kelvin-Voigt, SLS1 and SLS2 models obtained from all samples [185].

Table 4.4. *Parameters of Maxwell, Kelvin, SLS1 and SLS2 models calculated in average (Standard deviation in bracket).* ***Source:*** *Sciortino et. al. (2024) [185]*

	τ_0 [s]	τ_2 [s]	k [N/mm]	k_1 [N/mm]	k_2 [N/mm]
Maxwell	2967 (± 303)	-	91 (± 20)	-	-
Kelvin	12 (± 3)	-	461 (± 83)	-	-
SLS1	-	331 (± 159)	-	544 (± 83)	2003 (± 621)
SLS2	-	213 (± 56)	-	429 (± 77)	108 (± 25)

The parameters found for the power law have the following mean values: $C = 0,64 \pm 0,11$, $\beta = 0,06 \pm 0,01$ and $\alpha = 0,03 \pm 0,03$.

Figure 4.7 and 4.8shows respectively creep curves for each specimen fitted with Nutting's Power Law and SLS1 model [185].

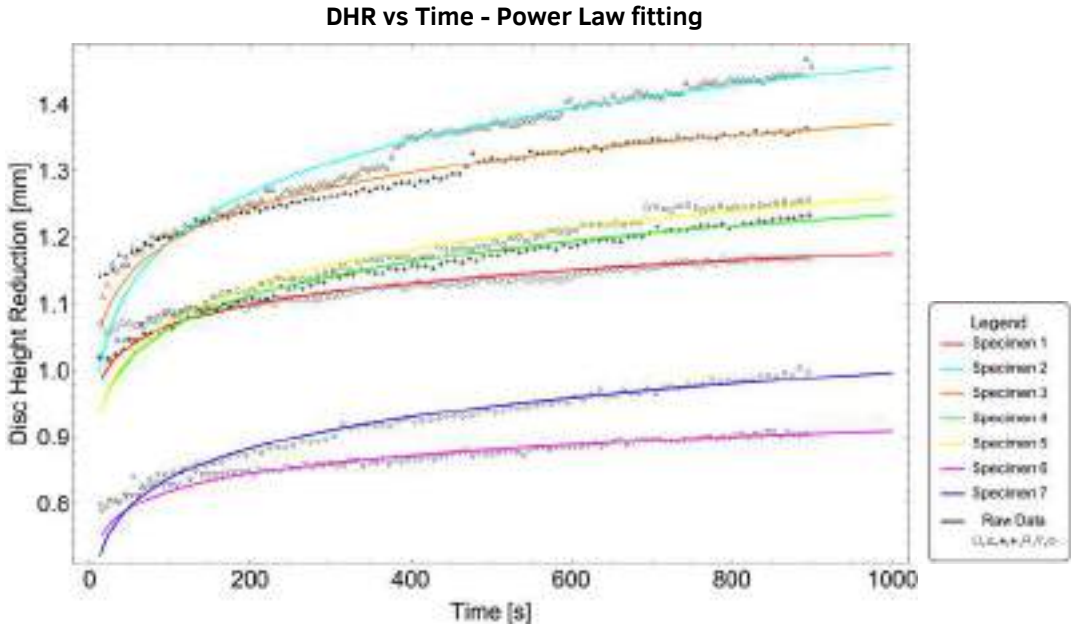

Figure 4.7. *Creep curves for each specimen without the initial slope part which were modelled with the Power law: Red-Specimen 1; Cyan-Specimen 2; Orange-Specimen 3; Green-Specimen 4; Yellow-Specimen 5; Magenta-Specimen 6; Blue-Specimen 7.* ***Source:*** *Sciortino et. al (2024) [185]*

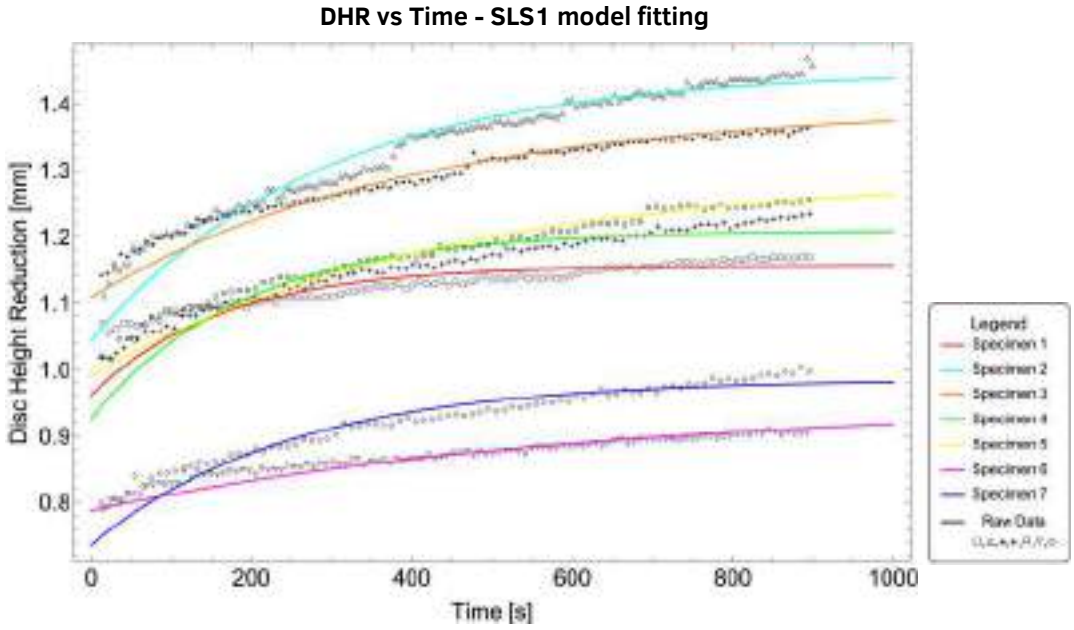

Figure 4.8. *Creep curves for each specimen without the initial slope part which were modelled with the SLS1 model: Red-Specimen 1; Cyan-Specimen 2; Orange-Specimen 3; Green-Specimen 4; Yellow-Specimen 5; Magenta-Specimen 6; Blue-Specimen 7.* ***Source:*** *Sciortino et. al (2024) [185]*

Lastly, a **correlation analysis** and a linear regression were done, see in Figure 4.9 and 4.10). Negative correlation were found between the parameters of the rheological models and the maximum value of the DHR for each specimen [185].

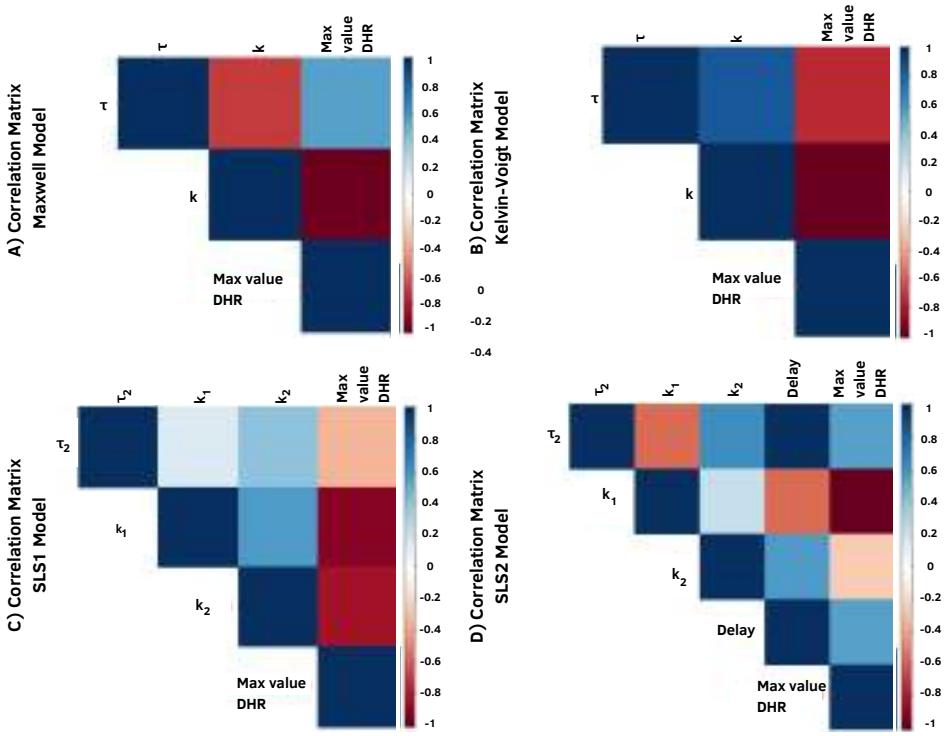

Figure 4.9. *Matrix Correlation between parameters of the models and DHR max:* ***A)*** *Maxwell;* ***B)*** *Kelvin-Voigt;* ***C)*** *SLS1;* ***D)*** *SLS2.* ***Source:*** *in Sciortino et. al (2024) [185]*

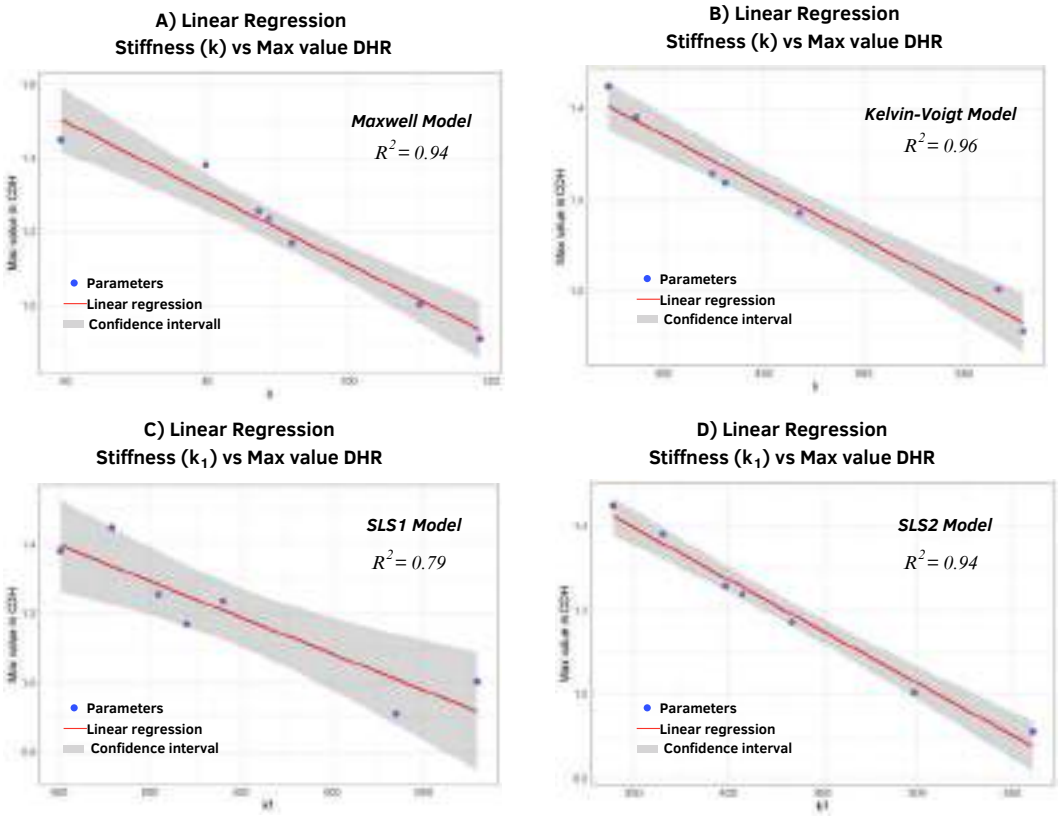

Figure 4.10. *Regression :* ***A)*** *Maxwell: k and DHR max;* ***B)*** *Kelvin-Voigt: k and DHR max;* ***C)*** *SLS1: k_1 and DHR max;* ***D)*** *SLS1: k_1 and DHR max.* ***Source:*** *in Sciortino et. al (2024) [185]*

4.3.5 Discussion and final remarks

This *in-vitro* experiment involved a creep test on human specimens under axial loading of 500 N for 15 minutes. The timing was chosen based on the in vivo IDP studies conducted by Wilke et al. in 1999 [53], since it had been determined that a 15-minute time was sufficient to achieve a constant IDP. The aim of this paper was to prove how classical rheological models and Nutting's law could model the creep behavior of human lumbar segments, showing how it **might be possible to simplify** through mathematical analytical approach the biphasic behavior of the disc. The modeling done has provided insight into how Maxwell's model cannot be a representative analytical model of creep curves, since its creep function is linear, and it is unable to represent the creep non-linear curves shown in the figure. Although the Kelvin-Voigt model has an exponential creep function, it is a very basic law unable to accurately describe the observed nonlinear trend [185].

The SLS1 and SLS2 models can fit the creep curves well, although they **fail to fit the starting ramp** of the curve, as shown in the enlargement of the SLS1 model's creep fitting curves in Figure 4.8. Instead, Nutting's law seems to be the best fit among the other laws (Figure 4.7), also capable of capturing the starting ramp of the curve, even though the fitting is not always effective. This may reflect that Nutting's law models the mechanical response at the macroscopic level, without considering what happens at the microscopic level with nutrient exchange, disc swelling and changes in disc height [185].

The *in-vitro* study has several limitations [185]. The specimens tested were frozen and thawed, thus affecting the results obtained, and distorting the true viscoelastic nature of the tissues considering the high-water content of biological tissues. The median age of the specimens is 48 years, with patients over 50 years of age. This is a limitation given the physiological degeneration that the intervertebral disc experiences with advancing age, which leads to a mechanical response that is certainly different from tissue of a young human being.

This study represents an **initial starting point** to assess the status of the literature on mathematical modeling for IVD mechanics and fully understand it, so that it will be feasible to investigate how the IVD deforms during daily and nocturnal activities. Indeed, the goal is to be able to model the biomechanical response of the IVD in a simple way, so that it can be replicated in clinical practice for the design of

disc prostheses that could be used to replace intervertebral discs damaged by disease.

4.4 Fractional calculus as a new frontier in IVD modeling

The last section of this chapter is about in vitro experiments on bovine tails involving a long-term loading test protocol. These experiment are extrapolated from a research paper which is not published yet by **Sciortino, V.** et al. (2025, out-going). The goal of this paper was to model creep curves of the IVD by using **fractional calculus,** providing an opportunity to demonstrate the potential and efficiency of this mathematical tool.

4.4.1 Materials and Methods

Eight fresh bovine tails from male cattle aged 12 to 24 months were selected from a local slaughterhouse, without signs of anatomical abnormalities, fractures or degeneration (Figure 4.11A), and the CY3/4 level segments were isolated from them. The specimens were stored at -20 °C in plastic bags and thawed at 4 °C for 16 h prior to testing. Spinal segments were prepared by removing all soft tissue and keeping the intervertebral discs intact (Figure 4.11B).

A) *Bovine tails RX and specimen prepared*

B) *Universal Testing machine (Zwick)*

C) *Heating System (Lauda)*

D) *Specimen during test in saline solution*

Figure 4.11. *© Materials and method:* ***A)*** *X-Ray Bovine tail and specimen prepared;****B)*** *Universal testing machine;* ***C)****Heating machine;* ***D)*** *Specimen fixed in saline solution.*

Furthermore, according to the procedures already outlined in the previous paragraphs, the cranial and caudal ends were embedded in PMMA (Technovit 3040, Heraeus-Kulzer, Wertheim/Ts, Germany) to allow fixation to the testing machine, reinforced by radiolucent screws inserted before embedding. A universal testing machine (Zwick&Roell, Figure 4.11C) was used for testing. Prior to testing, specimens were **hydrated** in a saline solution for 1 hour to hydrate the tissues that had been frozen. The entire test was conducted in **saline solution** at 37°C (Figure 4.11D-E) using a heating thermostat system (Lauda Alpha, LAUDA-Brinkmann, USA).

The **testing protocol** included a preconditioning phase with 10 cycles at 10% of the test loading force, followed by a compressive creep test with 80 N loading for 3 hours (see Figure 4.12 for the test protocol), from which the deformations of the specimens were measured as DHR.

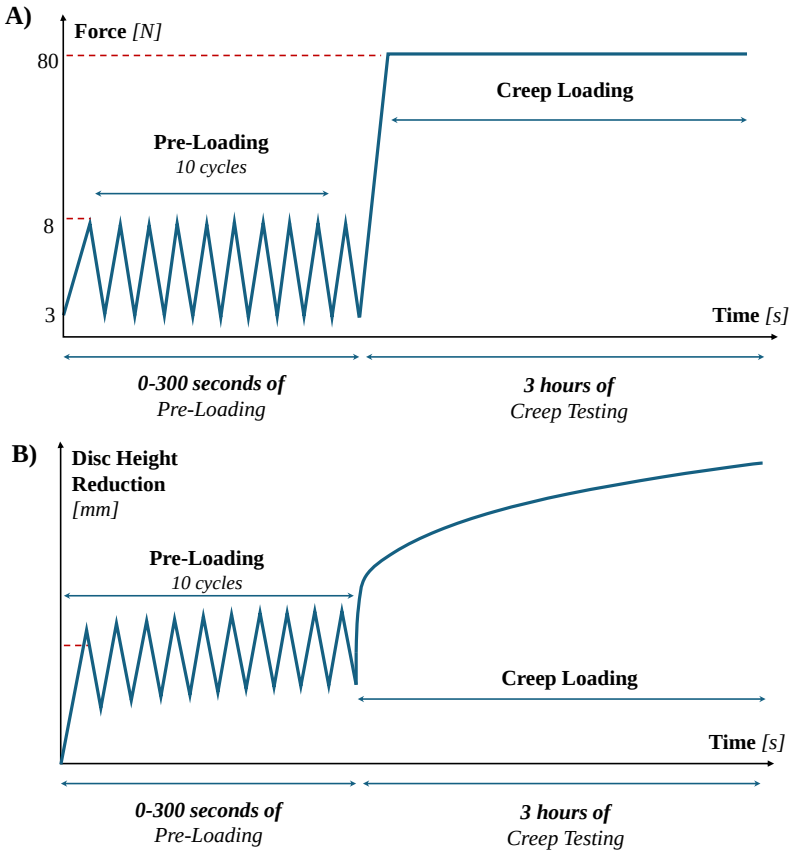

Figure 4.12. *© **A)** Test protocol; **B)** Curve disc height reduction vs. time.*

Additionally, an X-Ray for each specimen was done in the sagittal and coronal positions to measure the height, width, and cross-sectional area of the hydrated disc, from which stress and strain were calculated. Specifically, the cross-sectional area of the disc was modelled as an ellipse.

Once the raw data were collected from the experiment, these were evaluated. Creep functions were obtained in terms of strain and stress for each sample. Hence, the DHR strain was used to extrapolate the creep curves (see Figure 4.13A schematization of the specimen in the universal testing machine). The creep curves were mathematically modelled with the SLS1 and Kelvin-Voigt classical rheological models and the **Fractional Power Law and Fractional Maxwell Model** [43, 71–73, 166–173]. It was used Wolfram Mathematica v13.0 for the optimization of the cost function adopted for the modeling. Figure 4.13B shows the schematic representation for the intervertebral disc as a Fractional Maxwell Model.

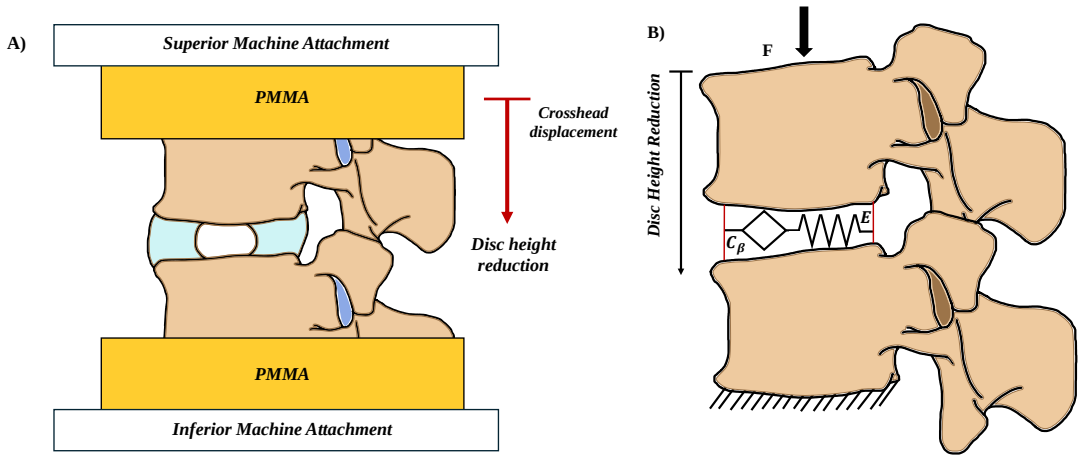

Figure 4.13. *© **A)** The specimen fixed in the universal testing machine to visualize how the measurements were considered. **B)** The mathematical modeling done for the IVD.*

The optimization method adopted was either Differential Evolution or Nelder-Mead method, since both methods can handle constraints and the nonlinear nature of the objective functions (optimization code in the Appendix). In addition, a correlation analysis was done between the identified model parameters and the maximum DHR values using RStudio software v2023.12.0, and significant correlations (Pearson correlations, r) were found by setting a p-value less than 0.05.

4.4.2 Fractional models' formulation

The **mathematical formulation** for the fractional models of the Power law and Maxwell's model will be briefly introduced. From the (4.20) equation and substituting it in (4.21), it is possible to obtain the creep function of the **Fractional Power law,** by considering a constant stress function (80N of compression force) [43, 71–73, 166–173] as follows:

$$\varepsilon(t) = \frac{1}{E_0 \tau^\beta} \left(I_{0^+}^\beta \sigma\right)(t) = \frac{\sigma_0}{E_0 \left[\Gamma(1+\beta)\right]} \left(\frac{t}{\tau}\right)^\beta \tag{4.37}$$

Where:

$$\left(I_{0^+}^\beta \sigma_0\right)(t) = \frac{\sigma_0 t^\beta}{\Gamma(1+\beta)} \tag{4.38}$$

About the **Fractional Maxwell's model,** its governing equation is the following:

$$C_\beta \sigma(t) + E\left(I_{0^+}^\beta \sigma\right)(t) = E C_\beta \varepsilon(t) \tag{4.39}$$

Where $C_\beta = E_0 {\tau_0}^\beta$ and $\sigma(t) = \sigma_0$. By solving the governing equation and by calculating the Fractional Integral as (5), the Creep Function of the **Fractional Maxwell's model is** the following:

$$\varepsilon(t) = \sigma_0 \left(\frac{1}{E} + \frac{1}{E_0 \Gamma(1+\beta)} \left(\frac{t}{\tau}\right)^\beta \right) \tag{4.40}$$

By considering also the Creep function of SLS1 and Kelvin-Voigt's models, the parameters of the models are the following:

- E_0, i.e., Young's Modulus, obtained from the $\sigma - \varepsilon$ curve of pre-load.
- E_1 and E_2, i.e., Young's Modulus of the SLS1 model.
- E, i.e., Young's Modulus of the Kelvin-Voigt and Fractional Maxwell model.
- τ and τ_2, i.e., time constants.
- η, i.e., viscosity of the dashpot, included in τ.
- β, i.e., the order of fractional derivative.

4.4.3 Results

After 3 hours of creep, the **disc height decreased** in average by 2.52, presenting an immediate reduction in disc height as 80N was reached in average by 0.77 mm. The Young's modulus of each specimen was extrapolated from the stress-strain curves of the final pre-load cycle, with a mean value of 4.82 MPa. Table 4.5 shows all the information about the samples.

Table 4.5. *© Information extracted for all specimens*

Specimen	Tool separation [mm]	Disc Height [mm]	Disc Width [mm]	Tested Disc height [mm]	DHR [mm]	Immediate DHR [mm]	Young's Modulus [MPa]
1	92.38	11.43	19.83	8.72	2.71	0.80	4.88
2	73.00	12.20	22.35	9.43	2.77	0.87	4.10
3	78.94	11.52	24.25	9.54	1.98	0.54	5.34
4	83.26	11.03	21.89	8.62	2.41	0.82	4.42
5	67.19	10.41	22.72	8.07	2.34	0.62	4.76
6	67.30	11.06	21.72	8.64	2.42	0.82	4.65
7	85.36	11.87	20.61	9.05	2.82	0.91	4.95
8	66.22	10.81	21.17	8.14	2.67	0.74	5.48

Table 4.6 shows the % error in average obtained by fitting the creep curves with the fours mathematical models considered for each specimen.

Table 4.6. *© % in error obtained by fitting the curve with all models considered for each specimen*

	Kelvin-Voigt	SLS1	Fractional Power Law	Fractional Maxwell
Specimen	**Err [%]**	**Err [%]**	**Err [%]**	**Err [%]**
1	7.26	1.1	0.81	0.62
2	7.97	1.09	1.32	0.43
3	7.69	0.96	1.65	0.35
4	7.78	1.02	1.04	0.54
5	7.08	1.57	1.02	0.35
6	8.30	1.16	1.37	0.39
7	7.39	1.05	0.83	0.63
8	7.39	1.21	0.97	0.35

Figure 4.14 shows the DHR creep curve in strain vs. time, from a specimen modeled through the four mathematical models listed previously (Figure 4.14A), with a **zoomed-in focus** on the first 1000 seconds of the test (Figure 4.14B) and the last 6000 seconds of the test (Figure 4.14C).

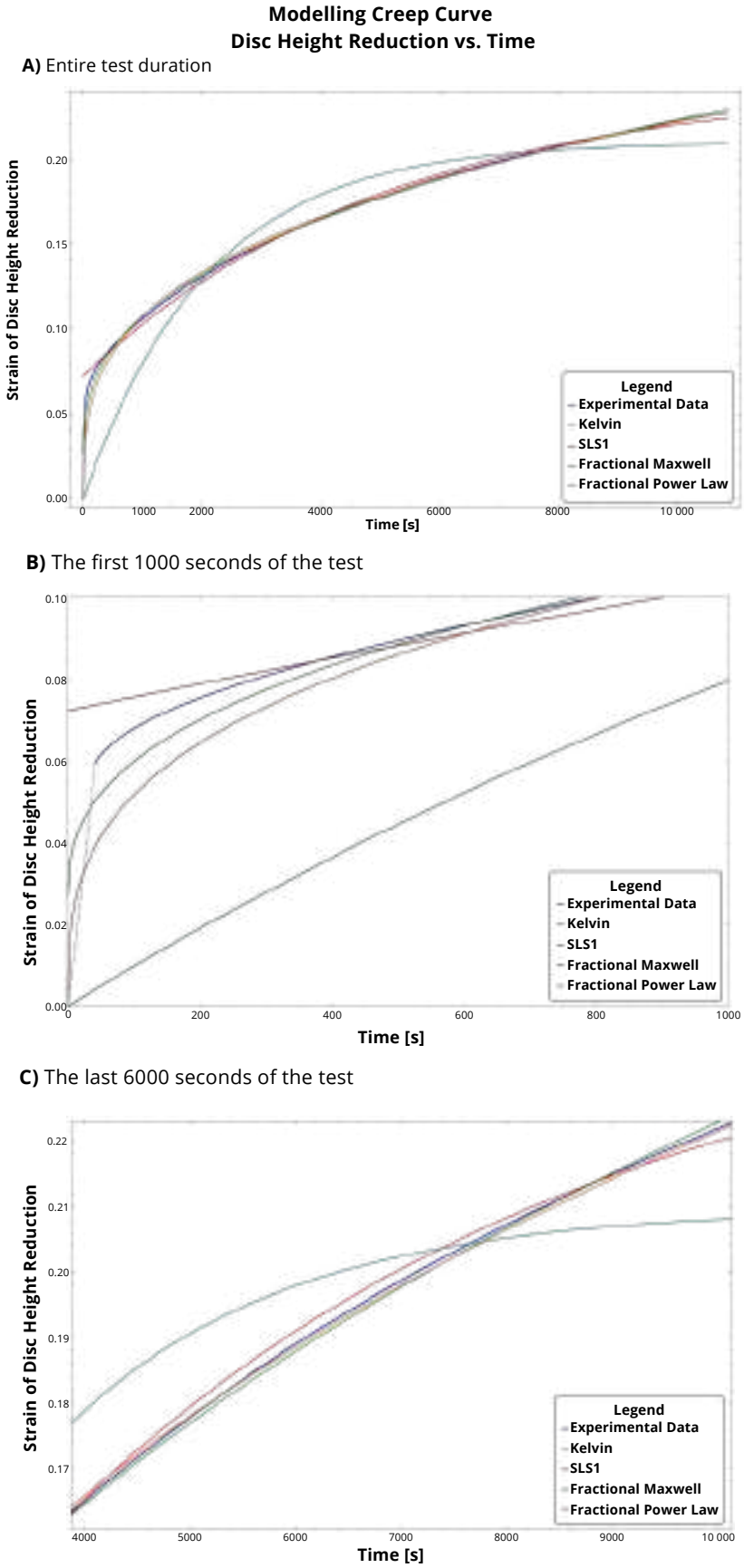

Figure 4.14. *© Creep curve for one specimen fitted with the four models:* ***A)*** *Entire test duration.* ***B)*** *Enlargement on the first 1000 seconds.* ***C)*** *Enlargement on the last 6000 seconds.*

Therefore, the **curve-fitting quality** for each modeling was evaluated by calculating the error rate, see tables. Figure 4.15 shows the creep curves for each sample superimposed on the raw data (curves with symbols) fitted with the Law of **Fractional Power and the Maxwell Fractional Rheological Model.**

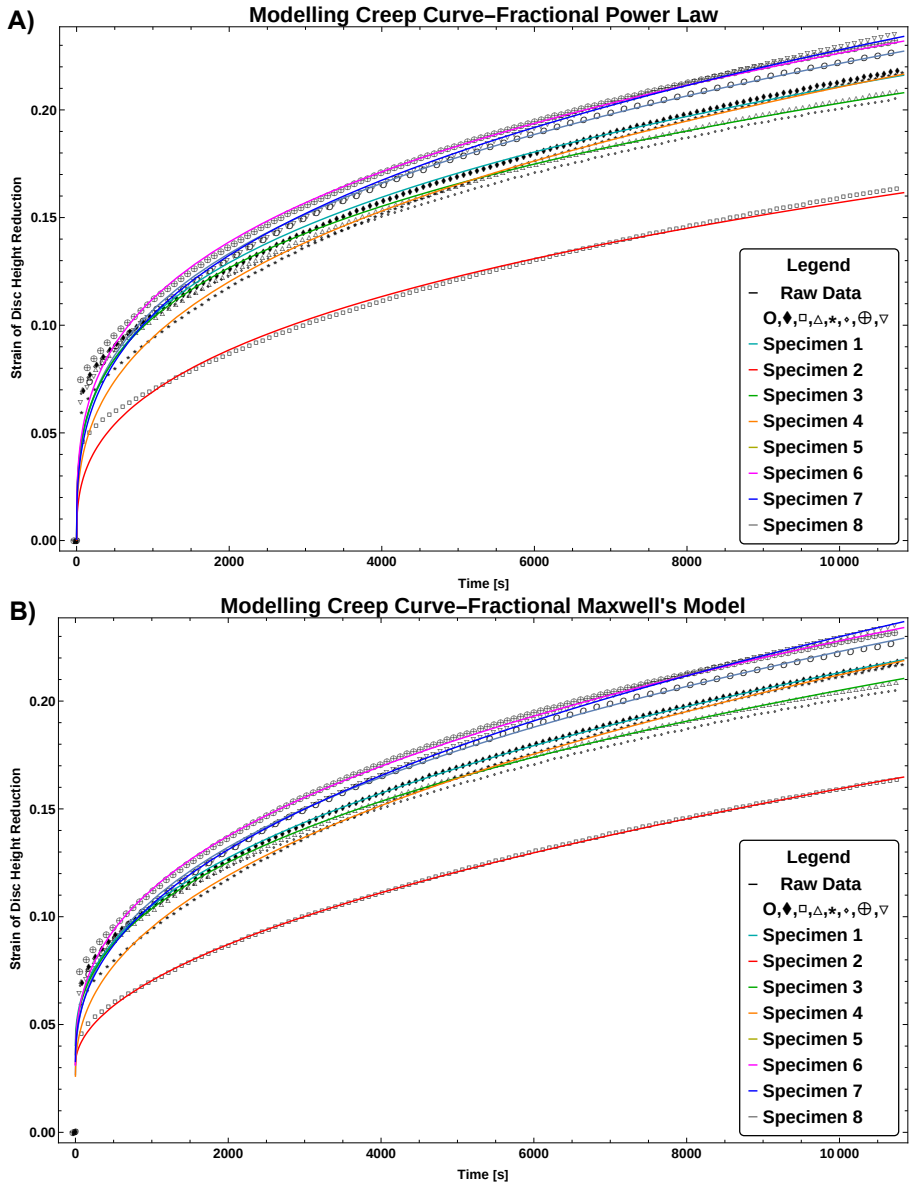

Figure 4.15. *© Creep curves fitted with the fractional power law* ***(A)*** *and Maxwell's model* ***(B)*** *for each specimen: Cyan-Specimen 1; Red-Specimen 2; Green-Specimen 3; Orange-Specimen 4; Dark Yellow-Specimen 5; Magenta-Specimen 6, Blue-Specimen 7 and Gray-Specimen 8.*

Lastly, Figure 4.16 shows the comparison between the classical rheological models and the Fractional Maxwell Rheological Model to testify to the power of fractional calculus.

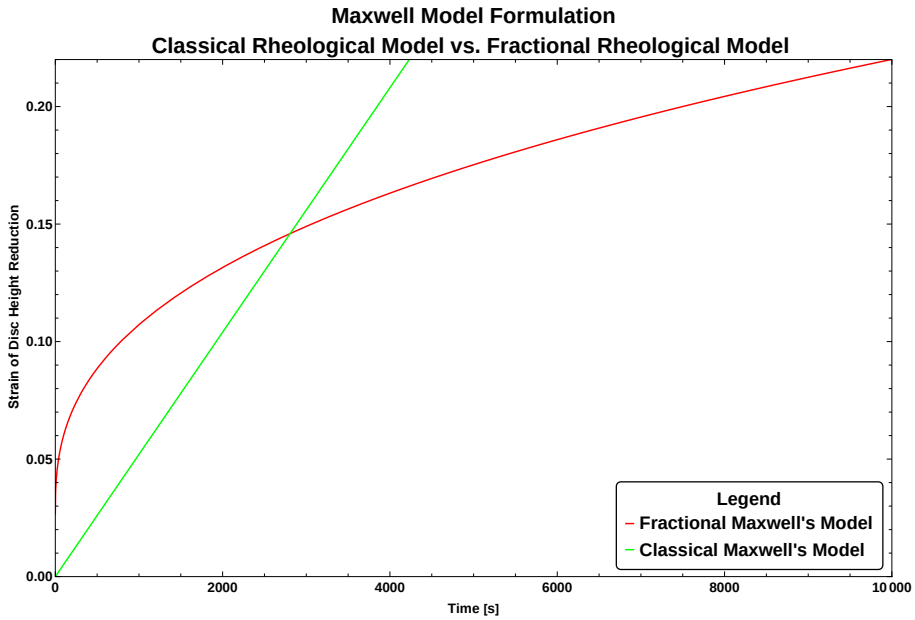

Figure 4.16. *© Comparison in fitting creep curve between Classical Maxwell and Fractional Maxwell*

From the correlation analysis, a negative correlation was found for the fractional power law between the immediate DHR at 80N and β ($r = -0.85$, with $R^2 = 0.73$), and τ($r = -0.87$, with $R^2 = 0.75$), while for Maxwell's fractional law, a negative correlation was found between the Hydrated Disc Width and the E_1 ($r = -0.79$, with $R^2 = 0.63$).

4.4.4 Final Remarks

A **comprehensive interpretation** of the disc mechanics under prolonged loads is critical to support clinical practice in the development of medical devices designed to replace and mimic native biomechanical features. This paper may be very useful in finding analytical laws which can model the creep curves, with very **low error rates** in curve fitting. The Kelvin-Voigt model had an average percentage fitting error of 7.61%, while the SLS1, Fractional Power Law and Fractional Maxwell Model models fit the experimental curves quite well, with an average fitting error of 1.15%, 1.13% and 0.46%, respectively. The SLS1 model has a rather low error fitting rate, but this model as also pointed out in the previous section, must be excluded since it cannot fit the first part of the creep curve.

The preliminary aim of this study was to test the **feasibility** of modeling creep curves by **fractional calculation.** Figure 4.16 shows the comparison of the experimental data adapted from the classical Maxwell model and the fractional

model. The clear difference between the creep functions of the two models can be seen here: a linear versus a nonlinear law. The fractional calculus enables the Maxwell model to fit the creep curves representing the model with the lowest average percent error of all adopted ones.

The **limitations** of this study first involve, as in the previous study, freezing and thawing of the specimens, thus altering the viscoelastic nature of the tissue. This problem was bypassed through hydration and maintenance in saline solution for the entire duration of the test. In addition, the stress and strain data manipulation which has been done also appears to be a limitation of the study. This manipulation is necessary to utilize fractional calculus for "removing" the **preload memory** component that is maintained by this mathematical operator. However, it was considered that neglecting these data did not significantly alter the fit of the creep curves.

Therefore, fractional calculus appears to be an excellent tool for modeling disc biomechanics, and as far as to date it has not been used in the literature. The next step will be to validate this modeling on human specimens, and then support the *Finite Element Modelling* (FEM) and the design of new medical devices that can mimic the IVD disc biomechanical characteristics. Further studies should focus on long-term testing, including loading and unloading cycles, to simulate daily and nightly activities, as well as understanding how the mechanisms of disc height loss and recovery may depend on each other, via fractional calculus and its memory capacity, which was not considered in this study.

Chapter 5

Finite element modeling of the spine

5.1 Rationale

This last chapter will focus on **Finite Element Modeling (FEM) of the spine.** The FEM approach is used to simulate the biomechanical response of the spine, allowing the reproduction of its complex geometry, anatomy, i.e., IVD's composition, ligaments and muscles actions, and stabilization mechanism.

As already described in previous chapters, intervertebral disc pathologies are **complex** and **multifactorial**, being that they are dependent on a wide range of factors. Indeed, experimental approaches present several limitations when studying multiple factors on which pathologies depend. Here, the **numerical approaches** are helpful in **overcoming** all the experimental **difficulties** encountered, i.e., availability of spine tester machines, finding specimens, specimens' transportation and cost, test feasibility issues and specimens' degradation [193–198].

Several studies [193–198] have taken place over the years, due to the evolution of technology which has made it possible to obtain FEM models that are **increasingly realistic** and conform to reality. Indeed, it is possible to create FEM models by using medical reverse engineering techniques, in which starting from a CT or MRI scan it is possible to reconstruct the anatomy and from this to create **patient-specific simulations.** However, there are several aspects and limitations that need to be considered in the numerical and computational approach. Hence, several difficulties encountered in FEM simulations of anatomical parts due to the complexity of the geometries involved, thus leading to long computation times, as well as the difficulties encountered are several to identify the properties and constitutive laws of the materials to be adopted.

5.2 Finite Element modeling of the spine

The following sections is extracted from a research paper published by **Sciortino, V.** et al. (2023) [199]. This paper aims to provide a **broad overview** about the FEM of the spine and to provide a general guideline to follow. The spine biomechanics is very complex since it involves many anatomical components. This complexity is reflected at the computational level, which is the reason why each component must be modelled in a specific way, either from a mechanical or geometrical point of view, as well as in the selection of material properties and constitutive models to adopt. The **vertebral bodies** are separately modelled in the cortical, spongy bone and posterior elements. The **intervertebral disc** is separately shaped in the nucleus pulposus and the fibrous annulus with the different layers and fibers of collagen. The **ligaments** shaped are the main seven that contribute to the stability of the spinal segments: Anterior Longitudinal (ALL), Posterior Longitudinal (PLL), Interspinous (IL), Intertransverse (TL), Flavum (FL), Supraspinous (SL) and Capsular (CL) [5,6]. Lastly, the **facet joints** and **cartilaginous endplates** are also modelled separately [193–199].

The computational approach enables assessment of the physiological and pathological state of the spine based on the loading conditions experienced in different situations by evaluating the IDP, ROM, and general stress states. Any FEM computational model must then be validated. Validation is done through experimental campaigns, in which specimens are tested according to well-defined protocol tests (as we have already seen in Chapter 4) and then compare the results obtained with the computational approach and verify that under the same loading and model conditions, the results are nearly identical.

5.2.1 Materials and Method

This paper was realized based on an extensive and thorough literature review conducted by using relevant scientific and engineering database platforms such as SCOPUS and Web of Science (see Figure 5.1 for the Prisma Diagram and Table 5.1 for steps followed in screening) [199].

A **keyword search** was conducted, whose purpose was to identify sources having FEM of the lumbar spine as their focus. The keywords used were **lumbar, spine, computational, model, modeling.** The records identified were screened through

exclusion/inclusion criteria, to exclude all those articles that had no information on the lumbar modeling. From each study the modeling information of cortical and spongy bone, posterior bone elements, cartilaginous endplates, fibrous annulus and its collagen fibers, nucleus pulposus, ligaments, the boundary and loading conditions were extracted [199].

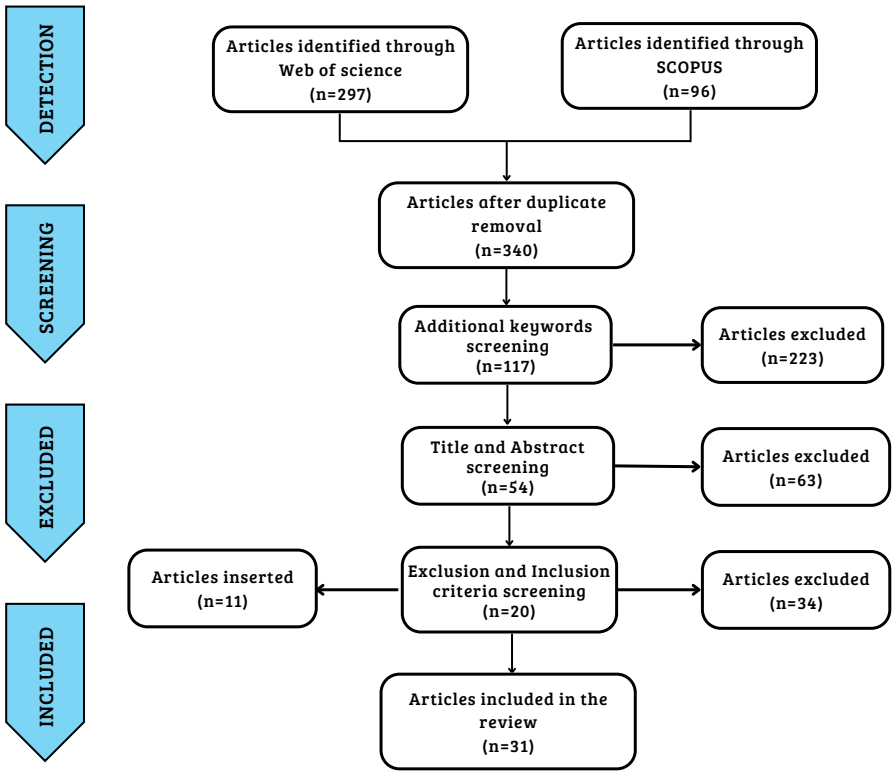

Figure 5.1. *Prisma diagram about the research strategy.* ***Source:*** *Sciortino et al. (2023) [199]*

Table 5.1. *Screening with keywords, exclusions and inclusion criteria.* ***Source:*** *Sciortino et al. (2023) [199]*

Keywords, exclusions and inclusion criteria	**Records selected**
TITLE-ABS-KEY ((lumbar AND spine) AND (computational) AND (modeling) AND (model))	393
After duplicate removal	340
TITLE-ABS-KEY ((lumbar AND spine) AND (computational) AND (modeling) AND (model) AND (biomechanics)) AND (finite AND element))	117
After screening done by abstracts and titles	54
Additional papers	11
Exclusion and inclusion criteria related to the presence of information about modeling (material properties, mesh, boundary conditions...)	31

5.2.2 Results

The database search resulted in the identification of 297 articles from Web of Science and 96 from Scopus using five keywords. A total of b were identified. The duplicates were removed, and it was done a screening by contents and exclusion/inclusion criteria, resulting in a total of 31 articles included in the review [199]. Figure 5.2 shows a visualization network between the main items identified in the initial dataset of 393 items, using the VOSviewer software, with the same methodology already described in Chapter 3. Figure 5.3 shows the number of articles identified year by year.

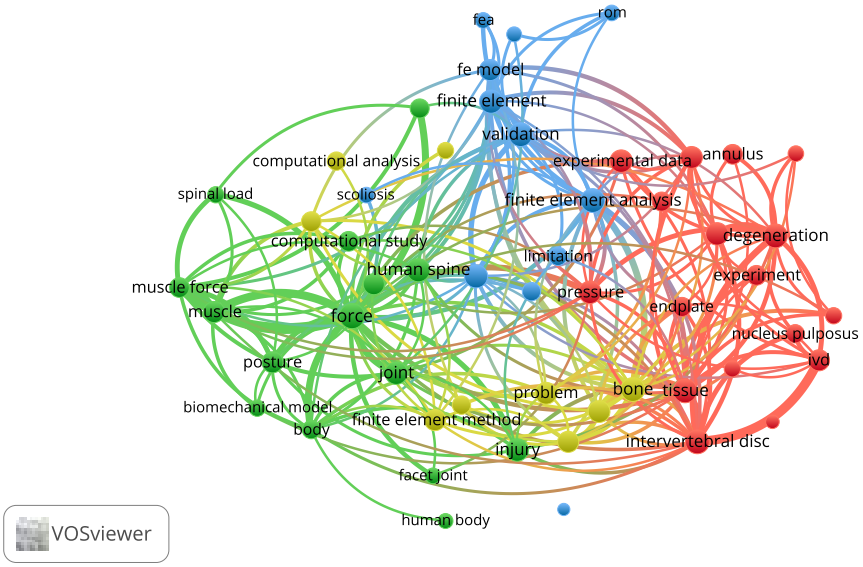

Figure 5.2. *Network of the main items in the database.* ***Source:*** *Sciortino et al. (2023) [199]*

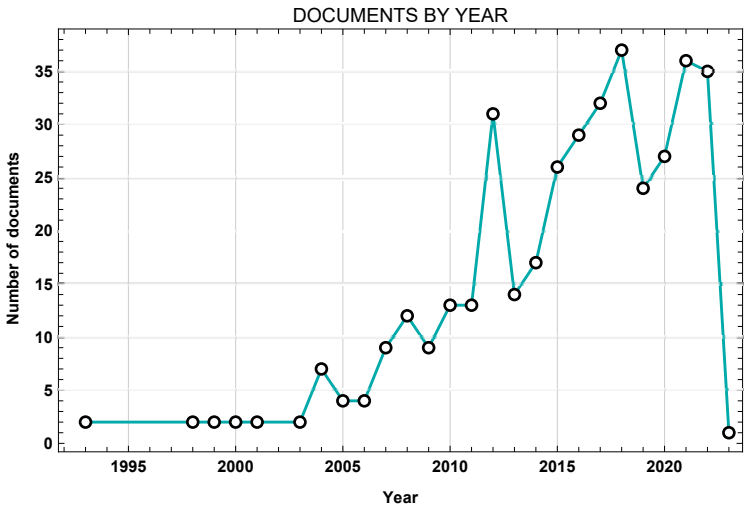

Figure 5.3. *Number of documents published over the years.* ***Source:*** *Sciortino et al. (2023) [199]*

5.2.3 Modeling for each component

The **main characteristics** by which the components of the spine are modelled were extrapolated and were schematically grouped in Table 5.2 [199].

Table 5.2. *FEM of the main spinal structures.* ***Source:*** *Sciortino et al. (2023) [199]*

	Finite element modeling	**FE elements**
Cortical and Cancellous Bone	Isotropic Elastic; Transversely Elastic; Poroelastic behaviour	Solid
Endplates	Isotropic Elastic	Solid
Nucleus Pulpous	Isotropic; Incompressible Fluid; Empty; cavity Hyperelastic	Solid; Fluid
Annular Substance	Hyperelastic behaviour	Solid
Collagen Fibers	Isotropic Elastic; Non-linear behaviour; Based on σ-ϵ curve	Truss; Beam, Connector
Ligaments	Isotropic Elastic; Non-linear behaviour; Based on σ-ϵ curve	Truss; Beam; Connector
Facet Joints	Isotropic Elastic; Hyperelastic behaviour; Surface to surface contact; Frictionless; Unidirectional gap contact	Solid; Contact

The modeling of **vertebral body bone** is distinguished into spongy and cortical bone. Spongy and cortical bone are modelled with elastic behaviour which can be isotropic or orthotropic, with preferential direction. It may also happen that the posterior bone elements are modelled separately, with different elastic characteristics, although this is not strictly necessary or recommended [199].

The **IVD** is shaped into its different components, NP and AF. The fibrous annulus is generally divided into annular substance and collagen fibers. The annular substance presents eight or more layers where the different collagen fibers are woven in alternating orientations, and it is modelled as hyperelastic material, employing a Neo-Hookean, Mooney-Rivlin or Ogden model. Instead, collagen fibers are modelled as isotropic elastic materials or with nonlinear models based on stress curves $\sigma - \varepsilon$ [199].

The major **ligaments** are all modelled in the same way as simple connector, truss, or beam elements, with an isotropic elastic material, with different Young's modulus mechanical response, or based on stress curves $\sigma - \varepsilon$. Cartilaginous endplates can be modelled as linear elastic or hyperelastic materials. Instead, articular facets are modelled as simple surface-to-surface contacts or as unidirectional gaps or other

different types of contacts; instead, if they are reconstructed, they will have a defined thickness and will be modelled with isotropic or hyperelastic elastic properties. Lastly, about the **muscle component,** this is not directly reconstructed considering the computational difficulties. Hence, muscle action can be simulated using connectors or truss elements, which act as tie rods, aiming to simulate the follower load path [199].

5.2.4 Loading and boundary conditions, and validation

Figure 5.4 shows some of the main loading conditions to which the spine is subjected. **Source:** Sciortino er al. (2023) [199].

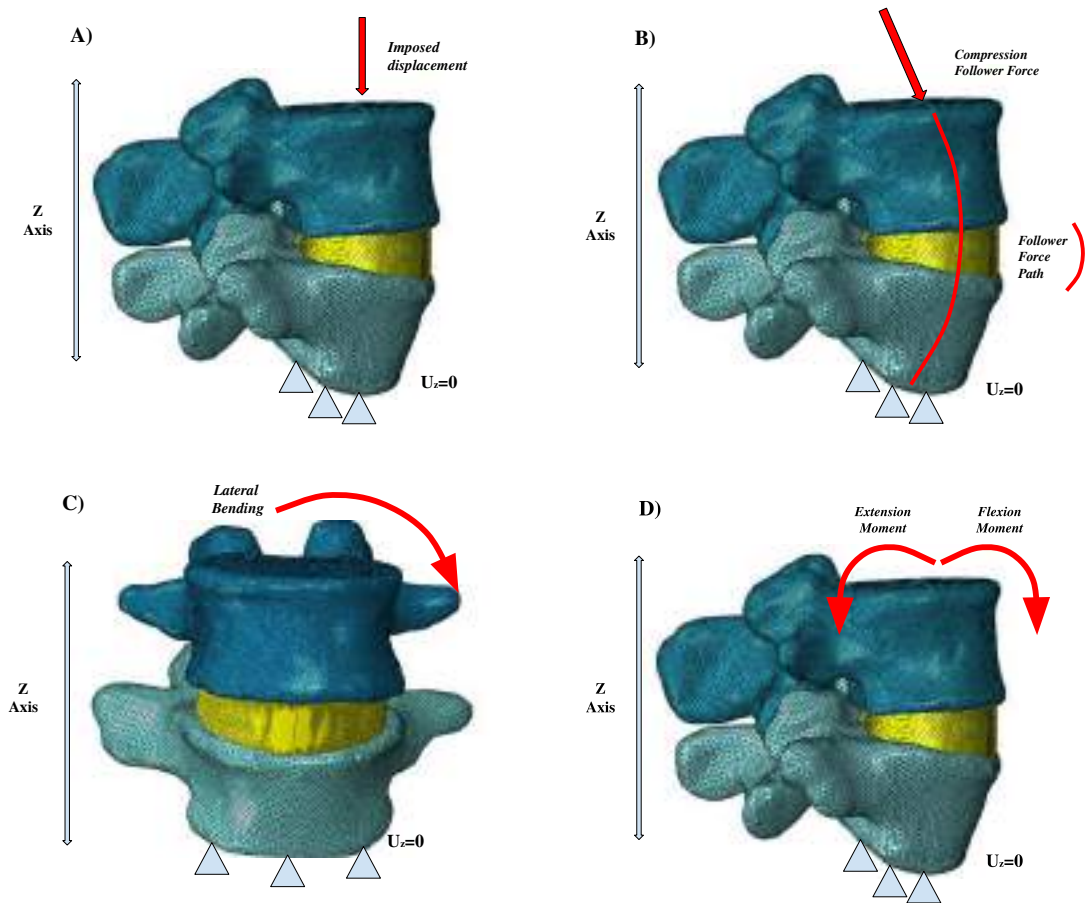

Figure 5.4. *Different loading and boundary conditions: A) displacement. B) Follower force. C) bending. D) Extension and Flexion.* ***Source:*** *Sciortino et al. (2023) [199]*

The boundary conditions generally involve fixing the bottom of the final vertebral segment, and allowing all three directions of movement, even though it may vary from case to case. The loading conditions can differ depending on what type of test protocol you want to study. It can include preloads, compression loads, or flexibility

tests for evaluating disc deformations, IDP, and ROM. Concerning validation, for a finite element model to be validated, it must be able to recreate experimental conditions in-vitro or in-vivo, thus serving as means of comparison [199].

5.2.5 Final remarks

This study provided a general overview of the existing literature in modeling the lumbar spine. Since these are biological tissues with intricate geometries, the numerical analyses to be adopted are nonlinear, which leads to computational issues. In addition, due to the number of components and the geometries, the element number generated by the meshing operation is very high, thus leading to large computational burdens . Indeed, the modeling of the components appears complex. Specifically, the intervertebral disc is reported to be the most articulated. The IVD biomechanics is very tricky; therefore, recreating it computationally is still a great challenge [193–203].

Based on the results obtained from the literature review, some general guidelines for modeling the lumbar spine can be outlined. Cortical and spongy bone should be represented using transverse elastic behaviour to better reflect their actual mechanical response. The posterior bone segments can be modelled in the same way or by linear isotropic elastic behaviors. For the intervertebral disc, it is important to correctly schematize its components: annular substance, annular collagen fibers, and nucleus pulposus. Mooney-Rivlin hyperelastic modeling is shown to be effective for the nucleus pulposus and annular substance, but future research could explore models which consider the viscoelastic creep characteristics of the disc or poroelastic models. About spinal ligaments, the current modeling involves elastic and nonlinear models. However, one aspect not yet adequately considered is the viscoelastic behaviour of the ligaments themselves. For this reason, future studies could adopt approaches which include such characteristics [193–203].

Lastly, this study allowed to consolidate existing knowledge and methodologies related to finite element modeling of the lumbar spine thus obtaining a starting point for future work considering the disc and ligament viscoelastic characteristics that have not been fully involved in the modeling analyzed in the literature.

5.3 Population 3D Atlas of the Pathological Lumbar Spine Segment

The opportunity to simulate the biomechanical behaviour of the spine becomes extremely important in the clinical field, given the practical and economic difficulties in performing in vivo and in vitro experiments. Moreover, describing the anatomical shape and geometry of the spine is **challenging**, which indeed results in the need to create a **3D atlas** of the spine, through the *Statistical Shape Modelling* (SSM) tool. This tool offers the possibility of generating an **infinite patient population** and provides the opportunity to study several situations, including the pathological ones. The concepts in this section are extracted from the research papers published by **Sciortino, V.** et al. in (2022) [204] and (2024) [205].

5.3.1 Material and methods

CT scans of 24 patients were considered as the population of this study (64 detector rows CT scanner, i.e., VCT 64; GE Medical Systems, Milwaukee, WI, USA). For each patient, assessment of the lumbar spine from L1 to L5 was done, including intervertebral discs. The patients included in the study had **scoliosis** and **herniated** disc diseases.

Table 5.3 shows the demographic data and anatomical parameters based on CT. 54.2% of the patients had a scoliosis grade between 5° and 16.74°, with 91.7% having disc herniation [204, 205].

Table 5.3. *Patient study population (mean ± standard deviation).* ***Source:*** *Sciortino et. al 2022 [204]*

Characteristic	Patients
Age (Years)	55.9 ± 7.5
Weight (Kg)	76.9 ± 7.5
Height (m)	1.70 ± 0.01
(Body Mass Index) BMI	26.6 ± 4.3
(Body Surface Area) BSA	1.90 ± 0.2
Male (%)	79.2
Herniated spine (%)	91.77
Scoliosis (%)	54.2

5.3.2 Segmentation and 3D reconstruction

CT scans were analyzed and used for doing **segmentation** and **reconstruction** of the anatomical part, through Mimics v21 medical imaging software (Materialise, Leuven, Belgium). Reconstructions were done through initial mask identification to identify the anatomical region with a semi-automatic thresholding of gray values for the lumbar spine from L1 to L5 followed by **manual editing** of the mask to remove artifacts [204, 205] (see Figure 5.5).

Figure 5.5. *© Automatic threshold mask for the vertebral body and the IVD.*

The reconstruction of the anatomical region was done separately for vertebral bodies and intervertebral discs. The reconstructed parts were smoothed for 20 iterations with a smoothing factor of 0.18, followed by wrapping with the smallest detail of 0.5 mm and a gap closure distance of 0.8 mm. Figure 5.6 shows the reconstruction for the patient who was selected as representative of population [204].

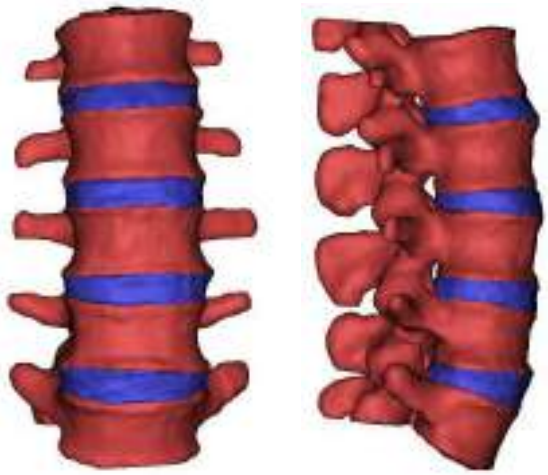

Figure 5.6. *3D reconstruction for the patient selected as representative of the average population size.* ***Source:*** *Sciortino et al. (2022) [204].*

5.3.3 Geometrical measurements

Some geometrical and anatomical measurements of the reconstructed regions were made through CT scans. Figure 5.7 shows the methodology used for the measurements made for the vertebral bodies and intervertebral disc, by using the analysis tools of Mimics. **Height and width measures** were taken at the centroids from the coronal e sagittal plane (Figure 5.7A-B), including the area and perimeter of the lower and inferior surface for the vertebral bodies and discs (Figures 5.7D). The **lordosis degree measurements** were taken (Figure 5.7C), proceeding to draw two straight lines in the sagittal plane. Finally, **Cobb's degree measurements** were taken by **Cobb's method**, drawing as straight lines those tangents to the upper and lower vertebrae that are most inclined. All measurements were taken for all 24 patients [204, 206–209].

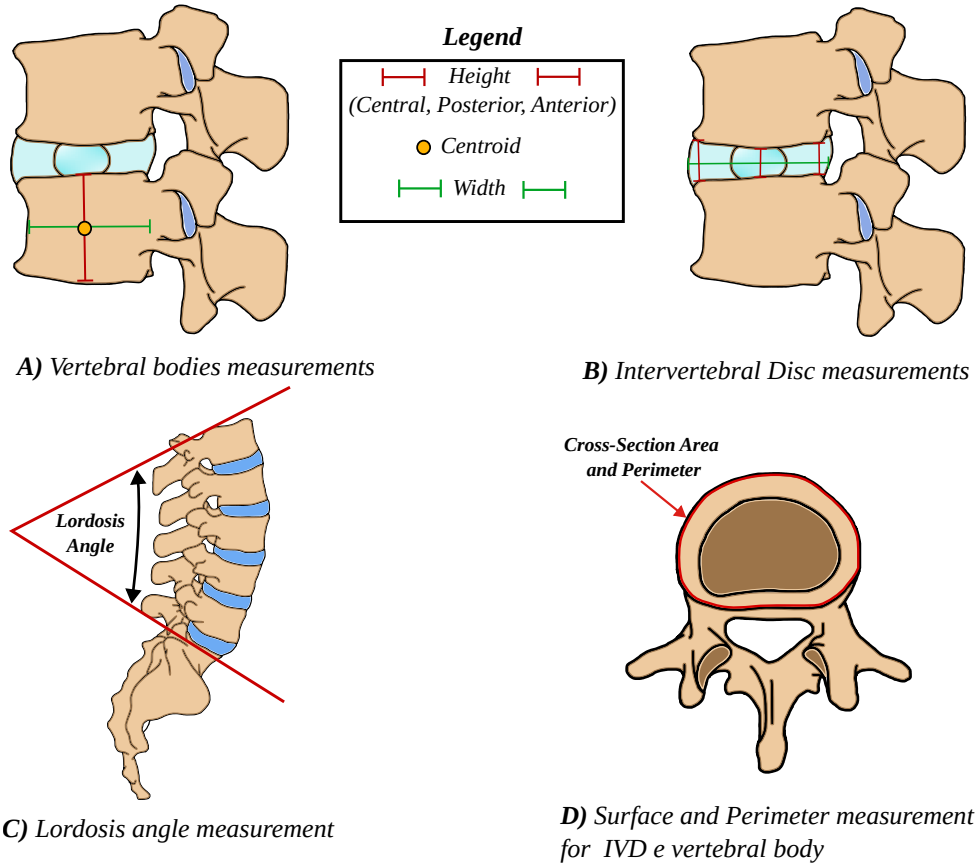

A) *Vertebral bodies measurements*

B) *Intervertebral Disc measurements*

C) *Lordosis angle measurement*

D) *Surface and Perimeter measurement for IVD e vertebral body*

Figure 5.7. *© **A)** Vertebral body measurements of height and width. **B)** IVD measurements of height and width. **C)** Lordosis Degree measurements. **D)** Surface and perimeter measurements.*

Table 5.4 and 5.5 show the population average measurements of geometric parameters for discs and vertebral body, respectively.

Table 5.4. *Measurements (mm) of 24 patients' disc (mean ± standard deviation).* ***Source:*** *Sciortino et al. (2022) [204].*

Medium shape	Surface	Height	Perimeter
L1-2	1470 ± 256	10 ± 2	148 ± 11
L2-3	1964 ± 288	11 ± 2	151 ± 12
L3-4	1630 ± 259	11 ± 2	153 ± 12
L4-5	1401 ± 284	10 ± 3	149 ± 12

Table 5.5. *Measurements of 24 patients' vertebral body (mean ± standard deviation).* ***Source:*** *Sciortino et al. (2022) [204].*

Medium shape	Surface	Height	Perimeter	Width
L1	1407 ± 216	28 ± 2	144 ± 10	40 ± 3
L2	1474 ± 223	28 ± 2	145 ± 11	42 ± 4
L3	1556 ± 230	28 ± 2	148 ± 11	44 ± 4
L4	1535 ± 223	28 ± 2	149 ± 11	45 ± 4
L5	1480 ± 199	30 ± 3	149 ± 10	45 ± 7

5.3.4 SSM of the lumbar spine

The SSM method is a statistical method for **image analysis**, which enables visualization and quantification of the **anatomical variability** by including all **geometric features** of the entire patient population. Hence, a script algorithm developed in the mathematical language MATLAB (R2020, MathWorks Inc., Natick, MA, USA) was used. First, the mean shape representative of the study population was identified (Figure 5.6), being the one with the geometric values closest to the identified mean values. From the **mean shape**, patient-to-patient, the algorithm allowed all iterative nearest points of individual patients to be aligned and shifted relative to the reference patient model. The alignment and displacement were performed through transformations that minimized the overall distance between model pairs until the error deviation was significantly reduced from the reference patient shape [204, 210–213].

The SSM method uses the statistical tool of *Principal Component Analysis* (PCA), which provides the ability to reduce the number of variables in the population and group them within different "shape modes." Using the built-in function implemented in MATLAB, orthogonal transformations together with PCA allowed the data to be projected onto a linear space of maximum variation, i.e., shape modes. **Shape**

modes represent distinct aspects of **variability in the anatomy** of the vertebral body or intervertebral disc. The shape modes, which are less than the number of included patients, exhibit the overall variability in the original set. Each shape mode is visualized by distorting the model from a low value of -3σ to a high value of +3σ of the deformation vector for each mode. The shape vectors numerically represent the contribution that each shape mode has on each spinal pattern [cit]. Lastly, Pearson's correlations (R) among the variables showed statistically significant values with a p-value (p) less than 0.05. In conclusion, a computational atlas of the pathological lumbar spine was created with the aim of exploring **how shape variations** are associated with anatomical features [204, 210–213].

5.3.5 Results

It was obtained an **atlas of the pathological lumbar spine**. Figure 5.8A shows the instance probability profile representing the occurrence probability of a specific shape mode for a specific boundary value, showing that for shape deviations of 0.5σ, 1σ, 1.5σ, 2σ, 2.5σ, 3σ, the probability of the deformed shape is 30.85%, 15.87%, 6.68%, 2.27%, 0.62%, and 0.13%, respectively. Whereas Figure 5.8B shows the cumulative variance up to 100% as the number of Modes increases, that is, it shows the ability of the number of modes to capture the variability of the population shape. The first 12 modes can capture up to 90% of the variability of the shapes [204].

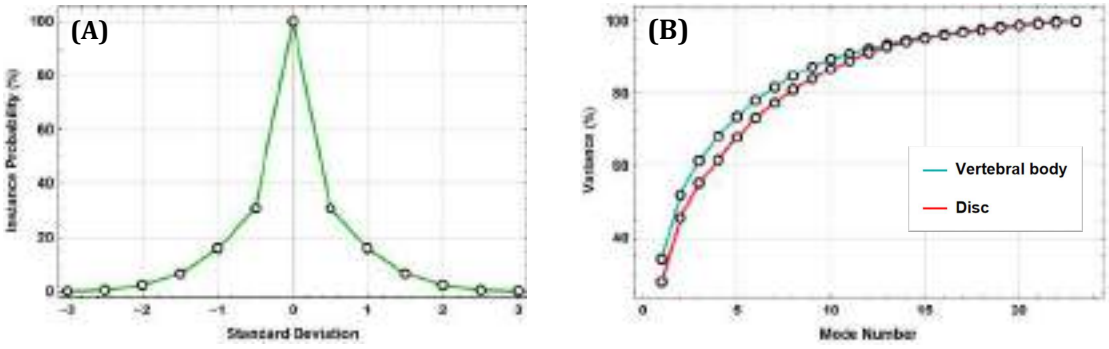

Figure 5.8. ***A)*** *Instance probability profile.* ***B)*** *Variability of the population shape.* ***Source:*** *Sciortino et al. (2022) [204].*

12 primary shape modes have been identified. Figure 5.9 shows mode 1 of the vertebral body (accounting for 34% of the total variance) and the IVD (accounting for 27% of the total variance), at different levels of standard deviation (±1 σ, ±2 σ, ±3 σ), where each deformed shape mode was overlapped with the mean shape.

Mode 1 of vertebral bodies is associated with variation in the height; while mode 1 of IVD is associated with variation in area, width, and scoliosis degree [204].

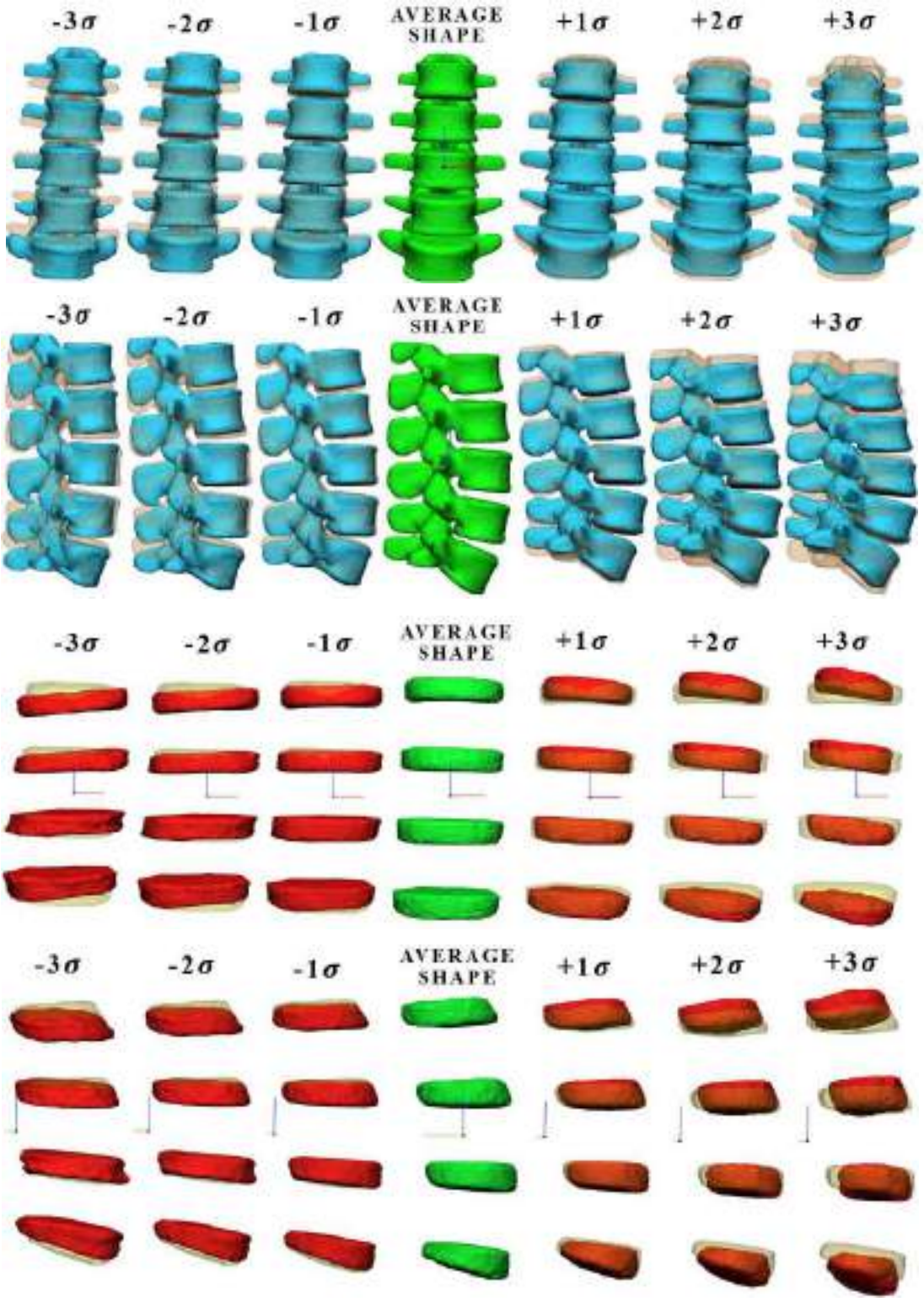

Figure 5.9. *Shape Mode 1 for the vertebral body and intervertebral disc at different σ values, where each deformed shape mode was overlapped with the mean shape (transparent shape).* ***Source:*** *Sciortino et al. (2022) [204].*

Figure 5.10 shows the comparison between mode 2 and 3 of the vertebral body, which account for 52% and 61% of the total variance, respectively; where mode 2 is associated with lordosis degree, while mode 3 with the scoliosis degree [204].

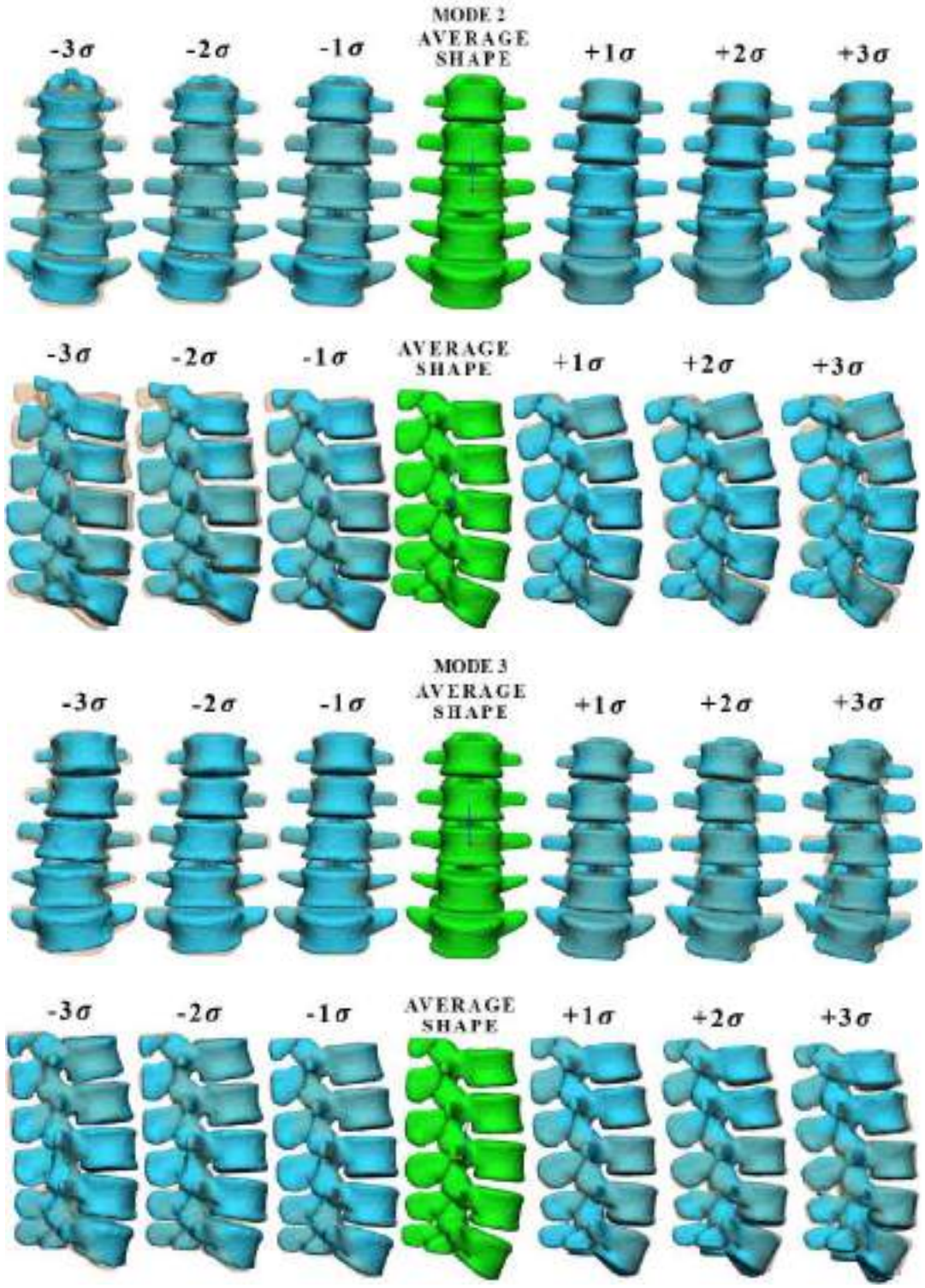

Figure 5.10. *Shape Mode 2 and 5 for the vertebral body at different σ values, where each deformed shape mode was overlapped with the mean shape (transparent shape).* ***Source:*** *Sciortino et al. (2022) [204].*

Lastly, Figure 5.11 shows the **comparison of shape modes** 4, 5, and 6 for disc and vertebral body. For disc shape modes 4,5, and 6 count 61%, 67% and 73% of the total variance, which are associated with changes in lumbar degree (mode 4), surface/scoliosis degree/width (mode 4, 5,6), height (mode 5,6), and disc heights (mode 6). Spinal shape modes 4, 5, and 6 count 68%, 73% and 78%, which are associated variations of width (mode 4), height (mode 4, 6), and spinal process dimensions (mode 4, 5, 6) [204]. Other shape modes can be found in the appendix.

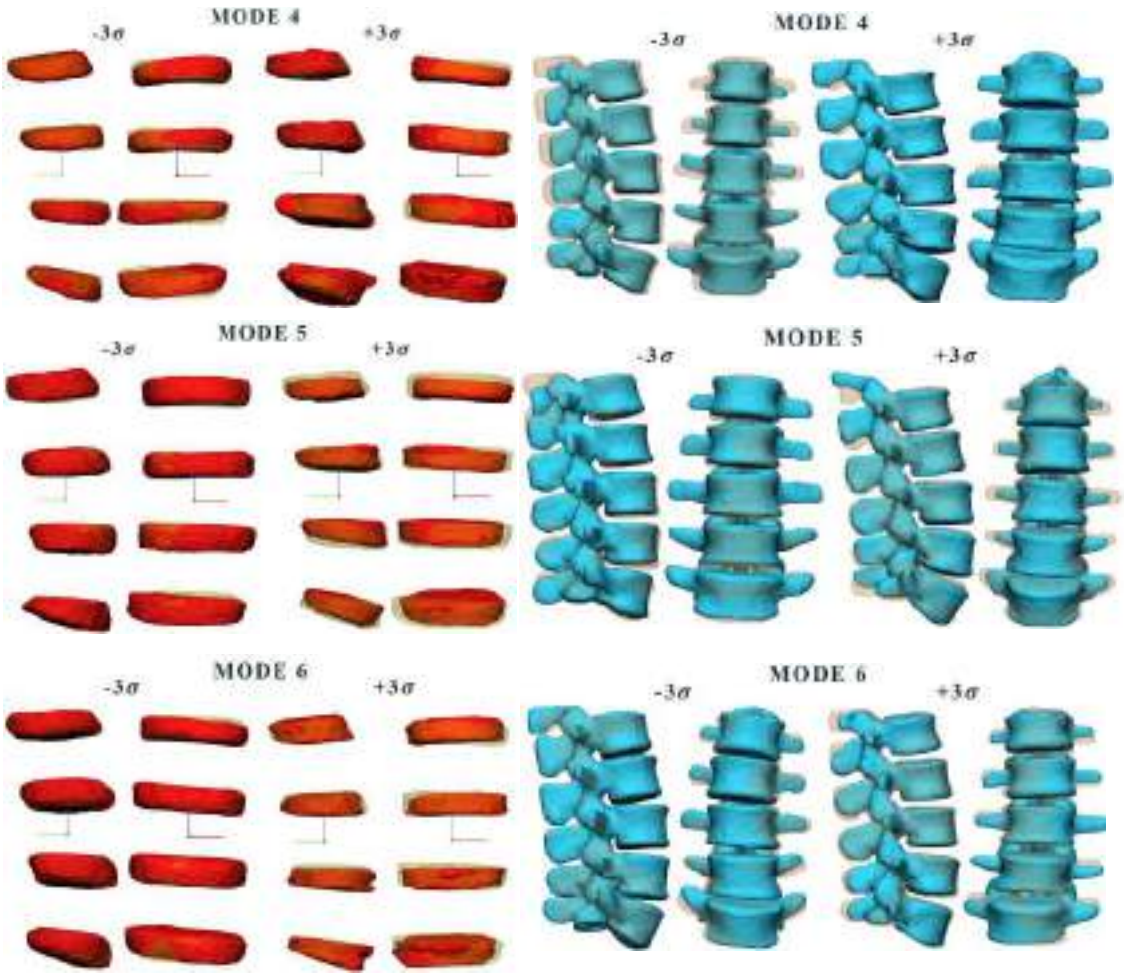

Figure 5.11. *Shape Mode 4, 5 and 6 for the vertebral body and IVD at different σ values, where each deformed shape mode was overlapped with the mean shape (transparent shape).* ***Source:*** *Sciortino et al. (2022) [204].*

Correlations were obtained (**Pearson Correlation**, p-value<0.005) between anatomical and pathological aspects and shape mode. A negative correlation was identified between Mode 6 and Cobb angle (Figure 5.12A) and a positive correlation between Mode 10 and mean column width (Figure 5.12B). In addition, a positive correlation was identified between Mode 9 and patient weight [204](Figure 5.12C).

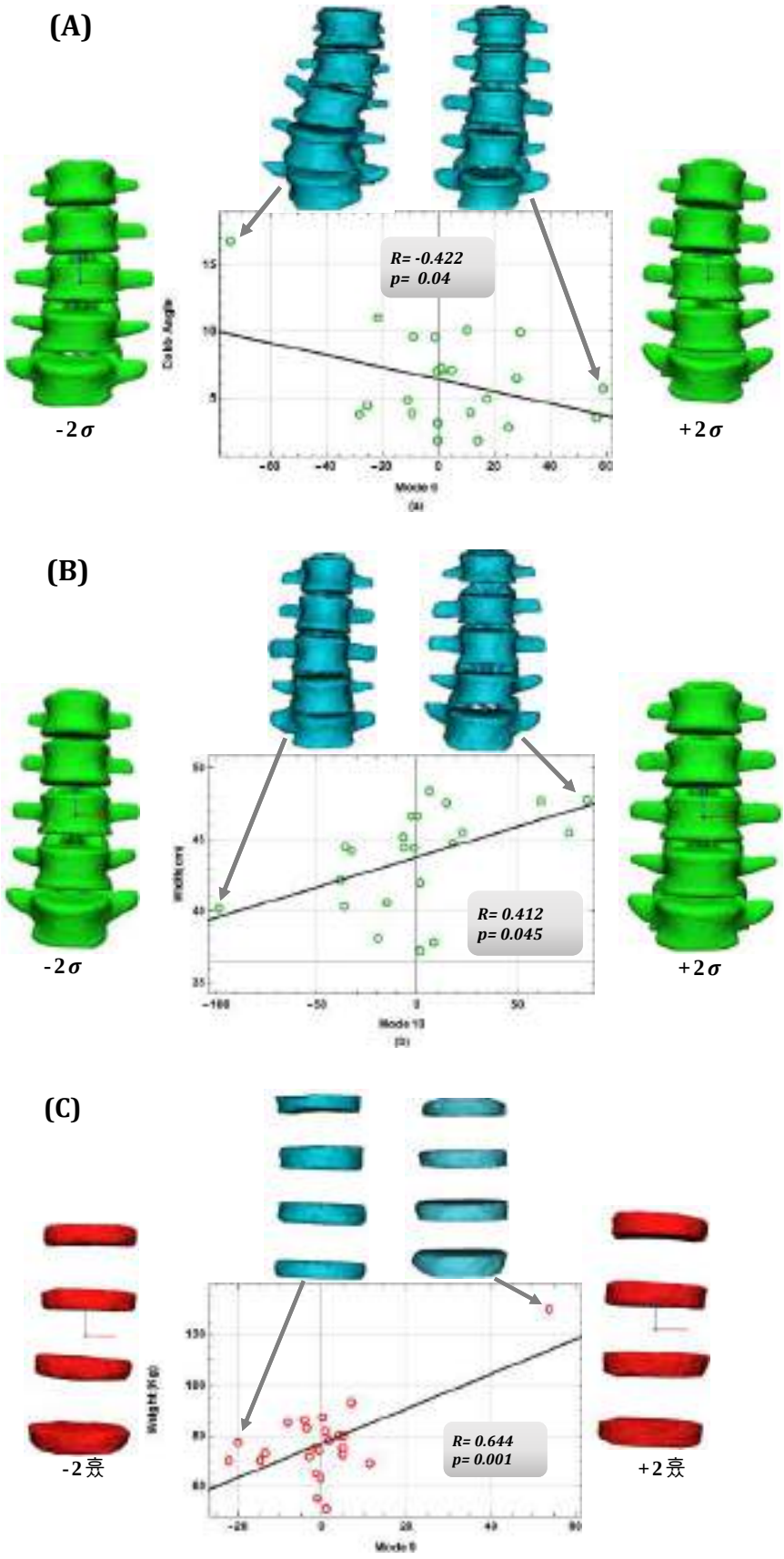

Figure 5.12. *A) Correlation for vertebral body between Mode 6 and Cobb's Angle. B) Correlation for intervertebral disc between Mode 9 and Weight. C) Correlation for vertebral body between Mode 10 and Width.* ***Source:*** *Sciortino et al. (2022) [204].*

5.3.6 Target and application of the lumbar spine atlas

The present study allowed the creation of a SSM (**3D atlas**) for the lumbar spine segment under pathological conditions, thus creating an infinite population of lumbar spine. Indeed, it was demonstrated through correlation analyses how each specific of shape mode was associated with variation in a specific feature of the spine anatomy. The number of patients used is limited, so increasing the number of patients would bring additional variability and broadness of achievable geometries as the shape modes are varied, which can be changed simultaneously, thus changing different geometric aspects not individually. Indeed, the correlations founded provide the actual link between the shape modes and the anatomical and pathological features [205, 214–218].

Technological and scientific evolution has reached high levels in medical research, indeed engineering tools, such as SSM, are crucial precisely to improve the tools available to physicians for patient care. The SSM just described exploits the principles of Medical ***Medical Reverse Engineering*** **(MRE)**, thus starting with CT scans of patients, it was possible to create this **3D digital population** of the anatomical area, thus offering the possibility of generating new models by deforming the average model of the lumbar spine within specific boundaries. MRE refers to all the tools and technologies used to fabricate 3D objects in a single step, starting from a CAD model following a precise guide. These technologies are often implemented for the fabrication of **medical devices**, which can be **customized** to the patient's specific anatomy [205].

Specifically, SSM could be an extremely useful tool in that it provides access to an infinite number of CAD models that can be used for a variety of purposes, from computational FEM analysis of the biomechanics of the lumbar spine, as well as **surgical planning** and implantation of devices, to the creation of medical devices. Indeed, with the second paper, it was explored the fields of application of the atlas they made, finding MRE as one of the main outcomes of use in the literature [205].

The infinite population of geometries could be followed by MRE data processing and CAD geometric modeling for **bioengineering** applications and research. **Biomedical applications** and research could include the implementation of FEM models, with biomechanical or surgical simulations [204, 205].

The study patient population included those with diseases such as **herniated**

discs and scoliosis, for which clinical treatments are not yet definitive. For herniated discs, there are several surgical solutions, which have already been discussed extensively in previous chapters. Specifically, for the insertion of spinal fusion cages, the choice of size is a critical step, and usually falls into specific standardized size alternatives. However, each patient has a different anatomy, so getting to choose which cage to use during surgery is not always straightforward, leading to questionable situations where the surgeon does not know which size is best.

Here, the ability to be able to simulate the effect that the different prosthesis might have on the patient could be of **crucial importance.** Similarly, surgery for scoliosis is particularly complex, requiring fusion of the affected spine segments and correction of rotation in the sagittal plane, leading to significant biomechanical changes and reduced , as has already been discussed. In this context, the use of the SSM could be of great help in situations where decisions are unclear by using a virtual **3D population** to study surgical outcomes in advance. This approach would lead to customized solutions for each patient. The 3D virtual population can reproduce any anatomical scenario without study limitations [205].

5.4 New Finite element model for a Lumbar FSU

This last section aims to present a new finite element model of a lumbar spine FSU to combine experimental and computational endeavors and combine them to validate a new finite element model of the spine, providing an initial starting point to perform computational simulations. The following concepts were extracted from a research paper not published yet by **Sciortino, V.** et al. (2025, out-going).

5.4.1 Materials and methods

The experimental long-standing test of the L4-5 lumbar spine performed by Heuer et al. (2007) was selected as the reference point for validating the new model based on a literature search. This model was chosen because these authors' research group has numerous in vitro experimental test results on the biomechanics of the human spine, and furthermore, a long-standing test was chosen to evaluate the long-term exposure of the IVD to constant loads (daily and nightly activities, already discussed in the previous chapter).

Only **one patient** was selected for this paper from the patient population study

described in the previous sections (**Sex:** Female; **Age:** 41; **Height:** 1.65 m; **Weight:** 55 kg; **BMI:** 20.2; **Pathology:** acute complicated dissection-Type B dissection) whose CT scan was used to do 3D reconstruction of the L4-5 vertebral bodies; meanwhile, the intervertebral disc was modeled by using geometric modeling software with a simple geometric shape.

Therefore, the intervertebral disc was constructed with a **cylindrical shape,** having an ellipsoidal base, which consisted of the fibrous annulus and the nucleus pulposus. The contacts were surface to surface between the vertebral portions and the disc. The **simple modeling** of the disc was **intentional**, as it was intended to model the disc to characterize its overall behavior as simply as possible. The lower part of L5 was constrained and segment movements were allowed only along the z-direction. Figure 5.13 shows the CAD model in frontal, lateral, and axonometric views, obtained from the patient's CT scan.

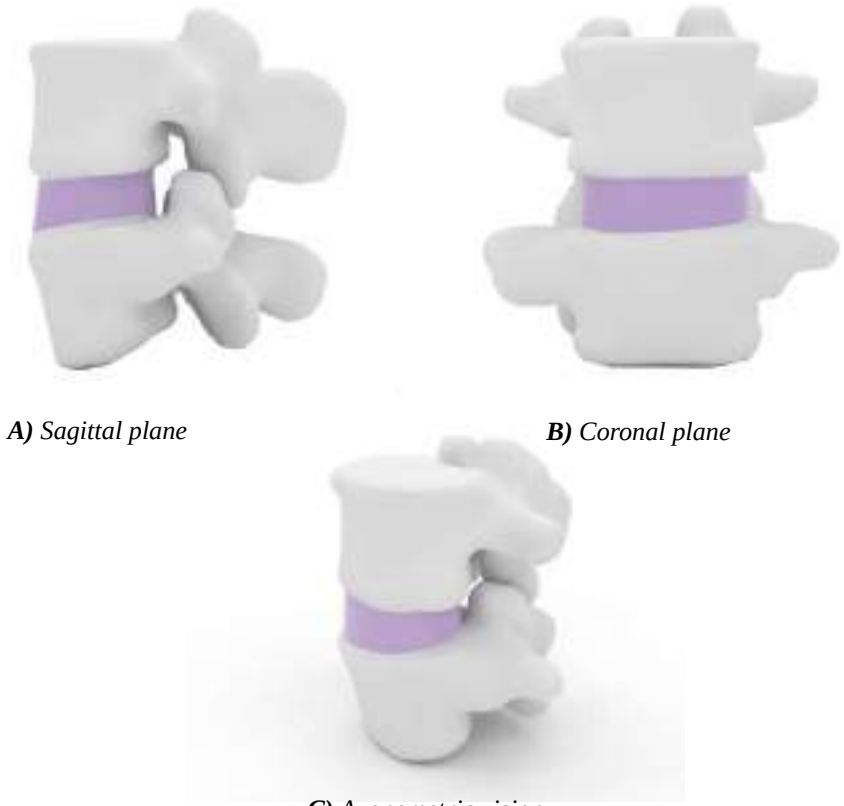

A) *Sagittal plane*

B) *Coronal plane*

C) *Axonometric vision*

Figure 5.13. *© The 3D CAD spinal model reconstructed from CT scan of the patients: A) Sagittal plane vision. B) Coronal plane vision. C) Axonometric vision.*

The experimental data used to validate the model were obtained through the online image data mining software **WebPlotDigitalizer** (https://apps.automeris.io/wpd/), where it was inserted Figure 2 from Heur et al 2007, resulting in Figure 5.14

representing the extracted raw data points. The test protocol involved human L4-5 lumbar segments subjected to creep test for 15 min under 500N **(raw data as a function of disc height reduction)**.

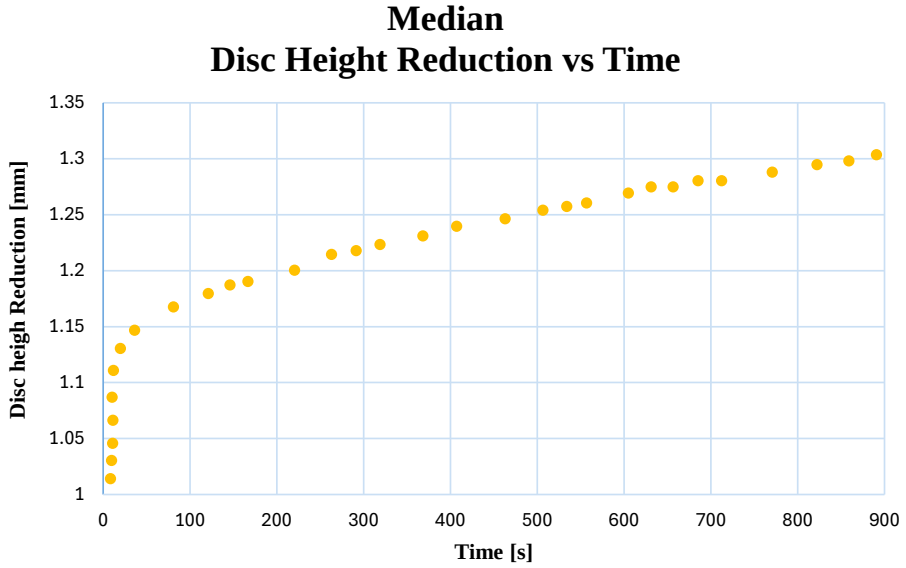

Figure 5.14. *© Raw data obtained from extrapolation manipulation of the median disc height reduction vs time. Source: WebPlotDigitalizer.*

Simulations in **Ansys** involved the same test protocol. The vertebral body was modelled as an **orthotropic material** with the material properties in the table. As for the intervertebral disc, however, this was modelled with two different constitutive models:

1. **Generalized Time Hardening creep model**, where the creep response is as follows:

$$\varepsilon = f t^r e^{\frac{-C_6}{T}} \tag{5.1}$$

Where $f = C_1\sigma + C_2\sigma^2 + C_3\sigma^3$ and $r = C_4\sigma + C_5\sigma$. Where ε is the equivalent creep strain, which is the change in equivalent creep strain with respect to time; σ is the equivalent stress; T is the temperature (absolute) and Ci with i=1...6 are constants defines via experimental data. These parameters were identified from the experimental source data.

2. **Poroelastic model** which parameters were extrapolated from the literature with the following characteristics: model permeability of 7.5e-16; zero pressure on the outer annulus surface; Young's modulus of nucleus equal to 1.5MPa and

Poisson coefficient equal to 0.45; Young's modulus of annulus equal to 2.5MPa and Poisson coefficient equal to 0.45.

Table 5.6. *© Parameters of the orthotropic behavior modelled for the vertebral bodies.*

	Value	Unit
Young's Modulus X	11300	MPa
Young's Modulus Y	11300	MPa
Young's Modulus Z	22000	MPa
Poisson's Ratio XY	0.484	-
Poisson's Ratio YZ	0.203	-
Poisson's Ratio XZ	0.203	-
Shear Modulus XY	3800	MPa
Shear Modulus YZ	5400	MPa
Shear Modulus XZ	5400	MPa

Figure 5.15 shows the finite element model with meshing done involving a tetrahedral mesh at 10 knocks with 47272 elements.

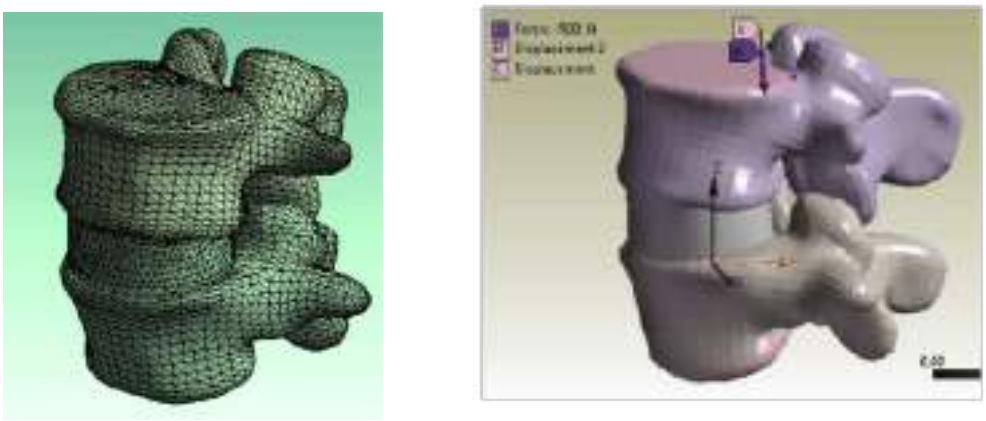

A) *Mesh* ***B)*** *Boundary conditions*

Figure 5.15. *© Tetrahedral mesh created for the L4-5 spine with boundary conditions.*

5.5 Result and final remarks

The experiments by Heuer et al. (2007) showed a median of disc height reduction was 1.30 mm (minimum value of 1.08 mm and maximum value of 1.57 mm). Following the simulations with the two models by which the disc was modelled, Figure 5.16 shows the results of the simulations compared with the experimental data extrapolated using the software. The Generalized Time Hardening creep model reached 1.292 mm

in disc height reduction; meanwhile, the Poroelastic model reached 1.256 mm in disc height reduction. Finally, Figure 5.17 shows the displacement map in which is also shown **bulging effect** of the intervertebral disc

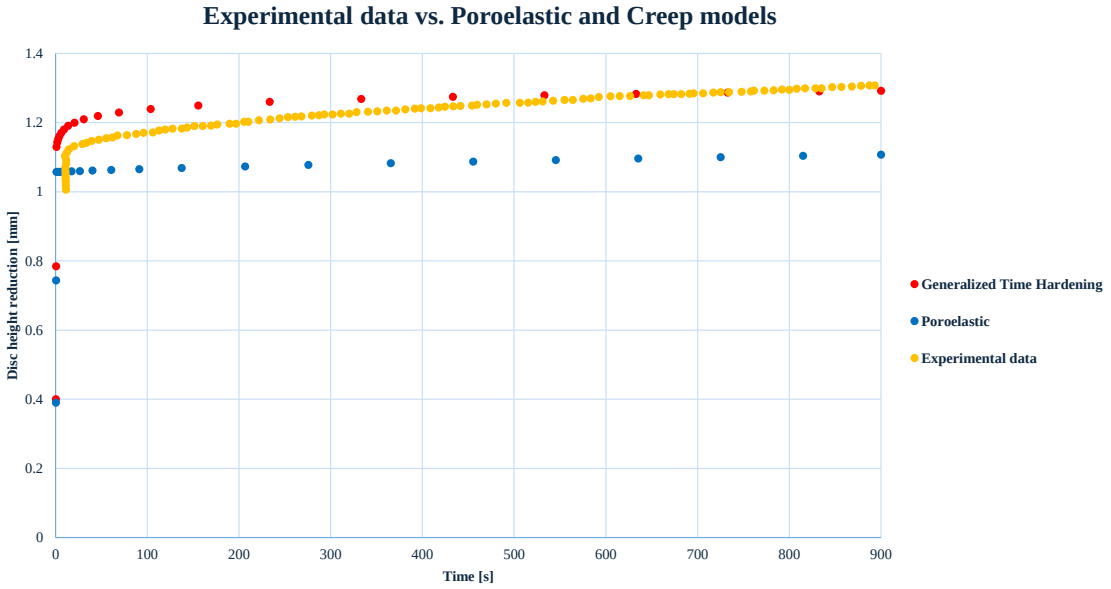

Figure 5.16. *© Comparison between creep curves of the experimental data, Generalized Time Hardening creep and poroelastic model.*

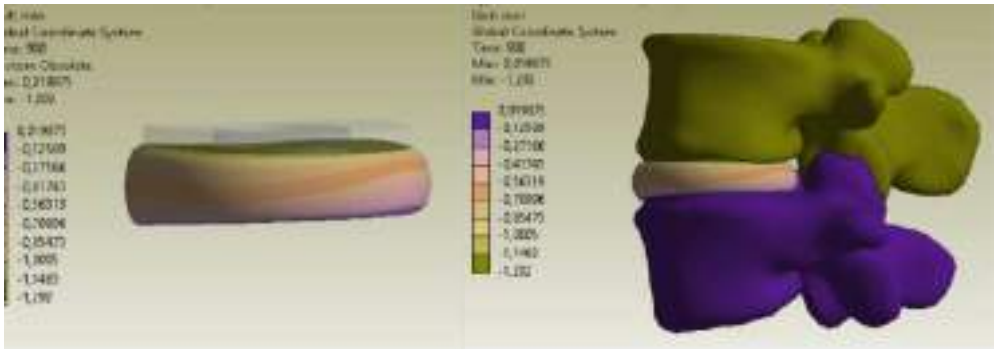

Figure 5.17. *© Simulations results displacement map of the Generalized Time Hardening creep model.*

The analysis performed showed that the newly realized model now used can **simulate** and **reproduce** the *in-vitro* experimental data almost faithfully, since the values of the simulations of the reduction in disc height are like the range of the median experimental values. The study has many **limitations** as the model is very simplified, since the ligamentous components, cartilaginous endplates, and collagen fibers are missing. Moreover, to fully validate the model, it needs to be tested on more patients. Overall, it can be stated that the model can provide a good approximation

to real experimental data. Future studies should engage in further **"complicating"** the finite element model and implementing the biomechanical modeling aspects of the intervertebral disc adopted in Chapter 4, with the goal of realizing a relevant computational model that could be used to study physiological and pathological conditions of the human spine.

Conclusions

This thesis is the result of three years of research. The starting point was the study of the anatomy and biomechanics of the spine in its physiological and pathological conditions. The spine is affected by several pathologies which can negatively affect human being's life. Although medicine and technology have made great progress over the past century, even to this day it is still unclear what triggers the mechanisms of disc degeneration, from which all other disc pathologies then start.

The aim of this thesis was to provide a significant contribution to the literature by enabling an integrated understanding of spinal biomechanics through an analytical and numerical approach, accompanied by an experimental campaign involving both human and animal specimens. By using human and animal specimens, physiological conditions were realistically replicated, contributing to the development of improved biomechanical models. These data are essential for the design of medical devices and the development of surgical techniques. Specifically, the ability to understand disc behavior under prolonged loads can help predict the occurrence of degenerative diseases and plan preventive treatments.

Disc herniation, in particular, is a condition in which the nucleus pulposus leaks out of the annulus fibrosus, causing spinal nerve compression and acute pain. This thesis explored in detail the different surgical approaches available to treat these conditions, such as spinal fixation and fusion, which are intended to stabilize the spine and reduce pain. However, the research also highlighted the limitations of these techniques, including reduced mobility and the risk of developing post-operative syndromes. Hence, research has shown that nucleus disc replacement has emerged as a promising alternative to fusion, as it offers the potential to preserve the natural spine mobility and reduce long-term complications. Nevertheless, nucleus replacement techniques are still not available in clinical practice due to manifold adverse events that have occurred in clinical trials for a variety of NR considered. Indeed, NR is still far away from being able to become a clinical gold standard.

Concerning the experimental section of the thesis work, an experimental campaign was performed twice on bovine and human discs, performing prolonged creep tests designed to gain insight into the viscoelastic properties of spinal tissues. The creep and stress relaxation phenomena are critical in understanding disc biomechanics, since the physiological working activities of the disc cover cycles of loading and unloading between night and day at prolonged loads.

A significant contribution of these experimental campaigns was to highlight how analytical modeling so far in the literature, i.e., classical rheological models and Nutting's law, cannot fully explain the complex viscoelastic response of the intervertebral disc. Therefore, it was suggested and verified how modeling based on the mathematical tool of fractional calculus can be extremely useful in disc biomechanics modeling. This innovative approach allowed a more accurate description of the complex mechanical behavior of the IVD, overcoming the limitations of traditional approaches. Fractional calculus could open new perspectives for the design of more targeted therapeutic interventions and for the prediction of the disease progression, due to the tool's inherent complexity and memory capabilities.

Finally, in the last thesis chapter, the use of finite element modeling (FEM) was presented as an advanced tool for the simulation of spinal biomechanics. The ability to create accurate 3D models of the spine, based on population data and real patients, is a significant step toward personalizing patient care through medical reverse engineering techniques. Indeed, the research made it possible to create a 3D atlas that provided an infinite population of spinal geometries, thereby becoming an important resource for physicians and surgeons in planning surgeries based on individual data and simulating the effects of different surgical techniques. Lastly, an FEM model was then developed and validated through long-term experimental test data, representing the starting point for a numerical model that may be further developed later.

In conclusion, this thesis represents an important contribution in studying spinal biomechanics and degenerative diseases. Continued research is imperative to further explore the relationships and interconnections that exist between biomechanical, environmental, and genetic factors, pathologies, and possible clinical treatments. The results obtained provide a solid basis for the development of new therapeutic and surgical approaches, as well as for the further advancement of biomechanical modeling through the implementation of fractional calculus, while also developing models that

can predict or simulate the progression of disc disease. Future research will then involve the application of this knowledge in the FEM model developed to validate the analytical approaches designed. The work done opens up new possibilities for improving the quality of patients' lives with spinal pathologies by offering innovative solutions for the diagnosis, treatment, and management of chronic pain related to spinal dysfunction. The knowledge gained and the results obtained not only enrich the existing literature but also offer insights for future research and clinical applications. Progress in this field will depend on continued collaboration among scientists, clinicians, and engineers to develop increasingly effective and innovative solutions.

Appendix A

Additional information

A.1 Basics of Fractional calculus

Fractional calculus is an extension of the concept of derivative and integral, as already seen in Chapter 4. For further details about this tools please refer to the following contents.

Euler's *Gamma Function*:

$$\Gamma(x) = \int_0^\infty \frac{e^{-t}}{t^{1-x}} dt, \quad \mathcal{R}(x) > 0 \tag{A.1}$$

***The Riemann-Liouville left-sided Fractional Integral*:**

$$\begin{gathered} \left({}_0I_t^\beta G\right)(t) = \frac{1}{\Gamma(\beta)} \int_0^t \frac{G(\tau)}{(t-\tau)^{1-\beta}} d\tau \\ n-1 < \beta < n, n = \lceil \beta \rceil \end{gathered} \tag{A.2}$$

The *Riemann-Liouville left-sided Fractional Derivative*:

$$\begin{gathered} \left({}_0D_t^\beta G\right)(t) = \frac{d^n}{dt^n}\left({}_0I_t^{1-\beta} G\right)(t) = \frac{1}{\Gamma(n-\beta)} \frac{d^n}{dt^n} \int_0^t \frac{G(\tau)}{(t-\tau)^{\beta-n+1}} d\tau \\ n-1 < \beta < n, n = \lceil \beta \rceil \end{gathered} \tag{A.3}$$

***The Caputo Fractional Derivative*:**

$$\begin{gathered} \left({}_0^C D_t^\beta G\right)(t) = \left({}_0I_t^{1-\beta} \frac{d^n G}{dt^n}\right)(t) = \frac{1}{\Gamma(n-\beta)} \int_0^t \frac{G^{(n)}(\tau)}{(t-\tau)^{\beta-n+1}} d\tau \\ n-1 < \beta < n, n = \lceil \beta \rceil \end{gathered} \tag{A.4}$$

Property of Left-inverse to Riemann-Liouville fractional derivative operator:

$$\left({}_0D_t^{\beta}\,{}_0I_t^{\beta}G\right)(t) = G(t) \tag{A.5}$$

Property for Caputo derivative:

$$\left({}_0^CD_t^{\beta}\,{}_0I_t^{\beta}G\right)(t) = G(t) \tag{A.6}$$

A.2 Optimization code

The following is the **Optimization code** used in Chapter 4.

```
(*Import Experiemental Data*)
dataX = Flatten@Import["FileBrowser from your computer", {"Data", 1}];
datay = Flatten@Import["FileBrowser from your computer", {"Data", 1}];

(*Definition of the model for data fitting*)
model[parameters_, t_] := MathematicalFormulation - CreepFunction;

(*Definition of the cost function (square sum of the differences)*)
costFunction[parameters_] := Total[(model[parameters, dataX] - dataY)^2]

(*Minimization of the cost function*)
minimizationResult = NMinimize[{costFunction[parameters], parametersrange}, {parameters}];

(*Estraction of optimal parameters*)
optimalParameters = {parameters} /. minimizationResult[[2]];

(*R² Calculaton*)
fittedValues = model[parameters, dataX] /. Thread[{parameters} → optimalParameters];
meanY = Mean[dataY];
totalVariation = Total[(dataY - meanY)^2];
residuals = dataY - fittedValues;
residualVariation = Total[residuals^2];
rSquared = 1 - residualVariation / totalVariation;

(*Error rate in fitting*)
percentageError = 100 Total[Abs[residuals]] / Total[dataY];

(*Model with the fitted parameters*)
fitCurve[t_] := model[parameters, t] /. Thread[{parameters} → optimalParameters];
```

Figure A.1. *Optimization code for the creep curve fitting with the mathematical models*

A.3 Shape modes

The following are the **other shape modes** for IVD and vertebral bodies presented in Chapter 5.

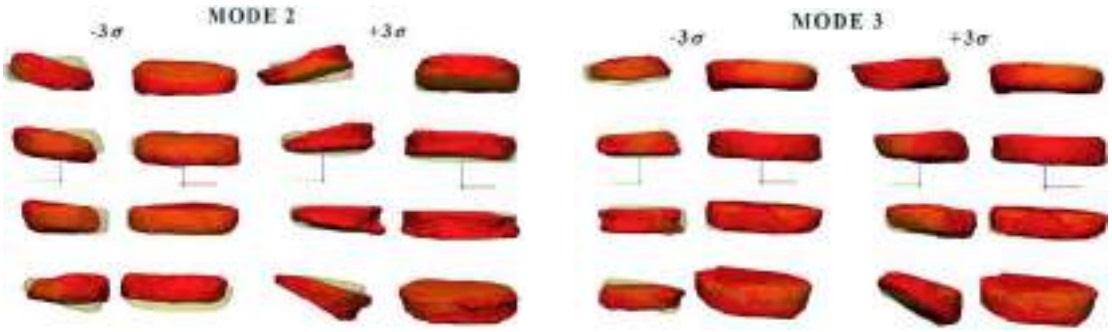

Figure A.2. *Graphic representation for mode 2 and 3 for the IVD (the deformed shape is overlapped with the mean one).*

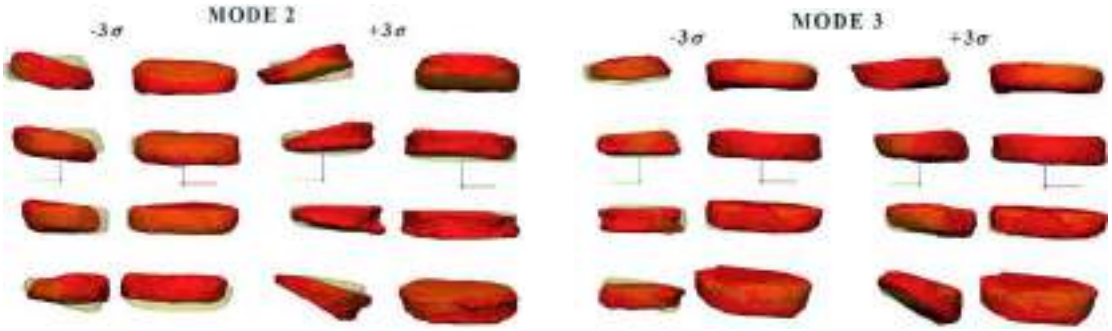

Figure A.3. *Graphic representation for modes 7 and 8 for* ***intervertebral disc*** *and vertebral body (the deformed shape is overlapped with the mean one).*

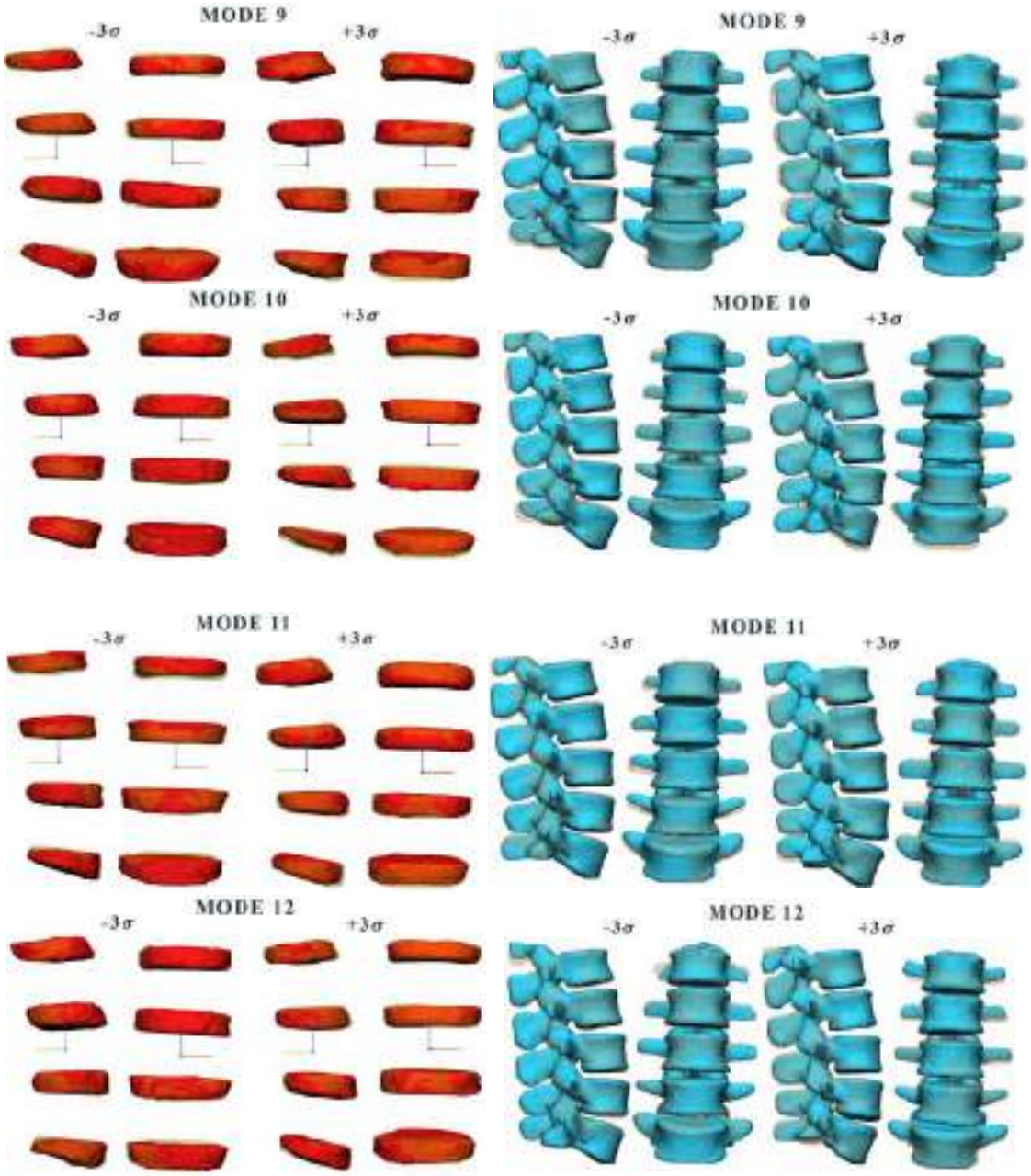

Figure A.4. *Graphic representation for modes 9, 10, 11 and 12 of the vertebral body and IVD (the deformed shape is overlapped with the mean one).*

Bibliography

[1] F. Martini, R.B. Tallitsch, and J. Nath. *Human Anatomy*. Pearson, 2017. ISBN: 9780134320762.

[2] F. Galbusera and H.-J. Wilke. *Biomechanics of the spine: Basic concepts, spinal disorders and treatments*. Academic Press, 2018.

[3] Michael W Devereaux. "Anatomy and examination of the spine". In: *Neurologic clinics* 25.2 (2007).

[4] Boyle Cheng. *Handbook of Spine Technology*. Springer, 2021.

[5] Ronan O'Rahilly, F Muller, and DB Meyer. "The human vertebral column at the end of the embryonic period proper. 1. The column as a whole." In: *Journal of anatomy* 131.Pt 3 (1980), p. 565.

[6] Anne M Gilroy et al. *Atlas of anatomy*. Thieme Stuttgart, 2008.

[7] Adriana Rigutti. *Atlante di anatomia*. Giunti Editore, 2007.

[8] Steven M Kurtz and Avram Edidin. *Spine technology handbook*. Elsevier, 2006.

[9] R. O'Rahilly, F. Müller, and Meyer DB. "The human vertebral column at the end of the embryonic period proper. 2. The occipitocervical region." In: *Journal of anatomy* 136 (1983), p. 181.

[10] Donald F Huelke and Guy S Nusholtz. "Cervical spine biomechanics: a review of the literature". In: *Journal of orthopaedic research* 4.2 (1986).

[11] R. O'Rahilly, F. Müller, and Meyer DB. "The human vertebral column at the end of the embryonic period proper. 4. The sacrococcygeal region." In: *Journal of anatomy* 168 (1990), p. 95.

[12] Irving M Shapiro and Makarand V Risbud. *Intervertebral Disc*. Springer, 2016.

[13] Luigi Manfrè and Johan Van Goethem. *The Disc and Degenerative Disc Disease: Remove Or Regenerate?* Springer, 2021.

[14] M. et al. Volz. “Computational modeling intervertebral disc pathophysiology: a review”. In: *Frontiers in physiology* 12 (2022), p. 750668.

[15] A. Ruffilli et al. “Mechanobiology of the human intervertebral disc: Systematic review of the literature and future perspectives”. In: *International Journal of Molecular Sciences* 24.3 (2023), p. 2728.

[16] Brody A Frost, Sandra Camarero-Espinosa, and E Johan Foster. “Materials for the spine: anatomy, problems, and solutions”. In: *Materials* 12.2 (2019), p. 253.

[17] Lance Twomey and James Taylor. “Age changes in lumbar intervertebral discs”. In: *Acta orthopaedica scandinavica* 56.6 (1985).

[18] Gerhard A Holzapfel et al. “Single lamellar mechanics of the human lumbar anulus fibrosus”. In: *Biomechanics and modeling in mechanobiology* 3 (2005).

[19] E. R. Acaroglu, J. C. Latridis, and L. A et al. Setton. “Degeneration and aging affect the tensile behavior of human lumbar anulus fibrosus”. In: *Spine* 20.24 (1995).

[20] Francoise Marchand and Abdul M Ahmed. “Investigation of the laminate structure of lumbar disc anulus fibrosus”. In: *Spine* 15.5 (1990).

[21] EF Johnson et al. “Elastic fibres in the anulus fibrosus of the adult human lumbar intervertebral disc. A preliminary report.” In: *Journal of anatomy* 143 (1985), p. 57.

[22] Azucena G Rodriguez et al. “Morphology of the human vertebral endplate”. In: *Journal of orthopaedic research* 30.2 (2012).

[23] K. et. al. Lakstins. “Characterization of the human intervertebral disc cartilage endplate at the molecular, cell, and tissue levels”. In: *Journal of Orthopaedic Research* 39.9 (2021).

[24] JPG Urban and JF McMullin. “Swelling pressure of the inervertebral disc: influence of proteoglycan and collagen contents”. In: *Biorheology* 22.2 (1985).

[25] S Holm et al. “Nutrition of the intervertebral disc: solute transport and metabolism”. In: *Connective tissue research* 8.2 (1981).

[26] Thijs Grunhagen et al. “Nutrient supply and intervertebral disc metabolism”. In: *JBJS* (2006).

[27] Jill PG Urban, Stanton Smith, and Jeremy CT Fairbank. "Nutrition of the intervertebral disc". In: *Spine* 29.23 (2004).

[28] Jill PG Urban and Sten H Holm. *Intervertebral disc nutrition as related to spinal movements and fusion*. Springer, 1986.

[29] Kaili Lin et al. "Advanced collagen-based biomaterials for regenerative biomedicine". In: *Advanced Functional Materials* 29.3 (2019).

[30] Néstor R Lago et al. "EXTRACELLULAR MATRIX-LIVER RELATIONSHIP". In: *CHRONIC LIVER DISEASE* (2015), p. 105.

[31] Lisa D. Muiznieks, Anthony S. Weiss, and Fred W. Keeley. "Structural disorder and dynamics of elastin". In: *Biochemistry and Cell Biology* 88.2 (2010). DOI: 10.1139/O09-161.

[32] P Adams, DR Eyre, and H Muir. "Biochemical aspects of development and ageing of human lumbar intervertebral discs". In: *Rheumatology* 16.1 (1977). DOI: 10.1093/rheumatology/16.1.22.

[33] H.-J. Wilke et al. "A universal spine tester for in vitro experiments with muscle force simulation". In: *European Spine Journal* 3.2 (1994). ISSN: 1432-0932. DOI: 10.1007/BF02221446.

[34] H. J. Wilke, K. Wenger, and L. Claes. "Testing criteria for spinal implants: recommendations for the standardization of in vitro stability testing of spinal implants". In: *European Spine Journal* 7 (1998). DOI: 10.1007/s005860050045.

[35] I. Busscher, A. J. van der Veen, and J. H. et al. van Dieën. "In Vitro Biomechanical Characteristics of the Spine: A Comparison Between Human and Porcine Spinal Segments". In: *Spine* 35.2 (2010). DOI: 10.1097/BRS.0b013e3181b21885.

[36] L. T. Topoleski et al. *Mechanical Testing of Orthopaedic Implants*. Woodhead Publishing, 2017. DOI: 10.1016/B978-0-08-100286-5.00003-2.

[37] A. A. E. Orías, J. He, and M. Wang. *Experimental Methods in Orthopaedic Biomechanics*. Academic Press, 2017. DOI: 10.1016/B978-0-12-803802-4.00009-3.

[38] Nihat Özkaya et al. *Fundamentals of Biomechanics: Equilibrium, Motion, and Deformation*. Springer Cham, 2016. DOI: 10.1007/978-3-319-44738-4.

[39] G. W. Schmid-Schönbein, S. Y. Woo, and B. W. Zweifach, eds. *Frontiers in Biomechanics*. Springer Science and Business Media, 2012.

[40] M. Dietrich, K. Kedzior, and T. Zagrajek. "A Biomechanical Model of the Human Spinal System". In: *Proceedings of the Institution of Mechanical Engineers, Part H: Journal of Engineering in Medicine* 205.1 (1991). DOI: 10.1243/PIME_PROC_1991_205_257_02.

[41] John H. Challis. *Experimental Methods in Biomechanics*. Springer Cham, 2021. DOI: 10.1007/978-3-030-52256-8.

[42] T. T. Dao and M. C. H. B. Tho. *Biomechanics of the Musculoskeletal System: Modeling of Data Uncertainty and Knowledge*. John Wiley and Sons, 2014.

[43] M. R et al. Asyraf. "Fundamentals of Creep, Testing Methods and Development of Test Rig for the Full-Scale Crossarm: A Review". In: *Jurnal Teknologi (Sciences and Engineering)* 81.4 (2019). DOI: 10.11113/jt.v81.13402.

[44] Albert J. van der Veen et al. "Flow-Related Mechanics of the Intervertebral Disc: The Validity of an In Vitro Model". In: *Spine* 30.18 (2005). DOI: 10.1097/01.brs.0000179306.40309.3a.

[45] S. Borrelli, G. Putame, G. Pascoletti, et al. "In Silico Meta-Analysis of Boundary Conditions for Experimental Tests on the Lumbar Spine". In: *Annals of Biomedical Engineering* 50 (2022). DOI: 10.1007/s10439-022-03015-x.

[46] Michael A. Adams and Patricia Dolan. "Spine biomechanics". In: *Journal of Biomechanics* 38.10 (2005), pp. 1972–1983. ISSN: 0021-9290. DOI: doi.org/10.1016/j.jbiomech.2005.03.028.

[47] Avinash G. Patwardhan et al. "A Follower Load Increases the Load-Carrying Capacity of the Lumbar Spine in Compression". In: *Spine* 24.10 (1999).

[48] Avinash G. Patwardhan et al. "Effect of compressive follower preload on the flexion–extension response of the human lumbar spine". In: *Journal of Biomechanics* 39.1 (2006). DOI: 10.1016/S0736-0266(02)00202-4.

[49] Kap-Soo Han et al. "Spinal muscles can create compressive follower loads in the lumbar spine in a neutral standing posture". In: *Medical Engineering and Physics* 33.4 (2011). DOI: doi.org/10.1016/j.medengphy.2010.11.014.

[50] Kyungsoo Kim and Yoon Hyuk Kim. “Role of Trunk Muscles in Generating Follower Load in the Lumbar Spine of Neutral Standing Posture”. In: *Journal of Biomechanical Engineering* 130.4 (May 2008), p. 041005. ISSN: 0148-0731. DOI: 10.1115/1.2907739.

[51] Hans-Joachim Wilke et al. “Influence of varying muscle forces on lumbar intradiscal pressure: an in vitro study”. In: *Journal of biomechanics* 29.4 (1996).

[52] Hans-Joachim Wilke et al. “Intradiscal pressure together with anthropometric data – a data set for the validation of models”. In: *Clinical Biomechanics* 16 (2001), S111–S126. ISSN: 0268-0033. DOI: doi.org/10.1016/S0268-0033(00)00103-0.

[53] Hans–Joachim Wilke et al. “New In Vivo Measurements of Pressures in the Intervertebral Disc in Daily Life”. In: *Spine* 24.8 (1999).

[54] C. Neidlinger-Wilke, F. Galbusera, H. Pratsinis, et al. “Mechanical loading of the intervertebral disc: from the macroscopic to the cellular level”. In: *European Spine Journal* 23.Suppl 3 (2014). DOI: 10.1007/s00586-013-2855-9.

[55] N. Newell et al. “Biomechanics of the human intervertebral disc: A review of testing techniques and results”. In: *Journal of the Mechanical Behavior of Biomedical Materials* 69 (2017), pp. 420–434. ISSN: 1751-6161. DOI: doi.org/10.1016/j.jmbbm.2017.01.037.

[56] Geoffrey Thor Desmoulin, Vikram Pradhan, and Theodore Edgar Milner. “Mechanical Aspects of Intervertebral Disc Injury and Implications on Biomechanics”. In: *SPINE* 45.8 (2020). DOI: 10.1097/BRS.0000000000003291.

[57] L. A. Setton. “Cell mechanics and mechanobiology in the intervertebral disc”. In: *European Cells and Materials* 10.Suppl. 3 (2005), p. 22.

[58] Amos Race, Neil D. Broom, and Peter Robertson. “Effect of Loading Rate and Hydration on the Mechanical Properties of the Disc”. In: *Spine* 25.6 (2000).

[59] S. D. Rockoff, E. Sweet, and J. Bleustein. “The relative contribution of trabecular and cortical bone to the strength of human lumbar vertebrae”. In: *Calcified Tissue Research* 3 (1969). DOI: 10.1007/BF02058659.

[60] Nikolai Bogduk and Susan Mercer. “Biomechanics of the cervical spine. I: Normal kinematics”. In: *Clinical Biomechanics* 15.9 (2000). ISSN: 0268-0033. DOI: doi.org/10.1016/S0268-0033(00)00034-6.

[61] Fratzl P. et al. “Nature’s hierarchical materials”. In: *Progress in Materials Science* 52.8 (2007). DOI: 10.1016/j.pmatsci.2007.06.001.

[62] Narayan Yoganandan, Srirangam Kumaresan, and Frank A Pintar. “Biomechanics of the cervical spine Part 2. Cervical spine soft tissue responses and biomechanical modeling”. In: *Clinical Biomechanics* 16.1 (2001), pp. 1–27. ISSN: 0268-0033. DOI: 10.1016/S0268-0033(00)00074-7.

[63] Filip Manek et al. *Biomechanical Study of Lumbar Spinal Fixation Device*. Vol. 232. Applied Mechanics and Materials. Trans Tech Publications Ltd, Dec. 2012. DOI: 10.4028/www.scientific.net/AMM.232.142.

[64] S. M. Moon, J. H. Yoder, A. C. Wright, et al. “Evaluation of intervertebral disc cartilaginous endplate structure using magnetic resonance imaging”. In: *European Spine Journal* 22 (2013). DOI: 10.1007/s00586-013-2798-1.

[65] Jesse C. Beckstein et al. “Comparison of Animal Discs Used in Disc Research to Human Lumbar Disc: Axial Compression Mechanics and Glycosaminoglycan Content”. In: *Spine* 33.6 (2008). DOI: 10.1097/BRS.0b013e318166e001.

[66] Hans-Joachim Wilke, Annette Kettler, and Lutz E. Claes. “Are Sheep Spines a Valid Biomechanical Model for Human Spines?” In: *Spine* 22.20 (1997). DOI: 10.1097/00007632-199710150-00009.

[67] David I. Simunic, Peter A. Robertson, and Neil D. Broom. “Mechanically Induced Disruption of the Healthy Bovine Intervertebral Disc”. In: *Spine* 29.9 (2004).

[68] Nicolas Newell et al. “Material properties of bovine intervertebral discs across strain rates”. In: *Journal of the Mechanical Behavior of Biomedical Materials* 65 (2017), pp. 824–830. DOI: doi.org/10.1016/j.jmbbm.2016.10.012.

[69] J. Yu et al. “Elastic fibre organization in the intervertebral discs of the bovine tail”. In: *Journal of Anatomy* 201.6 (2002). DOI: 10.1046/j.1469-7580.2002.00111.x.

[70] Lisa D. Muiznieks, Anthony S. Weiss, and Fred W. Keeley. "Structural disorder and dynamics of elastin". In: *Biochemistry and Cell Biology* 88.2 (2010), pp. 239–250. DOI: 10.1139/O09-161.

[71] William N. Findley and Francis A. Davis. *Creep and relaxation of nonlinear viscoelastic materials*. Courier Corporation, 2013.

[72] Richard M. Christensen. *Theory of viscoelasticity*. Courier Corporation, 2013.

[73] Y. C. Fung. *Biomechanics: Mechanical Properties of Living Tissues*. Springer Science and Business Media, 2013.

[74] Sertac Kirnaz et al. "Pathomechanism and Biomechanics of Degenerative Disc Disease: Features of Healthy and Degenerated Discs". In: *International Journal of Spine Surgery* 15.s1 (2021), pp. 10–25. ISSN: 2211-4599. DOI: 10.14444/8052.

[75] MA Adams. "Basic science of spinal degeneration". In: *Surgery* 30.7 (2012).

[76] A Wu et al. "Global low back pain prevalence and years lived with disability from 1990 to 2017: estimates from the Global Burden of Disease Study 2017". In: *Ann. Transl. Med.* 8.6 (2020).

[77] David F. Fardon and Pierre C. Milette. "Nomenclature and Classification of Lumbar Disc Pathology: Recommendations of the Combined Task Forces of the North American Spine Society, American Society of Spine Radiology, and American Society of Neuroradiology". In: *Spine* 26.5 (2001). DOI: 10.1097/00007632-200103010-00012.

[78] Isma Liza Mohd Isa et al. "Discogenic Low Back Pain: Anatomy, Pathophysiology and Treatments of Intervertebral Disc Degeneration". In: *International Journal of Molecular Sciences* 24.1 (2023), p. 208. DOI: 10.3390/ijms24010208.

[79] F. Galbusera, M. van Rijsbergen, K. Ito, et al. "Ageing and degenerative changes of the intervertebral disc and their impact on spinal flexibility". In: *European Spine Journal* 23.Suppl 3 (2014). DOI: 10.1007/s00586-014-3203-4.

[80] S. V. Kushchayev, T. Glushko, M. Jarraya, et al. "ABCs of the degenerative spine". In: *Insights Imaging* 9 (2018). DOI: 10.1007/s13244-017-0584-z.

[81] T. K. F. Taylor and J. et al. Melrose. “Spinal Biomechanics and Aging Are Major Determinants of the Proteoglycan Metabolism of Intervertebral Disc Cells”. In: *Spine* 25.23 (2000). DOI: 10.1097/00007632-200012010-00011.

[82] John E. A. O’Connell. “Protrusions of the Lumbar Intervertebral Discs”. In: *The Journal of Bone Joint Surgery British Volume* 33-B.1 (1951). DOI: 10.1302/0301-620X.33B1.8.

[83] T. Benzakour, V. Igoumenou, A. F. Mavrogenis, et al. “Current concepts for lumbar disc herniation”. In: *International Orthopaedics (SICOT)* 43 (2019). DOI: 10.1007/s00264-018-4247-6.

[84] Takeshi Oichi et al. “Pathomechanism of intervertebral disc degeneration”. In: *JOR SPINE* 3.1 (2020), e1076. DOI: 10.1002/jsp2.1076.

[85] J.P. Urban and S. Roberts. “Degeneration of the intervertebral disc”. In: *Arthritis Research and Therapy* 5 (2003), p. 120. DOI: 10.1186/ar629.

[86] Ankita Samanta, Thomas Lufkin, and Petra Kraus. “Intervertebral disc degeneration—Current therapeutic options and challenges”. In: *Frontiers in Public Health* 11 (2023), p. 1156749. DOI: 10.3389/fpubh.2023.1156749.

[87] Susan R.S. Bibby et al. “The pathophysiology of the intervertebral disc”. In: *Joint Bone Spine* 68.6 (2001), pp. 537–542. ISSN: 1297-319X. DOI: doi.org/10.1016/S1297-319X(01)00332-3.

[88] J. R. Hutchinson et al. “Structure and Function of the Lumbar Intervertebral Disk in Health, Aging, and Pathologic Conditions”. In: *Journal of Orthopaedic and Sports Physical Therapy* 31.6 (2001). DOI: 10.2519/jospt.2001.31.6.291.

[89] R. M. Amin, N. S. Andrade, and B. J. Neuman. “Lumbar Disc Herniation”. In: *Curr Rev Musculoskelet Med* 10 (2017). DOI: 10.1007/s12178-017-9441-4.

[90] HJ Wilke et al. “Effect of a prosthetic disc nucleus on the mobility and disc height of the L4–5 intervertebral disc postnucleotomy”. In: *J. Neurosurg. Spine* 95 (2001). DOI: 10.3171/spi.2001.95.2.0208.

[91] H Frei et al. “The effect of nucleotomy on lumbar spine mechanics in compression and shear loading”. In: *Spine* 26.19 (2001), pp. 2080–2089. DOI: 10.1097/00007632-200110010-00007.

[92] Gergana I. Hristova et al. “Calcification in Human Intervertebral Disc Degeneration and Scoliosis”. In: *Journal of Orthopaedic Research* 29.8 (2011). DOI: 10.1002/jor.21456.

[93] Lorin M. Benneker et al. “Vertebral Endplate Marrow Contact Channel Occlusions and Intervertebral Disc Degeneration”. In: *Spine* 30.2 (2005). DOI: 10.1097/01.brs.0000150833.93248.09.

[94] T Faciszewski et al. “Surgical technique of transsacral implantation of autograft bone for fusion of L5 to the sacrum in adolescent spondylolysis or spondylolisthesis: report of five cases”. In: *Spine* 20.12 (1995), pp. 1345–1350.

[95] Alexander R. Vaccaro et al. “AOSpine Thoracolumbar Spine Injury Classification System: Fracture Description, Neurological Status, and Key Modifiers”. In: *Spine* 38.23 (2013). DOI: 10.1097/BRS.0b013e3182a8a381.

[96] Ryan E. Will et al. “Cobb Angle Progression in Adolescent Scoliosis Begins at the Intervertebral Disc”. In: *Spine* 34.25 (2009). DOI: 10.1097/BRS.0b013e3181c11853.

[97] Hassan Serhan et al. “Motion-preserving technologies for degenerative lumbar spine: The past, present, and future horizons”. In: *SAS Journal* 5.3 (2011), pp. 75–89. ISSN: 1935-9810. DOI: doi.org/10.1016/j.esas.2011.05.001.

[98] Daniel H. Kim, Alexander R. Vaccaro, and Richard G. Fessler. *Spinal Instrumentation: Surgical Techniques*. Thieme, 2005. ISBN: 9781588903754. DOI: 10.1055/b-002-76305.

[99] M Szpalski, R Gunzburg, and M Mayer. “Spine arthroplasty: a historical review”. In: *Eur. Spine J.* 11 (2002). DOI: 10.1007/s00586-002-0474-y.

[100] MH Mayer and A Korge. “Non-fusion technology in degenerative lumbar spinal disorders: facts, questions, challenges”. In: *Eur. Spine J.* 11 (2002), S85–S91. DOI: 10.1007/s00586-002-0445-3.

[101] V.C. Traynelis. “Spinal arthroplasty”. In: *FOC* 13 (2002), pp. 1–7. DOI: 10.3171/foc.2002.13.2.11.

[102] Chen-Sheng Chen et al. “Stress analysis of the disc adjacent to interbody fusion in lumbar spine”. In: *Medical Engineering and Physics* 23.7 (2001), pp. 485–493. ISSN: 1350-4533. DOI: doi.org/10.1016/S1350-4533(01)00076-5.

[103] Ralph J. Mobbs et al. “Indications for Anterior Lumbar Interbody Fusion”. In: *Orthopedic Surgery* 5.3 (2013), pp. 162–166. DOI: 10.1111/os.12048.

[104] Kevin Phan and Ralph J. Mobbs. “Evolution of Design of Interbody Cages for Anterior Lumbar Interbody Fusion”. In: *Orthopedic Surgery* 8.1 (2016), pp. 1–6. DOI: 10.1111/os.12259.

[105] Ralph J. Mobbs, Kevin Phan, and Andrew Lennox. “Approach-Related Complications of Anterior Lumbar Interbody Fusion: Results of a Combined Spine and Vascular Surgical Team”. In: *Global Spine Journal* 6.2 (2021), pp. 103–109. DOI: 10.1055/s-0035-155714.

[106] R. J. Mobbs et al. “Lumbar interbody fusion: techniques, indications and comparison of interbody fusion options including PLIF, TLIF, MI-TLIF, OLIF/ATP, LLIF and ALIF”. In: *J Spine Surg* 1.1 (2015), pp. 2–18. DOI: 10.3978/j.issn.2414-469X.2015.10.05.

[107] Luke L. Viglione, Uphar Chamoli, and Ashish D. Diwan. “Is Stand-Alone Anterior Lumbar Interbody Fusion a Safe and Efficacious Treatment for Isthmic Spondylolisthesis of L5-S1?” In: *SAGE Open Medicine* 7 (6 2017), p. 219256821769921. DOI: 10.1177/219256821769921.

[108] H.-J. Wilke and V. Sciortino. “The past, present, and the future of disc nucleus replacement. A systematic review of a large diversity of ideas and experiences”. In: *Biomaterials* 312 (2025), p. 122717. ISSN: 0142-9612. DOI: 10.1016/j.biomaterials.2024.122717.

[109] EJ Carragee et al. “Clinical outcomes after lumbar discectomy for sciatica: the effects of fragment type and anular competence”. In: *JBJS* 85.1 (2003), pp. 102–108.

[110] C Thome et al. “Outcome after lumbar sequestrectomy compared with microdiscectomy: a prospective randomized study”. In: *J. Neurosurg. Spine* 2.3 (2005), pp. 271–278. DOI: 10.3171/spi.2005.2.3.0271.

[111] RW Murphy. “Nerve roots and spinal nerves in degenerative disk disease”. In: *Clin. Orthop. Relat. Res.* 129 (1977), pp. 46–60.

[112] RW Williams. “Microlumbar discectomy: a conservative surgical approach to the virgin herniated lumbar disc”. In: *Spine* 3.2 (1978), pp. 175–182.

[113] VK Goel et al. “Kinematics of the whole lumbar spine: effect of discectomy”. In: *Spine* 10.6 (1985), pp. 543–554.

[114] HJ Wilke et al. “Can prevention of a re-herniation be investigated?: establishment of a herniation model and experiments with an anular closure device”. In: *Spine* 38.19 (2013), E587–E593.

[115] H. Claude Sagi, Q. B. Bao, and Hansen A. Yuan. “Nuclear replacement strategies”. In: *Orthopedic Clinics* 34.2 (2003), pp. 263–267. DOI: 10.1016/S0030-5898(03)00007-5.

[116] Allen Carl et al. “New developments in nucleus pulposus replacement technology”. In: *The Spine Journal* 4.6, Supplement (2004), S325–S329. ISSN: 1529-9430. DOI: doi.org/10.1016/j.spinee.2004.07.030.

[117] Alberto Di Martino et al. “Nucleus Pulposus Replacement: Basic Science and Indications for Clinical Use”. In: *Spine* 30.16S (2005), S16–S22. DOI: 10.1097/01.brs.0000174530.88585.32.

[118] A.N. Sieber and J.P. Kostuik. “Concepts in nuclear replacement”. In: *Spine J.* 4 (2004), S322–S324. DOI: 10.1016/j.spinee.2004.07.029.

[119] R.D. Bowles and L.A. Setton. “Biomaterials for intervertebral disc regeneration and repair”. In: *Biomaterials* 129 (2017), pp. 54–67. DOI: 10.1016/j.biomaterials.2017.03.013.

[120] P.M. Klara and C.D. Ray. “Artificial nucleus replacement: clinical experience”. In: *Spine* 27 (2002), pp. 1374–1377. DOI: 10.1097/00007632-200206150-00022.

[121] Q.B. Bao and H.A. Yuan. “Artificial disc technology”. In: *FOC* 9 (2000), pp. 1–7. DOI: 10.3171/foc.2000.9.4.14.

[122] F. Heuer et al. “Biomechanical evaluation of conventional anulus fibrosus closure methods required for nucleus replacement, Laboratory investigation”. In: *SPI* 9 (2008), pp. 307–313. DOI: 10.3171/SPI/2008/9/9/307.

[123] L. Zengerle et al. “Nucleus replacement could get a new chance with annulus closure”. In: *Eur. Spine J.* 29 (2020), pp. 1733–1741. DOI: 10.1007/s00586-020-06419-2.

[124] P.-P.A. Vergroesen et al. “A biodegradable glue for annulus closure: evaluation of strength and endurance”. In: *Spine* 40 (2015), pp. 622–628. DOI: 10.1097/BRS.0000000000000792.

[125] S.R. Sloan et al. “Combined nucleus pulposus augmentation and annulus fibrosus repair prevents acute intervertebral disc degeneration after discectomy”. In: *Sci. Transl. Med.* 12 (2020). DOI: 10.1126/scitranslmed.aay2380.

[126] C.C. Guterl et al. “Challenges and strategies in the repair of ruptured annulus fibrosus”. In: *Eur. Cell. Mater.* 25 (2013), p. 1. DOI: 10.22203/ecm.v025a01.

[127] D.A. Frauchiger et al. “Annulus fibrosus repair using genetically engineered silk and genipin-enhanced fibringel”. In: *Global Spine J.* 6 (2016), s–0036. DOI: 10.1055/s-0036-1582588.

[128] R.G. Long et al. “Mechanical restoration and failure analyses of a hydrogel and scaffold composite strategy for annulus fibrosus repair”. In: *Acta Biomater.* 30 (2016), pp. 116–125.

[129] S.L. et al. Blumenthal. “Artificial intervertebral discs and beyond: a north American spine society annual meeting symposium”. In: *Spine J.* 2.6 (2002). DOI: 10.1016/s1529-9430(02)00540-5.

[130] M.L. Goins et al. “Nucleus pulposus replacement: an emerging technology”. In: *Spine J.* 5 (2005), S317–S324. DOI: 10.1016/j.spinee.2005.02.021.

[131] D.A. Cleveland. “The use of methylacrylic for spinal stabilization after disc operations”. In: *Marquette Med Rev* 20 (1955), pp. 62–64.

[132] R. Bertagnoli, A. Karg, and S. Voigt. “Lumbar partial disc replacement”. In: *Orthop. Clin. N. Am.* 36 (2005), pp. 341–347. DOI: 10.1016/j.ocl.2005.03.006.

[133] R. Bertagnoli et al. “Mechanical testing of a novel hydrogel nucleus replacement implant”. In: *Spine J.* 5 (2005), pp. 672–681. DOI: 10.1016/j.spinee.2004.12.004.

[134] R.D. Guyer and D.D. Ohnmeiss. “Intervertebral disc prostheses”. In: *Spine* 28 (2003), S15–S23. DOI: 10.1097/01.BRS.0000076843.59883.E1.

[135] C.M. Bono and S.R. Garfin. “History and evolution of disc replacement”. In: *Spine J.* 4 (2004), S145–S150. DOI: 10.1016/j.spinee.2004.07.005.

[136] M.H. Pelletier et al. *Comprehensive Biomaterials II*. Elsevier, 2017, pp. 216–245. DOI: 10.1016/B978-0-12-803581-8.10256-5.

[137] M.S. Marcolongo, M. Cannella, and C.J. Massey. *Spine Technology Handbook*. Elsevier, 2006, pp. 281–302. DOI: 10.1016/B978-012369390-7/50011-3.

[138] D. Coric and P.V. Mummaneni. "Nucleus replacement technologies". In: *Journal of Neurosurg Spine* (2008). DOI: 10.3171/SPI/2008/8/2/115.

[139] F. Grochulla, H.M. Mayer, and A. Korge. *Minimally Invasive Spine Surgery*. Springer-Verlag, 2006, pp. 374–378. DOI: 10.1007/3-540-29490-2_41.

[140] K. Muckley and T. Goswami. "Intervertebral disc and nucleus replacement devices and instrumentations". In: *BIOMENG* 6 (2013), pp. 136–157. DOI: 10.2174/1874764711306020007.

[141] Q.-B. Bao and H.A. Yuan. "New technologies in spine: nucleus replacement". In: *Spine* 27 (2002), pp. 1245–1247. DOI: 10.1097/00007632-200206010-00020.

[142] J.R. Meakin, J.E. Reid, and D.W.L. Hukins. "Replacing the nucleus pulposus of the intervertebral disc". In: *Clin. BioMech.* 16 (2001), pp. 560–565. DOI: 10.1016/S0268-0033(01)00042-0.

[143] G. Lewis. "Nucleus pulposus replacement and regeneration/repair technologies: present status and future prospects". In: *J. Biomed. Mater. Res.* 100B (2012), pp. 1702–1720. DOI: 10.1002/jbm.b.32712.

[144] Z. Li et al. "Polyurethane scaffold with in situ swelling capacity for nucleus pulposus replacement". In: *Biomaterials* 84 (2016), pp. 196–209. DOI: 10.1016/j.biomaterials.2016.01.040.

[145] O. Josimovic-Alesevic et al. "Three dimensional cultures of cells derived from fibrous disc cartilage for treatment of discopathy". In: *Cartilage Repair* (1997).

[146] M.C. Makhni et al. "Tissue engineering advances in spine surgery". In: *Regen. Med.* 11 (2016), pp. 211–222. DOI: 10.2217/rme.16.3.

[147] HJ Wilke et al. "Is a collagen scaffold for a tissue engineered nucleus replacement capable of restoring disc height and stability in an animal model?" In: *Eur. Spine J.* 15 (2006), pp. 433–438. DOI: 10.1007/s00586-006-0177-x.

[148] B.P. Chan and K.W. Leong. "Scaffolding in tissue engineering: general approaches and tissue-specific considerations". In: *Eur. Spine J.* 17 (2008), pp. 467–479. DOI: 10.1007/s00586-008-0745-3.

[149] S. Leckie and J. Kang. "Recent advances in nucleus pulposus replacement technology". In: *Current Orthopaedic Practice* 20 (2009), pp. 222–226. DOI: 10.1097/BCO.0b013e31819d5bdd.

[150] C.K. Lee and V.K. Goel. "Artificial disc prosthesis: design concepts and criteria". In: *Spine J.* 4 (2004), S209–S218. DOI: 10.1016/j.spinee.2004.07.011.

[151] F.C. Jr Pappou et al. "Screening for Nuclear Replacement Candidates in Patients with Lumbar Degenerative Disc Disease". In: *SAS Journal* (2008). DOI: 10.1016/SASJ-2007-0116-RR.

[152] F. Heuer et al. "Stepwise reduction of functional spinal structures increase vertebral translation and intradiscal pressure". In: *J. Biomech.* 40.4 (2007), pp. 795–803.

[153] H. J. Wilke, A. Kienle, S. Maile, et al. "A new dynamic six degrees of freedom disc-loading simulator allows to provoke disc damage and herniation". In: *European Spine Journal* 25 (2016), pp. 1363–1372. DOI: 10.1007/s00586-016-4416-5.

[154] L. Zengerle et al. "In vitro model for lumbar disc herniation to investigate regenerative tissue repair approaches". In: *Appl. Sci.* 11.6 (2021), p. 2847.

[155] A. Kettler et al. "Finite helical axes of motion are a useful tool to describe the three-dimensional in vitro kinematics of the intact, injured and stabilised spine". In: *Eur. Spine J.* 13 (2004), pp. 553–559. DOI: 10.1007/s00586-004-0710-8.

[156] A. Kettler and H.-J. Wilke H.-P. Kaps B. Haegele. "Biomechanical Behavior of a New Nucleus Prosthesis Made of Knitted Titanium Filaments". In: *SAS Journal* (2007).

[157] D.S. McNally and R.G.C. Arridge. "An analytical model of intervertebral disc mechanics". In: *Journal of Biomechanics* 28.1 (1995), pp. 53–68. ISSN: 0021-9290. DOI: 10.1016/0021-9290(95)80007-7.

[158] M. J. Gadd and D. E. T. Shepherd. “Viscoelastic properties of the intervertebral disc and the effect of nucleus pulposus removal”. In: *Proc Inst Mech Eng H* 225 (2011), pp. 335–341. DOI: 10.1177/2041303310393410.

[159] P. Kehr. *Edward C. Benzel: Biomechanics of Spine Stabilization*. Heidelberg: Springer, 2015. DOI: 10.1007/s00590-015-1684-4.

[160] Y. M. Lu, W. C. Hutton, and V. M. Gharpuray. “The effect of fluid loss on the viscoelastic behavior of the lumbar intervertebral disc in compression”. In: *J Biomech Eng* 120 (1998), pp. 48–54. DOI: 10.1115/1.2834306.

[161] F. Guilak et al. “Viscoelastic properties of intervertebral disc cells: identification of two biomechanically distinct cell populations”. In: *Spine* 24 (1999), p. 2475. DOI: 10.1097/00007632-199912010-00009.

[162] J. C. Iatridis et al. “The viscoelastic behavior of the non-degenerate human lumbar nucleus pulposus in shear”. In: *J Biomech* 30 (1997), pp. 1005–1013. DOI: 10.1016/S0021-9290(97)00069-9.

[163] R. Lakes and R. S. Lakes. *Viscoelastic Materials*. Cambridge: Cambridge University Press, 2009.

[164] N. D. Panagiotacopulos et al. “A mechanical model for the human intervertebral disc”. In: *J Biomech* 20.9 (1987), pp. 839–850.

[165] R. W. Ogden and G. A. Holzapfel. *Mechanics of Biological Tissue*. Berlin: Springer, 2006. DOI: 10.1007/3-540-31184-X.

[166] I. Podlubny. *Fractional Differential Equations: An Introduction to Fractional Derivatives, Fractional Differential Equations, to Methods of Their Solution and Some of Their Applications*. Amsterdam: Elsevier, 1998.

[167] F. Mainardi. *Fractional Calculus and Waves in Linear Viscoelasticity: An Introduction to Mathematical Models*. Singapore: World Scientific, 2010. DOI: 10.1142/p614.

[168] M. S. Stanković et al. “Theory and Applications of Fractional Differential Equations”. In: *Facta Universitatis, Series: Electronics and Energetics* 24.1 (2006), pp. 141–143.

[169] F.C. Meral, T.J. Royston, and R. Magin. "Fractional calculus in viscoelasticity: An experimental study". In: *Communications in Nonlinear Science and Numerical Simulation* 15.4 (2010), pp. 939–945. ISSN: 1007-5704. DOI: 10.1016/j.cnsns.2009.05.004.

[170] C. Ionescu et al. "The role of fractional calculus in modeling biological phenomena: A review". In: *Communications in Nonlinear Science and Numerical Simulation* 51 (2017), pp. 141–159. ISSN: 1007-5704. DOI: 10.1016/j.cnsns.2017.04.001.

[171] A. Bonfanti et al. "Fractional viscoelastic models for power-law materials". In: *Soft Matter* 16 (2020), pp. 6002–6020. DOI: 10.1039/D0SM00354A.

[172] G. Alotta et al. "The Finite Element Implementation of 3D Fractional Viscoelastic Constitutive Models". In: *Finite Elements in Analysis and Design* 146 (2018), pp. 28–41.

[173] A. Al Jarbouh. "Rheological Behaviour Modelling of Viscoelastic Materials by Using Fractional Model". In: *Energy Procedia* 19 (2012), pp. 143–157.

[174] V. Sciortino et al. "Fractional calculus as a new perspective in the viscoelastic behaviour of the intervertebral disc". In: *European Workshop on Structural Health Monitoring*. Cham: Springer International Publishing, 2023, pp. 915–925. DOI: 10.1007/978-3-031-07254-3_92.

[175] M. L. Burns, I. Kaleps, and L. E. Kazarian. "Analysis of compressive creep behavior of the vertebral unit subjected to a uniform axial loading using exact parametric solution equations of Kelvin-solid models—part I. Human intervertebral joints". In: *J Biomech* 17.2 (1984), pp. 113–130. DOI: 10.1016/0021-9290(84)90129-5.

[176] T. S. Keller, D. M. Spengler, and T. H. Hansson. "Mechanical behavior of the human lumbar spine. I. Creep analysis during static compressive loading". In: *J Orthop Res* 5 (1987), pp. 467–478. DOI: 10.1002/jor.1100050402.

[177] S. Li et al. "Limitations of the standard linear solid model of intervertebral discs subject to prolonged loading and low-frequency vibration in axial compression". In: *J Biomech* 28 (1995), pp. 779–790. DOI: 10.1016/0021-9290(94)00140-Y.

[178] L. Ekström et al. “Intervertebral disc response to cyclic loading—an animal model”. In: *Proc Inst Mech Eng H* 210 (1996), pp. 249–258. DOI: 10.1243/PIME_PROC_1996_210_421_02.

[179] Y. M. Lu, W. C. Hutton, and V. M. Gharpuray. “The Effect of Fluid Loss on the Viscoelastic Behavior of the Lumbar Intervertebral Disc in Compression”. In: *J Biomech Eng.* (1998). DOI: 10.1115/1.2834306.

[180] S. Campana et al. “Relationships between viscoelastic properties of lumbar intervertebral disc and degeneration grade assessed by MRI”. In: *J Mech Behav Biomed Mater* 4 (2011), pp. 593–599. DOI: 10.1016/j.jmbbm.2011.01.007.

[181] D. Hwang et al. “Role of load history in intervertebral disc mechanics and intradiscal pressure generation”. In: *Biomech Model Mechanobiol* 11 (2012), pp. 95–106. DOI: 10.1007/s10237-011-0295-1.

[182] A. Araujo et al. “Comparison between the dynamic and initial creep response of porcine and human lumbar intervertebral discs”. In: *2015 IEEE 4th Portuguese meeting on bioengineering (ENBENG)*. Porto: IEEE, 2015, pp. 1–6. DOI: 10.1109/ENBENG.2015.7088868.

[183] X. Yang et al. “Creep experimental study on the lumbar intervertebral disk under vibration compression load”. In: *Proc Inst Mech Eng H* 233 (2019), pp. 858–867. DOI: 10.1177/0954411919856794.

[184] A. Heinz. “Modelling the mechanical behavior of the intervertebral disc”. In: *RARC 2020* 3 (2020), p. 83.

[185] V. Sciortino, J. U. Jansen, D. Cerniglia, et al. “Intervertebral disc creep behaviour through viscoelastic models: an in-vitro study”. In: *Discover Applied Sciences* 6 (2024), p. 392. DOI: 10.1007/s42452-024-06092-w.

[186] Thomas Zander et al. “Diurnal variations in intervertebral disc height affect spine flexibility, intradiscal pressure and contact compressive forces in the facet joints”. In: *Computer Methods in Biomechanics and Biomedical Engineering* 13.4 (2009), pp. 551–557. DOI: 10.1080/10255840903337855.

[187] M. A. Adams, P. Dolan, and W. C. Hutton. “Diurnal variations in the stresses on the lumbar spine”. In: *Spine* 12.2 (1987), pp. 130–137. DOI: 10.1097/00007632-198703000-00008.

[188] M. Adams et al. “Diurnal changes in spinal mechanics and their clinical significance”. In: *J Bone Jt Surg Br Vol* 72 (1990), pp. 266–270. DOI: 10.1302/0301-620X.72B2.2138156.

[189] M. Jo and S. W. Chae. “Stress analysis of intervertebral disc during occupational activities”. In: *Comput Methods Progr Biomed* 208 (2021), p. 106298. DOI: 10.1016/j.cmpb.2021.106298.

[190] M. Żak. “Effect of support on mechanical properties of the intervertebral disc in long-term compression testing”. In: *J Theor Appl Mech* 52.3 (2014), pp. 677–686.

[191] L. A. Setton and J. Chen. “Cell mechanics and mechanobiology in the intervertebral disc”. In: *Spine* 29 (2004), pp. 2710–2723. DOI: 10.1097/01.brs.0000146050.57722.2a.

[192] F. Heuer et al. “Creep associated changes in intervertebral disc bulging obtained with a laser scanning device”. In: *Clin Biomech* 22 (2007), pp. 737–744. DOI: 10.1016/j.clinbiomech.2007.04.010.

[193] Sean M. Finley et al. “FEBio finite element models of the human lumbar spine”. In: *Computer Methods in Biomechanics and Biomedical Engineering* 21.6 (2018), pp. 444–452. DOI: 10.1080/10255842.2018.1478967.

[194] Ming Xu et al. “Lumbar spine finite element model for healthy subjects: development and validation”. In: *Computer Methods in Biomechanics and Biomedical Engineering* 20.1 (2017), pp. 1–15. DOI: 10.1080/10255842.2016.1193596.

[195] M. Kurutz and L. Oroszváry. “Finite element modeling and simulation of healthy and degenerated human lumbar spine”. In: *Finite Element Analysis—From Biomedical Applications to Industrial Developments*. London, UK: IntechOpen Limited, 2012, pp. 193–216.

[196] Lars G. Gilbertson et al. “Finite Element Methods in Spine Biomechanics Research”. In: *Critical Reviews in Biomedical Engineering* 23.5-6 (1995), pp. 411–473. DOI: 10.1615/CritRevBiomedEng.v23.i5-6.20.

[197] P.A. Kramer, A.G. Hammerberg, and A.D. Sylvester. “Modeling the Spine Using Finite Element Models: Considerations and Cautions”. In: *Spinal Evolution*. Ed. by E. Been, A. Gómez-Olivencia, and P. Ann Kramer. Springer, 2019. DOI: 10.1007/978-3-030-19349-2_17.

[198] Y. Guan et al. “Validation of a clinical finite element model of the human lumbosacral spine”. In: *Medical and Biological Engineering and Computing* 44 (2006), pp. 633–641. DOI: 10.1007/s11517-006-0066-9.

[199] Vincenza Sciortino et al. “On the Finite Element Modeling of the Lumbar Spine: A Schematic Review”. In: *Applied Sciences* 13.2 (2023), p. 958. DOI: 10.3390/app13020958.

[200] J. Noailly and D. Lacroix. “5 - Finite element modelling of the spine”. In: *Biomaterials for Spinal Surgery*. Ed. by Luigi Ambrosio and Elizabeth Tanner. Woodhead Publishing, 2012, 144–234e. DOI: doi.org/10.1533/9780857096197.1.144.

[201] M. Dreischarf et al. “Comparison of eight published static finite element models of the intact lumbar spine: Predictive power of models improves when combined together”. In: *Journal of Biomechanics* 47.8 (2014), pp. 1757–1766. ISSN: 0021-9290. DOI: doi.org/10.1016/j.jbiomech.2014.04.002.

[202] M.I. Godinho et al. “Computational modeling of lumbar disc degeneration before and after spinal fusion”. In: *Clinical Biomechanics* 90 (2021), p. 105490. ISSN: 0268-0033. DOI: doi.org/10.1016/j.clinbiomech.2021.105490.

[203] V. Moramarco et al. “An accurate validation of a computational model of a human lumbosacral segment”. In: *Journal of Biomechanics* 43.2 (2010), pp. 334–342. ISSN: 0021-9290. DOI: doi.org/10.1016/j.jbiomech.2009.07.042.

[204] Vincenza Sciortino et al. “A Population-Based 3D Atlas of the Pathological Lumbar Spine Segment”. In: *Bioengineering* 9.8 (2022), p. 408. DOI: 10.3390/bioengineering9080408.

[205] V. Sciortino et al. “Statistical Shape Modelling as a Tool for Medical Reverse Engineering”. In: *Design Tools and Methods in Industrial Engineering III*. Ed. by M. Carfagni et al. Lecture Notes in Mechanical Engineering. Springer, 2024. DOI: 10.1007/978-3-031-52075-4_25.

[206] Marco Cigoli et al. “Finite Element Analysis of the Lumbar Spine under Different Loading Conditions: A Systematic Review”. In: *Thoracic and Cardiovascular Surgeon* 66.2 (2018). DOI: 10.1055/s-0038-1632506.

[207] Konstantin V. Chernukha, Richard H. Daffner, and Donald H. Reigel. “Lumbar Lordosis Measurement: A New Method Versus Cobb Technique”. In: *Spine* 23.1 (1998). DOI: 10.1097/00007632-199801010-00016.

[208] Kevin G. Shea et al. “A Comparison of Manual Versus Computer-Assisted Radiographic Measurement: Intraobserver Measurement Variability for Cobb Angles”. In: *Spine* 23.5 (1998). DOI: 10.1097/00007632-199803010-00007.

[209] Robert Fernand and Daniel E. Fox. “Evaluation of Lumbar Lordosis: A Prospective and Retrospective Study”. In: *Spine* 10.9 (1985).

[210] J.Q. Campbell and A.J. Petrella. “Automated finite element modeling of the lumbar spine: Using a statistical shape model to generate a virtual population of models”. In: *Journal of Biomechanics* 49.13 (2016). DOI: 10.1016/j.jbiomech.2016.05.013.

[211] Laurent Mirel et al. “A study of the effects of variability in the vertebral model on the mechanical response of the lumbar spine”. In: *Inria Research Report* 2011.00616067 (2011). DOI: 10.1016/j.jbiomech.2016.12.014.

[212] S. Benameur et al. “A hierarchical statistical modeling approach for the unsupervised 3-D biplanar reconstruction of the scoliotic spine”. In: *IEEE Transactions on Biomedical Engineering* 52.12 (2005), pp. 2041–2057. DOI: 10.1109/TBME.2005.857665.

[213] Svante Wold, Kim Esbensen, and Paul Geladi. “Principal component analysis”. In: *Chemometrics and Intelligent Laboratory Systems* 2.1-3 (1987). DOI: 10.1016/0169-7439(87)80084-9.

[214] Vidosav Majstorovic et al. “Reverse engineering of human bones by using method of anatomical features”. In: *CIRP Annals* 62.1 (2013), pp. 167–170. DOI: 10.1016/j.cirp.2013.03.081.

[215] A. Ben et al. “Novel Approach for Estimating the Stiffness of Soft Tissue in Lumbar Spine Biomechanics”. In: *CMES 2017: 3rd International Conference on Computational Methods in Engineering and Science*. 2017.

[216] Jonathan Stradling. "The Development of a Finite Element Model of the Human Lumbar Spine". PhD thesis. University of Greenwich, 2016.

[217] I. Gibson. *Advanced manufacturing technology for medical applications: reverse engineering, software conversion and rapid prototyping*. Chichester, UK: John Wiley & Sons, 2006.

[218] J. Zhang, Z. Wei, and J. Li. "Finite Element Analysis of the Human Lumbar Spine Under Compression". In: *2010 3rd International Conference on Biomedical Engineering and Informatics*. Vol. 5. IEEE, 2010, pp. 1–5. DOI: 10.1109/BMEI.2010.5639244.